CHARACTERIZATION OF THE SHALLOW HYDROGEOLOGY WITH ESTIMATES OF RECHARGE AT A HIGH-ALTITUDE MOUNTAINOUS SITE, NIWOT RIDGE, FRONT RANGE, COLORADO

by

JESSICA J. KING

B.S., Tufts University, 2002

A thesis submitted to the

Faculty of the Graduate School of the

University of Colorado in partial fulfillment

of the requirement for the degree of

Master of Science

Department of Geological Sciences

2012

This thesis entitled:
Characterization of the shallow hydrogeology with estimates of recharge at a high-altitude mountainous site, Niwot Ridge, Front Range, Colorado
written by Jessica J. King
has been approved for the Department of Geological Sciences

_____
Shemin Ge

_____
Mark W. Williams

_____
Robert S. Anderson

Date_____

The final copy of this thesis has been examined by the signatories, and we find that both the content and the form meet acceptable presentation standards of scholarly work in the above mentioned discipline.

King, Jessica J. (M.S., Geological Sciences)

Characterization of the shallow hydrogeology with estimates of recharge at a high-altitude mountainous site, Niwot Ridge, Front Range, Colorado

Thesis directed by Professor Shemin Ge

Abstract

Mountains provide a source of essential water resources, including groundwater, for lower-lying valleys and plains. It is important to understand mountain systems to effectively manage and protect groundwater resources. Yet, basic questions remain regarding mountain recharge. The goal of this study was to improve understanding of spatial and temporal variability of groundwater flow and recharge in a mountainous watershed. It is the first attempt to characterize the hydrogeology of Niwot Ridge, an alpine study site in the Front Range, Colorado. The focus area included two headwater catchments: the Saddle catchment and the Martinelli catchment. Hydrogeology was characterized using results of groundwater level monitoring, infiltration tests, and slug tests. Recharge was estimated using water table fluctuation method and groundwater modeling. The water budget was determined.

The water table is at most 8.5 m below ground surface and is a subdued replica of topography. Water levels fluctuated seasonally, implying that one significant recharge period occurred per year. Infiltration capacity ranged 2.87×10^{-5}–6.71×10^{-4} m/s. Slug test results indicated hydraulic conductivity was 1.92×10^{-4} m/s for Quaternary-Tertiary diamicton, 8.74×10^{-4} m/s for Tertiary bedrock, and 8.42×10^{-6} m/s for Precambrian bedrock. Modeling results indicated hydraulic conductivity was 2.50×10^{-6} m/s for diamicton and 1.00×10^{-7} m/s for Tertiary bedrock. Groundwater flow was mostly shallow, flowed from high to low topography, recharged on ridgetops, and discharged to streams.

At the Saddle site, recharge averaged 1.25 m/y (3.96×10^{-8} m/s, 52% of precipitation) and ranged from 0.57 m/y in areas where little snow accumulates to 1.64 m/y in areas where snow depths reach several meters. At the Martinelli site, recharge was at a minimum through winter months, rose quickly to a maximum rate (1.22×10^{-7} m/s) in June when water table was highest, and gradually declined through the remainder of the year. Assuming 100% water input from precipitation, the annual water budget at Niwot Ridge included 33% evapotranspiration, 15% sublimation, 13% runoff, and 52% recharge (with 13% total error).

The results of this thesis contribute to scientific knowledge about the Niwot Ridge hydrologic system as well as to the broader understanding of how groundwater is replenished at its source by mountain recharge.

Acknowledgements

It is a pleasure to acknowledge the faculty, colleagues, friends, and family who made this thesis possible. The faculty of the University of Colorado at Boulder has provided me with an incredible graduate education. Several individuals deserve special recognition. First and foremost, I offer my sincerest gratitude to my adviser, Shemin Ge, for her support, patience, and guidance. Her remarkable knowledge of the science of hydrogeology was invaluable as I explored the groundwater system of Niwot Ridge. Shemin always encouraged me to pursue independent work, which has helped me become a confident and autonomous researcher. I thank her for working so hard with me during the final weeks of completing my thesis.

I also extend my appreciation to Mark Williams and Bob Anderson for their help as committee members. Mark's knowledge of the Niwot Ridge study area and snow hydrology was instrumental as I conducted my research. Bob taught me how to examine the physical world through math and encouraged me to work extra hard when faced with problems that seemed impossible. I thank Cliff Voss and Jeff McKenzie for allowing me to attend a SUTRA workshop and for answering my questions about SUTRA as I developed my models. Thank you to Anne Gardulski and Denis LeBlanc for introducing me to geology and hydrogeology and for encouraging me to apply to graduate school.

I am indebted to Jona King, Miori Yoshino, In Wook Yeo, Morgan Zeliff, Sandor Coscia, and Leah Meromy for their tireless assistance in the field under even the most intense alpine conditions. From conducting slug tests in below freezing weather, to hauling buckets of water upslope at 11,000 ft, to digging bottomless snowpits in search of wells, I couldn't have done it alone. Thank you also to the Niwot Ridge LTER for help in data compilation. My understanding of the climate and hydrology of Niwot Ridge would not have been possible

without Kurt Chowanski, Hope Humphries, Casey Flynn, Nel Caine, Jen Morse, and Rory Cowie. The support and camaraderie of my officemates, Miori Yoshino, Kali Abel, Matt Weingarten, Lyndsay Ball, Brent Aigler, In Wook Yeo, Jonathon Galeano, and Nadine Reitman, helped pass long hours in the hydrogeology lab.

I am grateful for the financial support of my graduate studies, which was provided by the National Science Foundation and the University of Colorado at Boulder Department of Geological Sciences. The research and teaching assistantships allowed me to focus my energy and time on learning.

A big thank you goes out to my friends and family for understanding my desire to move to Colorado to attend graduate school and for helping me enjoy the spaces in between studying. I appreciate the patience of my Jackson friends as it took me a little longer to skin out the Pass Ridge these past couple of years. I thank my parents, Pamela and David Cochrane, for providing inspiration. They are the hardest working and most supportive people I know. I thank my brother, Alec Cochrane, for his encouragement to follow my dreams. I thank Ella Rose for her loyal companionship and uncanny ability to make me smile. Above all, I want to thank my amazing husband, Jona, for his love, sacrifice, and compassion. His tireless commitment to my learning and my happiness provided me with the strength I needed to complete this journey.

Contents

Tables

Figures

Chapter 1
Introduction

1.1 Background

Mountains and high-elevation regions are natural "water towers" because they provide a source of essential water resources, including groundwater, and a steep hydraulic gradient for lower-lying valleys and plains (Viviroli et al., 2007). Precipitation in the form of snow accumulates in mountains over the winter months and melts through spring and summer when lowland demands are greatest. In arid and semi-arid regions, such as the western U.S., groundwater provides a primary source of freshwater, particularly during late summer and fall when surface flows decrease or dry up entirely (Scanlon et al., 2006). In addition, mountain groundwater often provides a source of high quality water supply (Abbott et al., 2000; Bossong et al., 2003). Yet, basic questions remain regarding how groundwater is replenished at its source by mountain recharge (Bales et al., 2006).

Groundwater constitutes 98% of accessible freshwater on Earth (Fetter, 2001). The enormous storing capacity and long residence time of groundwater make groundwater an effective buffer in regulating more drastic hydrologic events on the surface. Therefore, groundwater plays an important but often overlooked role in long-term sustainability of water resources. Recent trends show that precipitation in the western U.S. came more often as rain than as snow (Knowles et al., 2006), snow and snow cover extent declined (Hamlet et al., 2005; Karl et al., 1993; Mote, 2003; Mote, 2006), winter snowpack melted earlier in the spring (Regonda et al., 2005), and snowfed streams peaked earlier in the year (Regonda et al., 2005). These trends suggest that recharge areas may decrease in size, which would lead to declines in recharge to mountain aquifers. Mountain areas are rapidly developing in the western U.S. With

this development comes an increased use of mountain aquifers, so there is a need to understand better how mountain aquifers store and transport groundwater.

Prior studies in mountain hydrology have assumed negligible groundwater input, but recent studies show that mountain groundwater systems play a large role in regional groundwater systems, particularly in the western U.S. (Clow et al., 2003; Liu et al., 2004; Wilson and Guan, 2004; Smerdon et al., 2009). Wilson and Guan (2004) reviewed several studies showing that mountains are recharge zones that provide a primary source of water to basin alluvial aquifers in the western U.S. In the Colorado Front Range, injection-tracer tests (Clow et al., 2003) and isotopic and geochemical tracers (Liu et al., 2004) have been used to show that mountain groundwater provides more than half of total discharge to alpine streams, even after cessation of snowmelt. For this reason, mountain groundwater is vital to lowland rivers and aquifers. It is important to understand mountain systems to effectively manage and protect groundwater resources.

Groundwater recharge is defined as the movement of water from the unsaturated zone or from surface water into the saturated zone (Freeze and Cherry, 1979). It is typically expressed as either a volumetric flow rate, in terms of volume per unit time, (L^3/T), or as a flux, in terms of volume per unit surface area per unit time (L/T) (Healy, 2010). Recharge in mountainous terrain is characterized by the infiltration of snowmelt from the land surface to thin unconsolidated sediments and soils, mountain bedrock, and intervening valley fill deposits. Within unconsolidated surficial and valley fill deposits, groundwater occurs in porous granular sediments such as sand and gravel. Within bedrock, groundwater occurs primarily in fractures and flow depends on the interconnectivity of fracture networks. Where the water table is shallow and within a few meters of the land surface, recharge to the water table is more likely to occur.

In locations where the water table is deep, infiltrating water may take years or decades to recharge the water table, although recharge from groundwater inflow may still be significant. During peak snowmelt the water table may intersect the land surface leading to overland flow and reduced recharge. Recharge may also occur as water leaking from surface water to an underlying aquifer; however, in alpine settings this type of recharge is less common.

Groundwater recharge and flow patterns in mountain regions depend primarily on climate, surface topography, and geology (Forster and Smith, 1988b; Cherkauer and Ansari, 2005; Healy, 2010). Cold temperatures limit evaporation thereby increasing the amount of water available for recharge. The melting of the seasonal snowpack is the primary source of recharge to mountains and recharge is generally higher in mountains than in adjacent lowlands (Winter et al., 1999; Abbott, 2000). Areas that accumulate a deep seasonal snowpack provide a long-lasting source of groundwater recharge as snow melts throughout the summer. Areas where snowmelt occurs rapidly may be deprived of recharge for large portions of the year.

The spatial distribution of groundwater recharge is largely a function of surface topography. Groundwater recharge enters mountain systems at summits and high slopes and discharges to valleys (Tóth, 1963; Freeze and Witherspoon, 1967; Forster and Smith, 1988a; Wilson and Guan, 2004; Gleeson and Manning, 2008). Groundwater flow is driven by topographic gradients because water entering the system at topographic highs has a higher potential energy than groundwater in lower areas. The greater energy is reflected in higher elevation of the water table (Fetter, 2001). The steep topographic relief of mountainous terrain generates high hydraulic gradients. Slope aspect, shading, and exposure affect the amount of solar radiation that reaches that land surface and, therefore, the amount of snow that accumulates. In general, there is more water available for recharge on shaded, north-facing

slopes (in the Northern Hemisphere) oriented perpendicular to prevailing storm tracts (Stonestrom and Harrill, 2007).

The lithology and structure of the subsurface greatly affect recharge. Mountain geology is characteristically complex leading to heterogeneous patterns of recharge. Near-surface sediments in the mountains are generally thin and of higher permeability than the underlying bedrock. Recharge to these sediments occurs easily because water can infiltrate quickly. Lateral groundwater flow is common when the difference between sediment and bedrock permeability is high. Recharge to bedrock is mainly localized to fracture zones (Snow, 1973).

Recharge can be estimated by a variety of methods including physical, tracer, or numerical modeling approaches (Scanlon et al., 2002). Deciding what methods to use depends on the resources and data available and on the applicability and limitations of each method. Many studies recommend using multiple methods and comparing the results since much of the error associated with a recharge estimate is not quantifiable (Sophocleous, 1991; Halford and Mayer, 2000; de Vries and Simmers, 2002; Healy and Cook, 2002; Scanlon et al., 2002; Healy, 2010). The most common methods are discussed in Appendix II. Healy (2010) offers a thorough review of groundwater recharge and estimation methods.

Estimates of groundwater recharge are essential to the proper management and protection of groundwater resources. Recharge is also a key component of groundwater flow and contaminant transport models (Sanford, 2002). Accurate estimation of recharge is difficult because the processes involved are complex and depend on many factors, such as precipitation and snowmelt amounts and intensities, evapotranspiration, runoff, vegetation, topography, geology, and land use (Memon, 1995). In mountain regions, quantification of recharge is further hindered by the lack of hydrogeologic data and instrumentation for alpine regions worldwide

(Caine et al., 2006). Groundwater monitoring wells in high-altitude mountainous regions are rare. Where wells exist in the mountains, groundwater levels are likely to be the only hydrogeologic data available since well-core sampling, aquifer tests, and borehole geophysical tests are logistically challenging in difficult-to-access sites. Furthermore, the practical challenges of working in remote regions with harsh weather conditions are substantial.

The lack of groundwater data in mountain regions combined with the need for a better understanding of alpine groundwater systems provided the motivation to study recharge in a mountain aquifer. In addition, the existence of seven pairs of groundwater piezometers at Niwot Ridge, an alpine study site adjacent to the Continental Divide, provided a good opportunity to implement a hydrogeologic field investigation.

1.2 Water budget

The water budget method is the most fundamental approach to estimate recharge. Water budget techniques, including numerical modeling, depend on quantification of all contributing factors to the water budget of a basin. The water budget for a basin states that the amount of water entering a basin minus the amount of water leaving a basin is equal to the change in water stored in the basin. The water budget in equation form is (Scanlon et al., 2002):

$$P + Q_{in} - E - ET - Q_{out} = \Delta S \qquad [1.1]$$

where the inputs of water to the basin are precipitation that reaches the ground surface (P) and water flow into the basin (Q_{in}). The outputs of water from the basin are evaporation (E), evapotranspiration (ET), and water flow out of the basin (Q_{out}). ΔS is the change in water storage within the basin. A more useful water budget accounts for the individual components of water moving into and out of a basin and is written as (Scanlon et al., 2002):

$$P + Q_{in}^{sw} + Q_{in}^{gw} - E^{sw} - E^{gw} - ET - Q_{out}^{sw} - Q_{out}^{gw} = \Delta S^{sw} + \Delta S^{uz} + \Delta S^{gw} \qquad [1.2].$$

The superscripts refer to the location of water within the basin: surface water (*sw*) (e.g. lakes, streams, snow on the ground), unsaturated zone (*uz*), and groundwater (*gw*). The units of each term are a rate, either [L/T], [L^2/T], [L^3/T], or [M/T]. In the mountains, precipitation is typically the only input of water, so Q_{in} is assumed zero. The mountain water budget is written as (modified from Wilson and Guan, 2004):

$$P - E^{sw} - E^{gw} - ET - Q_{out}^{sw} - Q_{out}^{gw} = \Delta S^{sw} + \Delta S^{uz} + \Delta S^{gw} \quad [1.3].$$

Recharge (R) arriving at the water table either flows out of the basin as groundwater, is evaporated, or is retained in storage (Scanlon et al., 2002):

$$-R = -Q_{out}^{gw} - E^{gw} - \Delta S^{gw} \quad [1.4].$$

In most cases, the mountain water budget is applied by measuring or estimating all terms but one, which is calculated as a residual. In the case of recharge, R is the residual. Substituting the mountain water budget into Equation 1.4 leads to the following form of recharge equation:

$$R = P - E^{sw} - ET - Q_{out}^{sw} - \Delta S^{sw} - \Delta S^{uz} \quad [1.5].$$

Figure 1.1 illustrates the mountain water budget with precipitation arriving at the surface, evaporation and evapotranspiration, surface water outflow, recharge to groundwater, and changes in storage.

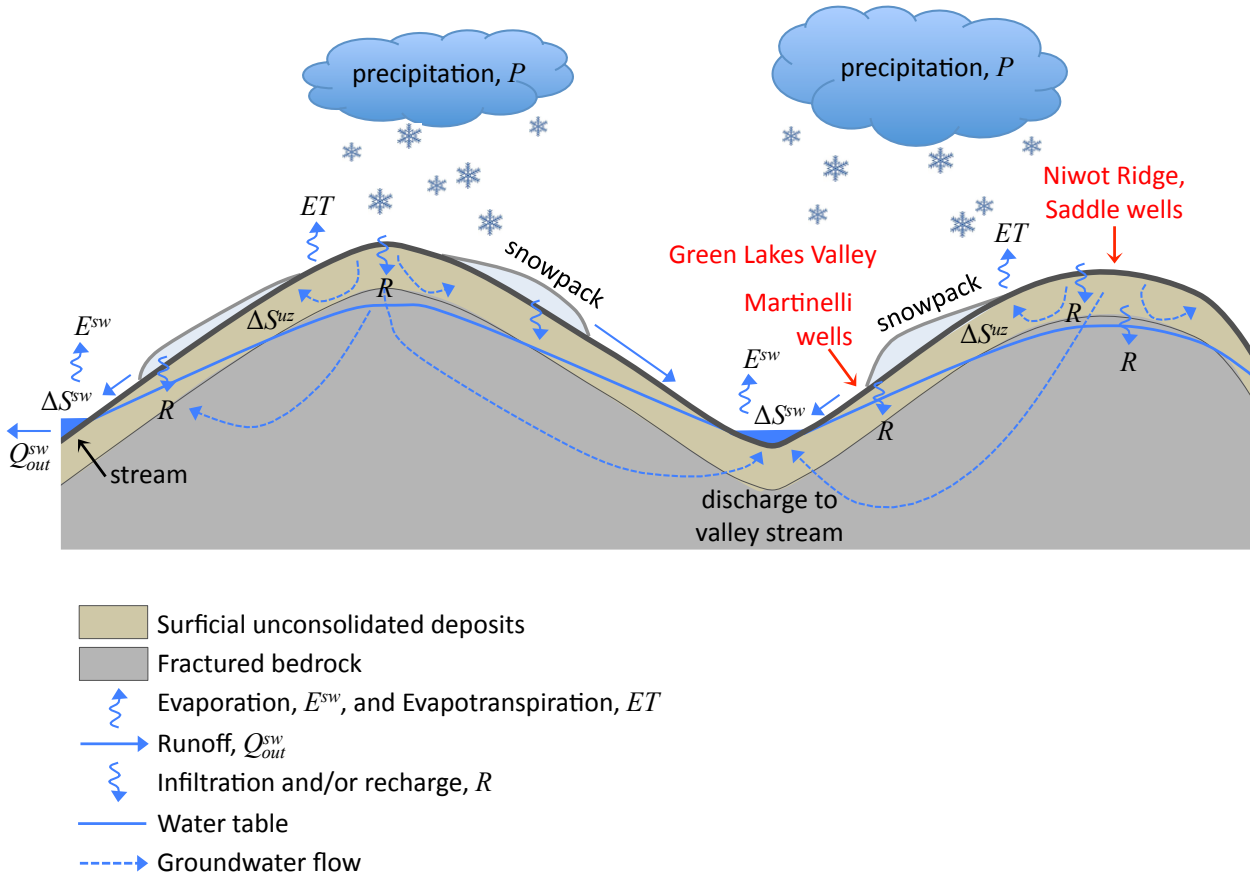

Figure 1.1. The mountain water budget. Input is precipitation (P). Outputs are evaporation from surface water (E^{sw}), evapotranspiration from the unsaturated zone (ET) and surface water flow out of the basin (Q^{sw}_{out}). ΔS^{sw} and ΔS^{uz} are the change in storage within surface water and the unsaturated zone, respectively. This figure illustrates a cross-sectional view of the conceptual model of the hydrogeology of Niwot Ridge, which is discussed in Chapter 2, Section 2.6.

A good recharge estimate from a water budget approach depends on how well the terms on the right-hand side of Equation 1.5 are estimated. The water budget method is data intensive, which is often a limiting factor in its use, particularly in alpine sites. Still, several studies have used the water budget method to estimate recharge in mountain regions. Huntley (1979) estimated 14% of precipitation recharges groundwater in the Sangre de Cristo Mountains in San Luis Valley, Colorado. Hely et al. (1971) estimated 19% of precipitation recharges groundwater in the Wasatch Range in Utah. In the mountains of Taiwan, Lee et al. (2006) estimated more than 20% of precipitation recharges groundwater.

1.3 Study objectives

The overall objective of this study is to improve understanding of spatial and temporal variability of groundwater flow and recharge at Niwot Ridge. In order to accomplish this primary objective, the hydrogeology of the field site needed to be characterized. Specific objectives are:

1. Determine the depth of the water table and examine the position of the water table change in space and time.
2. Determine the spatial distribution of infiltration capacity of the near surface material.
3. Determine the hydraulic conductivity of the shallow aquifer and its spatial variability.
4. Describe the pattern of groundwater flow rate and direction.
5. Estimate the rate and distribution of groundwater recharge.
6. Approximate the water budget of Niwot Ridge.

1.4 Thesis organization

Chapter 2 introduces the Niwot Ridge study area by presenting existing data on topography, land cover, geology, climate, and hydrology. The existing data were used to determine additional data needs and develop a conceptual model of the hydrogeology of Niwot Ridge. Chapter 3 describes the field investigation implemented to fill gaps in existing data and characterize the shallow subsurface hydrogeology of Niwot Ridge. Observations of water level and results of infiltration tests and slug tests are presented. Chapter 4 describes the use of the water table fluctuation method to estimate groundwater recharge. The water budget of Niwot Ridge is presented. Chapter 5 describes the development of a numerical groundwater flow model using the computer code SUTRA to estimate groundwater recharge. Chapter 6 presents the major findings of this study. Recommendations are made for future research.

Chapter 2
The Niwot Ridge study area

2.1 Introduction to the study area

Near the middle of the Colorado Front Range at a latitude of about 40°N, the Indian Peaks region dominates the topography with a mean altitude of over 4000 m (White, 1982). The Indian Peaks are characterized by their deep U-shaped valleys separated by long broad interfluves that narrow into arêtes at the Continental Divide. The longest of these interfluves, located near the midpoint of the Front Range, is Niwot Ridge (Ives, 1973).

Niwot Ridge is located roughly 35 km west of Boulder, Colorado (Figure 2.1a). It is a wind-swept alpine tundra landscape periglacial in origin (Madole, 1982). The focus area of this study included two adjacent headwater catchments located on Niwot Ridge: the Saddle site and the Martinelli site (Figure 2.1b). Both sites are alpine in nature, lie above the late Pleistocene ice limit (Gable and Madole, 1976; R. Madole, personal communication, 7 June 2001), and have similar climate. The sites differ in topography, landcover, subsurface geology, and snow accumulation patterns.

Niwot Ridge lies within the Arapaho and Roosevelt National Forests. There are no populated or developed areas within the study region (except for the Tundra Lab building at the Saddle site). Prior to 1910, the Snowy Range Mine, which is adjacent to Lake Albion, was an active although unproductive gold and lead mine (Lovering and Goddard, 1950; Pearson, 1980). Otherwise, the area has been entirely closed to mining activities. In addition, there are no groundwater withdrawal wells near the study area.

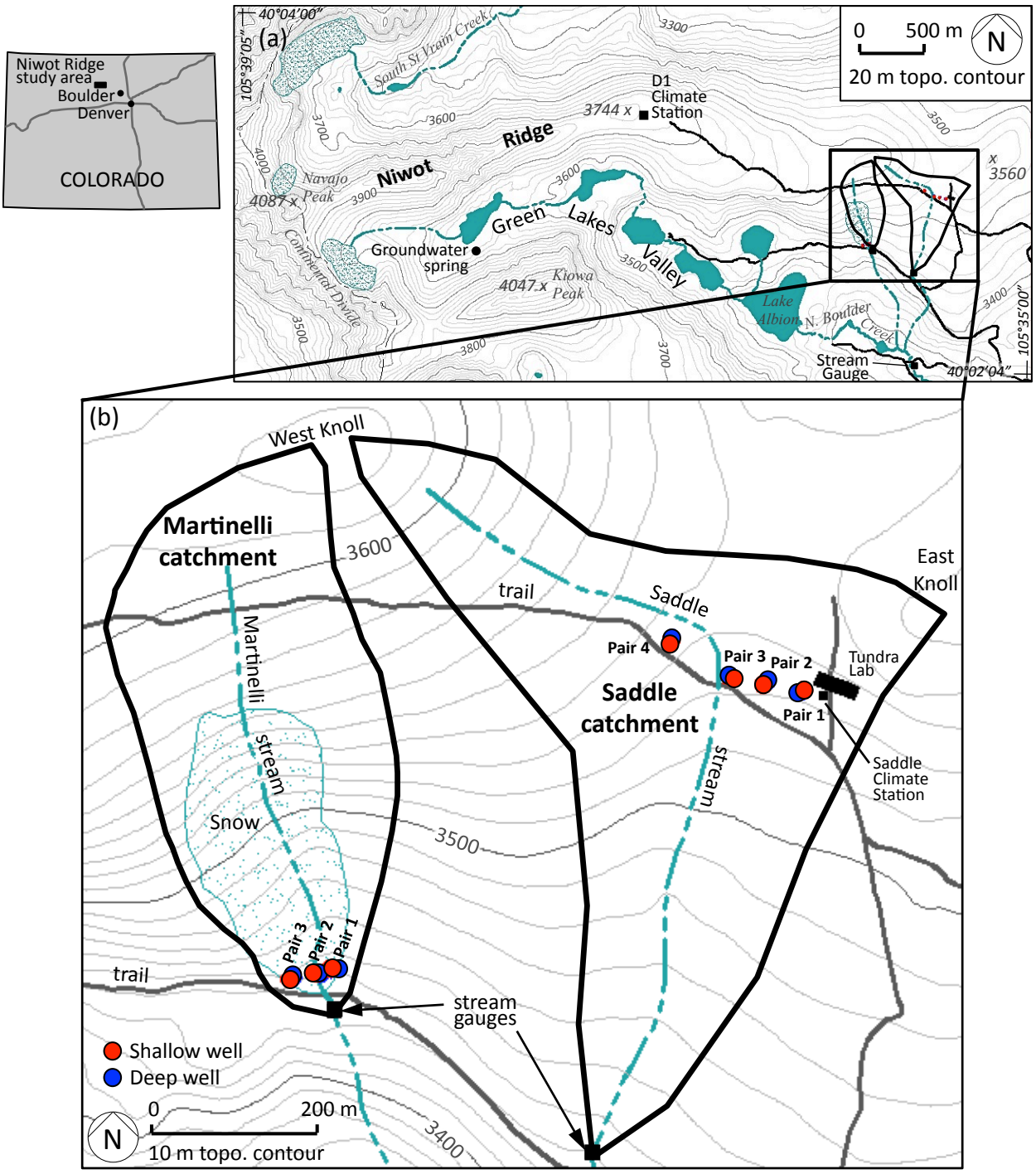

Figure 2.1. (a) Map of the Niwot Ridge area located in the Colorado Front Range of the Rocky Mountains, USA and (b) inset of the study sites "Saddle" and "Martinelli". Also shown are locations of four pairs of groundwater piezometers at Saddle site, three pairs of groundwater piezometers at Martinelli site, Saddle climate station, Tundra Lab building, and Saddle and Martinelli stream gauges. Contour lines and map features are from the Ward, CO (1957) 7.5' USGS Quadrangle (U.S. Geological Survey, 1957).

During the twentieth century, the site established its role as a primary player in alpine scientific research. In 1921, the University of Colorado founded the "Science Lodge" (later renamed the Mountain Research Station) at the base of Niwot Ridge to support alpine research activities (Bowman, 2001). In 1925, the City of Boulder purchased the Green Lakes Valley and its senior water rights as a municipal water source and, around 1930, closed the watershed to public use, including all recreational and grazing activities. The D-1 climate station (Figure 2.1a), located in the alpine tundra ecological zone, has been collecting nearly continuous data since 1952 (Dethier et al., 2003). The site is a National Experimental Ecological Reserves; a United Nations Educational, Scientific, and Cultural Organization (UNESCO) Biosphere Reserve; and a National Science Foundation Long Term Ecological Research (LTER) site.

The study area is accessed via the University of Colorado Mountain Research Station (MRS), which is located off Forest Road 298, a dirt road running west from Colorado State Highway 72 (i.e. The Peak-to-Peak Highway) between the towns of Nederland and Ward. During the snow-free months, an unpaved road leads to within 2 km of the Saddle and Martinelli sites. Vehicle access beyond the MRS is restricted in winter and access is gained by hiking about 7 km west up the road from the MRS.

This study area was selected for several reasons. (1) A U.S. Geological Survey geologic map (Gable and Madole, 1976) is available. (2) There exists field hydrology instrumentation, including automated and continuous discharge measurements at two gauging stations along with seven pairs of groundwater observations wells (Mark Williams, personal communication, 2009). (3) Digital archives of long-term data sets on climatology (~ 50 years) and hydrology (~30 years) are available. (4) An annual snow survey conducted at maximum snow accumulation has been conducted since 1996 and continues to present day. This research will capitalize on the existing

data from this site to investigate the groundwater flow processes from mountain recharge to stream discharge.

2.2 Topography and land cover

Niwot Ridge spans 9 km in length from Navajo Peak (4087 m) on the Continental Divide to timberline (~3350 m) at the eastern end of the Ridge (Figure 2.1a). Within less than 2 km of the Divide, the Ridge forms a rocky arête. It then widens into more gentle topography defined by rounded knolls and shallow saddles. Niwot Ridge drops south into Green Lakes Valley, a 7.1 km^2 east-facing catchment (Caine, 1995) containing headwaters of North Boulder Creek.

The Saddle catchment (0.24 km^2) lies along the crest of Niwot Ridge (3438 m) just south of a broad topographic saddle (Figure 2.1b and Figure 2.2). The catchment faces approximately 166° south and has a mean slope of 10° ranging from 0.1° to 30.4° (Hamann, 2002). Relief is approximately 190 m. The upper catchment is mantled with thick grasses, sedges, and low perennial herbs (Benedict, 1970) characteristic of alpine tundra. There is little exposed bedrock. Solifluction lobes create an irregular surface topography. Winter snow accumulation in the upper Saddle catchment is variable with maximum accumulation (< 4 m) occurring in the west and center of the catchment. The north and east portions of the catchment remain relatively snow free for most of the season due to high winds. The south portion of the Saddle catchment is covered with sub-alpine trees.

In contrast to the Saddle catchment, the Martinelli catchment (0.14 km^2) lies on the steep north wall of Green Lakes Valley (3410 m at the catchment low point) (Figure 2.1b and Figure 2.2). The catchment faces approximately 163° southeast with slopes that average 20.5° and range 4.5−39.2° (Hamann, 2002). Relief is approximately 155 m (Caine, 2001). Less than half the catchment is vegetated and no bedrock is exposed at the surface. A long-lasting seasonal

snowfield occupies 45% of the catchment area and reaches maximum depths of up to 20 m in the center of the catchment (Caine, 1989a, b). The snowfield does not support vegetation growth (Caine, 1989a). The east side of the catchment contains alpine vegetation and sub-alpine trees.

Figure 2.2. Photograph of the Niwot Ridge study area looking west on 12 August 2011. The Saddle site lies in a broad topographic saddle at the crest of Niwot Ridge. The Martinelli site lies on the south wall of Niwot Ridge and contains a permanent snowfield. Green Lakes Valley lies between Niwot Ridge and Kiowa Peak, shown in the background.

2.3 Geology

The bedrock and surficial geology of the region was most recently mapped by Gable and Madole (1976) and Gable (2000). Additional geologic advances include an assessment of the mineral resources of the Indian Peaks (Pearson, 1980), a description of the physical and geological nature of the Indian Peaks (White, 1982), analysis of diamicton deposits on Niwot Ridge (Madole, 1982), and geophysical surveys of the shallow subsurface of Niwot Ridge (Leopold et al., 2008 and Leopold et al., 2010). The primary units of Niwot Ridge include Proterozoic metamorphic and igneous bedrock, which were intruded by a large Tertiary pluton, and Quaternary deposits (Figure 2.3). The Mesozoic and Paleozoic Eras are absent from geologic record in this region of the Front Range.

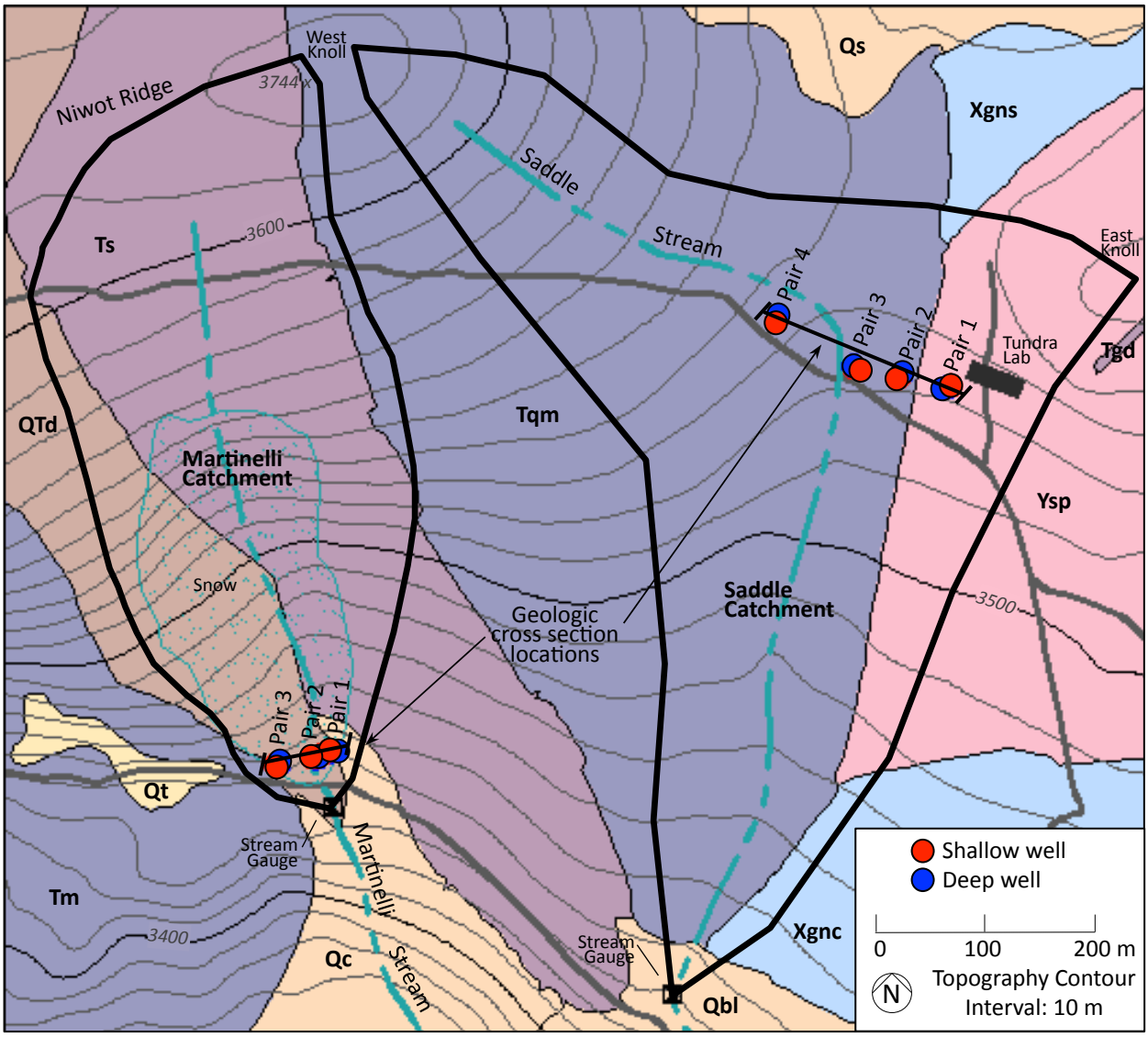

Quaternary Deposits
- Qt Talus deposit
- Qc Colluvium
- Qs Solufluction deposit
- Qbl Till of Bull Lake age

Quaternary–Tertiary Deposits
- QTd Diamicton

Tertiary Intrusive Rocks
- Tgd Granodiorite and biotite-quartz porphyry
- Ts Syenite
- Tqm Quartz monzonite
- Tm Monzonite

Precambrian Bedrock
- Ysp Silver Plume quartz monzonite
- Xgnc Cordierite-bearing garnet-sillimanite-biotite gneiss
- Xgns Cordierite- and magnetite-bearing sillimanite-biotite gneiss

Figure 2.3. Topographic and geologic map of the Saddle and Martinelli catchments with locations of geologic cross sections, which are illustrated in Figure 2.4. Geologic features are from Gable and Madole (1976). Contour lines and map features are from Ward, CO (1957) 7.5' USGS Quadrangle (U.S. Geological Survey, 1957).

2.3.1 Bedrock geology

The core of the Front Range Mountains consists of crystalline Precambrian rocks. The earliest Precambrian rocks in the study area are gneisses that intruded about 1.7 Ga (Gable and Madole, 1976). The protoliths of these gneisses were sedimentary rocks that have since been intensively folded and metamorphosed (White, 1982). About 1.4 Ga (Aleinikoff et al., 1993; Tweto, 1987) the Silver Plume quartz monzonite inundated the region as dikes, sills, and batholiths (Gable and Madole, 1976). Near the Saddle site, the Silver Plume intruded as a small stock and as abundant interlayers. It is light to pinkish gray, medium- to coarse-grained with a seriate (i.e. crystals gradually varying in size) porphyritic texture. In general, these older rocks contain few geologic structures, which permits them to withstand erosion and dominate the mountain summits (White, 1982; Tweto, 1987).

Beginning around 70 Ma, the Laramide Orogeny marked about 20 Ma of repeated uplifts of the Rocky Mountains, pulses of volcanism, crustal compression, faulting, and erosion. A variety of early Tertiary stocks intruded the region east of the Continental Divide (Gable and Madole, 1976; White, 1982). Valuable minerals including lead, gold, and silver were mined from these stocks, including the Snowy Range mine in Green Lakes Valley, during the early 1900s. The dominant stock of this period is the Audubon-Albion monzonite (68 ± 1 Ma), a "salt-and-pepper" colored medium-grained igneous rock (Gable and Madole, 1976). The primary Tertiary intrusive rocks found in the Saddle and Martinelli catchments include fractured quartz monzonite and syenite (Gable and Madole, 1976). Immediately west of the Saddle site, these units extend up the West Knoll and down into the valleys north and south of the Ridge. The syenite and monzonite underlying the Martinelli site are partially covered by Quaternary-Tertiary

diamicton deposits that have been transported downslope from Niwot Ridge. Figure 2.3 shows the geology of the Saddle and Martinelli catchments.

Fracture networks have not been mapped in detail at Niwot Ridge, but many studies have noted the presence of extensive bedrock fractures (Wahlstrom, 1940; Lovering and Goddard, 1950; Tweto, 1968; Pearson, 1980; Leopold et al., 2008). In addition, there are groundwater springs in Green lakes Valley, which are commonly associated with fractured rock aquifers. The Precambrian rocks of the area are broken by some Precambrian-age fractures and faults, but most of the structural features in the region date from the Laramide (Lovering and Goddard, 1950; Tweto, 1968). Fractured Silver Plume quartz monzonite bedrock is visible at about 1.5 m below the ground surface at an abandoned prospecting pit on East Knoll. Joints and fractures in the Silver Plume generally intersect at 90 degrees forming large rectangular blocks (Lester, 1992). Fracture and joint planes in the Albion-Audubon stock intersect at a variety of angles and are more numerous than those in the Precambrian rock (Lester, 1992). Wahlstrom (1940) observed cubical jointing of 0.6−0.9 m in width in the Tertiary monzonites. Faults in the study area are numerous, however most are less than 100 m long and show displacements of less than a meter or two (Tweto, 1968; Wahlstrom, 1933). No major faults or folds are known in the Saddle or Martinelli catchments (Gable, 2000).

Little tectonic activity for the last 40 Ma lead to erosion of the southern Rocky Mountains and resulted in relatively low-relief topography with broad upland surfaces (e.g. Niwot Ridge) (Anderson et al., 2006). About 5 Ma, in response to broad regional uplift, streams began to incise deep eastward trending bedrock canyons.

2.3.2 Quaternary geology

During the last 2 Ma (Pleistocene), the Front Range underwent numerous glacial-interglacial cycles, although neither of the Pleistocene advances covered the upper flanks Niwot Ridge (Benedict, 1970), including the Saddle and Martinelli study sites (Gable and Madole, 1976; R. Madole, personal communication, 2001). The topography of the study region reflects this glaciation history. Both Pleistocene glaciations produced deep U-shaped glacial valleys, such as Green Lakes Valley, with cirque basins, moraines, rock glaciers, and talus cones.

Niwot Ridge, as mentioned, was not glaciated during the Quaternary, but does have Quaternary-age deposits. Madole (1982) wrote an extensive account of diamicton (a nongenetic term for a poorly sorted sediment) deposits found on Niwot Ridge west of the Saddle site and covering a large portion of the Martinelli catchment (Figure 2.3). No definitive origin was determined, but the deposit is decidedly not glacial. It is more likely a mixture of alluvium and colluvium that accumulated on high Tertiary surfaces that predate adjacent Pleistocene valleys (Madole, 1982). The deposit is 3−30 m thick (Madole, 1982). Clasts within the coarse sand matrix are Precambrian in origin, subanglar to subrounded, and up to 3 m long (Gable and Madole, 1976). Diamicton deposits lie nonconformably on the Audubon-Albion stock and therefore must have been transported downslope into their current position (Madole, 1982).

Active solifluction deposits (Holocene and upper Pleistocene) composed of cobbles and pebbles in a fine-grained matrix are found in hummucks, turf-banked lobes, and terraces on the slopes north, northeast, and southeast of the Saddle site, many displaying sorted and patterned ground features (Gable and Madole, 1976; Benedict, 1970). The deposits are derived from weathering of near-surface bedrock and have been transported only short distances (Gable and Madole, 1976; Benedict, 1970). The Holocene colluvium downslope from the Martinelli

snowfield is mostly pebbles, cobbles, and some boulders and is typically only 1−3 m thick (Gable and Madole, 1976).

2.3.3 Geology of the shallow subsurface

The focus of this study is the shallow subsurface of the Saddle and Martinelli sites. The geology of shallow subsurface has not been well characterized. Geologic descriptions of the upper 15 m at the Saddle and Martinelli sites are limited to a surface geophysical survey conducted by Leopold et al. (2008) and imprecise drilling logs from the installation of seven pairs of groundwater piezometers (1.5−8.8 m depth). Aside from in the abandoned prospecting pit on East Knoll, bedrock is not exposed at either site. This section synthesizes results of Gable and Madole (1976), Leopold et al. (2008), and drilling logs. Figure 2.4 shows geologic cross sections of the shallow subsurface of the Saddle and Martinelli sites.

Due to the limitations of the geophysical methods, Leopold et al. (2008) did not classify the geologic units by lithology. Boreholes for the groundwater piezometers were drilled with a rotary/pneumatic hammer drill mounted on a skid steer, which is low-cost and easy to transport into remote or difficult-to-access sites such as Niwot Ridge (K. Chowanski, personal communication, 27 June 2011). However, the technique breaks up subsurface material and blows it out of the borehole so that precise lithological description is difficult. Description of geologic structure was made by observing the response of the drill rig since drilling is slower through rock that is more competent. Observations of the material blown out of the borehole were limited to degree of wetness, organic content, color, rough estimation of sand content, and depth to bedrock (Leopold et al., 2008).

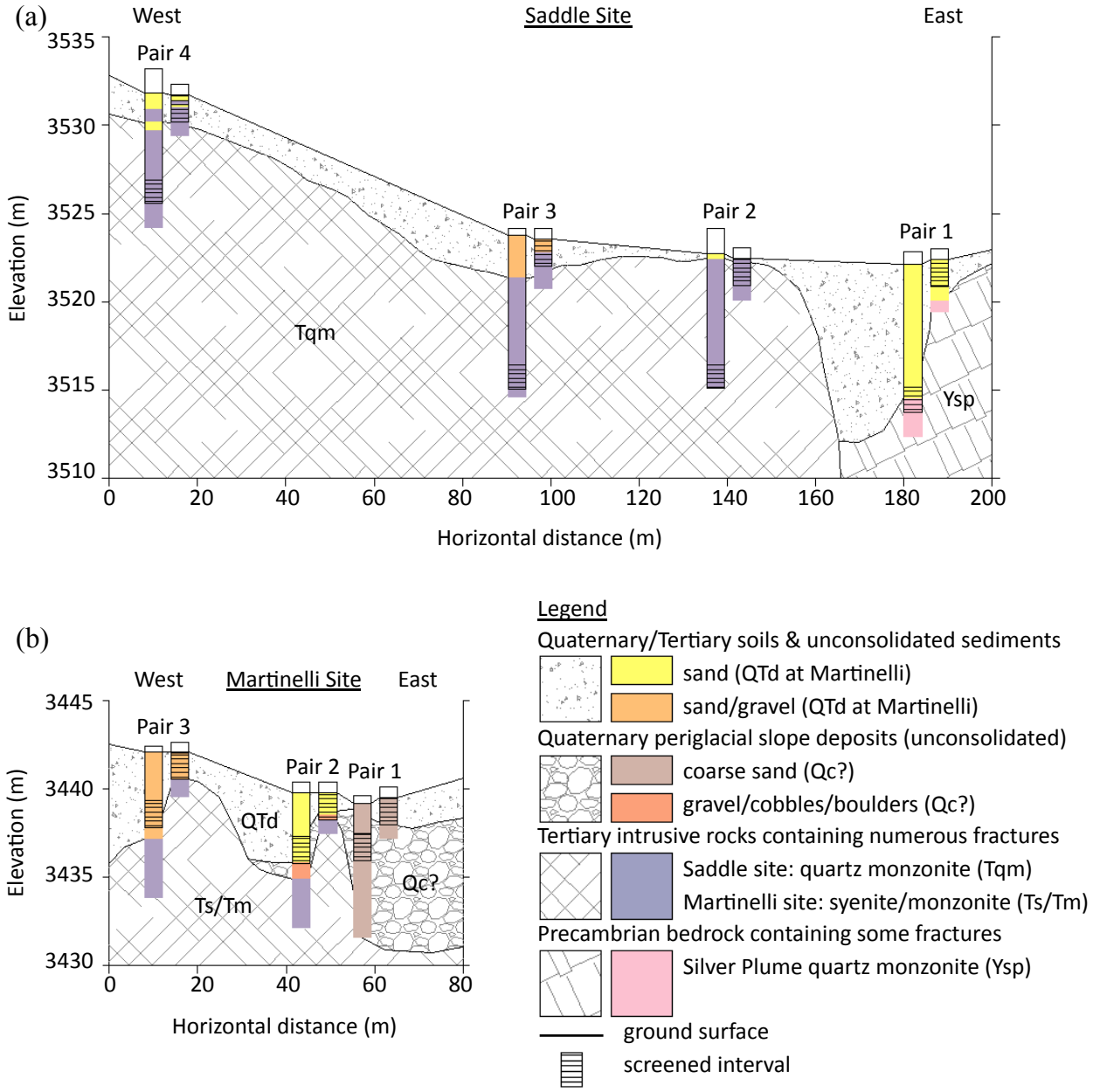

Figure 2.4. Geologic cross sections of (a) Saddle and (b) Martinelli study sites. Observations from driller's logs are shown in color (K. Chowanski, personal communication, 2010). Geologic interpretations are shown in black and white and are based on the author's interpretation of driller's logs, geologic map by Gable and Madole (1976), and geophysical study by Leopold et al. (2008). Vertical exaggeration is four times. The locations of the cross sections are shown in Figure 2.3.

Using shallow seismic refraction and ground penetrating radar at locations less than 500 m from the Saddle site, Leopold et al. (2008) indicated that stratigraphic layering, material composition, and depth to bedrock are highly variable on Niwot Ridge. In general, the shallow

subsurface near the Saddle site is composed of a thin layer of soil and unconsolidated material (< 7 m thick) overlying somewhat consolidated very poorly-sorted deposits of periglacial origin with depth to fractured bedrock ranging from 4 m to >10 m over horizontal distances of only tens of meters. Periglacial deposits between the surficial layer and fractured bedrock are 1−10 m thick and are composed of rock fragments, boulders, and fines. Several localized zones of either water saturated weathered bedrock or deposits of higher compaction such as periglacial slope deposits, rocks, and boulders were detected between the crystalline bedrock and the periglacial slope deposits.

Drilling logs from the installation of the Saddle piezometers generally corroborate the results of Leopold et al. (2008), although periglacial deposits were not detected between the surficial layer and bedrock (Figure 2.4). Logs show depth to bedrock ranges from 0.2 to 7.5 m with overlying sediments composed of unconsolidated sand or a mixture of sand and gravel (K. Chowanski, personal communication, 27 June 2011). Bedrock is predominantly Precambrian Silver Plume quartz monzonite and Tertiary quartz monzonite along the east and west sides of the Saddle site, respectively (Gable and Madole, 1976). Soils at the Saddle site are were mapped by Burns (1980) as Cryochrepts, 2 m in depth, and granitic in origin.

Results from the geophysical survey conducted at the Martinelli site show that the surficial layer is approximately 2−3 m thick and is composed of soil and poorly consolidated material (Leopold et al., 2008). The surficial layer is a Quaternary-Tertiary diamicton deposit (Gable and Madole, 1976). Along the lower flanks of the Martinelli catchment, the diamicton lies above unconsolidated deposits composed of layered rock fragments, boulders, and fines. These unconsolidated deposits overlie crystalline bedrock, are probably water saturated (Leopold et al., 2008), and are most likely Holocene colluvium (Gable and Madole, 1976). Across the

western side of the lower catchment, the Holocene colluvium is absent and the diamicton lies in contact with the bedrock. Depth to bedrock across the Martinelli catchment ranges from 6 to 11 m.

Borehole logs from the installation of piezometers along the lower flanks of the Martinelli catchment show similar patterns to the geophysical results except at MD1, which was described in drilling logs as containing water-saturated course sands and rock fragments over its entire depth of 7.5 m. Bedrock is predominantly Tertiary monzonite and syenite (Gable and Madole, 1976). Soil at the Martinelli site is poorly developed and contains little vegetation (Caine, 1989a).

Permafrost distribution in the study site has been described by Ives and Fahey (1971), Ives (1974), Greenstein et al. (1983), and Janke (2005). These studies place the lower elevation of discontinuous permafrost (2−5 m active layer thickness) between 3200 and 3500 m. The lower elevation of continuous permafrost (2 m active layer thickness) was reported to exist within the range of about 3600 to 3750 m. The large range in values is primarily due to differences in slope aspect, snow cover, and ground moisture, which strongly affect the development and maintenance of permafrost. In recent geophysical surveys of the shallow subsurface of Niwot Ridge, Leopold et al. (2008, 2010) found no evidence of permafrost suggesting a possible recent degradation of permafrost in the Front Range.

Although there has been no recent evidence of permafrost, Leopold et al. (2008, 2010) found evidence of seasonal ice lenses at roughly 2 m depth beneath active solifluction lobes on Niwot Ridge. Drilling at the Saddle site did not find any ice, but hollow zones were found which might be the uncollapsed voids left after ice lenses melted (Leopold et al., 2008). Due to high variation in the spatial distribution of snow, which when deep enough provides insulation to

underlying soil, ice lenses are probably uneven in distribution with nonuniform freezing and thawing. There has been no evidence of either ice lenses or permafrost at the Martinelli site because of its southern exposure, lower elevation, and deep winter snow cover.

2.4 Climate

Nearly continuous daily temperature and precipitation data are available from the D-1 climate station (Figure 2.1a) since 1952. The Saddle climate station (Figure 2.1b) has a variety of climate data from 1982 to the present. No climate data are available specifically for the Martinelli site. Snow depth and snow water equivalent data for upper Green Lakes Valley and the Saddle site are available from the early 1980s. Two National Resources Conservation Service (NRCS) snowpack telemetry (SNOTEL) sites (University Camp and Niwot C-1) have snowpack data from the late 1970s to present. However, these sites are of limited use since they are 500 m lower in elevation and nearly 5 km southeast of the Niwot Ridge study area.

The site has a continental high mountain climate (Caine and Thurman, 1990) characterized by steep gradients in temperature and precipitation with elevation, low temperatures throughout the year, extensive snow, strong winds, high solar radiation, and high interannual variability of hydrologic processes. Table 2.1 summarizes the climate of the area.

	Value	Climate station	Period of record	Source
Average annual temperature (°C)	-2.1	Saddle	1982−2010	Leopold et al., 2010
Average annual precipitation (m)	1.960	Saddle	1982−2010	NWT Meteorology/Climatology, 2011
Total precipitation that is snow (%)	80	D-1	na	Caine, 1995
Average annual evapotranspiration (m)	0.257	D-1	1951−1985	Greenland, 1989
Average annual wind speed (m/s)	8	D-1	1953−1964	Benedict, 1970

Table 2.1. Table summarizing the climate of the study area. The locations of the Saddle and D-1 climate stations are shown in Figure 2.1 (NWT Meteorology/Climatology, 2011).

Because of the high-altitude mid-continental location of Niwot Ridge, air temperatures are highly variable temporally. Figure 2.5a shows average daily minimum, maximum, and mean temperatures each month at the Saddle climate station for 2010. Only 5 months out of the year

are above freezing (May−September). Figure 2.5b shows average daily minimum, maximum, and mean temperatures each year at the Saddle climate station for the period of record (1982−2010). The mean annual air temperature at the Saddle climate station (3528 m) is -2.1°C (Leopold et al., 2010). Daily temperatures fluctuate about 7.5°C between day and night.

Precipitation at the site varies greatly in both time and space. Annual precipitation totals at the Saddle site range from year to year, but average 1.960 m (NWT Meteorology/Climatology, 2011). About 80% of precipitation falls as snow (Caine, 1995). Figure 2.5a shows total monthly precipitation for each month at the Saddle climate station for 2010. Figure 2.5b shows total annual precipitation at the Saddle climate station for the entire period of record (1982−2010). Most precipitation arrives in snowstorms from the west during winter and spring. Snow accumulates October to June and ablates June to September. Summer precipitation is minimal and arrives as rain produced by localized convective storms. Fall is the driest time of year.

In general, precipitation increases with elevation, but varies greatly between locations of equal elevation. Peak snow depths at the Saddle site range from zero to greater than 2 m near the wells with depths generally increasing with distance west. Snow depths measured at a row of four snow stakes located 40−60 m north of the piezometers at the Saddle site vary by a meter from year to year and from stake to stake (Figure 2.6). The Martinelli catchment accumulates a deep seasonal snowpack from wind drifting, which is often over 10 m thick in May at the end of the snow accumulation season (Caine, 1989a). The snow patch covers about 45% of the catchment (Caine, 1992) and lasts through late summer in most years.

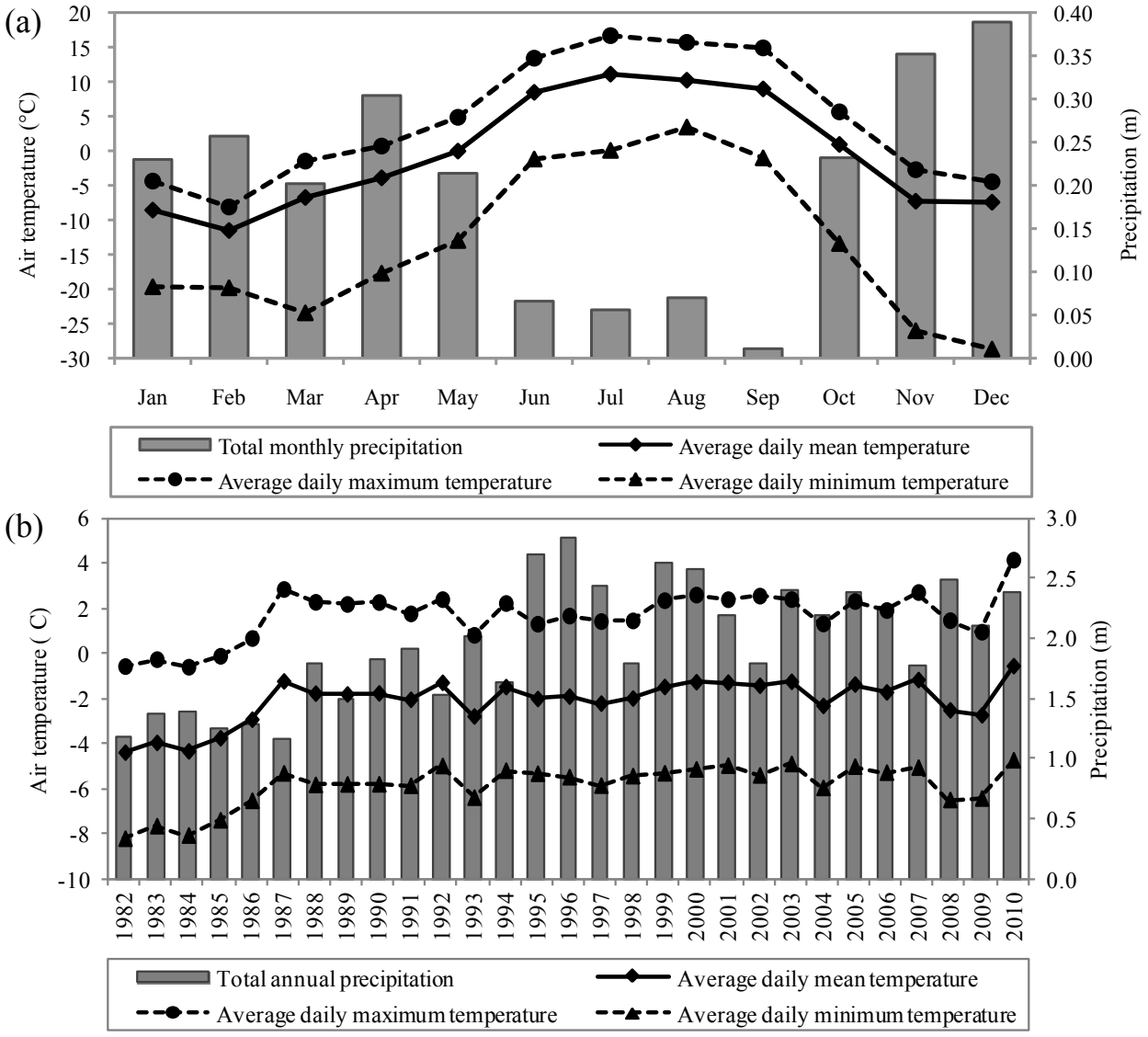

Figure 2.5. (a) Average monthly temperature (min., max., mean) and total monthly precipitation at the Saddle site in 2010. (b) Average annual temperature (min., max., mean) and total annual precipitation at the Saddle site for 1982−2010. Values were calculated from daily data collected at the Saddle climate station (3525 m) (NWT Meteorology/Climatology, 2011).

Prevailing winds are northwesterly, average 8 m/s, and gust at over 50 m/s (Benedict, 1970). Winds are strongest in winter but blow all year, leading to patchy snow accumulation on Niwot Ridge. Areas in the lee of topographic highs and depressions in the topography accumulate snow while areas facing west or exposed to more wind are scoured of snow. Green Lakes Valley, in the lee of the prevailing winds, accumulates a deep snowpack annually and

contains several permanent snowfields such as the Martinelli snow patch. Zones blown free of snow often lie immediately adjacent to deep snow accumulation areas and, therefore, there is a wide range in the magnitude and timing of snowmelt runoff (Benedict, 1970).

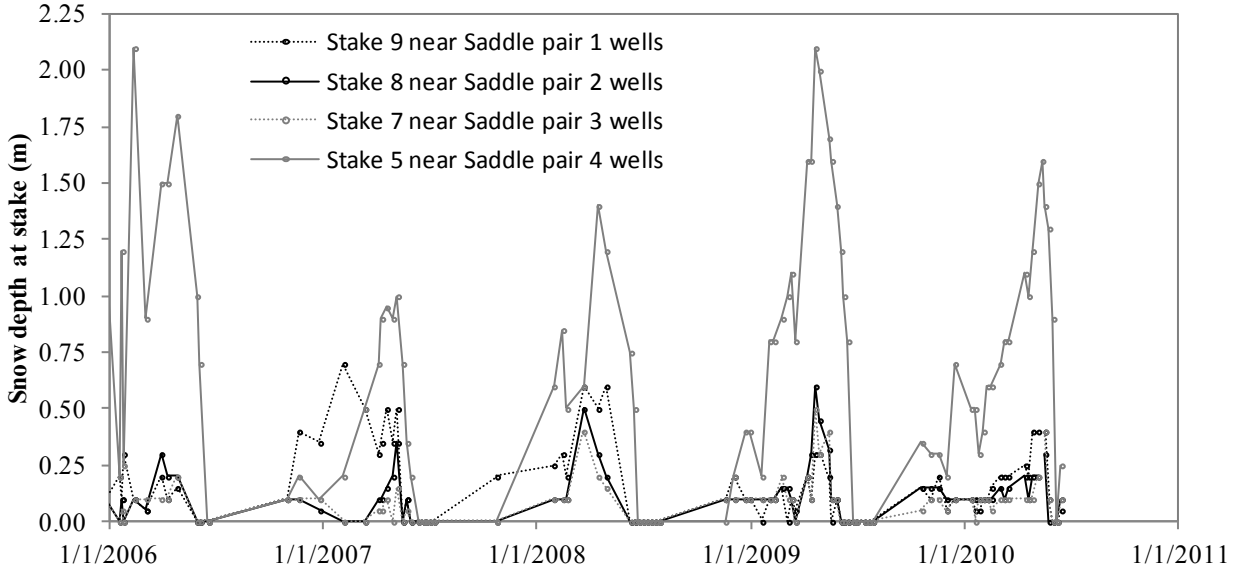

Figure 2.6. Snow depths measured at a row of snow stakes located roughly 40−60 m north of the piezometers at the Saddle site (2006−2010) (NWT Meteorology/Climatology, 2011).

At the D-1 climate station, about a third of precipitation is lost to evapotranspiration annually primarily during the growing season and snowmelt season (Berg, 1986; Greenland, 1989). At the Saddle site, about 15% of snow is lost to sublimation at maximum accumulation (Hood et al., 1999). The remainder of precipitation, approximately 52%, either runs off to streams or recharges groundwater. The low ratio of sublimation and evapotranspiration to precipitation indicates that the majority of water input from the atmosphere is not returned to the atmosphere but instead remains at or near the earth's surface.

2.5 Hydrology

2.5.1 Surface hydrology

Because there are no developed areas near the study area and because the site is located far up gradient from human impact, the site is a natural hydrologic setting. Water enters the

study site as precipitation primarily during the winter months. Water exits the study site through sublimation, evapotranspiration, or snowmelt discharge to streams and groundwater.

Niwot Ridge forms a surface water divide between South Saint Vrain Creek to the north and North Boulder Creek to the south. Both creeks are tributary to Saint Vrain Creek, which flows to South Platte River. North Boulder Creek flows from the base of the Arikaree Glacier eastward through Green Lakes Valley and connects a string of five alpine lakes: Green Lakes 2 through 5 and Lake Albion.

There are no perennial surface waters at either the Saddle or the Martinelli sites. Each year in midsummer, a small stream forms at each site and flows through the end of summer. The Saddle stream drains the 0.24 km^2 Saddle catchment, flows south to North Boulder Creek, and runs roughly parallel to and 0.5 km east of the Martinelli stream (Figure 2.1). The length of the Saddle stream channel is about 1.70 km. The average stream gradient is roughly 10%. The Saddle catchment is less steep and accumulates a shallower and more variable snowpack than the Martinelli catchment. The Martinelli stream flows south from the Martinelli basin, drains a 0.14 km^2 catchment, and connects with North Boulder Creek below Lake Albion (Figure 2.1). The length of the channel is about 0.35 km and the average stream gradient is 14% (Caine, 2001). Above the Martinelli piezometers (Figure 2.1b), the channel network is indistinct (Caine, 1992).

Snowmelt peaks in spring to replenish surface water and groundwater, but continues to provide a source of freshwater well into the late summer months. Hydrographs of the Saddle and Martinelli streams reflect this seasonality, peaking during spring melt, gradually declining through late summer, and reaching a low point in fall and winter when water inputs are minimal (Figure 2.7). Snowmelt runoff amount is difficult to predict because snowpack parameters (e.g. snow water equivalent, melt rate, ablation period) vary greatly from year to year (Cline, 1997).

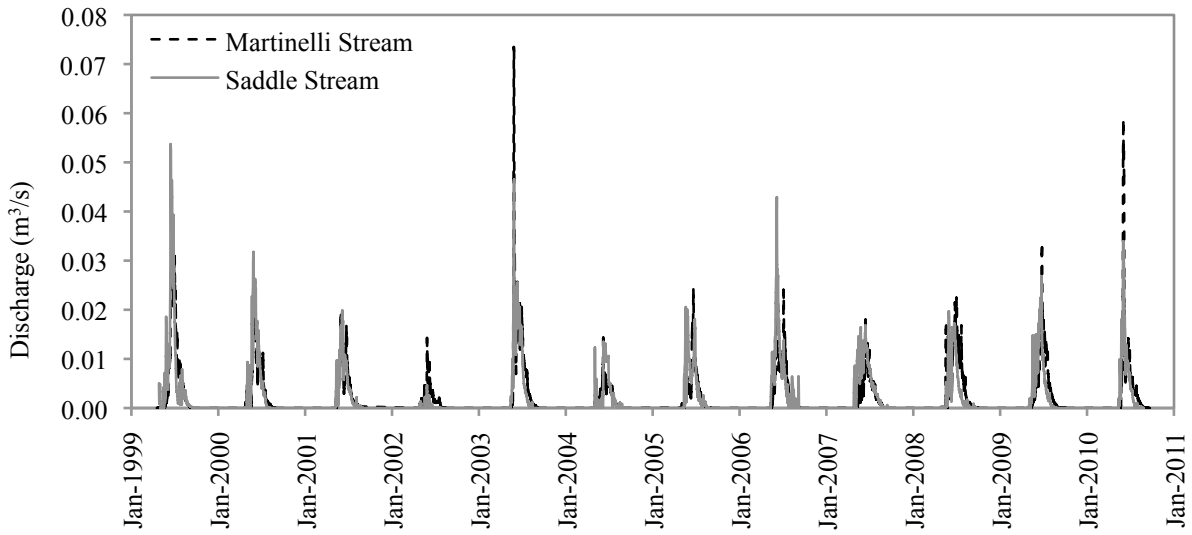

Figure 2.7. Daily stream discharge recorded at the Saddle and Martinelli stream gauges between 1999 and 2010 (NWT Hydrology, 2011).

Daily stream discharge records are available since 1983 for the Martinelli stream and 1999 for the Saddle stream. The locations of the stream gauges are show on Figure 2.1b. Table 2.2 summarizes discharge measurements at the Saddle and Martinelli stream gauges over the period of record. Peak flow occurs during May, June, or July and is due to snowmelt rather than summer rains. Peak discharge ranges greatly, but averages 0.028 m^3/s (standard deviation 0.015 m^3/s) at the Saddle stream and 0.035 m^3/s (standard deviation 0.019 m^3/s) at the Martinelli stream (NWT Hydrology, 2011). Discharge records from the Saddle and Martinelli streams, shown in Figure 2.7, do not indicate any significant differences in streamflow between the catchments. However, flow in the Saddle stream usually starts and ends before the Martinelli stream.

	Saddle Stream	Martinelli Stream
Approximate elevation of stream gauge (m amsl)	3430	3435
Basin area (m^2)	240,000	142,000
Period of record	1999 - 2010	1983 - 2010
Mean annual minimum discharge (m^3/s)	0	0
Mean annual maxiumum discharge (m^3/s)	0.028	0.035
Range of mean annual maxiumum discharge (m^3/s)	0.005 - 0.054	0.013 - 0.077
Mean date of annual maximum discharge	June 3	June 17
Range of date of annual maximum discharge	May 5 - June 26	May 24 - July 17
Mean duration of flow (d)	118	124
Mean annual total discharge (m^3)	56,934	78,142

Table 2.2. Summary of stream discharge recorded at the Saddle and Martinelli stream gauges (NTW Hydrology, 2011).

2.5.2 Subsurface hydrology

In October 2005, seven pairs of groundwater piezometers were installed on Niwot Ridge: four pairs at the Saddle site (Figure 2.8a) and three pairs at the Martinelli site (Figure 2.8b) (Mark Williams, personal communication, 2009). In addition, a groundwater-monitoring program was implemented to measure groundwater level, major cations and anions, dissolved organic matter, and stable isotopes of water (oxygen-18 and deuterium) (Mark Williams, personal communication, 2009). This program continues to the present day. The specifics of piezometer installation and the water level monitoring program are discussed in Chapter 3.

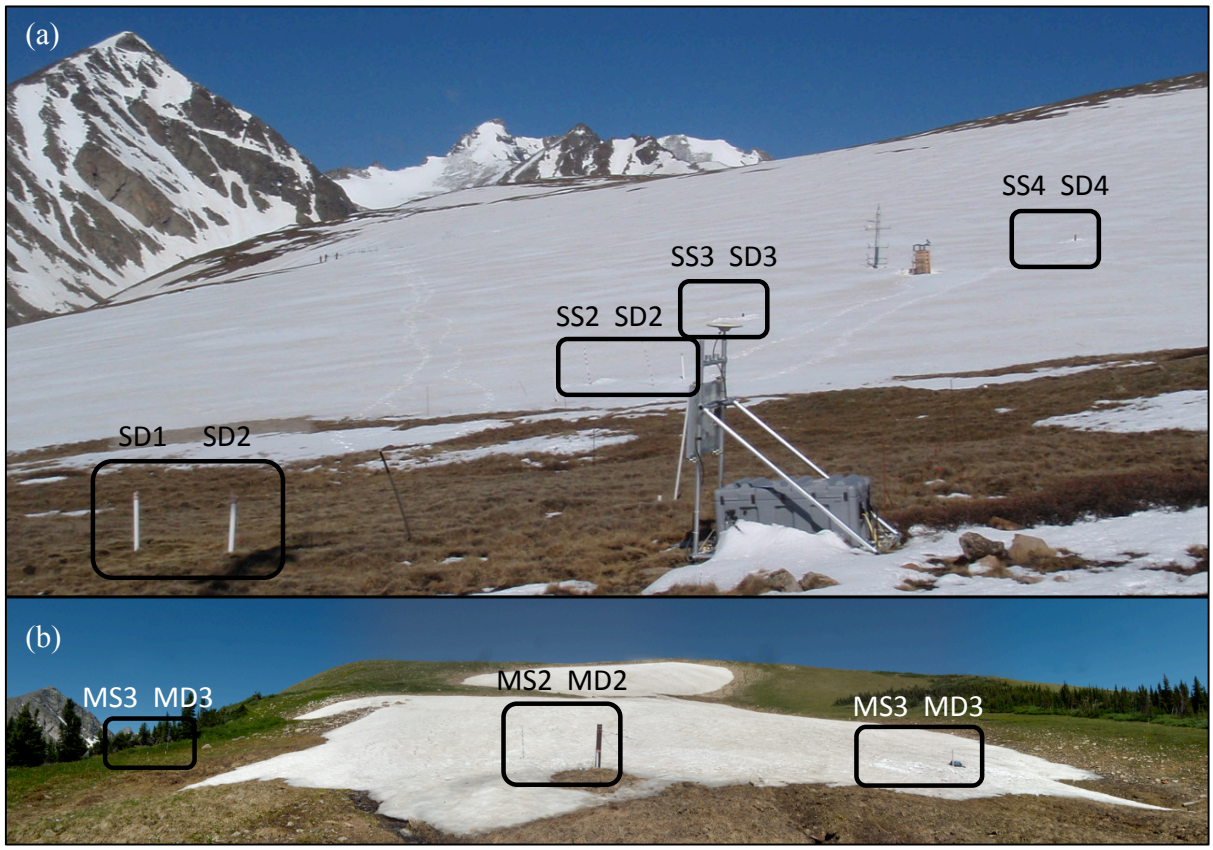

Figure 2.8. (a) Photograph of the "Saddle site," located in the upper Saddle catchment, looking southwest on 22 June 2011. Note the increase in snow cover toward the west and gentle topography. (b) Photograph of the Martinelli catchment taken looking north on 12 August 2011. Note the extensive snow cover and steep slope of the catchment. The pairs of piezometers at each site are indicated. Each pair consists of a deep and shallow well.

Few prior hydrogeologic studies have been conducted at Niwot Ridge, so little is known about the groundwater system. Davinroy (2000) used a constant head permeameter to examine the permeability of blockslope deposits (a thin deposit of angular blocks without a cliff above) in upper Green Lakes Valley and estimated 50% porosity and 1.1×10^{-3}–3.9×10^{-3} m/s hydraulic conductivity. For surficial materials in the Saddle catchment, Hamann (2002) conducted infiltration tests to estimate infiltration rate (5.6×10^{-8}–2.9×10^{-6} m/s) and Guelph permeameter tests to estimate hydraulic conductivity (2.3×10^{-4}–2.6×10^{-6} m/s). No prior studies have examined the water level data collected during the groundwater level monitoring program at the Saddle and

Martinelli sites. Furthermore, no studies have been conducted to delineate the extent of aquifers, calculate groundwater flow rates, or estimate groundwater recharge.

Prior studies have generally focused on geochemical and isotopic analysis of surface waters to determine source waters and flowpaths. Hamann (2002) examined snowmelt and stream chemistry in the Saddle and Martinelli catchments and found that there is diurnal and seasonal variability in the relative contribution of subsurface water to streams. Liu et al. (2004) used geochemical and isotopic tracers to show that subsurface flow, even during peak spring streamflow, contributes 28% of streamflow from a catchment in upper Green Lakes Valley and about 54% of streamflow from the Martinelli catchment. Hill (2005) used $\delta^{18}O$ concentrations from shallow groundwater wells and soil lysimeters at the Saddle site and found that upwelling groundwater and not snowmelt is most likely the dominant source of streamflow and soil moisture during the period of snowmelt runoff. Cowie (2010) presented the first analysis of groundwater sampled from the Saddle wells. He used geochemical analysis of the groundwater and streamflow to show that groundwater residence times are relatively short (1.12 years), flowpaths are shallow, and groundwater plays an important role in streamflow generation in alpine catchments. These studies show the importance of groundwater contribution to mountain streamflow where snowmelt runoff was traditionally assumed the primary source.

2.6 Conceptual model of hydrogeology

A conceptual model of hydrogeology takes all the factors affecting recharge into consideration to provide a concise and qualitative physical description of the system. The conceptual model of Niwot Ridge uses the existing data to identify dominant recharge mechanisms and estimate groundwater flow patterns. The conceptual model is illustrated in Figure 1.1. Many aspects of the hydrogeology of the Niwot Ridge study site are not well

understood. Additional data are required to estimate recharge, including groundwater levels, hydraulic conductivity, and specific yield. These data were collected for this project and are presented in Chapters 3−4.

Precipitation, mostly in the form of snow, is the only input of water to the Niwot Ridge study area. The potential for snowmelt to recharge groundwater is influenced by topography, land cover, climate, and geology. The relatively flat headwater area of the Saddle catchment increases the potential for recharge because of decreased runoff and greater infiltration. However, the ridge-top setting exposes the site to strong winds that blow away most snow accumulation, thereby limiting water available for groundwater recharge.

In contrast to the Saddle site, the Martinelli catchment is steep with little vegetative cover. The lack of vegetation limits infiltration as well as evapotranspiration, which decrease the potential for recharge. The Martinelli catchment is located in a depression, allowing prevailing wind to deposit a deep snowpack, which increases the potential for groundwater recharge. However, during the spring snowmelt season, the steep terrain increases the potential for runoff, which leaves less water available for recharge.

The primary aquifers at Niwot Ridge include unconsolidated surficial deposits and underlying fractured granitic bedrock. The thin veneer of unconsolidated surficial material at the Saddle site limits infiltration. However, large fractures in the underlying bedrock may provide conduits for recharge. Thick, highly conductive surficial sediments at the Martinelli catchment most likely increase the potential for recharge. The shape of the water table at both study sites is similar to the topography, with recharge occurring along ridgetops and discharge occurring at streams.

Chapter 3
Field characterization of the shallow hydrogeology

3.1 Groundwater level monitoring

3.1.1 Background on groundwater level monitoring

Water levels measurements in observation wells or piezometers are the primary source of information on the occurrence, movement, and storage of groundwater. Water levels are needed to characterize groundwater level change in space and time, to estimate groundwater recharge, and to construct numerical models.

Observation wells and piezometers are nonpumping wells used to observe the elevation of the water table or potentiometric surface. A piezometer differs from an observation well in that a piezometer is usually of small diameter and has a short well screen. It is not typically screened throughout the thickness of the aquifer. A piezometer nest consists of two or more piezometers laterally close to each other but screened over different depth intervals. The terms piezometer and well are used interchangeably in this thesis.

The water level in a piezometer indicates the hydraulic head in the aquifer. Hydraulic head is a measurement of potential energy per unit weight of groundwater above a specified datum and is usually expressed in units of length. The measurement point of hydraulic head is the location where water enters the piezometer. A measured groundwater level represents the depth-averaged hydraulic head over the screened interval.

Hydraulic head is defined as the sum of elevation head, pressure head, and velocity head (Freeze and Cherry, 1979; Fetter, 2001). Velocity head is assumed to equal zero because groundwater flow is relatively slow. Elevation head is the potential energy per unit weight due to the elevation of the groundwater at the measurement point. Pressure head is the potential

energy per unit weight due to the column of water in the piezometer above the measurement point. The equation that defines hydraulic head in groundwater hydrology is:

$$h = z + \frac{p}{\rho g} = z + h_p \qquad [3.1]$$

where h is hydraulic head [L], z is elevation head [L], p is fluid pressure [M/LT^2], ρ is density of water [M/L^3], g is gravitational acceleration [L/T^2], and h_p is pressure head [L].

The distribution of hydraulic head in an aquifer determines the rate and direction of groundwater flow. The difference in hydraulic head over a given distance is defined as the hydraulic gradient. Groundwater flows from high to low hydraulic head along the steepest hydraulic gradient.

Confined aquifers have an overlying geologic unit that limits, or confines, the upward or downward flow of groundwater. The confining layer exerts pressure on the aquifer pores. Recharge to a confined aquifer occurs as slow downward leakage through the confining layer or through an area where the confining layer is absent.

Unconfined, or water table, aquifers occur relatively close to the land surface and do not have an overlying confining layer. The upper boundary of an unconfined aquifer is the water table. Recharge to an unconfined aquifer occurs as downward infiltration of water through the unsaturated zone or through surface waters loosing water to the groundwater system. On the water table, pressure head equals zero and total hydraulic head is equal to elevation head. The configuration of the water table is influenced by surface water and topography. Where streams or lakes are present, the water table may intersect the ground surface. The water table is generally a subdued replica of land surface topography (Tóth, 1963; Freeze and Witherspoon, 1967; Gleeson et al., 2011).

Groundwater levels in wells fluctuate depending on the balance between recharge to, discharge from, and storage in the aquifer. Surface topography, porosity and permeability of aquifer material, saturated thickness of the aquifer, precipitation timing and amount, and evapotranspiration affect this balance. If recharge is greater than discharge, like during precipitation events, water levels rise. If discharge is greater than recharge, like during droughts, water levels decline. Water level fluctuations, particularly in mountain environments, are seasonal: rising with snowmelt in spring and gradually declining through the remainder of the year when water input is minimal. It should be noted that groundwater levels in wells represent the groundwater elevation at a specific point in space and time which may be controlled by local conditions and not necessarily represent conditions over a larger area or timescale.

Water levels observed in wells have been used by hydrogeologists for a variety of purposes. Water levels observed in wells can be used to construct a water table or potentiometric surface map, calculate hydraulic gradient, and determine groundwater flow direction (Freeze and Cherry, 1979; Fetter, 2001). Aquifer hydraulic properties can be determined from observing changes in water levels during aquifer tests (Thiem, 1906; Theis, 1935; Hvorslev, 1951; Bouwer and Rice, 1976) and from water level fluctuations induced by earth tides (Cutillo and Bredehoeft, 2010). Water levels are monitored to detect short-term trends in recharge (Healy and Cook, 2002) and long-term effects of climate variability (Allen et al., 2010; Weider and Boutt, 2010). Several studies have used groundwater levels to examine groundwater-surface water interactions (Sophocleous, 1991; Winter, 1984). Groundwater flow and transport models rely on observed water levels for input and calibration (Gburek et al., 1999; Marler and Ge, 2003; Zhang et al., 1998).

The elevation of groundwater in a well is most commonly measured by one of three methods. Prior to the wide availability of portable electrical water level indicators, most water level measurements were made with a wetted steel tape. The depth to water is subtracted from the elevation of the reference point to obtain the water level elevation. Electrical water level indicators consist an electrical probe at the end of a measuring tape. The probe is lowered into the well until it intersects the water level, completing an electrical circuit that activates a buzzer or light. The most modern method to measure groundwater levels is with a pressure transducer. A pressure transducer is a pressure sensor encased in a probe that measures the pressure exerted by the column of water above the probe. The advantage of a pressure transducer is that the probe can be deployed in a well to collect continuous data. In addition, pressure transducers can collect measurements on a fine timescale, which is useful when the water level changes rapidly like during aquifer tests.

3.1.2 Well installation

In October 2005, seven pairs of groundwater piezometers were installed on Niwot Ridge: four pairs at the Saddle site and three pairs at the Martinelli site. In addition, a groundwater level monitoring program was implemented and continues to the present day. Well installation and the monitoring program began nearly four years prior to the start of this study. However, to date, there has been no published account of drilling operations or of the methods used during the groundwater level monitoring program. The following sections serve to fill this gap.

The following description of drilling operations and well installation is based on personal communication between the author and Kurt Chowanski between September 2009 and June 2011. Interpretations of observations made during well installation are those of the author.

Four pairs of groundwater wells were installed along an east-west transect at the Saddle site (Figure 2.1b). Figure 3.1a–d shows the completed wells. Each pair consists of a *deep* well to a depth between 6.3 and 8.8 m and a *shallow* well to a depth of 1.5 m. Ground surface elevations at the Saddle wells range from about 3522 m at the eastern wells to 3532 m at the western wells. The transect is roughly 170 m from east to west, has an average slope of 0.06, and is perpendicular to the Saddle stream. Well locations were selected based on proximity to the headwater region of the Saddle stream channel. Saddle pair 3 was installed very close to the channel. Saddle pairs 2 and 4 were installed on opposite sides of the channel. Saddle pair 1 was installed furthest from the channel near a soil moisture probe located 2 m below the surface.

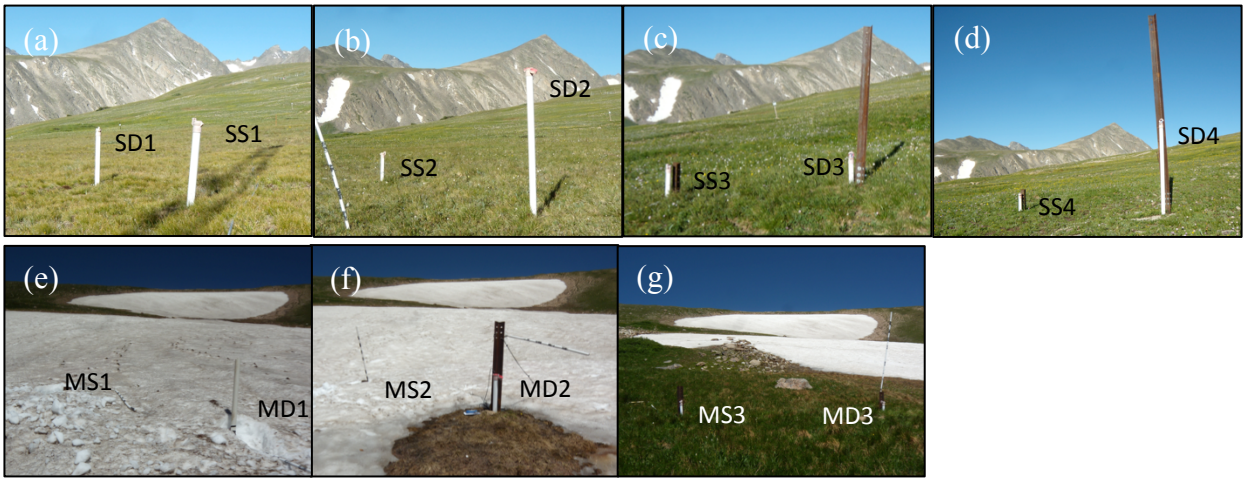

Figure 3.1. Photograph showing Saddle wells (a) pair 1, (b) pair 2, (c) pair 3, (d) pair 4, and Martinelli wells (e) pair 1, (f) pair 2, (g) pair 3. Photographs at Saddle site were taken looking west with Kiowa Peak in the background. Photographs at Martinelli site were taken looking north with the Martinelli snowfield in the background. Photographs were taken August 2011.

Three pairs of piezometers were installed along an east-west transect near the bottom of the Martinelli snowfield (Figure 2.1b). Figure 3.1e–g shows photographs of the completed wells. Each pair consists of a *deep* well to a depth between 3.3 and 4.3 m and a *shallow* well to a depth of 1.5 m. Ground surface elevations at the Martinelli wells range from approximately 3439 m at the eastern wells to 3442 m at the western wells. The transect is roughly 51 m from

east to west, has an average slope of 0.06, and is perpendicular to the Martinelli stream channel. Piezometer locations were determined based on proximity to the base of the Martinelli stream channel. Martinelli pair 2 was installed very close to the main channel. Martinelli pairs 1 and 3 were installed on opposite sides of the channel.

Piezometers were installed by Bandimere Geothermal Drilling Systems. Piezometer locations, depths, and design were determined by Niwot Ridge LTER lead researchers, Mark Williams and Nel Caine. The piezometers were installed primarily to monitor groundwater chemistry and water levels. The piezometers are maintained by the Niwot Ridge LTER program.

Boreholes at both sites were drilled with a rotary/pneumatic hammer drill mounted on a skid steer (Figure 3.2). The drilling stem was 1.5-inch diameter steel pipe. The drill bit was 3-inch diameter steel. The boreholes were cased with 2-inch nominal pipe size, Schedule 40 polyvinyl chloride (PVC), flush-threaded pipe, which was extended 0.3−1.5 m above ground. Well screens were constructed from 0.020-inch continuous slot PVC and installed in 5-ft (1.52 m) intervals. All of the piezometers have 1.52 m screens at the bottom of the well. The bottoms of the wells were capped with a PVC flush-threaded point cap. Following installation, well locations were mapped using global positional system (GPS). Table 3.1 summarizes the construction specifications of the wells.

Figure 3.2. Photographs showing drilling of a borehole at the Saddle site in October 2005 (courtesy of Kurt Chowanski).

Table 3.1. Construction specifications for the wells at the Saddle and Martinelli sites.

Saddle Piezometers	**SS1**	**SD1**	**SS2**	**SD2**	**SS3**	**SD3**	**SS4**	**SD4**
Latitude	40.05412	40.05411	40.05418	40.05421	40.05426	40.05428	40.05465	40.05468
Longitude	-105.58932	-105.58934	-105.58989	-105.58985	-105.59036	-105.59037	-105.59120	-105.59118
Easting	449735.80	449733.42	449687.23	449690.29	449646.78	449646.03	449575.78	449576.77
Northing	4433930.56	433929.03	4433937.13	4433940.62	4433946.64	4433948.69	4433990.54	4433993.41
Nominal casing/screen outside radius (m)	0.030	0.030	0.030	0.030	0.030	0.030	0.030	0.030
Nominal casing/screen inside radius, r_{nc} (m)	0.026	0.026	0.026	0.026	0.026	0.026	0.026	0.026
Approximate filter pack radius, r_w (m)	0.032	0.032	0.032	0.032	0.032	0.032	0.032	0.032
Casing type	2-in. NPS Sch. 40 PVC	2-in. NPS Sch. 40 PVC	2-in. NPS Sch. 40 PVC	2-in. NPS Sch. 40 PVC	2-in. NPS Sch. 40 PVC	2-in. NPS Sch. 40 PVC	2-in. NPS Sch. 40 PVC	2-in. NPS Sch. 40 PVC
Screen slot size (m)	0.000508	0.000508	0.000508	0.000508	0.000508	0.000508	0.000508	0.000508
Elevation top of well (m)	3523.05	3522.91	3522.97	3524.20	3524.00	3524.19	3532.11	3533.24
Elevation ground surface (m)	3522.39	3522.14	3522.44	3522.72	3523.54	3523.78	3531.74	3531.85
Elevation top of screen (m)	3522.45	3515.29	3522.37	3516.58	3523.40	3516.57	3531.51	3527.14
Elevation bottom of well (m)	3520.92	3513.77	3520.84	3515.06	3521.87	3515.05	3529.98	3525.62
Top of well stick-up (m)	0.66	0.77	0.53	1.48	0.46	0.41	0.37	1.39
Length of well below ground surface (m)	1.47	8.37	1.60	7.66	1.67	8.73	1.76	6.23
Length of screen, L (m)	1.52	1.52	1.52	1.52	1.52	1.52	1.52	1.52
Total length of well (m)	2.13	9.14	2.13	9.14	2.13	9.14	2.13	7.62
Formations penetrated by screened interval	Q (sand) (1.52 m)	Q (sand) (0.61 m) Ysp (0.91 m)	Q (sand) (0.08 m) Tqm (1.44 m)	Tqm (1.52 m)	Q (sand/gravel) (0.73 m) Tqm (0.79 m)	Tqm (1.52 m)	Q (sand) (0.27 m) Tqm (0.24 m) Q (sand) (0.14 m) Tqm (0.88 m)	Tqm (1.52 m)

Table 3.1. (continued)

Martinelli Piezometers	**MS1**	**MD1**	**MS2**	**MD2**	**MS3**	**MD3**
Latitude	40.05105	40.05105	40.05101	40.05099	40.05094	40.05096
Longitude	-105.59602	-105.59599	-105.59617	-105.59613	-105.59657	-105.59652
Easting	449161.42	449164.41	449148.84	449152.05	449114.51	449118.94
Northing	4433593.66	4433593.39	4433588.75	4433587.38	4433582.10	4433583.29
Nominal casing/screen outside radius (m)	0.030	0.030	0.030	0.030	0.030	0.030
Nominal casing/screen inside radius, r_{nc} (m)	0.026	0.026	0.026	0.026	0.026	0.026
Approximate filter pack radius, r_w (m)	0.060	0.060	0.060	0.060	0.060	0.060
Casing type	2-in. NPS Sch. 40 PVC	2-in. NPS Sch. 40 PVC	2-in. NPS Sch. 40 PVC	2-in. NPS Sch. 40 PVC	2-in. NPS Sch. 40 PVC	2-in. NPS Sch. 40 PVC
Screen slot size (m)	0.000508	0.000508	0.000508	0.000508	0.000508	0.000508
Elevation top of well (m)	3440.10	3439.70	3440.32	3440.31	3442.51	3442.36
Elevation ground surface (m)	3439.50	3439.19	3439.79	3439.77	3442.04	3442.06
Elevation top of screen (m)	3439.49	3437.54	3439.71	3437.26	3441.91	3439.31
Elevation bottom of well (m)	3437.97	3436.01	3438.19	3435.74	3440.38	3437.79
Top of well stick-up (m)	0.60	0.51	0.53	0.54	0.47	0.30
Length of well below ground surface (m)	1.53	3.18	1.60	4.03	1.66	4.27
Length of screen, L (m)	1.52	1.52	1.52	1.52	1.52	1.52
Total length of well (m)	2.13	3.69	2.13	4.57	2.13	4.57
Formations penetrated by screened interval	Q (coarse sand) (1.52 m)	Q (coarse sand) (1.52 m)	Q (sand) (1.20 m) Q (gravel) (0.28 m) T (0.04 m)	Q (sand) (1.34 m) Q (gravel) (0.18 m)	Q (sand/gravel) (1.48 m) T (0.04 m)	Q (sand/gravel) (1.52 m)

NPS = nominal pipe size, PVC = polyvinyl chloride, m amsl = meters above mean sea level, Q = Quaternary sediments,
T = Tertiary syenite, monzonite, or quartz monzonite, Tqm = Tertiary quartz monzonite, Ysp = Precambrian Silver Plume quartz monzonite

The annular space around each screen and pipe was backfilled with #10−20 silica sand to act as a filter. The PVC casing was shaken back and forth to further advance the silica into the borehole. Because of the relatively large difference in diameter between the drill stem and drill bit, the boreholes were not drilled perfectly straight. Consequently, the distance between the formation and well casing varied with depth into the borehole and settling of the silica filter was inconsistent. Ideally, a 0.5-inch filter was installed between the formation and the casing along the full length of the casing and screen. In reality, the filter thickness varies from 0 to 1 inches with the vertical distribution of filter thickness unknown. In addition, since the silica was poured, not packed, into the annular space, it is possible that voids exist around the casing and/or screen. The completed wells are not firmly installed in the ground and the above ground casing can be shaken back and forth. Since a bentonite seal was not used in the construction of these piezometers, it is likely that the screened portion is hydraulically connected with the surface through the filter. If this is the case, then the well is effectively open to the formation along its entire length and groundwater level measurements represent the average hydraulic head over the total length of the well and not just the screened interval. The shallow piezometers (1.5-m depth) are screened along the total length of the well, are therefore directly connected with the surface, and water level measurements equal the average hydraulic head over the length of the well.

Lithologic logs were created from direct observations of drill cuttings as the cuttings came out of each hole. The logs were supplemented with outcrop observations and information from prior mapping publications (e.g. Gable and Madole, 1976). The pneumatic drilling technique breaks up subsurface material and blows it out of the borehole and, therefore, precise lithological description is difficult. Well construction data were determined from pre-drilling

design and direct observation of construction of each well during drilling. Table 3.1 provides a summary of lithologic information.

As the boreholes were drilled, water was observed in the drill cuttings from several depths that were below the final static water level elevation measured after well completion. The driller referred to the occurrence of water in drill cuttings as *little aquifers*. One interpretation of this observation is that as drilling progressed downward, the drill bit intersected and exposed water-filled fractures or pockets of high permeability, which allowed the water to drain from the formation. If drilling progressed quicker than water draining from the formation filled the borehole, it was possible to observe multiple depth intervals where water drained into the borehole. Upon well completion, groundwater either filled the well until static water level was reached or drained back into the formation leaving the completed well dry.

Water in drill cuttings was observed in all Saddle and Martinelli boreholes except Saddle pair 1 (SS1 and SD1). SS1 was completely dry during drilling and after well completion. No water was observed during drilling of SD1, however, static water level in SD1 was above the bottom of the well after the well was completed. SD1 penetrates Precambrian bedrock that likely contains fractures through which water flowed very slowly into the well after cessation of drilling. After completion of the other deep wells (SD2, SD3, SD4, MD1, MD2, and MD3), water drained from the formation and filled the boreholes until static water level was reached.

McIntosh et al. (1999) found that in steep terrain with thin soil cover, water tends to perch at the interface between bedrock and overlying unconsolidated sediments. An isolated zone of wet drill cuttings was observed at this interface at the Saddle pair 4 and Martinelli pair 2 and pair 3 piezometers. This observation was most likely evidence of perched groundwater.

In Saddle pair 3 and Martinelli pair 2, artesian conditions were noted at the same depths as observations of wet drill cuttings. Artesian flow rates were not measured directly, but were estimated by the driller from visual inspection of water flowing out of the borehole. Flow rates varied from 0.32 to 0.50 L/s during drilling. After the well casing was installed, artesian conditions ceased. The presence of water in drill cuttings and artesian conditions suggest there was upward vertical flow of groundwater (i.e. groundwater discharge zone) in October 2005.

Each well was developed after completion to improve the viability to provide chemical and hydraulic data representative of the native groundwater. Each well was developed by the surging method using a bailer that was lowered into the well, allowed to fill with water and sediment, pulled out of the well, and emptied at the surface. Time was then permitted for water from the aquifer to flow into the well and return to static level. This process was repeated many times, which caused a surging action to develop the area around the well screen. Even after extensive surging, none of the Saddle or Martinelli wells produced sediment-free water and groundwater in the wells occasionally contains suspended sediment (e.g. following snowmelt in spring).

3.1.3 Measurement of water levels

Between October 2005 and August 2011, groundwater levels were measured with a weighted tape (accuracy 0.05 m) or an electrical water level indicator (ELE International water level indicator, 150 ft depth capacity, accuracy 0.005 m) (Figure 3.3). Measurements were collected weekly during snow-free months and monthly during winter (weather permitting) to examine the temporal and spatial characteristics in groundwater level. Measurements were not collected at the Martinelli wells during the winter due to deep snow covering the wells. Gaps in the time series data were typically due to adverse weather conditions or the lack of an available

field technician to visit the wells. Water level data at well MS1 were not collected in 2011 due to extensive damage to the well casing resulting from the weight of the heavy winter snowpack. Niwot Ridge LTER field technicians took the vast majority of these measurements.

Figure 3.3. ELE International electrical water level indicator. Weekly to monthly water level measurements were made with either an electronic water level indicator or weighted tape.

Depth to water was measured in each well from the reference point at the top of the well casing above ground. The elevation of the water level was calculated as the elevation of the ground surface plus the length of casing above ground minus the measured depth to water. The length of casing above ground, and therefore the height of the water level reference point, measured in October 2005 differed from that measured in September 2009 and in June 2011. Among all wells, casing stickup was on average 3 cm shorter in June 2011 than in October 2005 and ranged from 22 cm shorter in June 2011 to 7 cm taller in June 2011. In alpine environments, the shallow subsurface is subject to extensive freeze-thaw action that is capable of moving objects, such as large stones. It is assumed that freeze-thaw cycles shifted the vertical position of the Saddle and Martinelli wells, thereby changing the height above ground of the reference point on the casing stickup. To account for changes in vertical position of the well, groundwater level elevations were calculated using the most recent measurement of well stickup. Stickups at all

Saddle wells were measured in October 2005, August/September 2009, and June/July 2011. Stickups at all Martinelli wells were measured in October 2005 and July/August 2011.

Two deep wells at the Saddle site were instrumented with In-Situ Inc. Level Troll® 100 non-vented pressure transducers (Figure 3.4) to collect groundwater level data twice daily, measured at noon and midnight, between January 2010 and September 2011. Groundwater temperature data were collected in conjunction with depth data (Appendix IV). The accuracy of the Level Troll® 100 pressure sensor is 0.009 m. These water level data were downloaded 1 to 2 times per year using Win-Situ® v5.6.4.6 software. Water level data collected by pressure transducers were corrected for barometric pressure effects by subtracting the ambient barometric pressure, recorded by the Saddle climate station at noon and midnight. To correct for effects of freezing water on the tip of the probe, pressure transducer data were calibrated to manual measurements. When a manual measurement was taken, the pressure transducer measurement taken at the same time was set equal to the manual measurement. The amount added to or subtracted from the transducer measurement in order to set it equal the manual measurement was noted. This difference was then used to determine the appropriate linear function needed to calibrate transducer measurements taken between manual measurements.

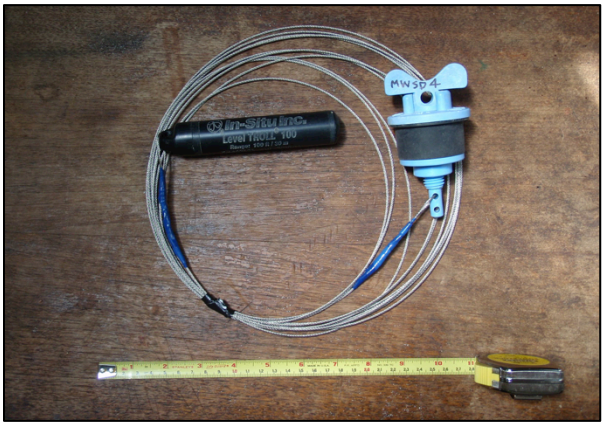

Figure 3.4. In-Situ Inc. Level Troll© 100 non-vented pressure transducer installed in piezometers SD3 and SD4.

The groundwater level data collected were used to analyze spatial and temporal trends, which give information on the magnitude and timing of recharge at each well location. Hydraulic gradients and relationships between water level fluctuations and climatic influences (precipitation, air temperature, snowmelt, and stream discharge) were also examined.

3.1.4 Results: Spatial and temporal trends in water levels

Figure 3.5 shows the elevation of groundwater levels over time and Figure 3.6 shows the trend in depth to water from the ground surface over time. Water level data from the shallow wells are shown only during a brief period in summer when water levels were above the bottom of the well. During the rest of the year, water levels dropped below the bottom of the shallow wells as indicated by the absence of data points. For this reason, trends in water levels in shallow wells will not be discussed as extensively as trends in deep wells. At the Martinelli site, the absence of data prior to summer reflects the cessation of data collection during winter when snow covered the well field and does not necessarily indicate that water levels were below the bottom of the well.

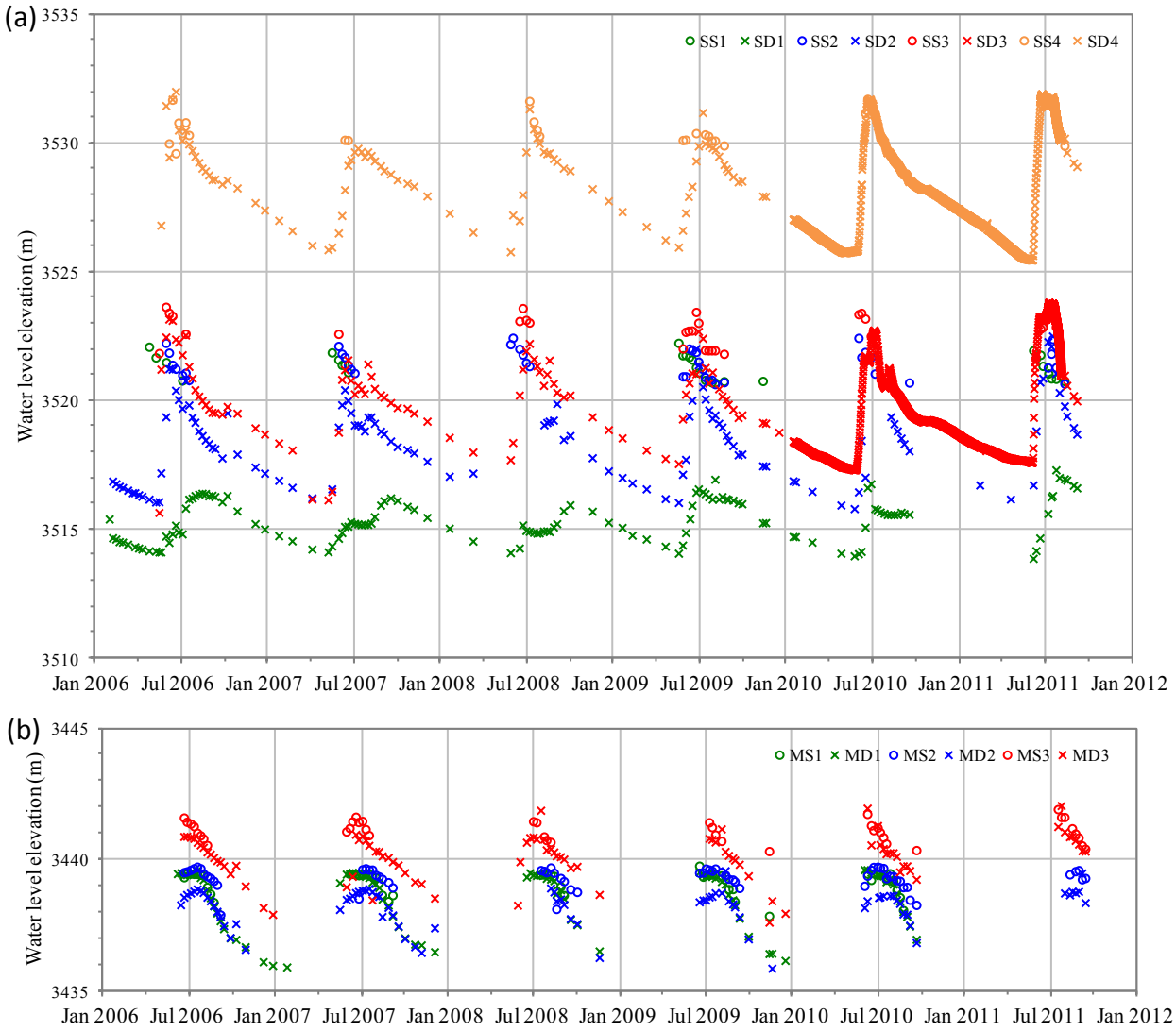

Figure 3.5. Seasonal variations in groundwater level elevations in wells at (a) Saddle site and (b) Martinelli site for the period of measurement (2006−2011).

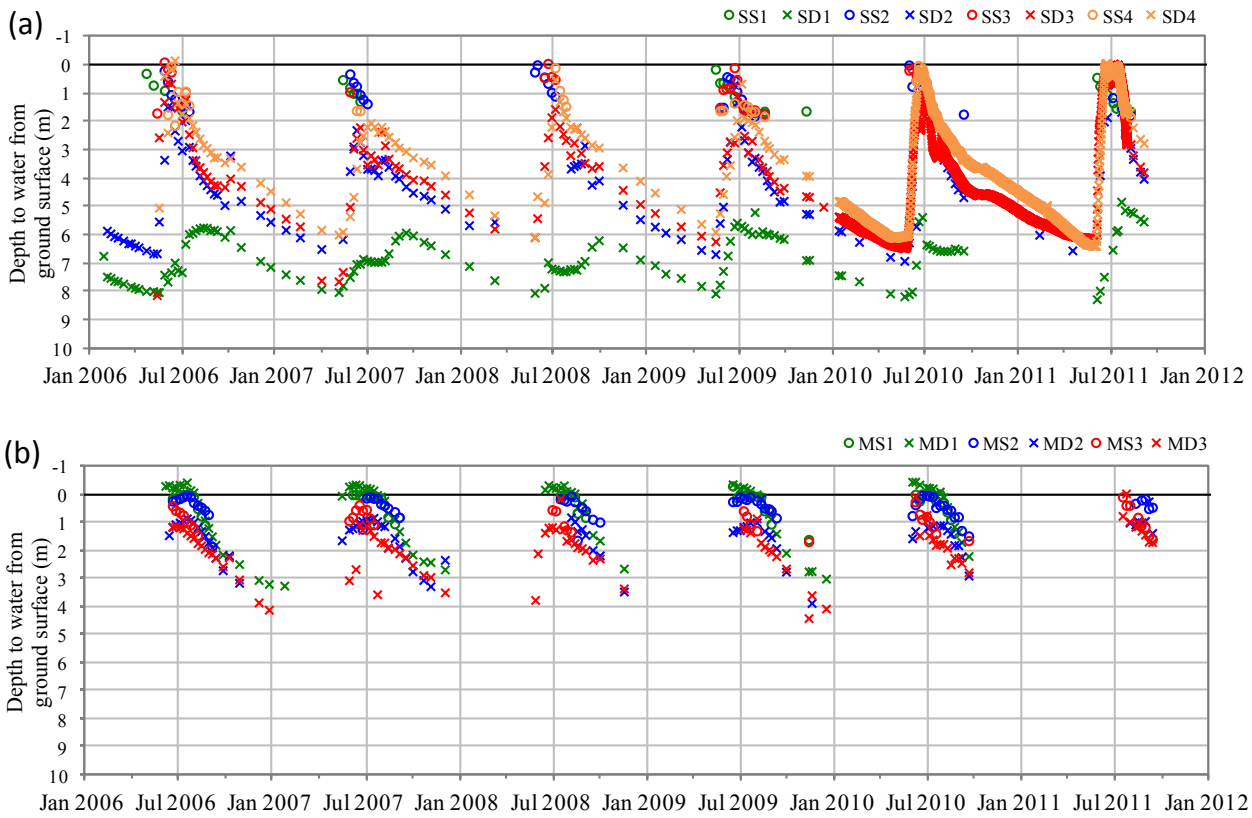

Figure 3.6. Seasonal variations in depth to groundwater in wells at (a) Saddle site and (b) Martinelli site for the period of measurement (2006−2011). Solid black line at 0 m depth represents ground surface.

Table 3.2 lists average values of annual minimum, maximum, and mean water level elevations (and corresponding depth to water). In addition, the average annual water level fluctuation, dates bracketing the fluctuation, and duration of the annual water level rise and subsequent decline are reported. Dates bracketing the seasonal fluctuation denote the period of potential recharge. At the Martinelli site, due to lack of data collection during winter when water levels were lowest, only the average annual minimum depth to water, corresponding water level elevation, and average date on which the minimum depth to water occurred are listed in the table.

	Depth to water (m)			Water level elevation (m amsl)			WLF	Date of	Date of	WL	WL
	min.	max.	mean	min.	max.	mean	(m)	max. DTW	min. DTW	rise (d)	decline (d)
SD1	5.54	8.07	6.80	3514.07	3516.60	3515.34	2.38	May 20	Aug. 16	92	260
SD2	1.17	6.70	3.94	3516.02	3521.55	3518.78	5.83	May 11	June 23	51	334
SD3	1.02	6.79	3.90	3516.99	3522.70	3519.85	5.77	May 23	June 28	37	332
SD4	0.52	5.91	3.22	3525.94	3531.33	3528.63	4.97	May 19	July 02	44	320
Mean	2.06	6.87	4.47	3518.26	3523.04	3520.65	4.74	May 18	July 10	56	311
SD	2.34	0.89	1.59	5.26	6.12	5.66	1.62	9 days	24 days	25	35
MD1	-0.37				3439.56				June 30		
MD2	0.55				3439.22				August 03		
MD3	0.55				3441.51				July 07		
Mean	0.24				3440.10				July 14		
SD	0.53				1.23				18 days		

WLF = annual water level fluctuation, DTW = depth to water from ground surface, WL = water level, SD = standard deviation

Table 3.2. Summary of depth to water (DTW) (minimum, maximum, and mean) in meters below the ground surface and water level elevation in meters for the period 2006−2010. Negative values indicate ponding of water on the ground surface during peak snowmelt. The average annual fluctuation of the water table, in meters, is also reported. Dates bracketing the seasonal fluctuation denote the period of potential recharge to groundwater. Values not reported for the Martinelli site reflect the period in winter when water level data were not collected.

Water levels at both sites fluctuated seasonally. This trend is most obvious in data collected from the deep wells at the Saddle site (Figures 3.5a and 3.6a). At SD2, SD3, and SD4, water levels rose rapidly with the onset of snowmelt in late spring and gradually declined through the drier and colder months when infiltration to the subsurface was minimal. The annual water level hydrograph at SD1 was less pronounced, rising gradually through late spring and summer and declining in fall and winter. The rising limbs of the well hydrographs were not captured in the deep wells at the Martinelli site because data were not collected in winter (Figure 3.5b). However, the falling limb of the hydrographs declined gradually through late summer and fall, like those observed at the Saddle site.

Figure 3.7 shows a map of the water table at the Saddle and Martinelli catchments. Figure 3.8 shows cross sections of the water table at the Saddle and Martinelli catchments. At both sites, water level elevation decreased eastward (Figure 3.7). Mean annual water level elevation at the Saddle site was greatest at SD4 (3528.63 m) and smallest at SD1 (3531.34 m)

(Table 3.2). Mean annual maximum water level elevation at the Martinelli site was greatest at MD3 (3441.51 m) and smallest at MD1 (3439.56 m) (Table 3.2). This trend mimicked the topography of the well transects, which also slope down to the east. Water levels were assumed to reflect the elevation of the water table. The water table at the study sites is a subdued replica of the topography. Because of the similar shape of the topography and water table and because depth to water table is shallow (Figure 3.8), the aquifer at Niwot Ridge is assumed to be unconfined. The deep wells generally had a lower water level than corresponding shallow wells (Figure 3.5). Lower water levels with increased depth in a piezometer pair indicated downward flow and that the location of the piezometer pair was a recharge area (Saines, 1981).

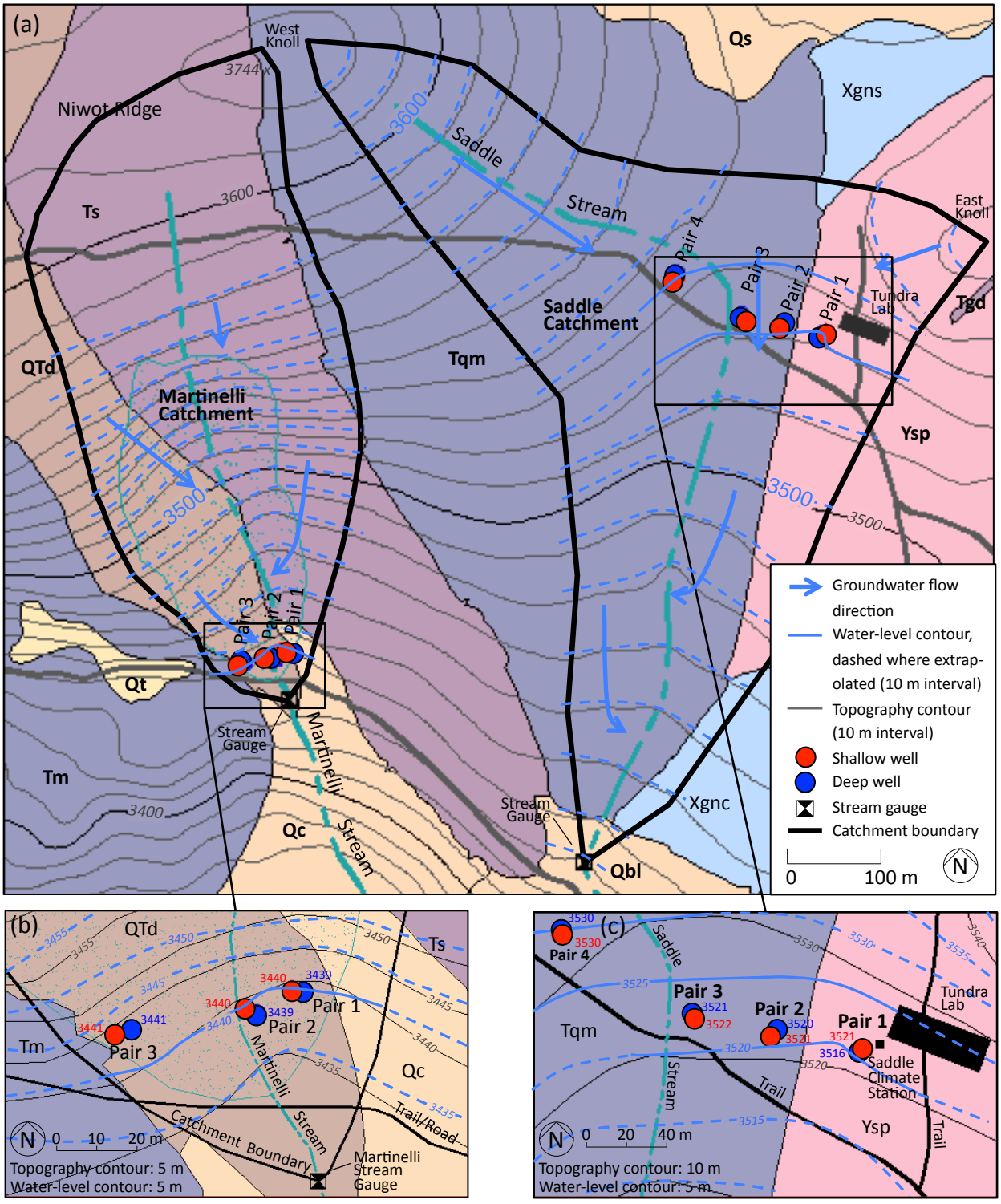

Figure 3.7. (a) Map of average peak water table elevation (m) (measured mid-May 2006−2011) at the Saddle and Martinelli catchments with underlying geology (Gable and Madole, 1976). Insets show water table at the (b) Saddle and (c) Martinelli sites during peak water level in mid-June 2009. Solid lines were drawn in regions where water level data were available. Dashed lines were drawn where the data were extrapolated.

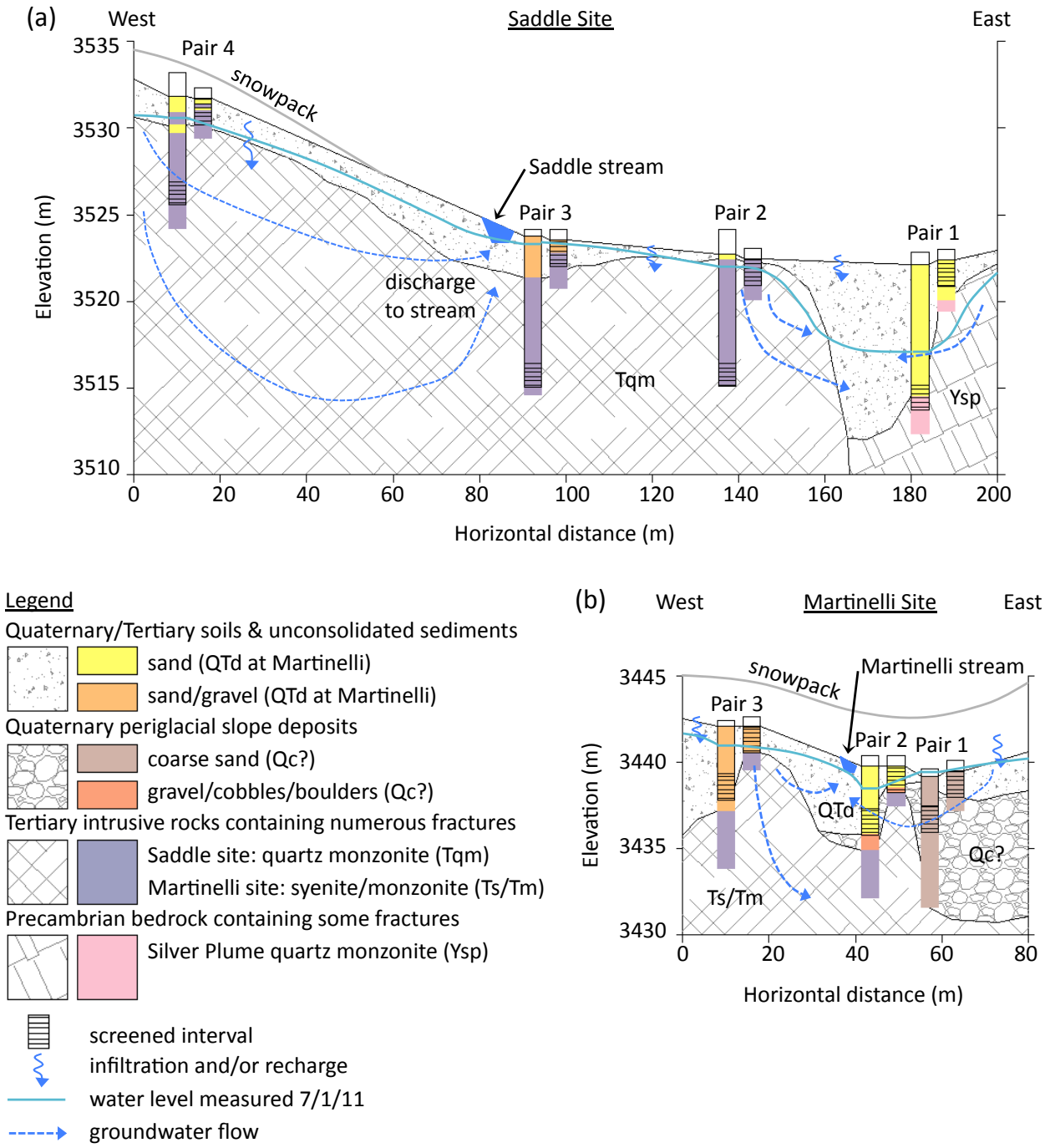

Figure 3.8. Cross section showing water table elevation (measured on 1 July 2011) at the (a) Saddle and (b) Martinelli sites. Vertical exaggeration is four times.

The timing of water level fluctuations varied depending on location. Mean annual peak water level elevation at the Saddle site occurred in mid to late May. Mean annual minimum occurred in late June and early July in wells SD2, SD3, and SD4 and nearly two months later on

August 16 in well SD1. Wells SD2, SD3, and SD4 are located in a recharge zone that accumulates a deep seasonal snowpack, so water infiltrating from the land surface does not travel far to recharge the water table. Well SD1, on the other hand, is located away from the recharge zone in an area that receives little snow.

The period between minimum and maximum water level corresponds to the period of potential groundwater recharge. SD3 had the shortest average duration of water level rise (37 d) and the greatest average fluctuation in water level (5.77 m), which resulted in the fastest rate of water level increase during the seasonal water level rise (0.16 m/d). SD3 is located in a slight topographic depression that gathered windblown snow and runoff. The proximity of SD3 to a recharge source was reflected in the large fluctuations in water level (Figure 3.5a). SD1 had the longest average duration of water level rise (92 d), the smallest average fluctuation in water level (2.38 m), and the slowest rate of water level rise (0.03 m/d). The ground surface at SD1 typically remains snow-free for most of the year, even during winter, so did not contribute much snowmelt to recharge. Therefore, there was less fluctuation in water levels at SD1.

The subsurface geology also affected water level fluctuations at the Saddle site. SD1 is screened across the contact between unconsolidated surficial sediments and Precambrian Silver Plume quartz monzonite. SD2, SD3, and SD4 are screened in Tertiary quartz monzonite. In permeable material, such as the unconsolidated sediments at SD1, the amplitude of the water table response is damped due to the higher storage capacity. In less permeable material, like the monzonite at SD2, SD3, and SD4, the amplitude of the water table response is heightened. The effect of subsurface geology was illustrated by water level fluctuations of small amplitude and gentle rise at SD1 (2.38 m over 92 days, 0.03 m/d) and fluctuations of large amplitude and steep rise at SD2, SD3, and SD4 (mean 5.52 m over 44 days, 0.13 m/d).

The water-level contours in Figure 3.7 were used to determine groundwater flow direction shown with blue arrows. Assuming the aquifer is homogeneous and isotropic, groundwater flows perpendicular to water level contours from high to low hydraulic head and flows faster where contours are closer together. Water level observations from the wells indicated that at the Saddle site, groundwater flows from the West Knoll toward the Saddle wells. At the Martinelli site, water level observations indicated that groundwater flows from the catchment boundary toward the Martinelli stream.

The latest year of measurement (2011) had the highest peak water levels in the deep Saddle wells, reflecting the record snow accumulation (Figure 3.5a). The lowest peak water levels at SD2, SD3, and SD4 occurred in 2007 when snow accumulation was the lowest over the period 2006−2011. At SD1, the lowest peak water levels occurred in 2008 reflecting minimal snow accumulation near SD1 due to wind scouring.

Figure 3.9 shows long-term trends in peak water levels in the deep wells at the Saddle site (Figure 3.9a) and the Martinelli site (Figure 3.9b). The rate of change, given by the slope of the equation of the trend line, and the R^2 value are also shown for each well. Over the 6-year period of record, trends in water levels increased in all wells except MD1 where water levels were relatively consistent. Unlike seasonal fluctuations in water level, which were on average 4.74 m/y at the Saddle site, long-term fluctuations were significantly smaller. At the Saddle site, water levels increased at an average rate of 0.23 m/y with the highest rate at well SD2 (0.35 m/y, $R^2 = 0.70$) and the lowest at SD4 (0.15 m/y, $R^2 = 0.11$). At the Martinelli site, water levels increased by an average of 0.13 m/y with the highest rate at well MD3 (0.23 m/y, $R^2 = 0.66$) and the lowest at MD1 (-0.0006 m/y, $R^2 = 0.0005$). Long-term changes in groundwater levels are caused by natural variations in vegetation, precipitation, air temperature, and snow depth or

anthropogenic effects (Healy, 2010). The net increase in water levels suggests that there was a net increase in groundwater stored at Niwot Ridge between 2006 and 2010. The significant variation in peak water level from year to year, as indicated by the low R^2 values, implies that the 6-year trend is not a good representation of decadal or longer-term trends.

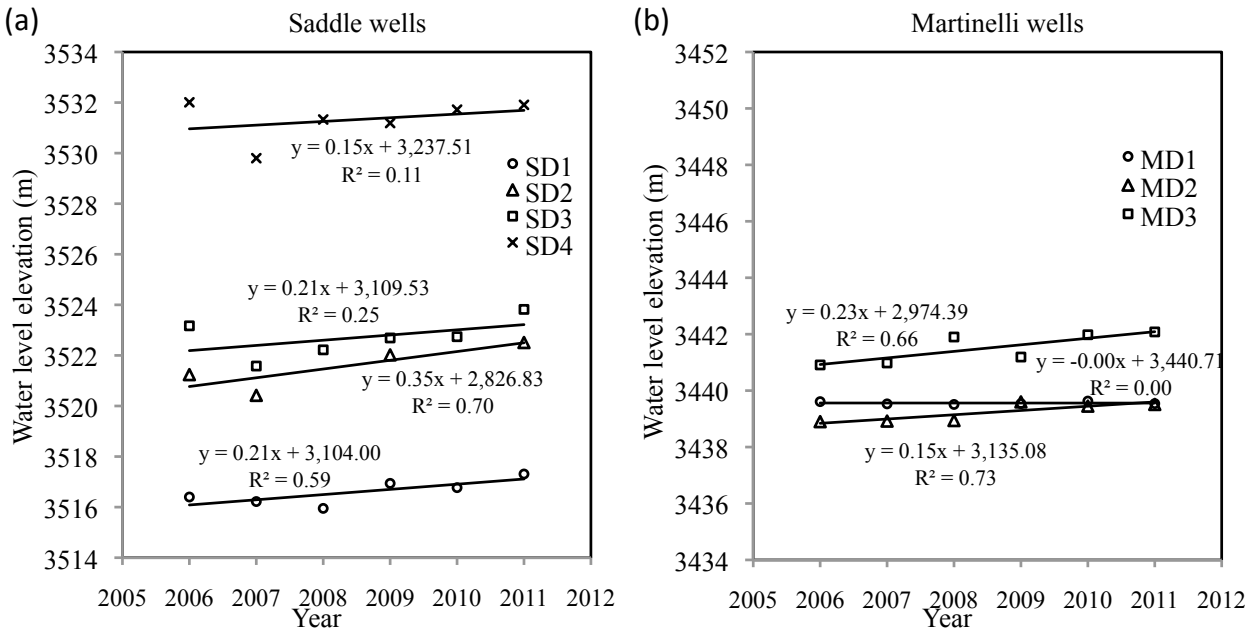

Figure 3.9. Long-term trends in peak water level elevation in the deep wells at (a) Saddle site and (b) Martinelli site for the period 2006−2011. The rate of change, given by the slope of the equation of the trend line, and the R^2 value are also shown for each well.

3.1.5 Results: Hydraulic gradients

Horizontal hydraulic gradient, *dh*/*dx*, is equal to the difference in hydraulic head between two piezometers divided by the horizontal distance between them. Mean horizontal hydraulic gradients, listed in Table 3.3a, were calculated using hydraulic head measured in the deep piezometers in mid-July and mid-May, which was approximately when peak and minimum water level occurred each year, respectively. Horizontal hydraulic gradients at the Saddle site indicated that the horizontal flow component of groundwater was from west to east, following the slope of the topography. At the Martinelli site, horizontal hydraulic gradients indicated that

groundwater was flowing toward the Martinelli stream. Mean horizontal hydraulic gradient measured at annual minimum water level in mid-May ranged from 0.01 between SD2 and SD3 to 0.11 between SD3 and SD4. Mean horizontal hydraulic gradient measured at annual peak water level in mid-July ranged from 0.03 between SD2 and SD3 to 0.10 between SD1 and SD2 and between SD3 and SD4. In general, horizontal hydraulic gradients did not change significantly between minimum and peak water level. However, between SD1 and SD2, mean horizontal hydraulic gradient more than doubled between mid-May ($dh/dx = 0.04$) and mid-July ($dh/dx = 0.10$) because water levels at SD1 did not rise nearly as much in spring as at SD2.

Vertical hydraulic gradient, dh/dz, is equal to the difference in hydraulic head between two closely spaced piezometers divided by the vertical distance between the middle of the screened intervals of the two piezometers. Mean vertical hydraulic gradients, listed in Table 3.3b, were calculated using hydraulic head measured in mid-July at each pair of piezometers, which was when peak water level occurred each year. In all seven pairs of wells, vertical hydraulic gradients indicated that groundwater flow was in downward, which was expected at peak water level, as infiltrating snowmelt recharged the groundwater system. Mean vertical hydraulic gradient was greatest at Saddle pair 1 ($dh/dz = 0.70$). Mean vertical hydraulic gradient was lowest at Martinelli pair 1 ($dh/dz = 0.4$). Greater vertical hydraulic gradient at the Saddle site suggests that there was more recharge at the Saddle site than at the Martinelli site, assuming similar values of hydraulic conductivity.

(a) Horizontal hydraulic gradient at peak water level:

	dx (m)	*dh* (m)	*dh/dx*
Between SD1, SD2	44.7	4.6	0.10
Between SD2, SD3	45.0	1.5	0.03
Between SD3, SD4	82.4	8.6	0.10
Between MD1, MD2	13.8	0.7	0.05
Between MD2, MD3	33.4	2.0	0.06

Horizontal hydraulic gradient at minimum water level:

	dx (m)	*dh* (m)	*dh/dx*
Between SD1, SD2	44.7	2.0	0.04
Between SD2, SD3	45.0	0.7	0.01
Between SD3, SD4	82.4	9.0	0.11
Between MD1, MD2	13.8	-	-
Between MD2, MD3	33.4	-	-

dx = horizontal distance between wells, *dh* = difference in hydraulic heads, *dh*/*dx* = horizonal hydraulic gradient

(b) Vertical hydraulic gradient at peak water level:

	dz (m)	*dh* (m)	*dh/dz*
Between SS1, SD1	7.1	5.0	0.70
Between SS2, SD2	5.8	0.7	0.12
Between SS3, SD3	6.8	0.8	0.12
Between SS4, SD4	4.4	0.3	0.06
Between MS1, MD1	2.0	0.1	0.04
Between MS2, MD2	2.5	0.9	0.39
Between MS3, MD3	2.6	0.3	0.13

dz = verical distance between middle of screened intervals, *dh* = difference in hydraulic heads, *dh*/*dz* vertical hydraulic gradient

dh/*dz* was not calculated at minimum water level because water levels were not measured in shallow wells during winter when water levels reached their annual minimum.

Table 3.3. Table of mean hydraulic gradients at the Saddle and Martinelli sites (2006−2011). (a) Values of mean horizontal hydraulic gradient were calculated using hydraulic head measured in the deep piezometers in mid-July and mid-May when peak and minimum water level occurred each year. (b) Values of mean vertical hydraulic gradient were calculated using hydraulic head measured in mid-July at each pair of piezometers when peak water level occurred each year.

3.1.6 Results: Trends in water levels related to climate and streamflow

Seasonal fluctuations in water levels are caused by seasonal fluctuations in climatic parameters. Daily measurements of precipitation, air temperature, and streamflow over the period 2006−2011 and daily measurements of snowmelt for 2010 were plotted over time with water levels measured at the Saddle and Martinelli sites to determine what effect, if any, these parameters had on seasonal groundwater level fluctuations. Total daily precipitation and mean daily air temperature were measured at the Saddle climate station (NWT

Meteorology/Climatology, 2011). Daily snowmelt was measured with snowmelt lysimeters at a site near wells SS3 and SD3 (Rory Cowie, personal communication, 25 April 2011). Total daily streamflow was measured at the Saddle and Martinelli stream gauges (NWT Hydrology, 2011). The locations of the climate station and stream gauges are shown in Figure 2.1b.

Water level fluctuations in the Saddle and Martinelli wells are shown plotted with precipitation in Figure 3.10 and with air temperature in Figure 3.11. The groundwater level response to precipitation was delayed. The effect of air temperature on groundwater levels is indirect since increasing air temperature does not alone cause groundwater levels to rise. Because air temperature during winter on Niwot Ridge was below freezing, winter precipitation arrived in the form of snow, accumulated on the ground surface, and was not available to recharge groundwater. For this reason, groundwater levels declined throughout the winter months. As soon as air temperature rose above 0°C in June, groundwater levels began their seasonal rise due to infiltration of snowmelt. During summer, air temperature was warm enough for precipitation to arrive as rain. However, precipitation was so low that water inputs were minimal (Figure 3.10). Groundwater levels therefore declined at a relatively constant rate during summer. When air temperature dropped below freezing in October, groundwater levels were already well into their seasonal decline.

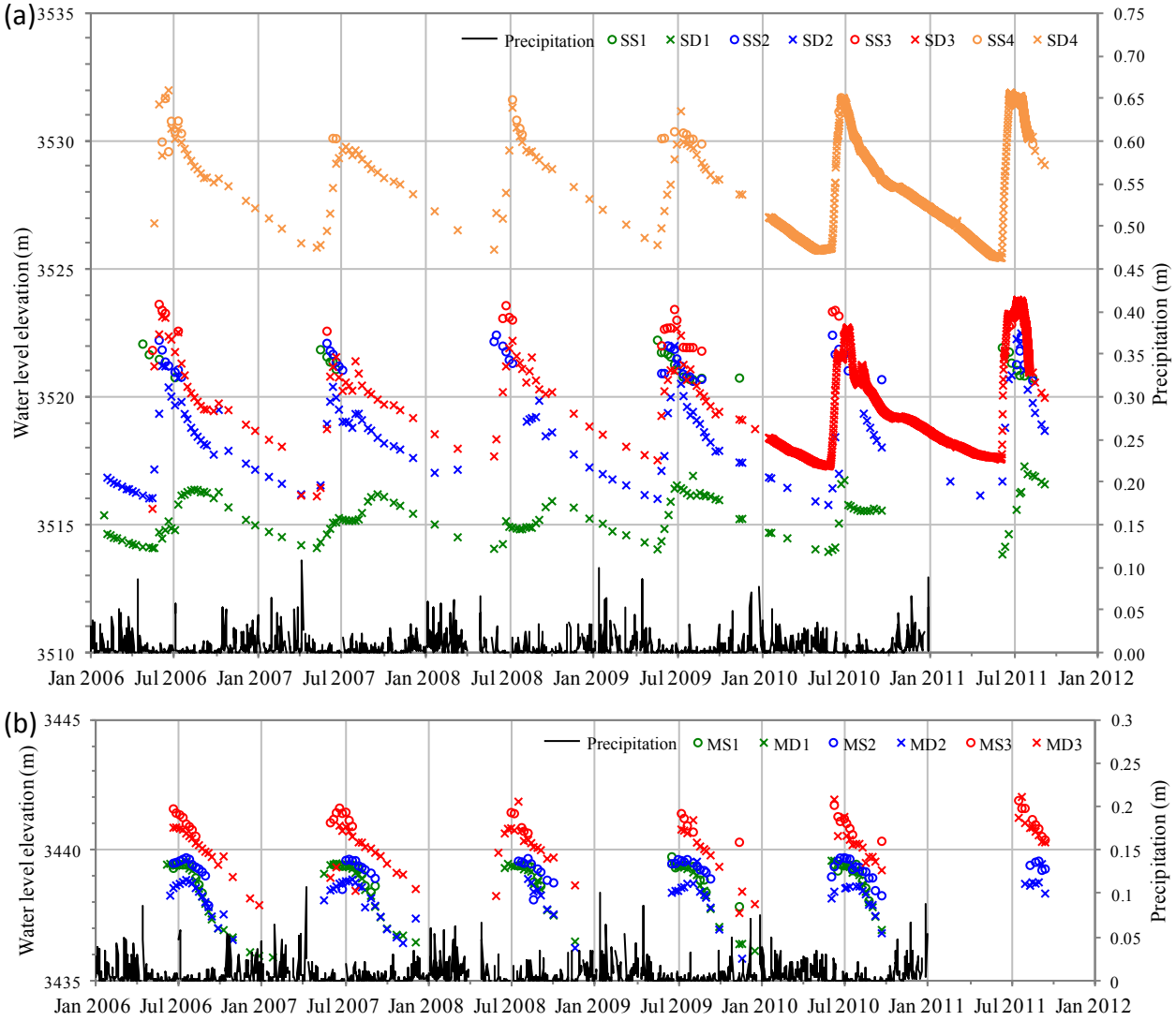

Figure 3.10. Graph of daily precipitation measured at the Saddle climate station (NWT Meteorology/Climatology, 2011) and water levels measured at (a) Saddle piezometers and (b) Martinelli piezometers for the period 2006−2011. Precipitation data were not available for 2011.

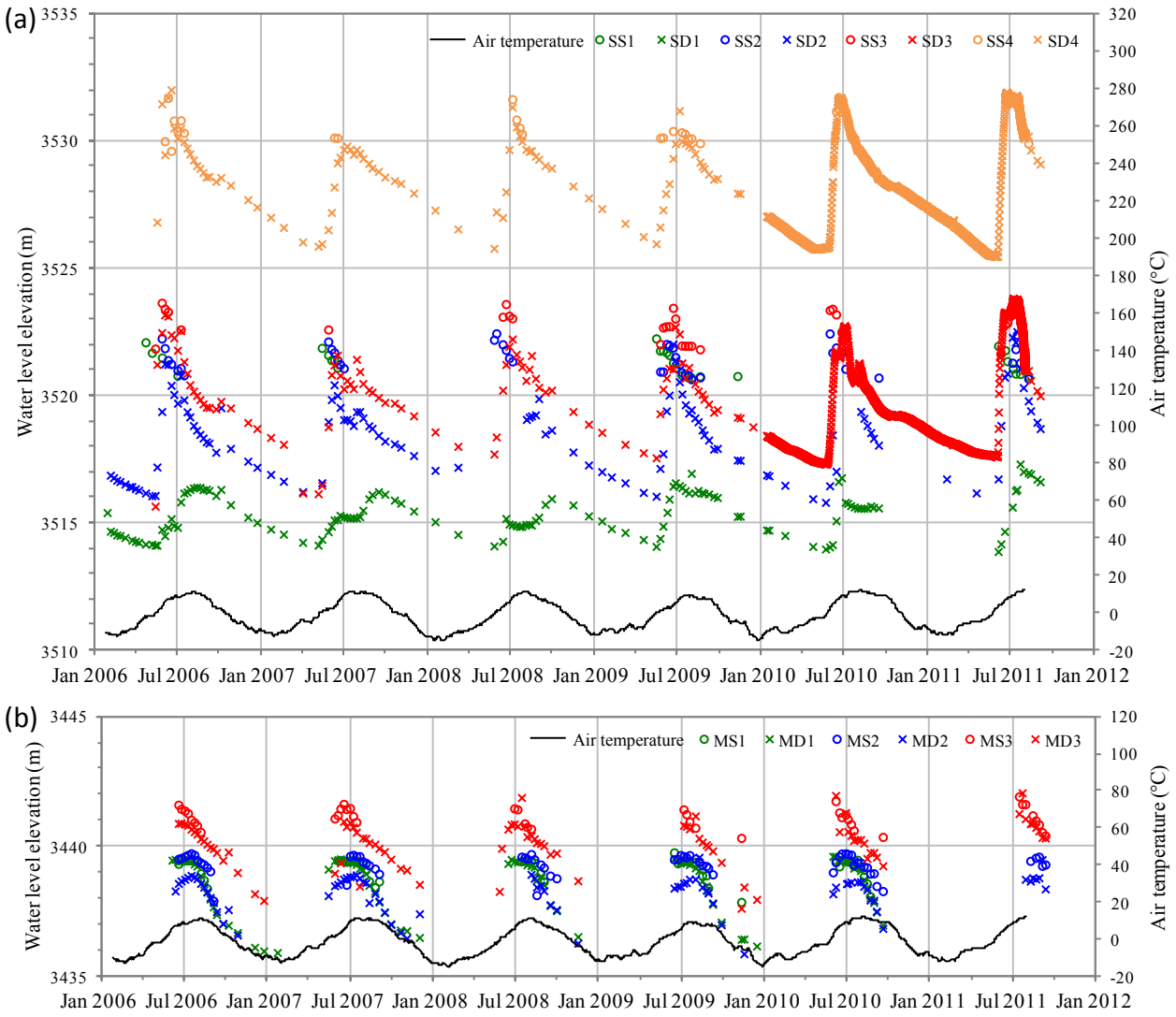

Figure 3.11. Graph of daily mean air temperature measured at the Saddle climate station (NWT Meteorology/Climatology, 2011) and water levels measured at (a) Saddle piezometers and (b) Martinelli piezometers for the period 2006−2011.

Figure 3.12 illustrates the relation between snowmelt and groundwater levels measured at the Saddle wells in 2010. The timing between peak snowmelt and peak groundwater levels was lagged. Snowmelt peaked on June 6 in 2010. Groundwater levels in the shallow wells peaked approximately one week after snowmelt peaked. In the deep wells, groundwater levels peaked about a month after snowmelt due to the greater distance between the ground and the well screen.

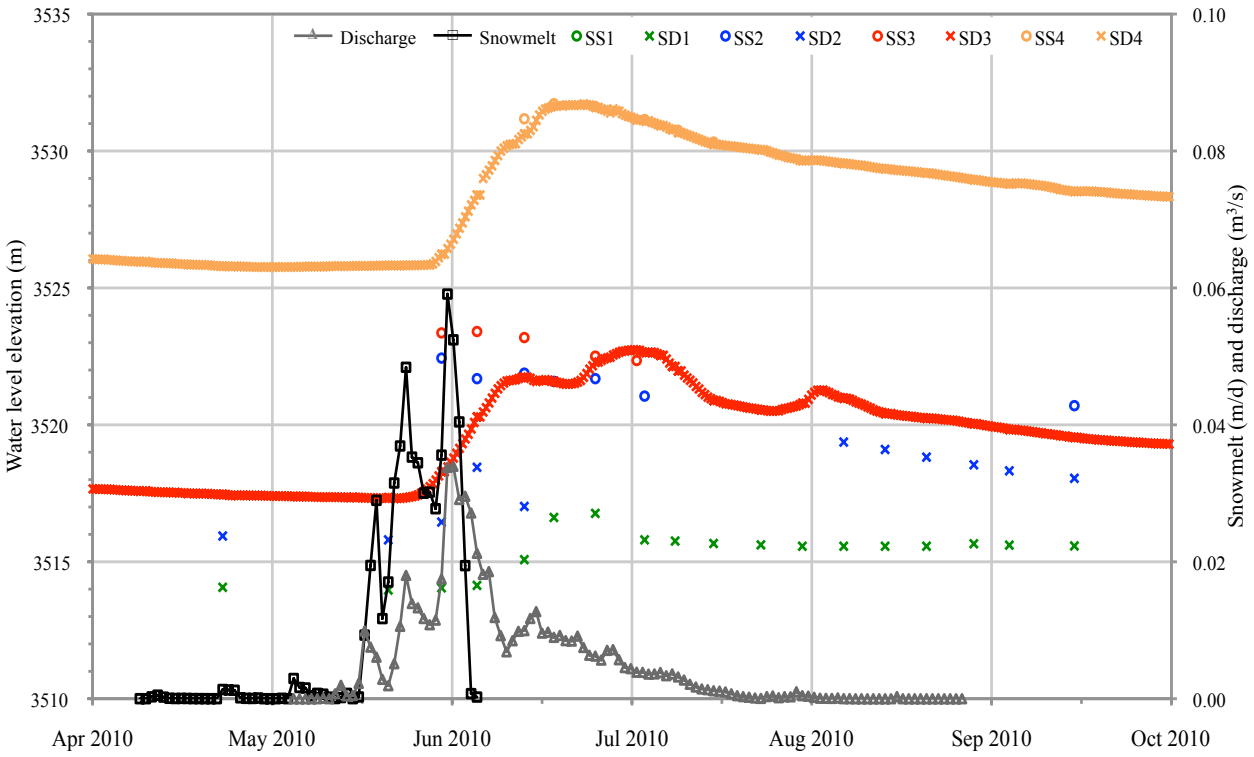

Figure 3.12. Graph of snowmelt measured at the Saddle snowmelt lysimeters (Rory Cowie, personal communication, 25 April 2011), stream discharge measured at the Saddle stream gauge (NWT Hydrology, 2011), and water levels measured at (a) Saddle piezometers and (b) Martinelli piezometers for April to October 2010.

Similar to snowmelt, there was a lagged relation between peak groundwater levels and peak streamflow. Figure 3.13 shows that peak groundwater levels occur after peak streamflow at the Saddle and Martinelli sites. As discussed above, peak water level at the deep Saddle wells varied by location. Therefore, the lag between peak streamflow and water levels also varied by location. The lag at the Saddle site was on average 29 days and ranged from 16 days at SD2 (peak water level on June 23) to 65 days at SD1 (peak water level on August 20) (Table 3.4). The lag between streamflow and water levels at the Martinelli site was on average 26 days and ranged from 12 days at MD1 to 46 days at MD2. Peak streamflow occurred before peak water level because the flow of snowmelt to the water table was slowed by the long and tortuous path of groundwater through the porous media.

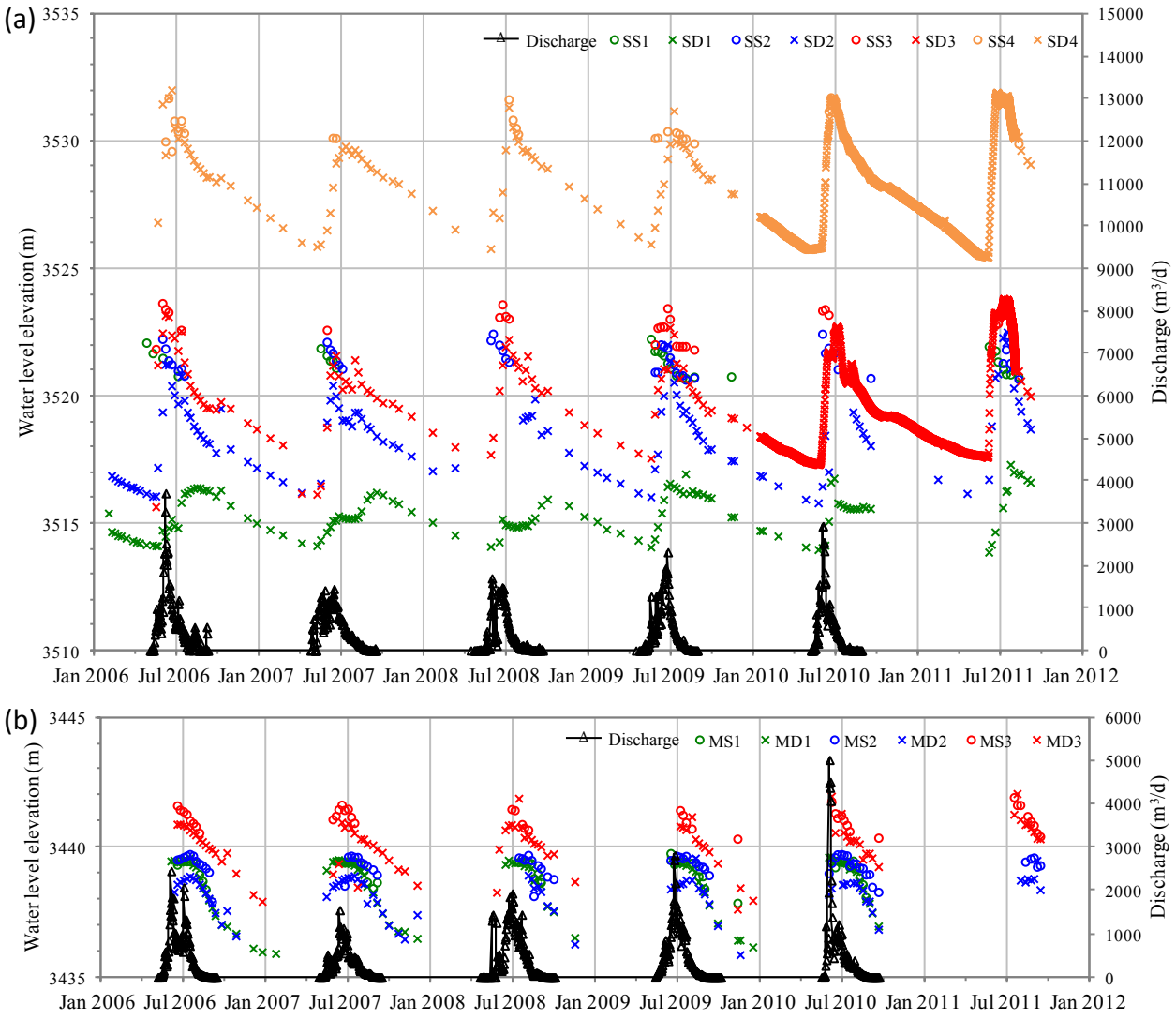

Figure 3.13. Graph of daily stream discharge measured at (a) Saddle stream gauge and (b) Martinelli stream gauge (NWT Hydrology, 2011) and water levels measured at (a) Saddle piezometers and (b) Martinelli piezometers for the period 2006−2011.

Well	Date of peak water level	Date of peak streamflow	Lag between peak water level and streamflow
SD1	8/16	6/11	65
SD2	6/23	6/11	12
SD3	6/28	6/11	17
SD4	7/2	6/11	21
Mean	7/10	6/11	29
SD	25	0	25
MD1	6/30	6/18	12
MD2	8/3	6/18	46
MD3	7/7	6/18	19
Mean	7/14	6/18	26
SD	18	0	18

SD = standard deviation

Table 3.4. Table listing average dates of peak groundwater levels in deep wells at the Saddle and Martinelli sites, average dates of peak streamflow in the Saddle and Martinelli streams, and lag (in days) between peak water level and peak streamflow (2006−2011).

3.1.7 Summary and discussion of groundwater level monitoring

The water level data collected in this study provide valuable insight into groundwater recharge and the overall behavior of the Niwot Ridge aquifer. Several key observations are noted. First, water level fluctuations were similar in all Saddle wells except SD1. Water levels at the Saddle site showed a large and rapid increase in late spring and gradually declined through the remainder of the year. At SD1, however, the rise in water level in late spring was small and slow. Second, water levels in all Niwot Ridge wells showed one significant recharge event per year, which demonstrates that climate (e.g. snowmelt) controls groundwater recharge to the Niwot Ridge aquifer. Water level rise occurred nearly exclusively in response to snowmelt in late spring and early summer. The rise was quick and lasted one to two months (except at SD1). Declines in water level occurred from late summer to early spring, lasted ten to eleven months (except at SD1), and reflected less recharge to the shallow aquifer due to minimal input of water at the surface. Third, depths to groundwater were shallow, at most 8.5 m below ground surface, and the water table was a subdued replica of the topography, which suggest that the Niwot Ridge

groundwater system is unconfined. These observations demonstrate the complexity in features controlling groundwater behavior at Niwot Ridge.

3.2 Estimation of infiltration capacity

3.2.1 Background on infiltration

The primary source of groundwater recharge to the study area is water infiltrating from the surface. Therefore, an understanding of infiltration is essential for estimating the timing and amount of groundwater recharge. Infiltration is the process by which water from rain or snowmelt at the surface enters the ground. The infiltration capacity is the maximum rate that infiltration can occur, has units of [L/T], and is approximately equal to the saturated hydraulic conductivity of the near-surface material at that location (Dingman, 2002).

Infiltration is affected by many factors including the rate of water input at the surface, chemical and physical properties of the infiltrating water, surface slope and roughness, antecedent soil moisture content, and hydraulic conductivity (Dingman, 2002). If the rate of water input from rain or snowmelt is less than the infiltration capacity of the near-surface material, water will infiltrate. If the rate of water input is greater than the infiltration capacity, water will either pond on the surface or move downslope via overland flow. As snowmelt is more constant and occurs over a longer period than rain events, infiltration from snowmelt is more likely than from rain. Overland flow is more likely to occur following heavy precipitation events than during snowmelt. Frozen ground can hinder infiltration and result in overland flow.

Topography affects the amount of infiltration. Steeper slopes are more likely to produce overland flow, while ponding and infiltration are likely to occur on gentle or flat slopes. A smooth ground surface results in higher rates of overland flow and less infiltration. Rough surfaces may allow for pooling and infiltration.

The soil moisture content of the unsaturated zone plays a significant role in the rate of infiltration. If a soil is dry prior to a water input event, the infiltration capacity is high due to capillary forces drawing the water downward into the soil. As the soil moisture content increases, infiltration capacity decreases until a more or less steady rate is reached. This steady rate is approximately equal to the saturated hydraulic conductivity. In areas where snowmelt occurs over a longer period, soil saturation is maintained, which increases the amount of infiltration and the probability that water will recharge the aquifer.

Many factors influence the porosity and permeability of the near-surface material and therefore the hydraulic conductivity (i.e. infiltration capacity) of the material. The hydraulic conductivity affects infiltration rate and amount. If the material is porous (e.g. gravel) or highly fractured, water will more easily enter the ground. The contrast in permeability between surficial sediments and the underlying bedrock affects the direction of flow of infiltrating water. Thin permeable sediments over bedrock of a lower permeability leads to lateral flow along the boundary between sediments and bedrock, which limits deep infiltration. Frost at the surface impedes infiltration as well. However, frost in rock with low moisture content can result in frost cracking over long timescales, which can increase permeability and infiltration rate. The transport of fine sediments into larger pore spaces can decrease porosity and therefore infiltration. Vegetation and organic matter at the surface and insects and other burrowing animals generally increase porosity and permeability, and hence infiltration, near the surface.

Quantifying the rate and amount of infiltration in a mountainous field setting such as Niwot Ridge is difficult because of the high spatial variability of topography, near-surface material, and snowpack. In addition, these variables are rarely well defined for mountain regions. Infiltration rates can be estimated from lysimeters, sprinkler-plot studies, observations

of soil-water changes, environmental isotopes, numerical models, and ring infiltrometers (Dingman, 2002). Lysimeters measure the amount of water that moved from the ground surface and through a column of soil. In sprinkler-plot studies, infiltration rates are determined by applying a known rate of artificial rainfall to the ground surface and the rate of infiltration is determined from the derived relation between soil tension and water content. Many types of tracers, including applied, historical, and environmental tracers, can be used to estimate infiltration. Numerical models, such as the Green-Ampt model, can simulate the infiltration process (Dingman, 2002). The aforementioned methods require costly specialized equipment and/or complex application techniques.

The ring infiltrometer method, on the other hand, is efficient and requires only simple and affordable equipment. A ring infiltrometer is a device used to directly measure infiltration capacity in the field. The infiltrometer is set in the ground surface and water is added such that several centimeters of ponded water fills the device. Infiltration test data are obtained by measuring the rate of water level decline or measuring the rate water must be added to maintain a constant water level (Dingman, 2002). The double-ring infiltrometer is better than a single-ring infiltrometer because the double-ring system minimizes the effects of lateral water movement. Water infiltrating from the outer ring buffers lateral flow of water infiltrating from the inner ring.

3.2.2 Methods: Double-ring infiltrometer tests

Double-ring infiltrometer tests were performed in representative locations at the Saddle and Martinelli catchments to obtain the infiltration capacity (i.e. saturated hydraulic conductivity) of the near surface material. Resulting infiltration capacity values were compared with values of hydraulic conductivity for the materials reported in the well lithologic logs and on the geologic map by Gable and Madole (1976).

The double-ring infiltrometer used in this study consisted of two concentric vertical steel rings attached to a horizontal steel handle (Figure 3.14). The inner ring had a diameter of 0.15 m and the outer ring had a diameter of 0.30 m. The height of the rings was 0.10 m.

Figure 3.14. Double-ring infiltrometer used in this study. A tape measure affixed to the inside of the inner ring was used to measure the level of the ponded water. A stopwatch was used to measure the change in water level over time.

The procedure used to measure infiltration capacity was as follows (adapted from League, 1990 and Dingman, 2002). After a test area was selected, the exact location was chosen to be on as flat ground as possible for ease of recording measurements. If the surface of the test location was sloped, the infiltrometer was inserted into the ground slightly more on the uphill side to make the instrument as level as possible. If vegetation was thick, it was cut to about 0.02 m. Where conditions allowed, a narrow slit was cut into the ground directly below where the bottom edge of the infiltrometer rings was to be placed. The infiltrometer was then uniformly pressed into the ground about 0.01−0.03 m to form a seal with the surface. Modeling clay or topsoil was pressed between the ground and the base of the infiltrometer at locations where the surficial material was too coarse to form an adequate seal. Approximately 0.18 m^3 and 0.35 m^3 water at ambient temperature was then poured into the inner and outer rings, respectively, to

create a condition of 0.08−0.10 m ponding in the inner ring. In locations where the infiltrometer was pressed further into the ground, water was allowed to spill over from the inner to the outer ring. The water in the outer ring served to reduce lateral flow of water infiltrating from the inner ring. The infiltration rates were high during the beginning of a test and gradually decreased to a steady rate. The rate of water level decline in the inner ring was recorded until a steady decline rate was reached. The ground cover, slope aspect, and slope angle were noted at each location. In addition, the underlying geology, as determined from lithologic logs of the piezometers and from the geologic map by Gable and Madole (1976), was noted.

Without disturbing the position of the infiltrometer, the test was repeated a total of three tests per location. Loague (1990) recommended repeating the test at the same location until two consecutive measurements converged to within $5x10^{-7}$ m/s of each other. Burgy and Luthin (1956) recommended taking the average of at least six tests per location to obtain an estimate within 30% of the true value. Due to limited water supply at the Saddle and Martinelli sites, the mean value of infiltration capacity obtained from three tests performed at each location was assumed to equal the true infiltration capacity at that location. Infiltration rate was calculated for each test by plotting ponded water level versus time and fitting a linear trend line to the data. The slope of the line equaled infiltration rate. The infiltration rate measured during the last test was assumed to equal the infiltration capacity (i.e. saturated hydraulic conductivity) at a location.

Forty-one double-ring infiltrometer tests were conducted at 15 locations. Test locations, shown in Figure 3.15, were selected to test each type of surficial material observed during drilling and each type of underlying bedrock noted on the geologic map by Gable and Madole (1976). Test locations were distributed across the two catchments to capture spatial variability.

Tests were performed during July 3−12, 2010 and July 9−15, 2011. The resulting infiltration capacity values were used as input for hydraulic conductivity in the numerical model.

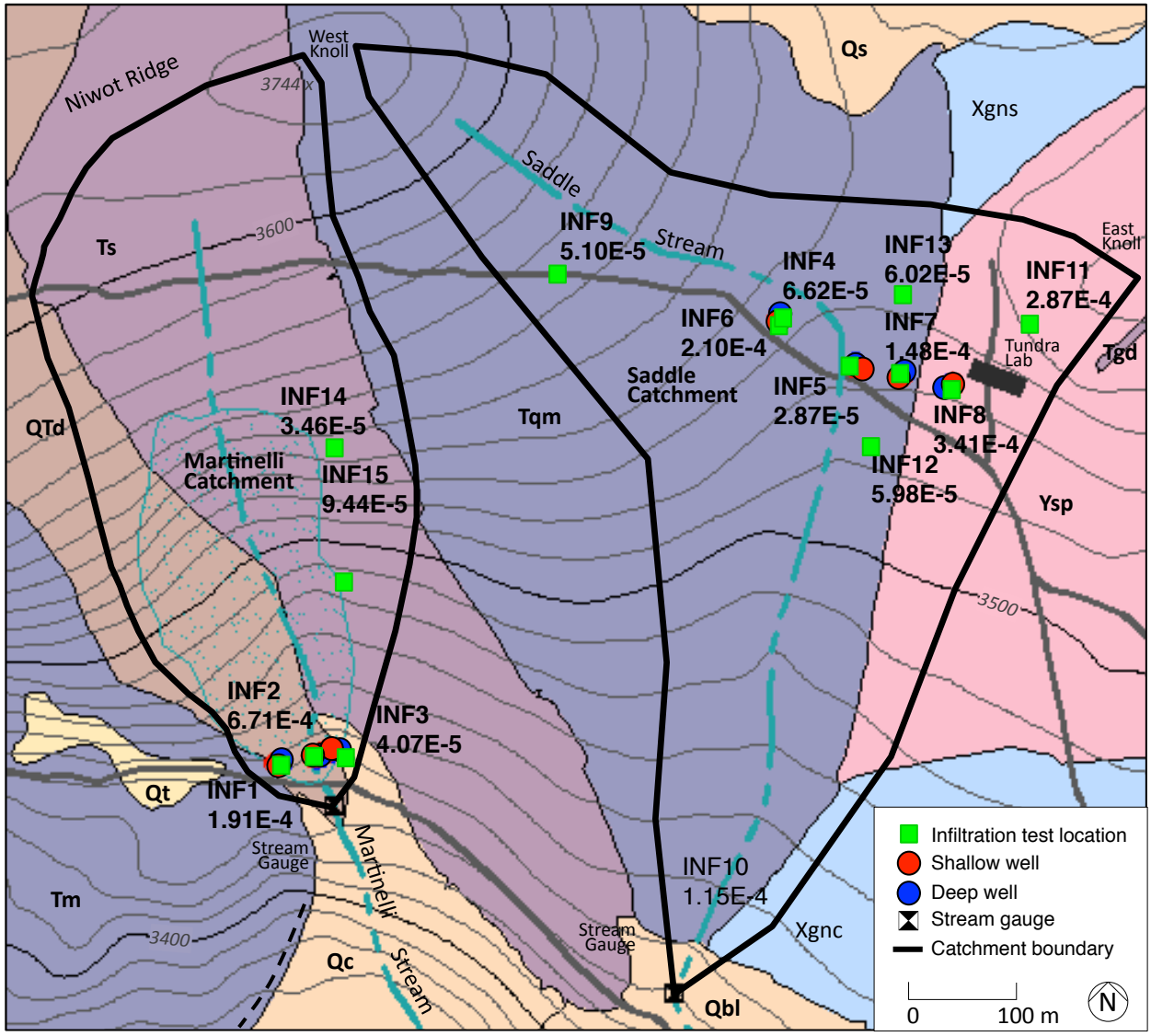

Figure 3.15. Map showing locations of infiltration tests conducted in the Saddle and Martinelli catchments. Also shown, is the spatial distribution, in relation to topography and underlying geology (Gable and Madole, 1976), of average infiltration capacity calculated from the results of the infiltration tests. One to three tests were conducted at each test location. Results are in m/s.

Twenty-eight tests were performed at 10 locations at the Saddle catchment (Figure 3.15). The types of surficial materials reported on lithologic well logs from the Saddle site were sand, sand/gravel, and alternating layers of sand and rock. Each type of surficial and bedrock material

was tested. Three tests were conducted near the Pair 1 piezometers (location INF8). Lithologic logs from drilling reported 2.32−7.62 m sand overlying Precambrian Silver Plume quartz monzonite near this location. Three tests were conducted near the Pair 2 piezometers (location INF7). Lithologic logs from drilling reported 0.09−0.31 m sand overlying Tertiary quartz monzonite near this location. Three tests were conducted near the Pair 3 piezometers (location INF5). Lithologic logs from drilling reported 0.74−2.44 m sand/gravel overlying Tertiary quartz monzonite near this location. Four tests were conducted near the Pair 4 piezometers (locations INF4 and INF6). Lithologic logs from drilling reported 0.65−2.13 m alternating sand and rock layers overlying Tertiary quartz monzonite near this location. Three tests were conducted near the center of the Saddle catchment in soil overlying Tertiary quartz monzonite (location INF12). Three tests were conducted in soil overlying Precambrian Silver Plume quartz monzonite near the northeast corner of the Saddle catchment (location INF11). Three tests were conducted in soil overlying Tertiary quartz monzonite near the north-central Saddle catchment (location INF13). Three tests were conducted in soil overlying Tertiary quartz monzonite near the northwest corner of the Saddle catchment (location INF9). Three tests were conducted in soil overlying Tertiary quartz monzonite near the south corner of the Saddle catchment (location INF10). The biotite gneiss found along the north and southeast margins of the Saddle catchment and the till found at the southern end of the Saddle catchment were not tested because these units comprise a relatively small portion of the catchment area.

Thirteen tests were performed at five locations at the Martinelli catchment (Figure 3.15). The types of surficial materials reported on lithologic well logs were coarse sand, sand overlying gravel, and sand/gravel. Gable and Madole (1976) mapped the surficial deposits covering the Martinelli catchment as Pleistocene or Tertiary diamicton transported from above via solifluction

and Holocene colluvium. Leopold et al. (2008) described the surficial unit as periglacial slope deposits. Bedrock at the Martinelli catchment includes Tertiary-aged syenite and Audubon-Albion monzonite, which are both fractured (Gable and Madole, 1976). Each type of surficial and bedrock material was tested. Three tests were conducted east of the Pair 1 piezometers (location INF3) where there is a coarse sand layer of 2.32−7.62 m overlying bedrock. The coarse sand is Holocene colluvium and the bedrock Tertiary syenite or monzonite (Gable and Madole, 1976). Three tests were conducted near the Pair 2 piezometers (location INF2) where there is 1.21−3.96 m sand overlying 0.28−0.92 m gravel overlying Tertiary syenite or monzonite. The sands and gravels are composed of Pleistocene/Tertiary diamicton. Three tests were conducted near the Pair 3 piezometers (location INF1) where there is 1.49−4.88 m sand/gravel (Pleistocene/Tertiary diamicton) overlying Tertiary syenite or monzonite. One test was conducted in soil overlying Tertiary syenite near the north corner of the Martinelli catchment (location INF14). Only one test was performed at this location because of incoming thunderstorms. Three tests were conducted in soil overlying Tertiary syenite near the east-central Martinelli catchment (location INF15). The upper west side of the Martinelli catchment is too steep to conduct infiltration tests.

3.2.3 Results: Double-ring infiltrometer tests

Figure 3.16 shows graphs of change in ponded water level over time during the 41 infiltration tests conducted at 15 locations throughout the Saddle and Martinelli catchments. The graphs indicate that infiltration occurred fastest during the first test at a location. Infiltration rates decreased with subsequent tests. Infiltration was initially high due to the combination of gravity and capillary effects drawing the water downward. As saturation increased, capillary effects diminished, flow became gravity driven, and the infiltration rate decreased until a more or

less steady rate was reached. The steady state infiltration rate measured during the final test was assumed to equal the infiltration capacity.

All tests reached steady-state infiltration within 30 minutes, but most reached steady state in less than 10 minutes. At location INF8, field observations of infiltration indicated steady state was reached, however, the graph of the data (Figure 3.16h) shows that more data would confirm steady-state infiltration. If infiltration did not reach a steady rate, then saturated conditions were never met, and resultant estimates of infiltration capacity were likely overestimated.

Table 3.5 summarizes the data collected (location, date, location description, ground cover, underlying geology, aspect, and slope angle) at each test location and the infiltration capacity (e.g. hydraulic conductivity) calculated for each test. Figure 3.15 shows the spatial distribution, in relation to the topography and underlying geology, of infiltration capacity calculated from the results of the infiltration tests. The following two sections present the results, sorted by underlying geology, for the Saddle and Martinelli catchments.

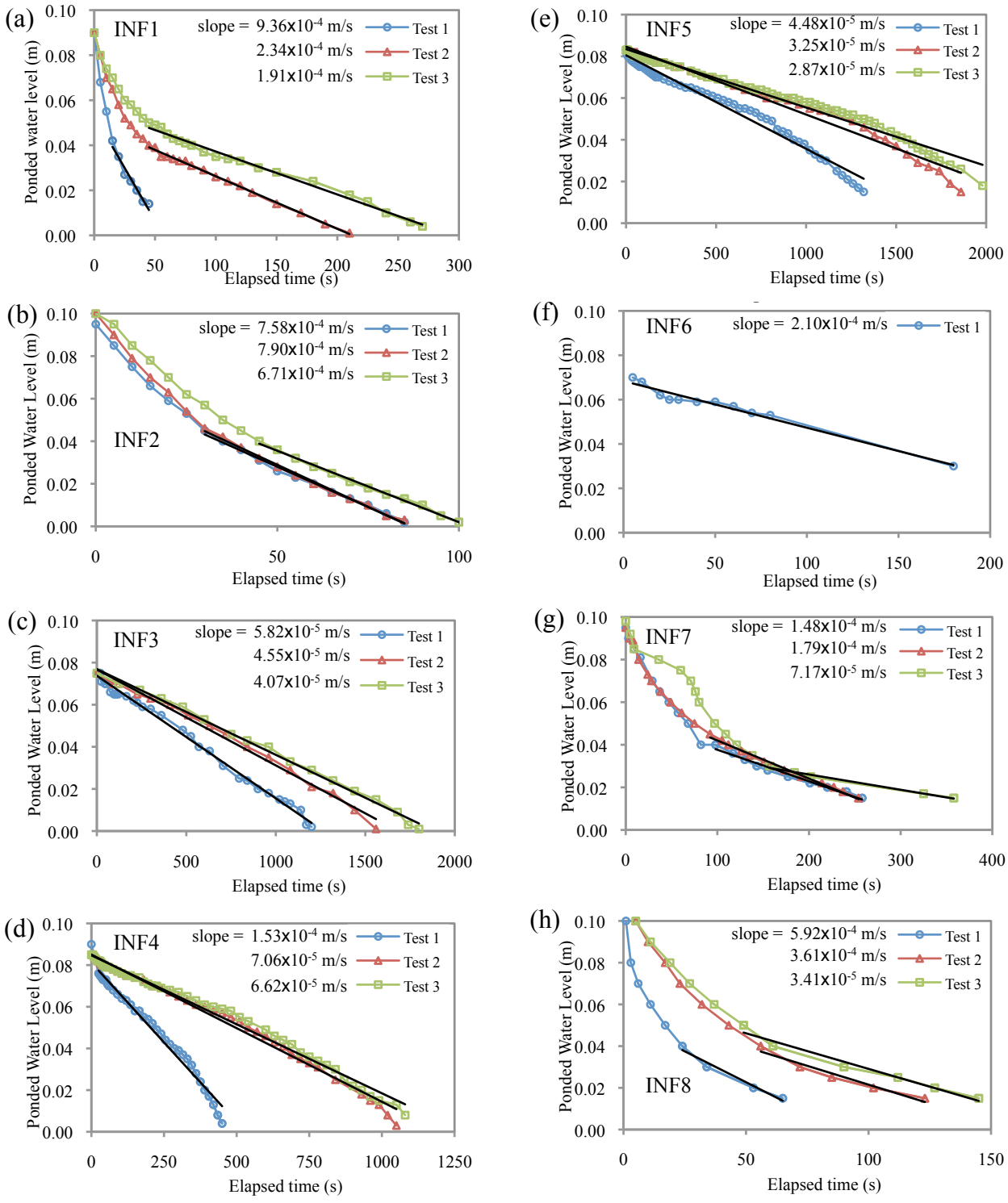

Figure 3.16. Change in ponded water level over time at 15 infiltration test locations. Black line overlying each test's data indicates best-fit line used to estimate infiltration capacity for that test.

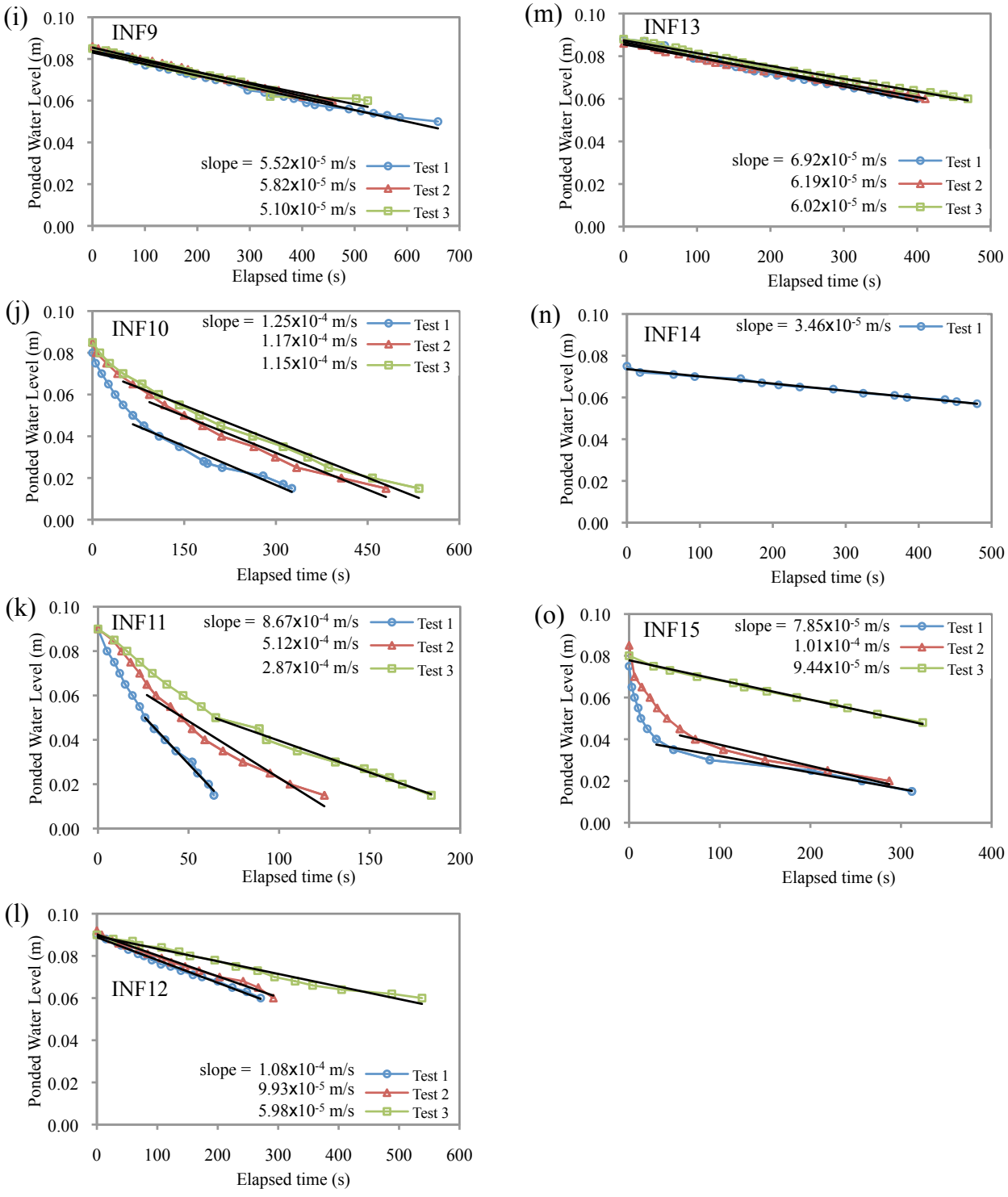

Figure 3.16. (continued)

Location	Date	Location Description	Ground cover	Underlying geology *	Aspect	Slope angle	Test No.	*K* (m/s)
INF1	7/3/10	Martinelli pair 3 piezometers	thick grasses; moist, brown, silty/gravely soil	QTd (sand/gravel) over Tm	155°	15°	1	9.36E-04
							2	2.34E-04
							3	1.91E-04
							Infiltration capacity	**1.91E-04**
INF2	7/3/10	Martinelli pair 2 piezometers	thick grasses; moist, brown, silty/gravely soil	QTd (sand) over QTd (gravel) over Qc, Ts, or Tm	na	0°	1	7.58E-04
							2	7.90E-04
							3	6.71E-04
							Infiltration capacity	**6.71E-04**
INF3	7/3/10	Martinelli pair 1 piezometers	no vegetation; very dry, orange/red, sandy gravel of granitic origin	Qc (thick layer coarse sand)	219°	12°	1	5.82E-05
							2	4.55E-05
							3	4.07E-05
							Infiltration capacity	**4.07E-05**
INF4	7/10/10	Saddle pair 4 piezometers	thick lichens with some grasses; moist, dense, dark-brown soil with some sand and cobbles	(thin layer sand) over Tqm	na	0°	1	1.53E-04
							2	7.06E-05
							3	6.62E-05
							Infiltration capacity	**6.62E-05**
INF5	7/10/10	Saddle pair 3 piezometers	thick grasses; very moist, dense, dark-brown soil with some sand and cobbles	(sand/gravel) over Tqm	168°	5°	1	4.48E-05
							2	3.25E-05
							3	2.87E-05
							Infiltration capacity	**2.87E-05**
INF6	7/12/10	Saddle pair 4 piezometers	thick grasses; moist, dense, dark-brown soil with some sand and cobbles	(thin layer sand) over Tqm	na	0°	1	2.10E-04
							2	-
							3	-
							Infiltration capacity	**2.10E-04**
INF7	7/9/11	Saddle pair 2 piezometers	some grasses and lichen; moist, dense, dark-brown soil with some sand and cobbles	(thin sand layer) over Tqm	194°	4°	1	1.48E-04
							2	1.79E-04
							3	7.17E-05
							Infiltration capacity	**1.48E-04**
INF8	7/9/11	Saddle pair 1 piezometers	thick grasses; dry, dark-brown soil with some sand and cobbles; hummocky ground	(thick layer sand) over Ysp	188°	6°	1	5.92E-04
							2	3.61E-04
							3	3.41E-04
							Infiltration capacity	**3.41E-04**
INF9	7/9/11	northwest corner Saddle basin	dormant, flattened grasses; very moist, dark-brown silty soil with some cobbles; snowpack recently melted	Tqm	120°	8°	1	5.52E-05
							2	5.82E-05
							3	5.10E-05
							Infiltration capacity	**5.10E-05**
INF10	7/15/11	south corner Saddle basin; 5 m west of Saddle stream	no vegetation; dry, brown, silty/sandy soil; ground covered in pine needles and pine cones	Tqm	196°	9°	1	1.25E-04
							2	1.17E-04
							3	1.15E-04
							Infiltration capacity	**1.15E-04**
INF11	7/9/11	northeast corner Saddle basin	thick grasses and small plants; dry, dark-brown soil containing many cobbles and boulders 0.1-0.6 m diameter	Ysp	191°	10°	1	8.67E-04
							2	5.12E-04
							3	2.87E-04
							Infiltration capacity	**2.87E-04**

Table 3.5. Results of the infiltration tests conducted at the Saddle and Martinelli sites. The steady-state infiltration rate measured during the last test was assumed to equal the infiltration capacity at a location. Underlying geology was determined from driller's logs of the well pair nearest to the infiltration test location and the geologic map by Gable and Madole (1976). Aspect and slope angle were measured at the infiltration test site using a hand-held compass.

INF12	7/9/11	central Saddle basin	dormant, flattened grasses; very moist, dark-brown soil with some cobbles; snowpack recently melted	Tqm	190°	8°	1 2 3 **Infiltration capacity**	1.08E-04 9.93E-05 5.98E-05 **5.98E-05**
INF13	7/9/11	north-central Saddle basin	grasses and small plants; very moist, dark-brown silty soil	Tqm	na	0°	1 2 3 **Infiltration capacity**	6.92E-05 6.19E-05 6.02E-05 **6.02E-05**
INF14	7/9/11	north corner Martinelli basin	dormant, flattened grasses; saturated, dark-brown silty and cobbly soil snowpack recently melted	Ts	184°	14°	1 2 3 **Infiltration capacity**	3.46E-05 - - **3.46E-05**
INF15	7/15/11	east-central Martinelli basin	only a couple small plants; dry, brown,silty and cobbly soil	Ts	189°	13°	1 2 3 **Infiltration capacity**	7.85E-05 1.01E-04 9.44E-05 **9.44E-05**

* Geology noted in parentheses was reported on lithologic well logs. Geology not in parentheses is from Gable and Madole (1976). Qc = Holocene colluvium, QTd = Pleistocene or Tertiary diamicton, Ts = Tertiary syenite, Tqm = Tertiary quartz monzonite, Tm = Tertiary monzonite, Ysp = Silver Plume quartz monzonite
K = hydraulic conductivity of near-surface materials (i.e. infiltration capacity)

Table 3.5. (continued)

Saddle infiltration tests results

Six tests at two locations in the Saddle catchment were conducted in surficial deposits overlying Precambrian Silver Plume quartz monzonite. Infiltration capacity at location INF8 was 3.41×10^{-4} m/s, which was the highest rate measured in the Saddle catchment (Figure 3.16h). Infiltration capacity at location INF11 was 2.87×10^{-4} m/s (Figure 3.16k).

Twenty-two tests at eight locations in the Saddle catchment were conducted in surficial deposits overlying Tertiary quartz monzonite (INF4, INF5, INF6, INF7, INF9, INF10, INF12, and INF13). Infiltration capacity at location INF4 was 6.62×10^{-5} m/s (Figure 3.16d). Infiltration capacity at location INF5 was 2.87×10^{-5} m/s, which was the lowest rate measured in either the Saddle or the Martinelli catchments (Figure 3.16e). Only one test was done at location INF6 that yielded an infiltration capacity of 2.10×10^{-4} m/s (Figure 3.16f). This value is probably an overestimate of the true value because infiltration is fastest during the first test. Infiltration capacity at locations INF7, INF10, and INF13 was 1.48×10^{-4} m/s, 1.15×10^{-4} m/s, and 6.02×10^{-5}

m/s, respectively (Figure 3.16g, j, and m). Infiltration capacity at location INF9 and INF12 was 5.10×10^{-5} m/s and 5.98×10^{-5} m/s, respectively (Figure 3.16i and Figure 3.16l). The winter snowpack had melted from these locations two or three days prior to conducting the infiltration tests; however, no frozen ground was noted.

Martinelli infiltration tests results

Three tests at one location in the Martinelli catchment were conducted in Quaternary colluvium. Infiltration capacity at INF3 was 4.07×10^{-5} m/s (Figure 3.16c).

Six tests at two locations in the Martinelli catchment were conducted in surficial deposits overlying Tertiary syenite. Due to imposing thunderstorms, only one test was done at location INF14. The winter snowpack had melted from the location two or three days prior to conducting the infiltration test; however, no frozen ground was noted. Infiltration capacity for the test was 3.46×10^{-5} m/s, which was the lowest rate measured at the Martinelli catchments (Figure 3.16n). At location INF15, three tests were conducted and infiltration capacity was 9.44×10^{-5} m/s (Figure 3.16o). The first test, unlike the second and third tests, did not display high initial infiltration. Instead, infiltration during test 3 was steady from start to finish indicating that the soil did not drain and remained saturated between tests 2 and 3.

Four tests at two locations were conducted in surficial deposits overlying Pleistocene/Tertiary diamicton. Three tests were conducted at location INF1. Infiltration capacity was 1.91×10^{-4} m/s (Figure 3.16a). At location INF2, three tests were conducted and infiltration capacity was 6.71×10^{-4} m/s, which was the highest rate measured in either the Saddle or the Martinelli catchments (Figure 3.16b).

3.2.4 Summary and discussion of infiltration capacity

Infiltration capacity estimated for the Niwot Ridge study area ranged from 2.87×10^{-5} to 6.71×10^{-4} m/s. Results for the Saddle and Martinelli catchments were similar. Variations in rates between test locations depended on the underlying geology, composition of the surficial material, moisture content, and vegetative cover. Infiltration capacity was highest in the deposit composed of Pleistocene/Tertiary diamicton (mean 4.31×10^{-4} m/s) and lowest in the Quaternary colluvium (mean 4.07×10^{-5} m/s). Infiltration capacity averaged 6.45×10^{-5} m/s in the Tertiary syenite, 3.41×10^{-4} m/s in the Tertiary quartz monzonite, and 3.14×10^{-4} m/s in the Precambrian Silver Plume quartz monzonite. High infiltration rates, such as those observed in the deposit composed of diamicton, increased the probability that water recharged the water table and was not evapotranspired.

Surficial materials containing gravel (INF1 and INF2) had higher infiltration rates (mean 8.62×10^{-4} m/s) than materials containing sand and cobbles (INF4−INF8, mean 7.94×10^{-4} m/s). Where surficial deposits were dry or slightly moist (INF 1, INF2, INF4, INF6, INF7, INF8, INF10, INF11, and INF15), infiltration capacity was relatively high. Where surficial deposits were very moist or saturated (INF5, INF9, INF12, INF13, and INF14), infiltration capacity was relatively low. The presence of vegetation did not affect infiltration rates in very moist or saturated material. However, in dry or slightly moist material, the presence of thick grasses resulted in higher infiltration capacity (INF1, INF2, INF6, INF8, and INF11). Results from location INF3 did not follow these trends. Infiltration capacity was expected to be relatively high in the unvegetated, very dry surficial material at INF3. However, resultant average infiltration capacity was 4.07×10^{-5} m/s, which was similar to results from locations with very

moist or saturated soils. A large boulder, ice lens, or other zone of low permeability may have been located directly below the test site and limited infiltration.

Tabulated values of hydraulic conductivity for earth materials (Table 3.6) (Domenico and Schwartz, 1990) corroborated results of the infiltration tests. Table 3.6 designates the deposit composed of Pleistocene/Tertiary diamicton (mean infiltration capacity 4.31×10^{-4} m/s) as medium/coarse sands and gravel (range 9×10^{-7} to 3×10^{-2} m/s), the Quaternary colluvium (mean 4.07×10^{-5} m/s) and Tertiary syenite (mean 6.45×10^{-5} m/s) as sands (range 2×10^{-7} to 6×10^{-3} m/s), and the Tertiary quartz monzonite (mean 3.41×10^{-4} m/s) as fractured igneous and metamorphic rocks (range 8×10^{-9} to 3×10^{-4} m/s). Table 3.6 suggests the material overlying Silver Plume quartz monzonite (mean 3.14×10^{-4} m/s) may be characterized as either medium/coarse sands and gravel (range 9×10^{-7} to 3×10^{-2} m/s) or fractured igneous and metamorphic rocks (range 8×10^{-9} to 3×10^{-4} m/s), which makes sense because depth to bedrock above the Silver Plume can be up to 10 m and infiltrating water likely did not reach bedrock over the duration of the infiltration test.

Hamann (2002) conducted infiltration tests at the Saddle site using a single-ring infiltrometer and the constant water-level method. She found that infiltration ranged from 5.6×10^{-8} to 2.9×10^{-6} m/s, which is lower than the rates measured during this study. Hamann conducted the tests during the snowmelt season when the ground was likely partially frozen. Frozen ground limits infiltration, which may explain the lower infiltration rates.

		Hydraulic conductivity (m/s)
Sedimentary rocks	Karst limestone	$1 \times 10^{-6} - 2 \times 10^{-2}$
	Limestone and dolostone	$1 \times 10^{-9} - 6 \times 10^{-6}$
	Sandstone	$3 \times 10^{-10} - 6 \times 10^{-6}$
	Siltstone	$1 \times 10^{-11} - 1 \times 10^{-8}$
	Salt	$1 \times 10^{-12} - 1 \times 10^{-10}$
	Anhydrite	$4 \times 10^{-13} - 2 \times 10^{-8}$
	Shale	$1 \times 10^{-13} - 2 \times 10^{-9}$
Crystalline rocks	Weathered granite	$3 \times 10^{-6} - 5 \times 10^{-5}$
	Weathered gabbro	$6 \times 10^{-7} - 4 \times 10^{-6}$
	Permeable basalt	$4 \times 10^{-7} - 2 \times 10^{-2}$
	Fractured igneous and metamorphic rocks	$8 \times 10^{-9} - 3 \times 10^{-4}$
	Basalt	$2 \times 10^{-11} - 4 \times 10^{-7}$
	Unfractured igneous and metamorphic bedrock	$3 \times 10^{-14} - 2 \times 10^{-10}$
Unconsolidated sediments	Gravel	$3 \times 10^{-4} - 3 \times 10^{-2}$
	Coarse sand	$9 \times 10^{-7} - 6 \times 10^{-3}$
	Medium sand	$9 \times 10^{-7} - 5 \times 10^{-4}$
	Fine sand	$2 \times 10^{-7} - 2 \times 10^{-4}$
	Silt, loess	$1 \times 10^{-9} - 2 \times 10^{-5}$
	Clay	$1 \times 10^{-11} - 5 \times 10^{-9}$
	Till	$1 \times 10^{-12} - 2 \times 10^{-6}$
	Unweathered marine clay	$8 \times 10^{-13} - 2 \times 10^{-9}$

Table 3.6. Reported values of hydraulic conductivity for unconsolidated materials and rocks (modified from Domenico and Schwartz, 1990).

3.3 Estimation of aquifer hydraulic conductivity

3.3.1 Background on hydraulic conductivity

In order to characterize recharge and groundwater flow, the hydraulic conductivity of the aquifer must be known. Hydraulic conductivity is the ability of a saturated porous medium to transmit fluid (Fetter, 2001). It is a function of both the medium and the fluid flowing through the medium. An aquifer composed of rock with small pores or pores that are not well connected will not transmit water efficiently and will have a lower hydraulic conductivity. An aquifer filled with a viscous fluid, such as crude oil, will have a lower hydraulic conductivity than an aquifer filled with water. In this study, the fluid considered is water.

Values of hydraulic conductivity range over twelve orders of magnitude (Table 3.6) (Domenico and Schwartz, 1990). The hydraulic conductivity of unconsolidated sediments is

generally high and ranges from 10^{-13} to 10^{-2} m/s. The hydraulic conductivity of unfractured rock is low, ranging from 10^{-14} to 10^{-6} m/s, but can increase to 10^{-9} to 10^{-2} m/s in rock containing faults, fractures, or karst.

Henry Darcy, a French hydraulic engineer, first described in 1856 the relationship between the bulk flow of water through a saturated porous medium and hydraulic gradient. Darcy's Law states that the discharge of water through saturated porous media proportional to the cross-sectional area through which flow occurs and the hydraulic gradient:

$$Q = -AK\frac{\Delta h}{\Delta l} \qquad [3.2]$$

where Q is the discharge or volume flow rate [L^3/T], A is cross-sectional area [L^2], K is the proportionality constant, saturated hydraulic conductivity [L/T], h is hydraulic head, and l is the length of flow. $\Delta h/\Delta l$ is the hydraulic gradient [1]. The negative sign in Darcy's Law indicates that groundwater flow is in the direction of decreasing hydraulic head. Darcy's Law can also be expressed in terms of specific discharge:

$$q = \frac{Q}{A} = -K\frac{\Delta h}{\Delta l} \qquad [3.3]$$

where q is specific discharge or Darcy velocity [L/T] that describes the flow rate.

Hydraulic conductivity is used to estimate groundwater flow and recharge and identify aquifers with high yield for water supply. Hydraulic conductivity can be obtained from grain size analysis, laboratory measurements, and aquifer tests. Grain size analysis consists of evaluating lithologic logs of wells and drill cuttings and assigning a hydraulic conductivity value to each unit based on its grain size according to tabulated values. Hydraulic conductivity can be measured in a laboratory using a permeameter. Hydraulic conductivity is calculated using Darcy's Law and measurements of head and rate of water flow from the permeameter. The

primary limitation of grain size analysis and laboratory tests is that only a small volume of material is evaluated, which may not represent the bulk properties of the aquifer.

Aquifer tests integrate a larger volume of aquifer material to estimate the hydraulic properties of an aquifer. In an aquifer test, a head gradient is induced between a test well and the surrounding aquifer. Changes in hydraulic head in response to the induced head gradient are measured and used to calculate hydraulic conductivity and storage parameters. The accuracy of estimated parameters depends on the reliability of the aquifer test data, which is largely contingent on the quality of well construction and proper execution of test protocol. There are two categories of aquifer tests. The first is pumping tests in which a well is pumped and the rate of water level decline in a nearby well is measured. The second is slug tests in which a small volume of water is displaced in a well and the rate of water level change in the test well is measured. The advantage of pumping tests over slug tests is that hydraulic parameters are provided for a larger volume of aquifer material. The advantage of slug tests is that they are cost effective, relatively quick and easy to employ, no water needs to be handled, only one well is required, and analysis is more straightforward (Butler, 1998).

Slug tests have been used extensively to measure hydraulic conductivity in the field since the pioneering work of Hvorslev in 1951 (Butler, 1998; Weight, 2008). During a slug test, after a near-instantaneous change in hydraulic head is imposed in a well through the introduction or removal of a slug in the well, recovery of hydraulic head is measured (Butler, 1998). A slug can be a known volume of water, but is most often a solid object of known volume. When the slug is added to the well, the water level rapidly rises and then slowly falls as it recovers. This test is called a *falling-head* or *slug* test. When the slug is removed from the well, the water level rapidly drops and then slowly rises as it recovers. This test is called a *rising-head* or *bail* test. A

pressure transducer is typically used to measure the water level over time. During both falling-head and rising-head tests, the recovery of the water level, or hydraulic head, is measured until the displaced water level returns to its pre-test static level. The time required for hydraulic head to return to static conditions is proportional to the hydraulic conductivity of the near-well aquifer materials affected by the perturbed groundwater. Mathematical models of idealized test conditions are used to analyze the recovery data and calculate hydraulic conductivity. The geometry for a falling-head slug test in an unconfined aquifer is shown in Figure 3.17.

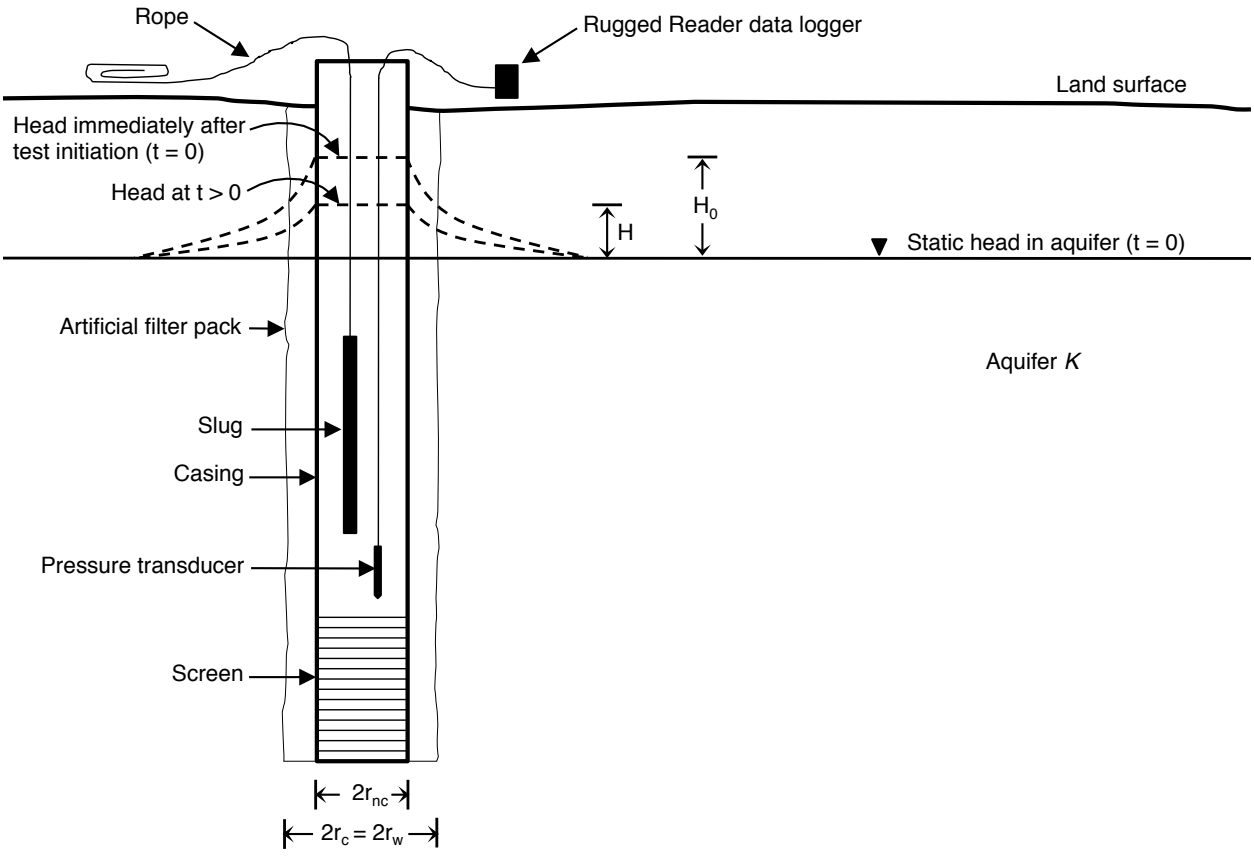

Figure 3.17. Schematic showing the geometry for a falling-head slug test in an unconfined aquifer (adapted from Butler, 1998 and Weight, 2008). See Appendix I for notation definitions.

3.3.2 Design of the slug test

For aquifer material below the water table, hydraulic conductivity was obtained from the results of slug tests conducted in selected wells at the Saddle and Martinelli sites. The slug tests,

field protocol, and data analysis were designed and executed following the guidelines of Butler (1998).

Three slug sizes were used (Figure 3.18). The small, medium, and large slugs were 0.75 m, 1.08 m, and 1.61 m long, respectively. The dimensions of each slug are listed in Table 3.7. The slugs were constructed from 0.032 m or 0.034 m diameter PVC pipe filled with sand. PVC end caps were glued on both ends of the PVC pipe to form a watertight seal. A stainless-steel eyebolt was screwed into the top end of each slug and a long rope was attached to each eyebolt.

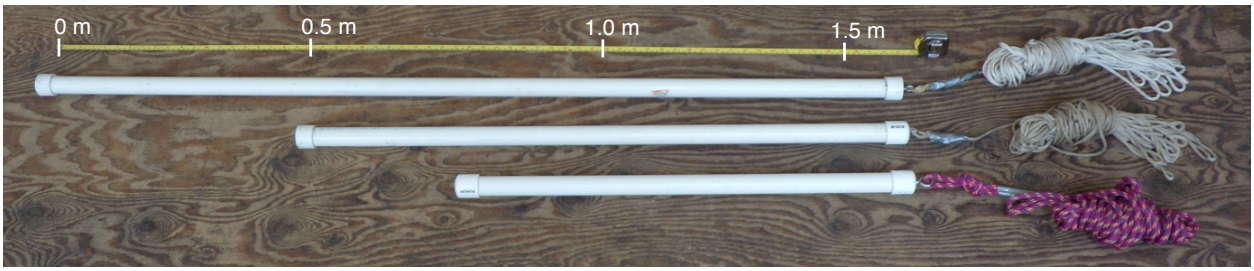

Figure 3.18. Photograph of the three PVC slugs used to conduct slug tests. The small, medium, and large slugs were 0.75 m, 1.08 m, and 1.61 m long, respectively.

Slug size	Length (m)	Radius (m)	Volume (m^3)	H_0^* (m)
Small	0.71	0.016	6.41E-04	0.336
Medium	1.08	0.016	8.59E-04	0.450
Large	1.61	0.016	1.28E-03	0.669

H_0^* = expected inititial displacement

Table 3.7. Dimensions of the PVC slugs used to conduct slug tests.

Slug tests were conducted in each of the deep piezometers at the Saddle site on 9 and 14 July 2011 and at the Martinelli site on 12 August 2011. Tests were not conducted in MD1 because the well casing above ground was broken and the slug could not be inserted into the well. The series of tests performed in each test well is listed in Table 3.8. Slug tests were not conducted in the shallow piezometers because the top of the well screen coincides with the ground surface in the shallow piezometers. Instead, infiltration tests were conducted near each shallow piezometer to test the hydraulic conductivity of the near-surface material (Section 3.2).

Well	Dominant geology of the screened interval	Test date	WT position with respect to TOS	Test No.	Test type	Slug size	H_0^* (m)	H_0 (m)	Translation method used?
SD1	sand overlying Ysp	7/9/11	1.1 m above TOS	1	Falling-head	Large	0.669	0.139	Yes
				1	Rising-head	Large	0.669	0.272	Yes
				2	Falling-head	Small	0.336	0.075	Yes
				2	Rising-head	Small	0.336	0.101	Yes
				3	Falling-head	Large	0.669	0.140	Yes
				3	Rising-head	Large	0.669	0.315	Yes
SD2	Tqm	7/14/11	5.6 m above TOS	1	Falling-head	Large	0.669	-	-
				1	Rising-head	Large	0.669	0.183	Yes
				2	Falling-head	Small	0.336	0.171	No
				2	Rising-head	Small	0.336	0.140	Yes
				3	Falling-head	Large	0.669	0.456	No
				3	Rising-head	Large	0.669	0.177	Yes
SD3	Tqm	7/9/11	7.2 m above TOS	1	Falling-head	Large	0.669	-0.349	No
				1	Rising-head	Large	0.669	0.137	No
				2	Falling-head	Medium	0.450	-0.211	No
				2	Rising-head	Medium	0.450	0.138	No
				3	Falling-head	Large	0.669	-0.258	No
				3	Rising-head	Large	0.669	0.171	No
SD4	Tqm	7/9/11	4.72 m above TOS	1	Falling-head	Large	0.669	0.378	Yes
				1	Rising-head	Large	0.669	0.548	Yes
				2	Falling-head	Medium	0.450	-	-
				2	Rising-head	Medium	0.450	0.452	No
				3	Falling-head	Large	0.669	0.670	Yes
				3	Rising-head	Large	0.669	0.556	Yes
MD1	Qc: coarse sand	-	-	-	-	-	-	-	-
MD2	QTd: sand	8/12/11	1.49 m above TOS	1	Falling-head	Large	0.669	0.764	No
				1	Rising-head	Large	0.669	0.877	No
				2	Falling-head	Medium	0.450	0.756	No
				2	Rising-head	Medium	0.450	0.702	No
				3	Falling-head	Large	0.669	1.168	No
				3	Rising-head	Large	0.669	0.803	No
MD3	QTd: sand/gravel	8/12/11	1.65 m above TOS	1	Falling-head	Large	0.669	1.078	No
				1	Rising-head	Large	0.669	0.484	No
				2	Falling-head	Medium	0.450	0.603	No
				2	Rising-head	Medium	0.450	0.422	No
				3	Falling-head	Large	0.669	0.989	No
				3	Rising-head	Large	0.669	0.518	No

Ysp = Precambrian Silver Plume quartz monzonite, Tqm = Tertiary quartz monzonite, Qc = Quaternary colluvium, QTd = Quaternary/Tertiary diamicton, WT = water table, TOS = top of screen, H_0^* = expected initial displacement, H_0 = measured initial displacement, r_{nc} = nominal casing radius, r_c = effective well casing radius, K = hydraulic conductivity, H_0^+ = apparent value for initial displacement, L_e = effective length of water column in well, C_d = dimensionless damping parameter

Table 3.8. Results of the slug tests conducted at the Saddle and Martinelli sites. Geology of the screened interval was determined from driller's logs and the geologic map by Gable and Madole (1976). See Appendix III for details on slug test analysis models.

Well	Model	r_{nc} (m)	Calculated r_c (m)	Method to calculate r_c	K (m/s)	H_0^+ (m)	L_e (m)	C_d
SD1	Bouwer-Rice, unconfined (1976)	0.025	0.214	Equation 4.6b	1.51E-05	0.009		
	Bouwer-Rice, unconfined (1976)	0.025	0.054	Equation 4.6b	4.60E-06	0.138		
	Bouwer-Rice, unconfined (1976)	0.025	0.066	Equation 4.6b	8.99E-06	0.047		
	Bouwer-Rice, unconfined (1976)	0.025	0.055	Equation 4.6b	7.48E-06	0.067		
	Bouwer-Rice, unconfined (1976)	0.025	0.070	Equation 4.6b	9.31E-06	0.082		
	Bouwer-Rice, unconfined (1976)	0.025	0.053	Equation 4.6b	5.08E-06	0.148		
				Mean:	**8.42E-06**	**0.082**		
				Standard deviation:	**3.80E-06**	**0.054**		
SD2	-	0.025	-	-	-	-	-	-
	-	0.025	-	-	-	-	-	-
	-	0.025	-	-	-	-	-	-
	-	0.025	-	-	-	-	-	-
	-	0.025	-	-	-	-	-	-
	-	0.025	-	-	-	-	-	-
				Mean:	**-**	**-**	**-**	**-**
				Standard deviation:	**-**	**-**	**-**	**-**
SD3	Springer-Gelhar (1991)	0.025	-	-	1.19E-03		7.884	0.72
	Springer-Gelhar (1991)	0.025	-	-	1.78E-03		8.122	0.48
	Springer-Gelhar (1991)	0.025	-	-	1.32E-03		7.862	0.65
	Springer-Gelhar (1991)	0.025	-	-	1.76E-03		8.328	0.48
	Springer-Gelhar (1991)	0.025	-	-	1.23E-03		9.353	0.64
	Springer-Gelhar (1991)	0.025	-	-	1.80E-03		7.824	0.48
				Mean:	**1.51E-03**		**8.229**	**0.57**
				Standard deviation:	**2.96E-04**		**0.584**	**0.11**
SD4	Hvorslev, unconfined (1951)	0.025	0.033	Equation 4.5b	1.07E-04	0.014		
	Hvorslev, unconfined (1951)	0.025	0.027	Equation 4.5b	1.67E-04	0.306		
	-	0.025	-	-	-	-		
	Hvorslev, unconfined (1951)	0.025	-	-	8.19E-05	0.239		
	Hvorslev, unconfined (1951)	0.025	-	-	7.65E-05	0.209		
	Hvorslev, unconfined (1951)	0.025	0.027	Equation 4.5b	1.04E-04	0.382		
				Mean:	**1.07E-04**	**0.230**		
				Standard deviation:	**3.58E-05**	**0.138**		
MD1	-	0.025	-	-	-	-	-	-
MD2	Dagan, unconfined (1978)	0.025	-	-	9.63E-05	0.351		
	Dagan, unconfined (1978)	0.025	-	-	1.11E-04	0.422		
	Dagan, unconfined (1978)	0.025	-	-	9.20E-05	0.219		
	Dagan, unconfined (1978)	0.025	-	-	9.53E-05	0.270		
	Dagan, unconfined (1978)	0.025	-	-	1.04E-04	0.326		
	Dagan, unconfined (1978)	0.025	-	-	9.14E-05	0.390		
				Mean:	**9.82E-05**	**0.330**		
				Standard deviation:	**7.56E-06**	**0.075**		
MD3	Dagan, unconfined (1978)	0.025	-	-	3.36E-04	0.473		
	Dagan, unconfined (1978)	0.025	0.029	Equation 4.5b	2.15E-04	0.278		
	Dagan, unconfined (1978)	0.025	-	-	4.07E-04	0.408		
	Dagan, unconfined (1978)	0.025	0.026	Equation 4.5b	1.93E-04	0.225		
	Dagan, unconfined (1978)	0.025	0.020	-	3.52E-04	0.411		
	Dagan, unconfined (1978)	0.025	-	Equation 4.5b	2.10E-04	0.327		
				Mean:	**2.85E-04**	**0.354**		
				Standard deviation:	**9.04E-05**	**0.093**		

Ysp = Precambrian Silver Plume quartz monzonite, Tqm = Tertiary quartz monzonite, Qc = Quaternary colluvium, QTd = Quaternary/Tertiary diamicton, WT = water table, TOS = top of screen, H_0^* = expected initial displacement, H_0 = measured initial displacement, r_{nc} = nominal casing radius, r_c = effective well casing radius, K = hydraulic conductivity, H_0^+ = apparent value for initial displacement, L_e = effective length of water column in well, C_d = dimensionless damping parameter

Table 3.8. (continued)

Butler (1998) lists the following criteria for the design of a slug test program: (1) conduct a minimum of three paired falling-head and rising-head tests per well, (2) the expected initial displacement (H_0^*) and measured initial displacement (H_0) should be in close agreement, (3) the magnitude of the initial displacement should vary between subsequent paired tests by at least a factor of two, (4) the first and last paired tests should be conduced with the same size slug, and (5) there should be a close match between observed response data and a theoretical type curve. Each of these criteria is discussed further below.

The first criterion states that a minimum of three paired falling-head and rising-head tests should be conducted per well. For this study, three paired tests were performed in each test well. A paired test consists of a falling-head test and a rising-head test in the same well. Using this method, six tests were conducted in each test well. The graphs of response data, normalized by the measured initial displacement, were plotted. Overlapped data were evidence that there was no dependence on the direction of flow. Falling-head and rising-head test data that did not coincide, but showed a dependence on flow direction (Figure 3.19), were indicative of well-skin effects or a changing water table position. A well skin is a zone in the immediate vicinity of the well that typically has a lower hydraulic conductivity than the surrounding formation.

Response data may be affected by a changing water table position in situations where the water table intersects the well screen and/or the filter pack. Changes in the water table position typically result in a reproducible dependence on flow direction (i.e. there is a repeatable difference between rising-head and falling-head response data) due to changes in the effective casing radius and/or the effective screen length through which groundwater flows during a test. In the case where the effective casing radius changes, normalized response data from falling-head tests will typically lag behind rising-head tests (Figure 3.19a). This pattern reflects the

larger effective casing radius during a falling-head test, which results from expansion of water into the unsaturated zone, and the relatively slow movement of water in the unsaturated zone due to capillary tension retarding the flow of water back into the well. During the paired rising-head test, the effective casing radius does not change as much and water moves relatively quickly in the saturated zone because there is no capillary tension. In this study, changes in effective casing radius were accounted for using Equation 3.4 or Equation 3.5 (discussed below).

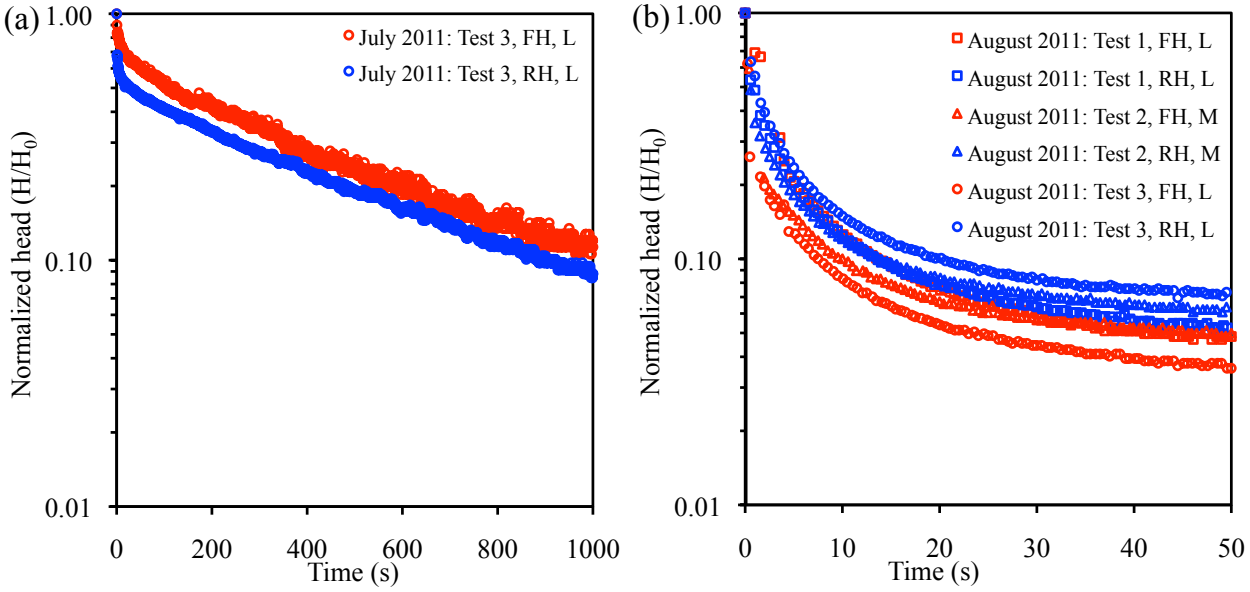

Figure 3.19. Dependence of response data on flow direction. (a) Plot showing normalized response data from a paired slug test conducted in well SD1. Data from the falling-head test lag behind data from the rising-head test indicating that the effective casing radius changed during testing due to a changing water table position. (b) Plot showing response data from the series of slug tests conducted in well MD2. Data from the rising-head test lag data from the falling-head test indicating that the effective screen length changed during testing due to a changing water table position.

In the case where changes in the effective screen length result in a reproducible dependence on flow direction, normalized response data from rising-head tests will typically lag behind falling-head tests (Figure 3.19b). In addition, the rising-head and falling-head response data often exhibit concave-down and concave-up shapes, respectively. In wells where the water table intersects the well screen or the filter pack, the effective screen length is larger during a

falling-head test than during a rising-head test due to a changing water table position. In other words, even though the same volume of water is displaced during the rising-head and falling-head tests, however during the falling-head test, that volume of water has a larger area of screen to flow through because the water table moved upward upon introduction of the slug. For slug tests during which the effective screen length changed, the Dagan method (Dagan, 1978) was used to solve for hydraulic conductivity.

The second, third, and forth criteria concern the magnitude of the initial displacement. Criterion (2) requires a comparison between the expected initial displacement (H_0^*) and measured initial displacement (H_0). In wells where the water table intersected either the screen or the filter pack, close agreement between H_0^* and H_0 indicated that the effective casing radius was not changing during the test and the nominal casing radius could be used in data analysis. A H_0 value that was less than H_0^* suggests that the effective casing radius was larger than the nominal casing radius. Response data were analyzed using an effective casing radius calculated from the following mass balance equation (Butler, 1998 Equations 3.1 and 3.2):

$$\pi r_c^2 H_0 = \pi r_{nc}^2 H_0^* \qquad [3.4a]$$

which can be rewritten as:

$$r_c = r_{nc}\sqrt{\frac{H_0^*}{H_0}} \qquad [3.4b]$$

where r_c is effective casing radius, and r_{nc} is nominal casing radius.

In wells where the filter pack intersects the water table and the filter pack is markedly more permeable than the formation, the plot of normalized response data will likely exhibit a double-straight line (Figure 3.20). This response is due to rapid drainage of the filter pack (the first straight line) followed by a slower response reflecting the hydraulic conductivity of the

formation (the second straight line). In these cases, response data were analyzed using an effective casing radius calculated from the following equation, which incorporates the drainable porosity of the filter pack (Butler, 1998 Equations 6.11a and 6.11b):

$$H_0^* \pi r_{nc}^2 = H_0^+ \pi (r_{nc}^2 + n(r_w^2 - r_{nc}^2)) = H_0^+ \pi r_c^2 \qquad [3.5a]$$

where n is drainable porosity of the filter pack [1] and r_w is effective well screen radius [L]. Equation 3.5a can be rewritten as:

$$r_c = r_{nc} \sqrt{\frac{H_0^*}{H_0^+}} \qquad [3.5b]$$

where H_0^+ is the apparent magnitude of the initial displacement estimated from the y-intercept of the fitted straight line to the second straight-line segment. Equation 3.5b accounts for n without having to provide an estimate of n.

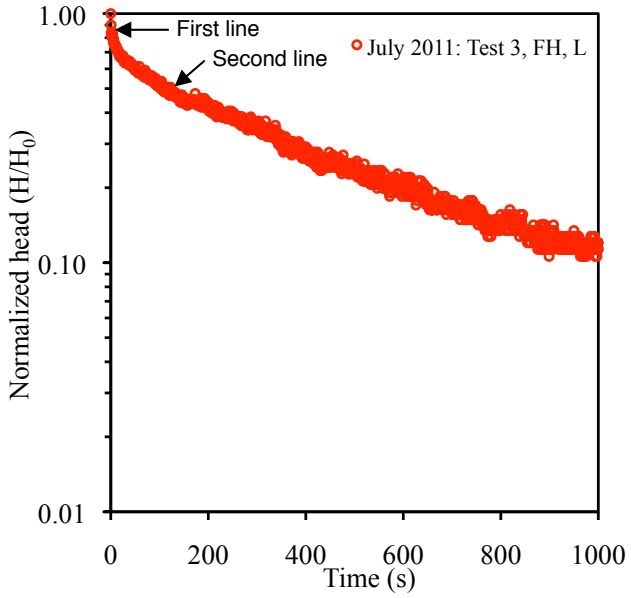

Figure 3.20. Plot showing normalized response data from a falling-head test conducted in SD1. Data exhibit a double-straight line because the filter pack in SD1 intersects the water table, which caused a change in effective casing radius. The first line segment reflects rapid filter pack drainage. The second line segment reflects slower response of the formation. Data showing a double-straight line were analyzed using an effective casing radius calculated from Equation 3.5.

Per criterion (3), the magnitude of the initial displacement (H_0) was varied between subsequent paired tests by varying the size of the slug used. The dimensions of the three sizes of slugs used in this study are listed in Table 3.7. Larger slugs were preferred over smaller slugs in order to test the greatest volume of aquifer possible. For that reason, H_0 was not necessarily varied by the minimum factor of two recommended by Butler (1998). The particular slug sizes selected for use in each test well depended on the volume of standing water in the well prior to test initiation. The slug needed to be small enough that it would be fully submerged when added to the well. In wells with a larger volume of standing water, larger size slugs were used. In wells with a smaller volume of standing water, smaller size slugs were used. The slug sizes used for each test are listed in Table 3.8.

The graphs of normalized response data from tests using different sized slugs should coincide to indicate that the response data are independent of H_0 (Figure 3.21a). If they do not coincide (Figure 3.21b), there is a dependence on H_0 due to either a changing water table position or dynamic well-skin effects (Butler, 1998). In the case of a changing water table position, the dependence on H_0 is often reproducible such that tests conducted with the same size slug coincide, but tests conducted with different size slugs do not coincide (Figure 3.21b). A reproducible dependence on H_0 indicated that the Dagan method should be used.

The forth criterion recommends that the first and last paired tests be conducted with the same size slug to detect dynamic well-skin effects. In this study, the large size slug was used for the first and last paired test at all test wells. Plots of normalized response data in which the first and last tests did not coincide were evidence of a well skin changing position with each subsequent test. No theoretical models are available to estimate hydraulic conductivity in wells with dynamic skins.

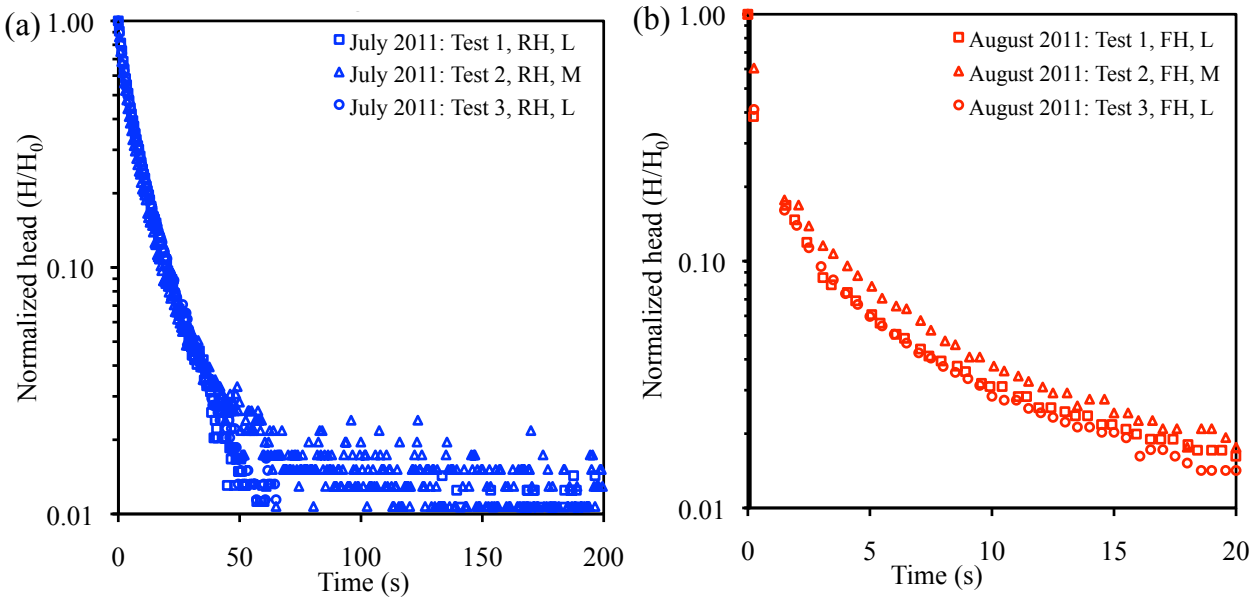

Figure 3.21. Dependence on observed initial displacement (H_0). (a) Plot showing normalized response data from a series of tests conducted in well SD4. The response data from tests conducted with medium (M) and large (L) slugs coincide indicating that there was no dependence on H_0. (b) Plot showing normalized response data from a series of tests conducted in well MD3. The response data from tests conducted with the same size slug (L) coincide, but tests conducted with different size slugs (M and L) do not coincide, indicating that there was a reproducible dependence on H_0.

The final criterion states that observed response data should closely match a theoretical type curve. If the normalized response data, plotted on log-linear axes, were not linear, then conventional theoretical models could not be used to estimate hydraulic conductivity. The exception to this rule was data that displayed a concave-up curvature (e.g. Figure 3.33). For wells screened across the water table, this pattern was caused by drainage of the filter pack and the Bouwer-Rice (1976) model was used. For wells screened below the water table, this pattern was caused by the effect of elastic storage mechanisms and the Hvorslev (1951) or Dagan (1978) model were used (Butler, 1998). For response data that displayed an oscillatory shape, an unconventional model (Springer and Gelhar, 1991) was used to estimate hydraulic conductivity.

3.3.3 Field protocol

The following protocol was followed to perform slug tests in the deep piezometers at the Saddle and Martinelli sites.

1. General information about the well was recorded including casing stick-up, total depth, location and length of screen, radius of casing and screen, length and radius of filter pack.
2. A static water level measurement was made. The water level was checked a few times prior to beginning the test to verify static water level was constant.
3. Calculations were made to determine which size slugs to use. The entire slug needed to be submerged upon introduction to the well. In addition, there needed to be at least 0.3 m between the bottom of the slug and the top of the pressure transducer. Smaller slugs were used in wells in which the water level was relatively low. A mark was made on the rope attached to the slug at the point where, when the slug was submerged, the mark on the rope would be at the top of the well casing and the bottom of the slug would be 0.3 m above the pressure transducer.
4. The selected slug size also depended on the location of the top of the well screen with respect to static water level. In wells where the water table was above the screen, it was preferable to not allow the water level to drop below the top of the screen during a rising-head test. Calculations were made to verify that the expected initial displacement (H_0) during a rising-head test, which depended on the slug size, would maintain a minimum of 0.1 m of head above the top of the screen. In wells screened across the water table, this step would have been skipped. However, all tests in this study were run in wells where the water table was above the top of the screen.

5. Calculations were then made to determine the height to set the pressure transducer in the water column. The pressure transducer should be placed close to static water level to avoid the need for type-curve correction for the effects of water-column acceleration on pressure transducer data collection (Butler et al., 2003). The pressure transducer was set at a depth such that the slug would be fully submerged and there was 0.3 m between the bottom of the slug and the top of the pressure transducer.
6. After all calculations were complete, an In-Situ Level Troll© 700 pressure transducer connected to a cable was lowered to the calculated position. The cable coming from the pressure transducer was secured to the well casing so that the transducer did not move during the test. The cable was connected to an In-Situ Rugged Reader© data logger and the logger was set up to begin the test. The data logger was programmed to collect a data point every 0.5 s.
7. The static water level was measured with an electrical water-level indicator again to ensure it had returned to static after emplacement of the pressure transducer. In addition, water level reported by the data logger was checked to verify consistency with the manual measurement.
8. Falling-head tests were conducted before rising-head tests to save time in the field. Figure 3.22a shows the author preparing for a falling-head test. Figure 3.22b shows a falling-head test in progress. The falling-head test was performed with the following procedure.
    a. The slug was lowered into the well until the bottom of the slug was just above the static water level. Placing the slug in this position minimized oscillation of the water level, which can result in erroneously large pressure transducer readings.

b. Data logger recording began shortly before the slug was rapidly and completely submerged below the static water column in the well. The slug should be introduced "instantaneously" relative to the formation response.

c. The slug was stopped from falling into the well when the marked point on the rope from Step 2 reached the top of the well casing. The rope was tied off.

d. H_0 was determined by examining the test log and identifying the data point of greatest displacement. Data recording continued until residual deviation from static returned to less than or equal to 5% of H_0 (Butler, 1998). The static water level was measured with an electrical water-level indicator to confirm that this was the case. Then, data collection was stopped. The slug was left in position in preparation for the paired rising-head test.

9. The rising-head test was performed with the following procedure.

   a. A new test was set up on the data logger. Recording began shortly before the slug was rapidly and completely removed from the well.

   b. Recording continued until the residual deviation from static returned to less than or equal to 5% of H_0. The static water level was measured with an electrical water-level indicator to confirm that this was the case. Then, data collection was stopped.

10. Steps 8 and 9 were repeated two more times to obtain a total of three paired tests in a single well. The second paired test was performed with a smaller size slug. The third paired test was performed with the same size slug as the first paired test.

11. Steps 1 through 10 were repeated in each well of interest. Because water quality was high and cross-contamination was not a concern, the slug and pressure transducer did not need to be decontaminated before transfer to another well.

12. In-Situ Win-Situ 5© software was used to download the data from the pressure transducer to the data logger and from the data logger to a personal computer.
13. The data were then pre-processed and the appropriate theoretical model was selected to estimate hydraulic conductivity of the near-well aquifer material. These steps are explained in the following sections.

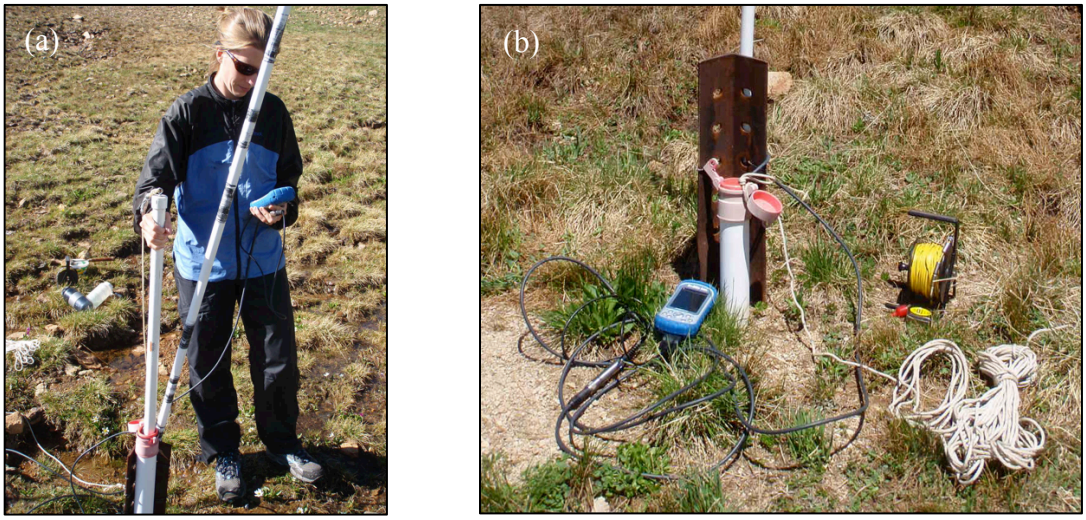

Figure 3.22. (a) Photograph of the author preparing for a falling-head test. (b) Photograph of a falling-head test in progress. The cable going into the well connects the Rugged Reader© data logger, shown left of the well, to the pressure transducer. The rope going into the well is attached to the slug.

3.3.4 Data analysis

The first step in the analysis of slug test response data is preprocessing the data so that they are suitable for analysis with theoretical models. The pressure transducer response data were exported from Win-Situ 5© into Microsoft Excel©. The data were then converted from units of *level depth to water* to *deviation of total head from static conditions*. Static water level was determined from the average water level recorded prior to the introduction of the slug. This value was then subtracted from all *level depth to water* measurements. The absolute value was taken to get the positive *deviation of total head from static conditions.*

The next step in preprocessing response data was to determine the measured initial displacement (H_0) and the time of test initiation (t_0). H_0 was obtained from examination of the data record. t_0 was set equal to the time the slug was completely submerged (falling-head test) or withdrawn (rising-head test) minus any early-time noise in the response data. Noise resulted from non-instantaneous slug introduction relative to the formation response. A test was assumed to start following early-time noise. For response data that plotted linearly on log(H) versus t, the point (t_0, H_0) was located at the point immediately following early-time noise. For oscillatory response data, the point (t_0, H_0) was located at either a trough or a peak in the response data (Butler, 1998).

The third step in preprocessing the data was to normalize the *deviation of total head from static* data by the measured initial displacement (H_0). The *deviation of total head from static* data were divided (normalized) by H_0. The final step was to reinitialize the time record to the actual time at which the test began (when *deviation of total head from static* equaled H_0). The value of t_0 was subtracted from all recorded time values. Data prior to point (t_0, H_0) were deleted and data following point (t_0, H_0) were used in subsequent analysis. The final product of preprocessed data was a record of the deviation of head from static conditions that were normalized by H_0 and reinitialized to t_0. This new data set was then used to find hydraulic conductivity.

The theoretical model for calculating hydraulic conductivity was selected depending on the characteristics of the response data. For normalized response data that coincided when plotted together, were not dependent on H_0, and did not display evidence of filter pack drainage, the Hvorslev solution (Hvorslev, 1951) was matched to the data. For normalized response data that coincided when plotted together, were not dependent on H_0, and displayed evidence of filter

pack drainage (e.g. double straight-line effect), the Bouwer and Rice solution was matched to the data (Bouwer and Rice, 1976). For normalized response data that coincided when plotted together and displayed a reproducible dependence on H_0, the Dagan solution was matched to the data (Dagan, 1978). In highly conductive aquifers, the displaced column of water may recover quickly enough such that the momentum of the water column overcomes the viscous forces of the water. As a result, the water level in the well oscillates from above to below static water level. This response is termed underdamped. Normalized response data that displayed an oscillatory response were analyzed using the method of Springer and Gelhar (1991). Appendix III describes each of these models in detail.

Data analysis was implemented using AQTESOLV© version 4.5 computer software (Duffield, 2007). Analytical solutions within AQTESOLV© software were obtained by manually fitting the selected model to the normalized response data. The automatic curve-matching option was not used because it did not produce reasonable match between the data and the model.

3.3.5 Results: Slug tests

Table 3.8 lists information collected at each test location, methods used to estimate hydraulic conductivity, and the resultant hydraulic conductivity. The average hydraulic conductivity and standard deviation for each well is also listed. The hydraulic conductivities estimated from multiple tests performed in each well did not vary by more than a factor of four, which is reasonable considering that hydraulic conductivity of earth materials ranges over many orders of magnitude (Table 3.6). Figure 3.23 shows the spatial distribution, in relation to the topography and underlying geology, of average hydraulic conductivity calculated from the results of the slug tests. Slug tests were not performed in well MD1 because the well casing was

broken and the slug could not be inserted into the well. The following two sections present the results for the Saddle and Martinelli sites.

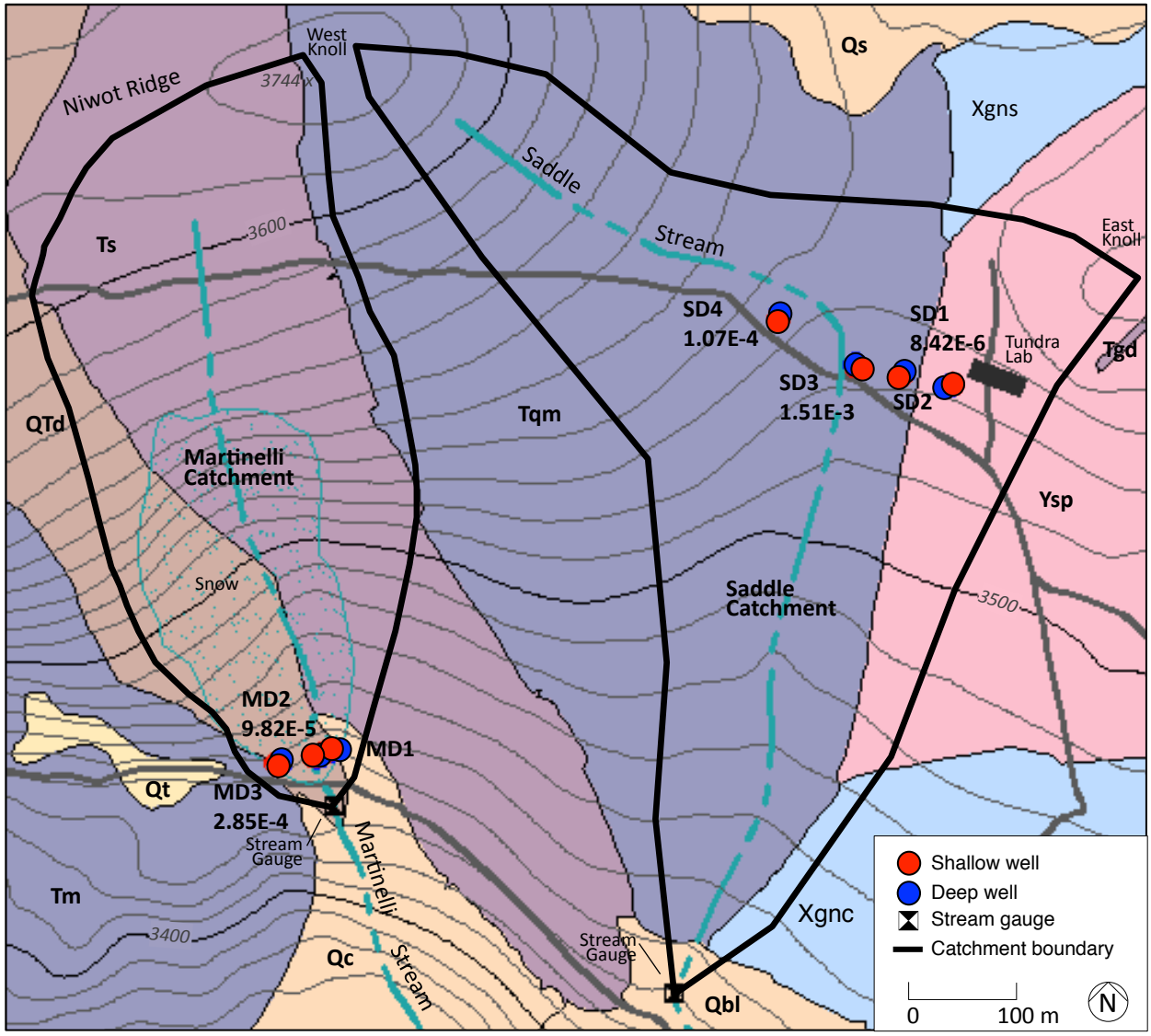

Figure 3.23. Map showing the spatial distribution, in relation to topography and underlying geology (Gable and Madole, 1976), of average hydraulic conductivity calculated from the results of slug tests. Three paired tests were conducted at each test location. Results are in m/s.

Saddle slug test results

Three paired slug tests were conducted in well SD1, which is screened across the contact between unconsolidated surficial deposits of sand and Precambrian Silver Plume quartz monzonite. Figure 3.24 shows that the normalized response data from the tests coincided. The

results of falling-head test 1 did not entirely coincide with the other results of the other tests, however within the recommended head range of 0.10−0.20 the deviation of falling-head test 1 from the other tests was relatively minor. Because the water table was near the top of the screened interval and the data exhibited a double-straight line indicative of filter pack drainage, the Bouwer and Rice method was used to estimate hydraulic conductivity of the aquifer around well SD1. Equation 3.5b was used to calculate the effective casing radius. Figure 3.25 shows the results of each falling-head and rising-head test with the best-fit line of the Bouwer and Rice model. Average hydraulic conductivity for the three paired tests was 8.42×10^{-6} m/s, which was the lowest value at both the Saddle and Martinelli sites. Tabulated values of hydraulic conductivity for earth materials place the results of slug tests in SD1 in the range of sands, silt, loess, fractured igneous and metamorphic rocks, and weathered granite (Table 3.6), which corresponds well with observed lithology of the screened interval.

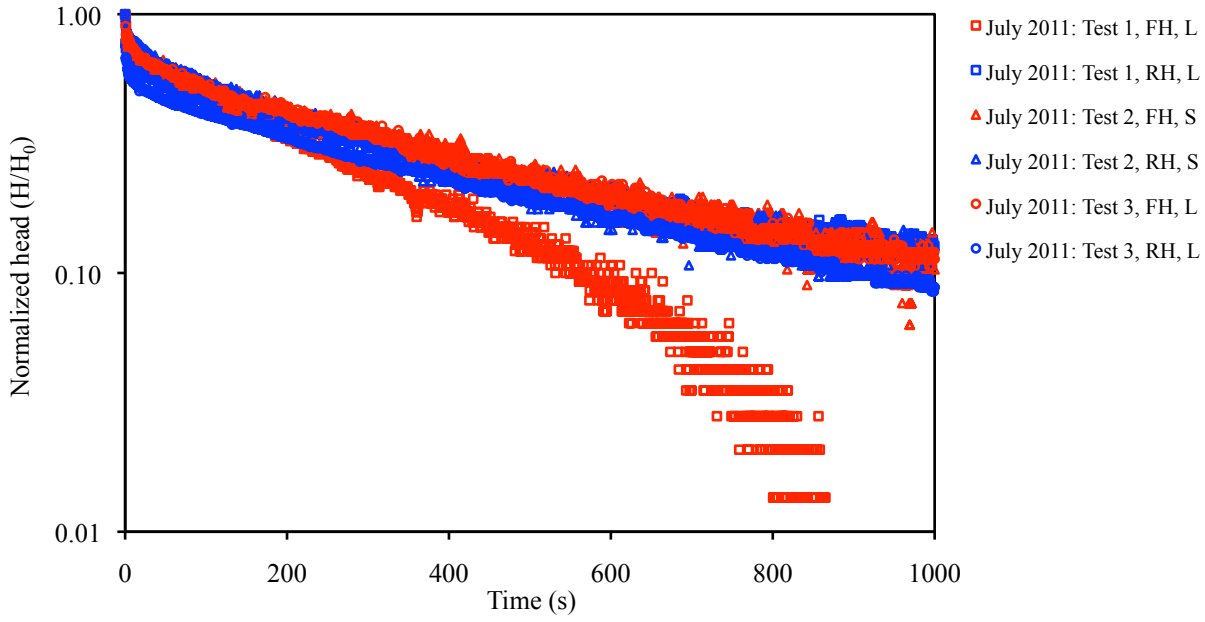

Figure 3.24. Normalized response data versus time for the series of slug tests performed in SD1.

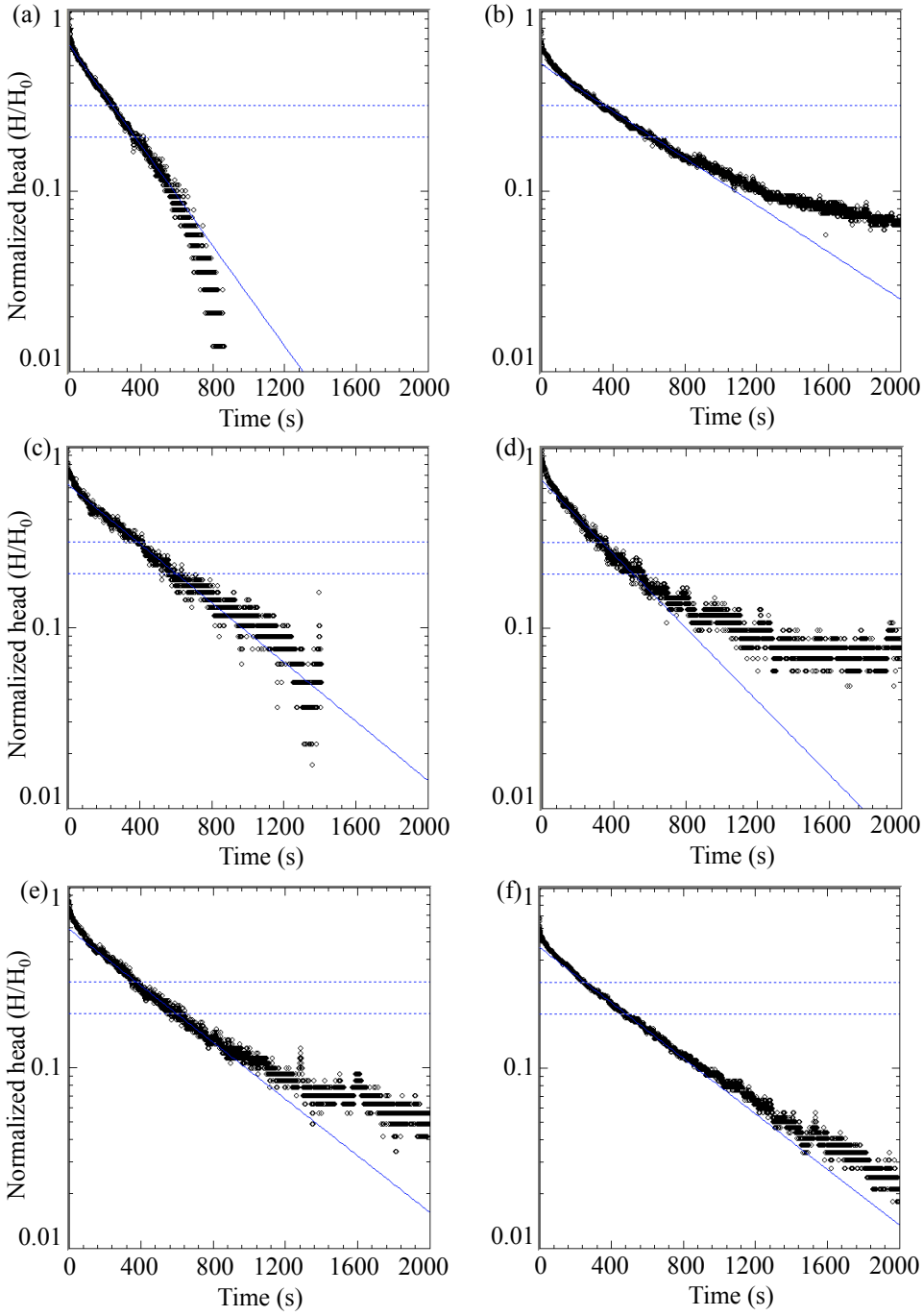

Figure 3.25. Normalized response data versus time for each slug test performed in well SD1: (a) test 1 falling-head large slug, (b) test 1 rising-head large slug, (c) test 2 falling-head small slug, (d) test 2 rising-head small slug, (e) test 3 falling-head large slug, (f) test 3 rising-head large slug. Solid line shows the Bouwer and Rice model fit to the response data. Dashed lines indicate the recommended head range.

Three paired slug tests were performed in well SD2, which is screened in Tertiary quartz monzonite. Figure 3.26 shows that the normalized response data from the tests were oscillatory. However, the oscillations did not fluctuate about static water level ($H/H_0 = 0$) and there was not a reproducible dependence on H_0, suggesting that a dynamic well skin or other mechanism was influencing the response. Each spring, a thick ice lens forms in well SD2. It is possible that during testing ice was present in the formation near the well, which would prevent water from flowing into and out of the test well and result in abnormal response data. The response data could not be analyzed with conventional theoretical models and a hydraulic conductivity value was not obtained for the material around well SD2.

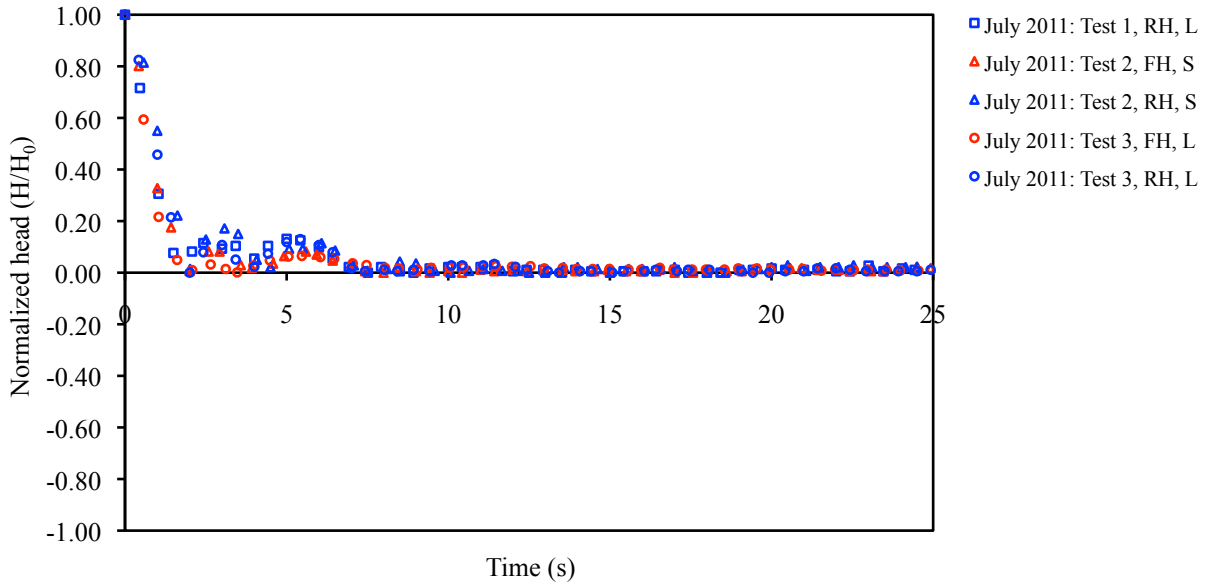

Figure 3.26. Normalized response data versus time for the series of slug tests performed in SD2.

Three paired slug tests were conducted in well SD3, which is screened in Tertiary quartz monzonite. Figure 3.27 shows that the normalized response data from the tests were oscillatory and that there was a dependence on both H_0 and flow direction. The Springer and Gelhar method was used to estimate hydraulic conductivity of the material around well SD3. Figure 3.28 shows the results of each falling-head and rising-head test with the best-fit curve of the Springer and Gelhar model. Average hydraulic conductivity for the three paired tests was 1.51×10^{-3} m/s, which was the highest rate measured at the Saddle and Martinelli sites. This value is slightly greater than the accepted range of 8×10^{-9} to 3×10^{-4} m/s for fractured igneous and metamorphic rocks (Table 3.6). The calculated hydraulic conductivity may be an overestimate of the actual hydraulic conductivity due to the movement of displaced water through the filter pack or the presence of larger fractures in the aquifer material around the well.

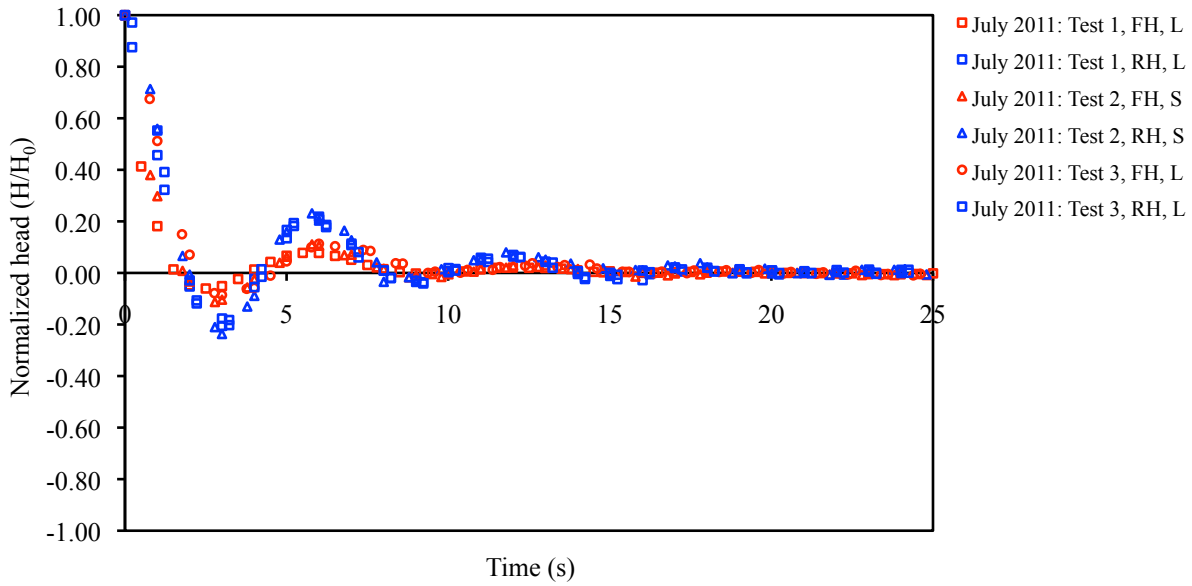

Figure 3.27. Normalized response data versus time for the series of slug tests performed in SD3.

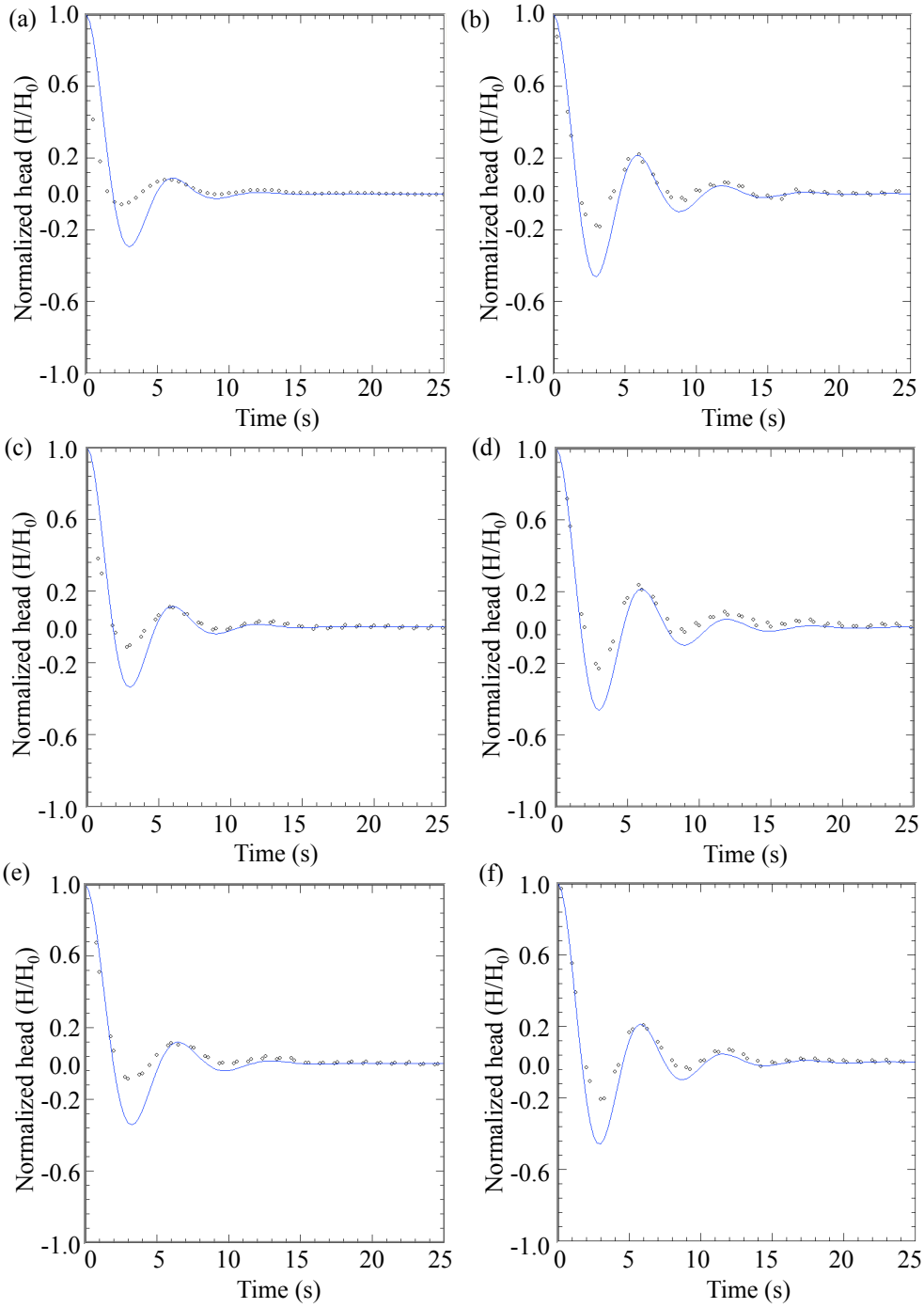

Figure 3.28. Normalized response data versus time for each slug test performed in well SD3: (a) test 1 falling-head large slug, (b) test 1 rising-head large slug, (c) test 2 falling-head medium slug, (d) test 2 rising-head medium slug, (e) test 3 falling-head large slug, (f) test 3 rising-head large slug. Solid line shows the Springer and Gelhar model fit to the response data.

Three paired slug tests were conducted in well SD4, which is screened in Tertiary quartz monzonite. Figure 3.29 shows that the normalized response data from the tests coincided. Because the static water table was above the top of the screened interval, the Hvorslev method was used to estimate hydraulic conductivity of the aquifer around well SD4. In cases where H_0 was less than H_0^*, indicating the effective casing radius was changing during the test, Equation 3.4b was used to calculate the effective casing radius. Figure 3.30 shows the results of each falling-head and rising-head test with the best-fit line of the Hvorslev model. The data logger failed during test 2 falling-head, so hydraulic conductivity was not obtained. Average hydraulic conductivity for the set of tests was 1.07×10^{-4} m/s, which corresponds with tabulated values of hydraulic conductivity for fractured igneous and metamorphic rocks (Table 3.6).

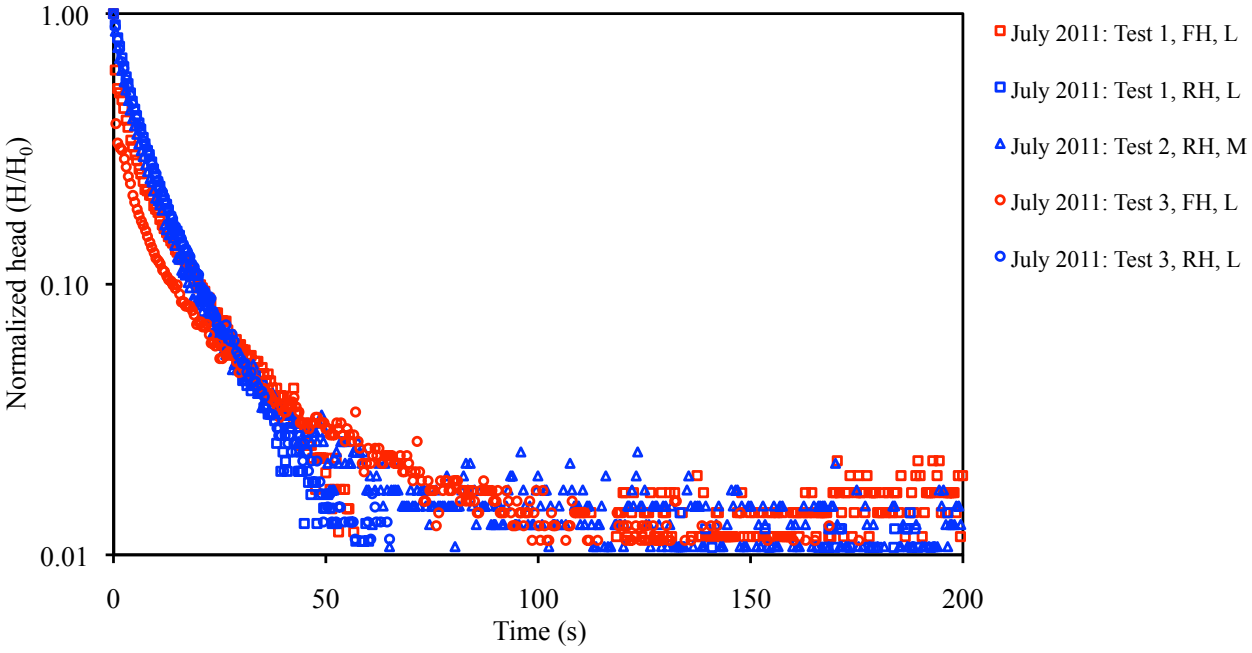

Figure 3.29. Normalized response data versus time for the series of slug tests performed in SD4.

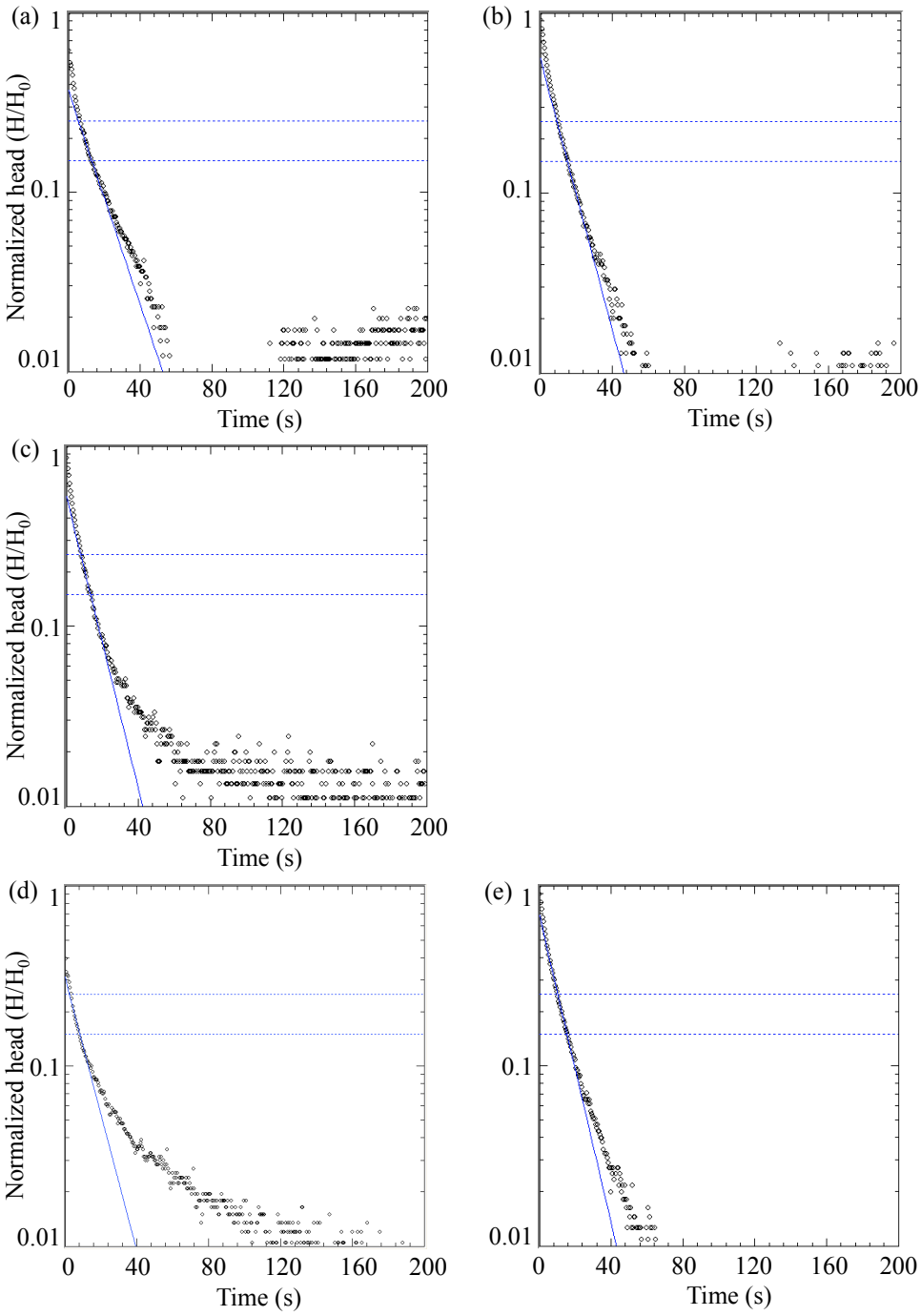

Figure 3.30. Normalized response data versus time for each slug test performed in well SD4: (a) test 1 falling-head large slug, (b) test 1 rising-head large slug, (c) test 2 rising-head medium slug, (d) test 3 falling-head large slug, (e) test 3 rising-head large slug. Solid line shows the Hvorslev model fit to the response data. Dashed lines indicate the recommended head range.

Martinelli slug test results

Three paired slug tests were conducted in well MD2, which is screened in Quaternary-Tertiary diamicton described as sand in the driller's log. Figure 3.31 shows that the normalized response data from the tests did not coincide, but there was a reproducible dependence on H_0 and flow direction. Since the data were not oscillatory, the Dagan method was used to calculate hydraulic conductivity of the aquifer around well MD2. The concave-up shape of plots in Figure 3.31 shows that elastic storage effects were influencing the data, so the straight line model was fit to normalized heads in the recommended range of 0.20−0.30. Figure 3.32 shows the results of each falling-head and rising-head test with the best-fit line of the Dagan model. Average hydraulic conductivity for the three paired tests was 9.82×10^{-5} m/s. Tabulated values of hydraulic conductivity place the results of slug tests in MD2 in the range of sands (Table 3.6), which corresponds with the observed lithology of the screened interval.

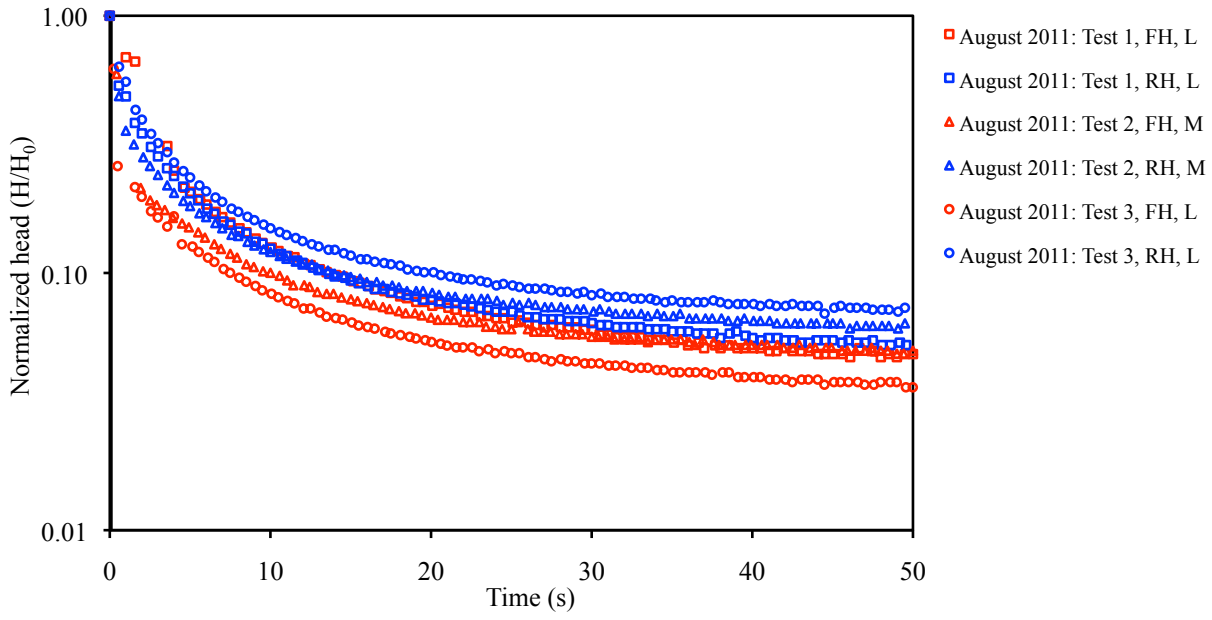

Figure 3.31. Normalized response data versus time for the series of slug tests performed in MD2.

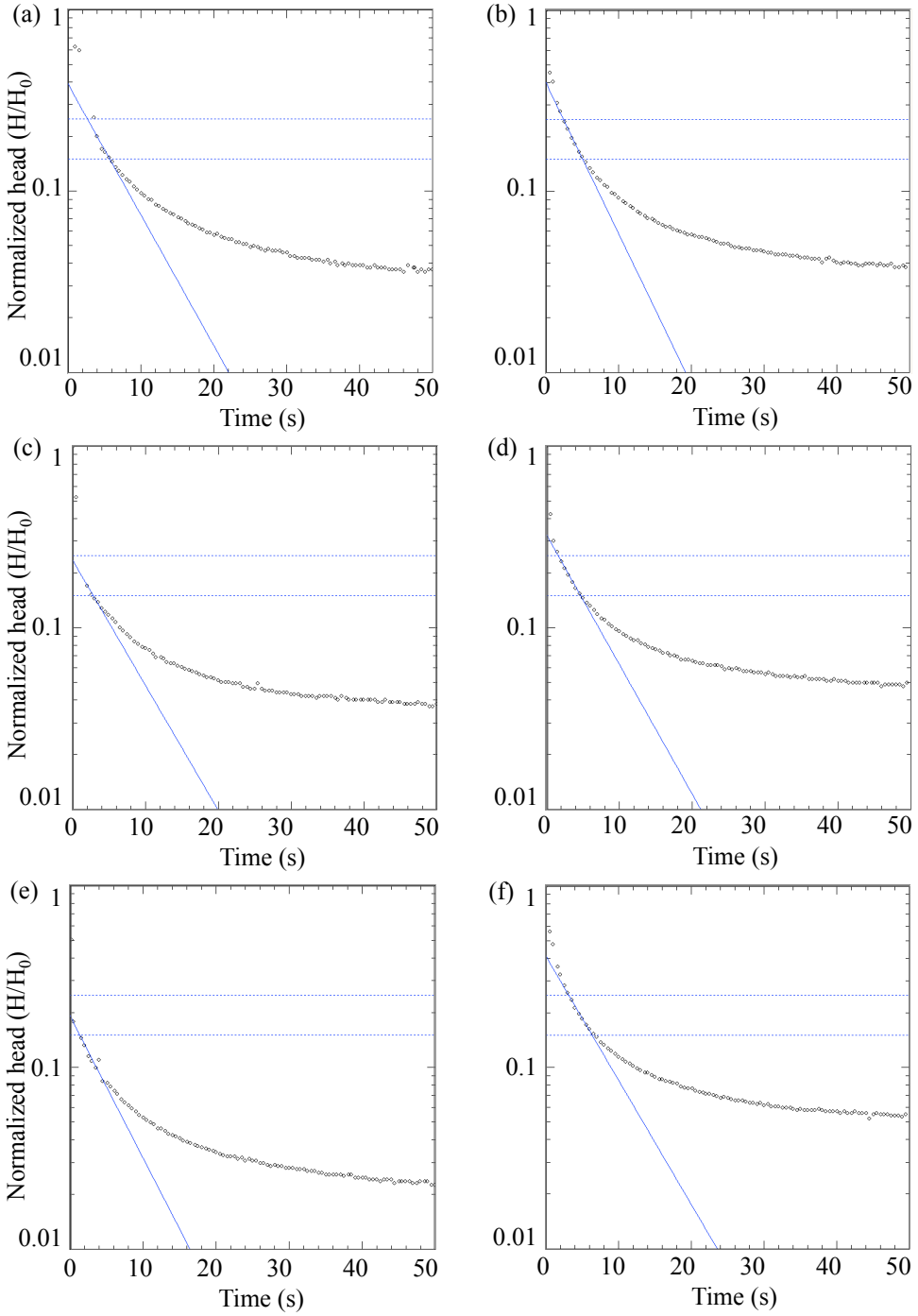

Figure 3.32. Normalized response data versus time for each slug test performed in well MD2: (a) test 1 falling-head large slug, (b) test 1 rising-head large slug, (c) test 2 falling-head medium slug, (d) test 2 rising-head medium slug, (e) test 3 falling-head large slug, (f) test 3 rising-head large slug. Solid line shows the Dagan model fit to the response data. Dashed lines indicate the recommended head range.

Three paired slug tests were conducted in well MD3, which is screened in Quaternary-Tertiary diamicton described as sand/gravel in the driller's log. Figure 3.33 shows that the normalized response data from the tests did not coincide, but were dependent on H_0 and strongly dependent on flow direction. Therefore, the Dagan method was used to calculate hydraulic conductivity of the aquifer around well MD3. In cases where H_0 was less than H_0^*, indicating that the effective casing radius was changing during the test, Equation 3.4b was used to calculate the effective casing radius. Similar to well MD2, the concave-up shape of plots indicates that elastic storage effects were influencing the data and the model was matched to normalized heads in the recommended range of 0.20−0.30. Figure 3.34 shows the results of each falling-head and rising-head test with the best-fit line of the Dagan model. Average hydraulic conductivity for the three paired tests was 2.85×10^{-4} m/s, which corresponds with tabulated values of hydraulic conductivity for sands (Table 3.6).

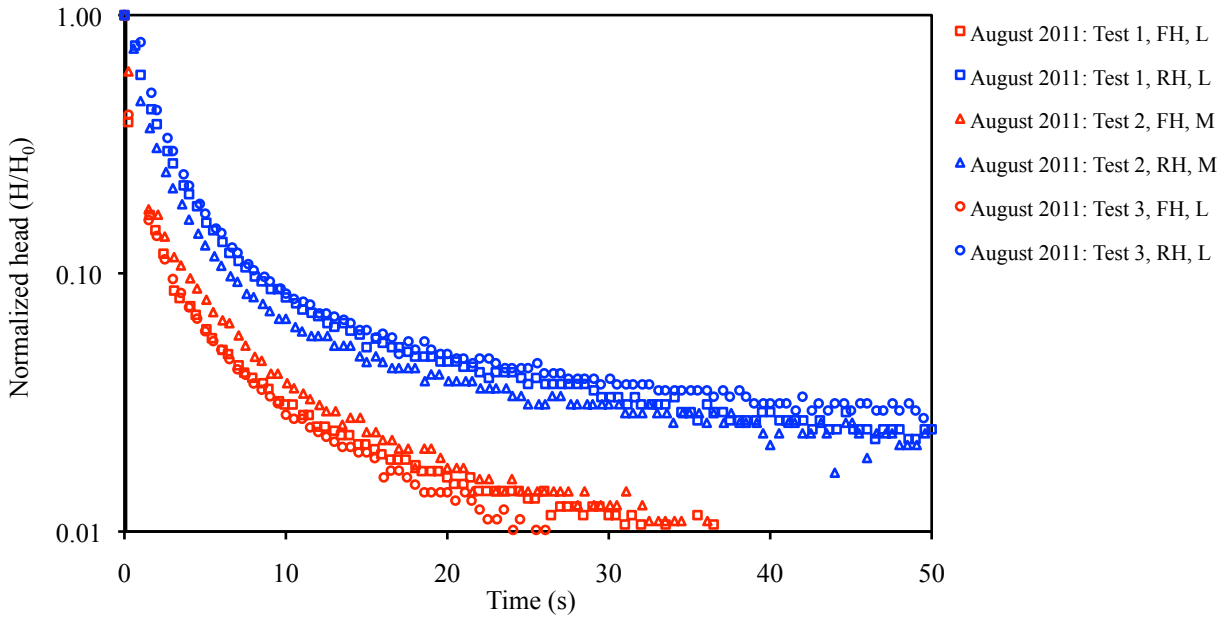

Figure 3.33. Normalized response data versus time for the series of slug tests performed in MD3.

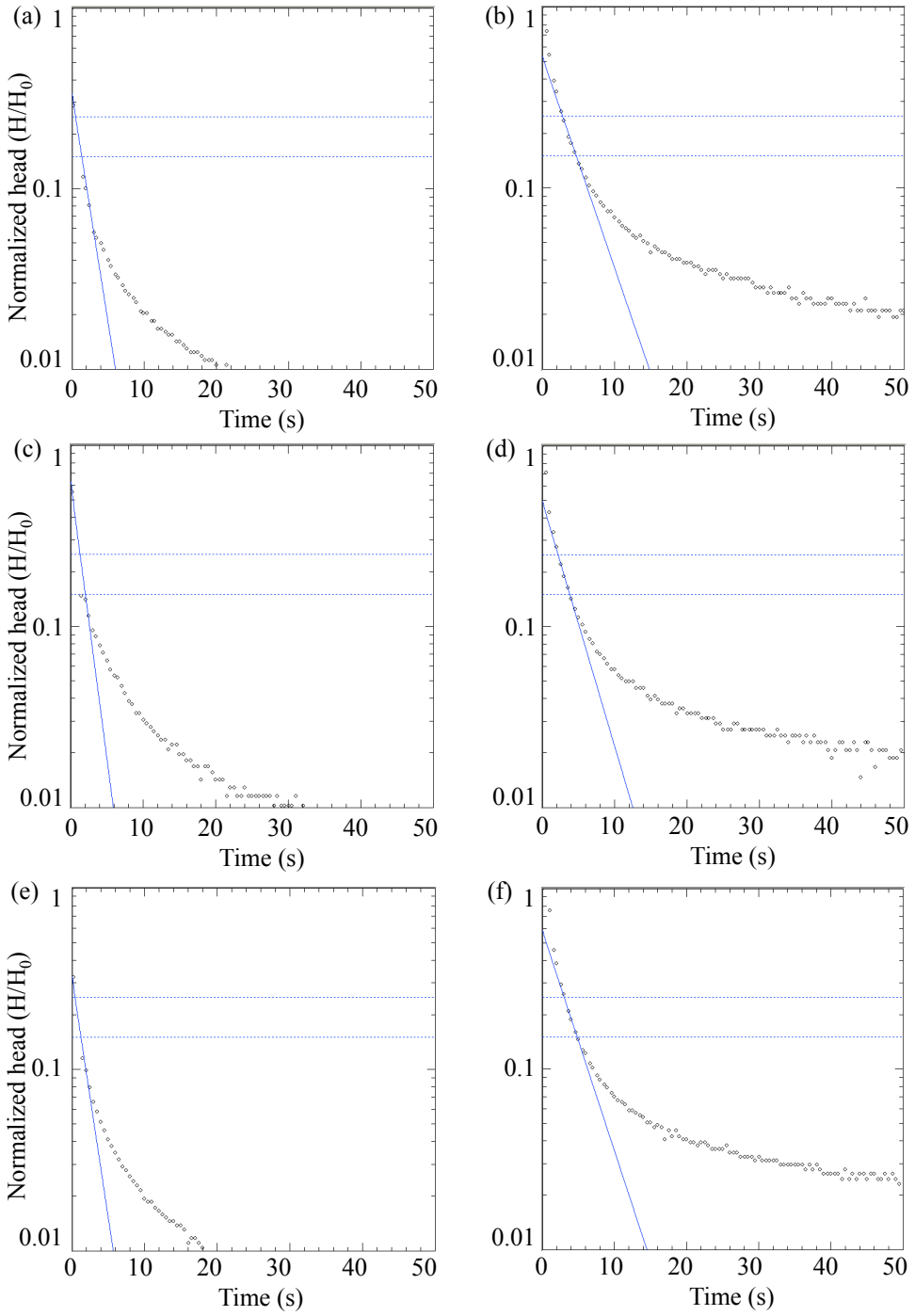

Figure 3.34. Normalized response data versus time for each slug test performed in well MD3: (a) test 1 falling-head large slug, (b) test 1 rising-head large slug, (c) test 2 falling-head medium slug, (d) test 2 rising-head medium slug, (e) test 3 falling-head large slug, (f) test 3 rising-head large slug. Solid line shows the Dagan model fit to the response data. Dashed lines indicate the recommended head range.

3.3.6 Summary and discussion: Slug tests

Hydraulic conductivity estimated for the Niwot Ridge study area ranged from 8.42×10^{-6} to 1.51×10^{-3} m/s. Variations in permeability between test wells depended on the geology of the screened interval. Hydraulic conductivity was highest in the Tertiary quartz monzonite at wells SD3 and SD4 (mean 8.74×10^{-4} m/s) and lowest in SD1, which is screened across the contact between Quaternary sands and Precambrian Silver Plume quartz monzonite (mean 8.42×10^{-6} m/s). Hydraulic conductivity in the Quaternary-Tertiary diamicton at wells MD2 and MD3 averaged 1.92×10^{-4} m/s. Average hydraulic conductivity from slug tests performed in the Tertiary quartz monzonite around wells SD3 and SD4, which are 82 m apart, varied by more than an order of magnitude. This variation was expected, since the distribution of fractures in the bedrock is probably nonuniform. Variation in hydraulic conductivity over short distances provides evidence of aquifer heterogeneity and supports the results of Hamann (2002) who conducted Guelph permeameters tests and found high variation in the hydraulic conductivity (2.3×10^{-4}–2.6×10^{-6} m/s) of near-surface material at the Saddle site.

The results of the slug tests at the Saddle site suggest that hydraulic conductivity is higher in Tertiary quartz monzonite than in Precambrian quartz monzonite, which contradicts the results of infiltration tests. The infiltration tests assessed the shallow subsurface materials while slug tests provided estimates of the hydraulic conductivity of deeper materials. Therefore, the results of slug tests provide better estimates of the hydraulic conductivity of the saturated aquifer. That hydraulic conductivity of the aquifer was higher in locations composed of Tertiary quartz monzonite than in locations composed of Precambrian quartz monzonite suggests that the Tertiary rock is more fractured than the Precambrian rock. Multiple prior studies have noted the presence of fractures in both the Precambrian and Tertiary quartz monzonites on Niwot Ridge

(Wahlstrom, 1940; Lovering and Goddard, 1950; Tweto, 1968; Pearson, 1980; Lester, 1992; Leopold, 2008), but there have been no efforts to map their distribution, orientation, aperture, or conductivity. The results of this study present the first direct measurements of hydraulic conductivity of the fractured bedrock on Niwot Ridge.

Results of slug tests conducted in bedrock at the Saddle site (range 8.42×10^{-6} to 1.51×10^{-3} m/s) corroborate with hydraulic conductivities reported for similar lithologies at nearby sites. Snow (1968) used borehole logs and pressure-injection tests and found that hydraulic conductivity of fractured Precambrian granite and granite gneiss of the Front Range decreased logarithmically from ~10^{-4} m/s near the surface to ~10^{-7} m/s at 60 m depth. Using the values reported by Snow (1968), Clow et al. (2003) estimated hydraulic conductivity in the shallow bedrock at Loch Vale, located 30 km north of Niwot Ridge, to be 1×10^{-5}–1×10^{-2} m/s, although these values may be overestimates because the estimates of Snow (1968) were for more weathered bedrock than that found at Loch Vale.

Hydraulic conductivities estimated for the unconsolidated deposits at the Martinelli site (range 9.82×10^{-5} to 2.85×10^{-4} m/s) were somewhat lower than values reported from nearby sites. Davinroy (2000) used a constant-head permeameter to obtain hydraulic conductivity values of 1.1×10^{-3}–3.9×10^{-3} m/s for blockslope deposits (a thin deposit of angular blocks without a cliff above) in upper Green Lakes Valley. In the Loch Vale catchment, Clow et al. (2003) estimated hydraulic conductivity of 1.1×10^{-3}–2.6 m/s for blockslope deposits. Hydraulic conductivity of the unconsolidated deposits at Martinelli is likely lower than that of nearby sites because the deep permanent snowfield at the Martinelli catchment probably produces some compaction of the surficial sediments, which would lower the conductivity. However, the artificial filter pack

around the wells, which was not sealed with bentonite, may serve as a conduit for vertical flow, which would lead to overestimates of hydraulic conductivity determined from slug test results.

3.4 Estimation of specific discharge

3.4.1 Methods: Specific discharge

Results from water level monitoring and slug testing enabled calculation of specific discharge, the flow rate at which water would flow in an aquifer if the aquifer were an open conduit (Fetter, 2001). Equation 3.3 states that specific discharge between two points is equal to the product of hydraulic conductivity and the horizontal hydraulic gradient. The negative sign on the right-hand side of Equation 3.3 indicates that groundwater moves from high head toward low head. The average hydraulic conductivity between a pair of test wells (e.g. SD1 and SD3) was calculated using average hydraulic conductivity from each slug test well (Table 3.8). Average horizontal hydraulic gradients were calculated using annual minimum water levels and annual peak water levels over the period 2006−2011. Specific discharge was calculated at the annual minimum water level and at the annual peak water level for wells SD1/SD3 and SD3/SD4. Since minimum water levels were not measured at the Martinelli site due to deep snow cover, specific discharge was only calculated at the annual peak water level for wells MD2/MD3. The values of hydraulic conductivity and hydraulic gradient used in the calculations and the resultant specific discharges are listed in Table 3.9.

			At annual minimum water level				At annual peak water level			
	mean *K* (m/s)	*dx* (m)	*dh* (m)	*dh/dx*	*q* (m/s)	*q* (m/d)	*dh* (m)	*dh/dx*	*q* (m/s)	*q* (m/d)
Between SD1, SD3	7.59E-04	89.6	2.6	0.03	-2.2E-05	-1.9	6.1	0.07	-5.2E-05	-4.5
Between SD3, SD4	8.09E-04	82.4	9.0	0.11	-8.9E-05	-7.7	8.6	0.10	-8.5E-05	-7.3
Between MD2, MD3	1.92E-04	33.4	-	-	-	-	2.0	0.06	-1.1E-05	-1.0

K = saturated hydraulic conductivity, *dx* = horizontal distance between wells, *dh* = vertical distance between hydraulic heads, *dh*/*dx* = hydraulic gradient, *q* = specific discharge

Minimum water levels were not measured at MD2 and MD3 due to deep snow cover.

Table 3.9. Values of hydraulic conductivity and hydraulic gradient used to calculate specific discharge. Minimum water levels were not measured at MD2 and MD3 due to deep snow cover.

3.4.2 Results: Specific discharge

Specific discharge ranged from 1.1×10^{-5} m/s (1.0 m/d) between MD2 and MD3 at annual peak water level to 8.9×10^{-5} m/s (7.7 m/d) between SD3 and SD4 at annual minimum water level (Table 3.9). Higher values of specific discharge at the Saddle site reflect higher hydraulic conductivity and steeper hydraulic gradient between wells. Smaller values at the Martinelli site reflect lower hydraulic conductivity and gentler hydraulic gradient between wells. Between SD1 and SD3, specific discharge was greater at peak water level in mid-July (5.2×10^{-5} m/s or 4.5 m/d) than at minimum water level in mid-May (2.2×10^{-5} m/s or 1.9 m/d). This change was due to an increase in hydraulic gradient between the time of minimum and peak water levels, which resulted from a larger increase in water level at SD3 than at SD1. The opposite was observed between SD3 and SD4, where specific discharge was slightly lower at peak water level (8.5×10^{-5} m/s or 7.3 m/d) than at minimum water level (8.9×10^{-5} m/s or 7.7 m/d). The decrease reflected a decline in hydraulic gradient through spring when the ground became saturated near SD3 and SD4. Specific discharge, and therefore flow, moved in the same direction as topographic gradients confirming results of water level mapping (Figure 3.7).

Chapter 4
Estimation of groundwater recharge using water table fluctuations

4.1 Introduction to the water table fluctuation method

Techniques that rely on water levels measured in groundwater wells are among the most commonly used methods for estimating recharge because of the comparative simplicity. Water table fluctuations occur in unconfined aquifers in response to groundwater recharge and discharge. The water table fluctuation (WTF) technique uses water table fluctuations to provide an estimate of recharge that reaches the water table. This method is based on the relation between changes in measured water level and changes in the amount of water stored in the aquifer (Healy, 2010). Difficulties in using the WTF technique are related to appropriately estimating aquifer specific yield and ensuring that water level fluctuations are due to recharge (Scanlon et al., 2002). Healy (2010) describes the WTF method in detail.

The advantage of the WTF method is that it is relatively simple, easy to use, and inexpensive if hydrographs are available from existing observation wells. In addition, it requires no assumptions on the movement of water through the unsaturated zone, so the presence of preferential flow paths, such as fractures, does not limit its use (Healy, 2010). The technique is best applied to wells that show a relatively rapid rise in water level relative to the rate at which water moves away from the water table (Healy and Cook, 2002). The rising limb of the hydrographs for the deep Saddle wells displayed this trend, rising quickly and steeply following initiation of snowmelt (Figures 3.13).

The limitations of the WTF approach stem from the simplification of the complex recharge process to a simple model with only two parameters: specific yield (S_y) and water level rise rate ($\Delta h/\Delta t$). Estimates of S_y are rarely available, so uncertainty in a representative estimate

of S_y is a drawback to the WTF method. Further limitation of the WTF method emerges if water level rises do not exclusively reflect recharge due to precipitation or snowmelt events. For example, water table fluctuations can occur in response to processes such as evapotranspiration, change in atmospheric pressure, changes in surface water elevations, earthquakes, or earth tides (Freeze and Cherry, 1979). At Niwot Ridge, effects from evapotranspiration were minimal because temperatures only rose above 4°C, the lower limit for evapotranspiration to occur (Linsley et al., 1982), 30% of the time between 2006 and 2011 (NWT Meteorology/Climatology, 2011). Atmospheric pressure effects were removed from the water level data (see Chapter 3). The impact of other effects was unlikely more than a few centimeters per year (Healy and Cook, 2002).

A groundwater recharge study conducted by Risser et al. (2005) concluded that water table fluctuations observed in fractured rock aquifers should be used with caution because of spatial variability of $\Delta h/\Delta t$ and the sensitivity of recharge to small errors in S_y that are typical of low-storage fractured rock systems. Thus, care must be taken in selecting S_y. To achieve the best possible estimate of recharge to fractured rock aquifers, Risser et al. (2005) recommends applying the technique to multiple observation wells within the study site. The WTF method was applied to the four deep piezometers at the Saddle site (Figure 2.1b).

The WTF method has been employed in numerous studies and over a wide range of climates. Delin et al. (2007) estimated recharge at 60−560 mm/y (21% of annual precipitation) for humid forested watersheds in Minnesota. Coes et al. (2007) used the technique at a North Carolina coastal plain and estimated recharge to be 250−940 mm/y (56% of annual precipitation). Risser et al. (2005) determined that recharge to a fractured rock aquifer in Pennsylvania was 190−480 mm/y (24% of annual precipitation). The WTF method has not been

used to estimate recharge to high-altitude snow-dominated groundwater systems. Estimation of recharge on Niwot Ridge will advance the scientific understanding of snowmelt-dominated mountain groundwater systems.

4.2 Methods

4.2.1 Compilation of water level records

The groundwater level elevation data presented in Chapter 3 were used to estimate recharge by the WTF method. To be included in this recharge estimation method, a well needed to have a minimum of one water level measurement taken every other month for each water year. (A water year is defined as October 1 to September 30. For the duration of this chapter, all descriptions using the words "year" or "annual" refer to the water year and not the calendar year.) In most cases, water levels were collected on a monthly to weekly basis. The four shallow wells at the Saddle site were excluded from WTF analysis because water level during winter dropped below the bottom of the well. All wells at the Martinelli site were excluded because measurements were not collected during winter when deep snow covered the wells. The four deep wells at the Saddle site (SD1, SD2, SD3, SD4) met the specified criteria. However, data from water years 2007 and 2010 at SD2 were not included because ice in the well prevented measurement for several consecutive months. The compiled groundwater level datasets were used to calculate annual groundwater recharge rates for 2006−2010 at the Saddle site.

To assess what portion of water input to Niwot Ridge resulted in recharge versus runoff, precipitation and streamflow data were compiled and compared with estimates of recharge. In addition, the estimate of recharge was used to approximate the water budget of the Saddle catchment. Precipitation was measured at the Saddle climate station between October 2006 and December 2010 (NWT Meteorology/Climatology, 2011). Streamflow data, measured at the

Saddle stream gauge, for October 2006 to December 2010 (NWT Hydrology, 2011). To obtain a depth of streamflow, streamflow volume was divided by the area of the Saddle catchment (240,000 m^2). Precipitation and streamflow data were not available after December 31, 2010 because the Niwot Ridge LTER staff had not yet processed these data.

4.2.2 Estimation of groundwater recharge

The WTF method is based on the principle that rises in groundwater levels in unconfined aquifers are the result of recharge water arriving at the water table (Healy, 2010). Recharge is determined for individual recharge events. Estimates for annual recharge were obtained by summing individual recharge events over year of interest. The spatial scale represented by the recharge estimate obtained by the WTF method ranges from 1 to 1000s m^2 (Healy, 2010). The time scale represented ranges from individual event to seasonal (Scanlon et al., 2002). Recharge, R, by the WTF method is calculated as:

$$R = S_y \frac{dh}{dt} = S_y \frac{\Delta h}{\Delta t} \qquad [4.1]$$

where R is recharge [L/T] occurring over the time period Δt [T], S_y is the specific yield of the aquifer [1], h is water table height [L], and t is time [T] (Healy, 2010). The rise in water table height (Δh) is equal to the difference between the peak of the rise and the low point on the extrapolated antecedent recession curve at the time of the peak (Healy, 2010) (Figure 4.1).

The WTF relies on three assumptions: (1) a water level rise observed in the well hydrograph is caused only by recharge arriving at the water table, (2) specific yield is known and constant over the period of water table fluctuations, and (3) the pre-recharge water level recession can be extrapolated to determine $\Delta h/\Delta t$. Application of the WTF method involved two steps: (1) estimation of the water level rise, $\Delta h/\Delta t$, and (2) estimation of specific yield, S_y. In this study, graphical estimation was used to determine $\Delta h/\Delta t$.

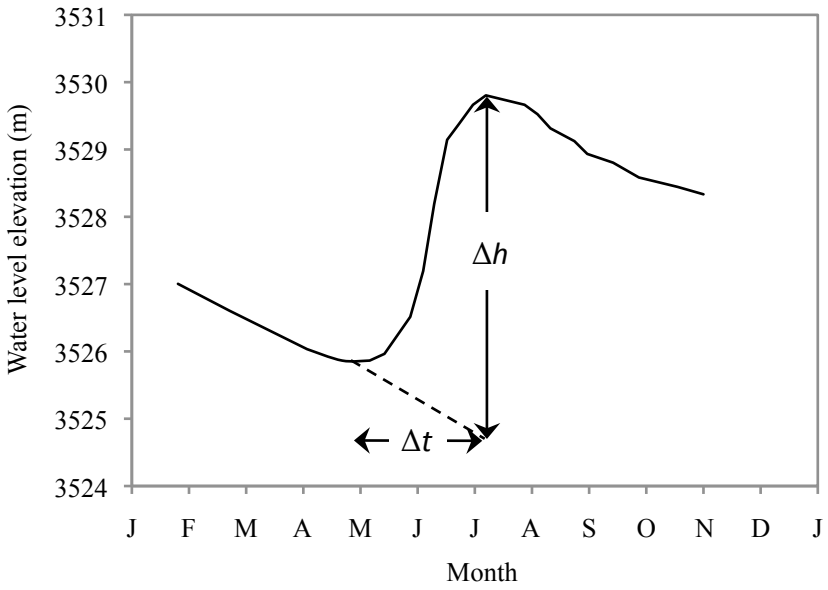

Figure 4.1. Determination of water level rise, Δh, using the graphical approach to the WTF method, illustrated with hypothetical data.

Specific yield is defined as "the ratio of the volume of water that drains from a saturated rock under gravity to the total volume of the rock" (Fetter, 2001). The theoretical maximum value of S_y is porosity. S_y is usually determined from laboratory methods (e.g. column drainage experiments), field methods (e.g. aquifer tests), water budget methods, or numerical modeling. Healy (2010) presents detailed information on the techniques available. For this study, neither laboratory nor field estimates of S_y were available. Instead, a water budget method was used to estimate S_y (Hall and Risser, 1993; Delin et al., 2007; Healy, 2010).

The water budget method combines a water budget (Equation 1.5) with Equation 4.1 to estimate S_y. This method was applied in mid-summer during the period following snowmelt when both streamflow and groundwater levels were in recession and all precipitation arrives as rain. During the period of streamflow recession, it was assumed that all streamflow out of the catchment was derived from baseflow and precipitation runoff. In addition, all precipitation during that period was assumed to either run off as streamflow or recharge the water table. Immediately following snowmelt, air temperature was low and vegetation was still dormant, so

evaporation and evapotranspiration were negligible. Furthermore, soil moisture contents were at their greatest, meaning that unsaturated zone storage was negligible. Applying these assumptions to the mountain water budget from Equation 1.5, the simplified water budget is written as:

$$R = P - \left(\frac{Q_{out}^{sw}}{A_{Saddle}} \right) \qquad [4.2]$$

where R is recharge [L/T], P is precipitation measured at Saddle climate station [L/T], Q_{out}^{sw} is Saddle streamflow measured at Saddle stream gauge [L^3/T], and A_{Saddle} area of Saddle catchment [L^2] (240,000 m^2). Substituting Equation 4.1 into Equation 4.2 and solving for S_y yields:

$$S_y = \frac{P - \left(\frac{Q_{out}^{sw}}{A_{Saddle}} \right)}{\Delta h / \Delta t}. \qquad [4.3]$$

where Δh is groundwater level decline [L] over time period Δt [T]. Equation 4.3 was applied to SD4 for a 7-day period in mid-summer when snowmelt had ceased and streamflow and groundwater levels were in baseflow recession. SD4 was used because it had the most consistent water level record during mid-summer. S_y for the Saddle site was determined from the average of S_y values estimated at SD4 for 2007−2010. The final value of S_y was for bedrock, as opposed to surficial deposits, because the water table fluctuates primarily in bedrock at the Saddle site.

The WTF method was used to quantify recharge on an annual timescale for water years 2006−2010 at the deep Saddle wells. To obtain $\Delta h/\Delta t$, the antecedent recession curves were extrapolated manually by visual inspection of the yearlong well hydrographs. Using Equation 4.1, the annual $\Delta h/\Delta t$ was multiplied by S_y to obtain a range of estimated recharge at each well. This approach is somewhat subjective and interpretation of the data by different researchers would undoubtedly result in slightly different extrapolations (Healy and Cook, 2002).

4.3 Results

4.3.1 Estimation of specific yield

The results of the S_y calculation are listed in Table 4.1. Average S_y at SD4 between 2007 and 2010 was 0.033. This estimate of S_y was consistent with tabulated values of S_y based on the known geology of the site and with S_y values measured at similar field settings. Best estimates from driller's logs and surficial mapping by Gable and Madole (1976) indicate that the Saddle site is largely underlain by fractured quartz monzonite (Figure 2.4). S_y of fractured-rock systems is typically equal to the fracture porosity (Healy, 2010), although fracture porosity is unknown since the fracture network at Niwot Ridge has not been delineated. Risser et al. (2005) used a range of S_y values between 0.0035 and 0.035 for a fractured siltstone and shale aquifer in Pennsylvania. Maréchal et al. (2006) estimated S_y at 0.014 for fractured granite in eastern India. The value of S_y used in this study fell within the range of previously reported values of S_y.

Year	P (m/d)	Q/A_{Saddle} (m/d)	Δh (m)	Δt (d)	S_y
2007	0.002	0.002	0.10	7	0.010
2008	0.003	0.001	0.34	7	0.047
2009	0.002	0.001	0.15	15	0.060
2010	0.002	0.002	0.12	7	0.017
				Mean	0.033
				SD	0.024

P = precipitation, Q/A_{Saddle} = streamflow divided by area Saddle catchment (240,000 m^2), Δh = change in water level, Δt = change in time, S_y = specific yield, SD = standard deviation

Table 4.1. Input values of precipitation, streamflow, and change in water level at SD4 and resultant value of S_y using a water budget approach.

4.3.2 Estimation of groundwater recharge

Table 4.2 summarizes the calculations and results of the graphical approach to the WTF method, which was used to estimate annual recharge rates, R, for 2006−2010 and the percentage of precipitation, % of P, for 2006−2009. Figure 4.2 shows the trends in annual recharge, precipitation, and streamflow over time at the Saddle site. Mean annual recharge was lowest at

SD1 (0.57 m) for the five years examined reflecting relatively shallow snowpack that developed near the well each year. Mean annual recharge was greatest at well SD4 (1.64 m) reflecting the deep snowpack near the well. From year to year, the well in which the largest annual recharge occurred varied. Variation in recharge reflects differences in the distribution of precipitation and snowmelt and differences in underlying geology. Across the Saddle site, recharge averaged 1.25 m/y or 52.5% of *P*. Recharge generally increased over time in the Saddle wells, although with only five years of record, this trend is not statistically significant to make long-term assessments.

	Water year	S_y	Δh (m)	Δt (d)	R (m/y)	P (m/y)	% of P	Q (m/y)
SD1	2006	0.033	2.61	144	0.22	2.10	10.4	0.32
	2007	0.033	2.67	175	0.18	2.45	7.5	0.29
	2008	0.033	3.34	48	0.84	1.91	44.0	0.21
	2009	0.033	3.43	64	0.65	2.09	30.9	0.25
	2010	0.033	3.81	48	0.96	-	-	0.22
				Mean	0.57	2.14	23.2	0.26
				SD	0.35	0.23	17.4	0.05
SD2	2006	0.033	5.68	76	0.90	2.10	42.8	0.32
	2007	0.033	-	-	-	2.45	-	0.29
	2008	0.033	6.17	37	2.01	1.91	105.4	0.21
	2009	0.033	3.97	77	0.62	2.09	29.8	0.25
	2010	0.033	-	-	-	-	-	0.22
				Mean	1.18	2.14	59.3	0.26
				SD	0.73	0.23	40.5	0.05
SD3	2006	0.033	7.42	90	0.99	2.10	47.2	0.32
	2007	0.033	6.45	66	1.18	2.45	48.0	0.29
	2008	0.033	6.10	49	1.50	1.91	78.7	0.21
	2009	0.033	7.38	41	2.17	2.09	103.9	0.25
	2010	0.033	7.77	43	2.18	-	-	0.22
				Mean	1.60	2.14	69.5	0.26
				SD	0.55	0.23	27.3	0.05
SD4	2006	0.033	4.46	104	0.52	2.10	24.6	0.32
	2007	0.033	5.53	40	1.67	2.45	67.9	0.29
	2008	0.033	5.89	51	1.39	1.91	73.0	0.21
	2009	0.033	6.72	58	1.40	2.09	66.9	0.25
	2010	0.033	7.21	27	3.22	-	-	0.22
				Mean	1.64	2.14	58.1	0.26
				SD	0.98	0.23	22.5	0.05

S_y = specific yield, Δh = water level rise, Δt = change in time, R = recharge, P = precipitation, Q = streamflow, SD = standard deviation

Table 4.2. Table summarizing input values and results of the graphical approach to the WTF method (2006−2010). Values of Δh, Δt, R, P, and Q are annual totals.

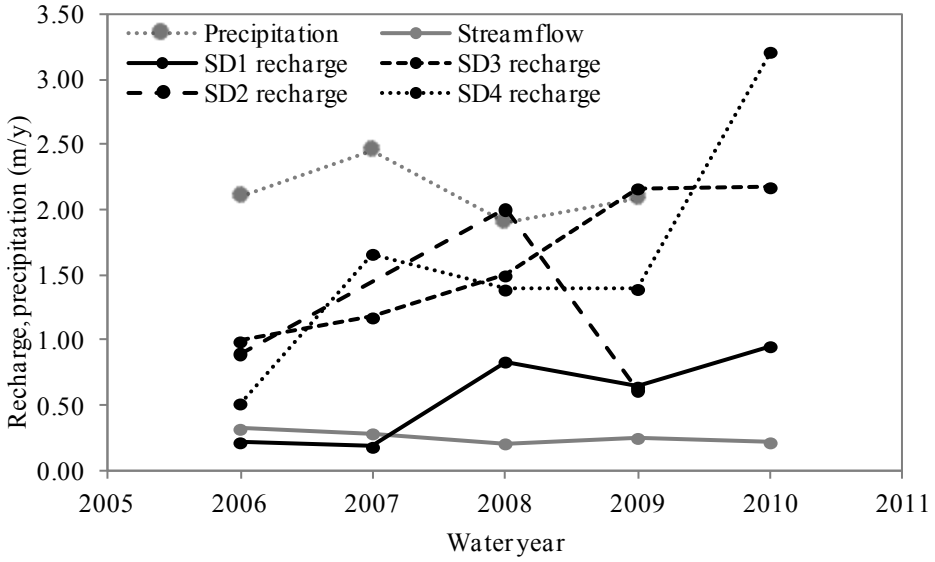

Figure 4.2. Plot showing annual recharge estimated using the graphical approach to the WTF method (2006−2010). Annual precipitation measured at the Saddle climate station (NWT Meteorology/Climatology, 2011) and stream discharge measured at the Saddle stream gauge (Nel Caine, personal communication, 4 July 2011) are also shown. Precipitation in 2008 and 2009 are less than recharge at wells SD2 and SD3, respectively, due to high variability in the spatial distribution of snow at the Saddle site.

4.4 Water budget

Recharge estimated using the WTF method was used to approximate the water budget of Niwot Ridge for 2006−2009, specifically the Saddle catchment (Table 4.3). Mean annual precipitation at the Saddle climate station was 2.14 m for 2006−2009 (standard deviation 0.23 m) (NWT Meteorology/Climatology, 2011). Each year, 33% of precipitation is lost to ET (Berg, 1986; Greenland, 1989) (0.71 m 2006−2009) and 15% sublimates (Hood et al., 1999) (0.32 m 2006−2009). Streamflow in the Saddle stream averaged 64,288 m^3/y (0.27 m/y depth over the 0.24 km^2 catchment area, standard deviation 0.04 m/y) for 2006−2009 (NWT Hydrology, 2011), which was 13% of annual precipitation. By the WTF method, the Saddle site produced on average 1.25 m/y (standard deviation 0.50 m/y) of groundwater recharge, which was 52% of annual precipitation. Assuming 100% of water input was from precipitation for 2006−2009, there was an additional 13% in the water budget.

	Value (m/y)	% of precipitation	Source
Precipitation	2.14	100	NWT Meteorology/Climatology, 2011
Evapotranspiration	0.71	33	Berg, 1986; Greenland, 1989
Sublimation	0.32	15	Hood et al., 1999
Runoff to Saddle stream	0.27	13	NWT Hydrology, 2011
Groundwater recharge	1.25	52	WTF method

Table 4.3. Water budget of Niwot Ridge, specifically the Saddle catchment.

The additional 13% most likely reflects error in the calculations due to limitations in data collection. The Saddle climate station measures precipitation at only the ridge crest, so measurements of precipitation may not represent the Saddle catchment as a whole. Due to complex interactions gusty winds, extensive snow, and varied topography, the spatial distribution of precipitation in mountain regions is highly heterogeneous and is, therefore, difficult to measure (Erickson et al., 2005). Williams et al. (1998) found that precipitation gauges at the Saddle site largely overcollect snowfall accumulation due to wind effects. The estimate of ET was made over 20 years ago and may not represent recent conditions. Recharge may have been overestimated by the WTF method if the effects of ET and other influences had a larger effect on water level fluctuations than was assumed or if the S_y value used was not representative of the subsurface material. The 13% extra water in the water budget may also be a product of changes in unsaturated zone storage, which was not calculated as part of this study. Given the diversity of sources of error in the water budget calculation, 13% error is reasonable. However, further work should be done to refine the water budget equation.

4.5 Summary and discussion

Results of this study indicated that groundwater recharge rates at the Saddle site varied over small spatial scales and on annual timescales. Mean annual recharge at SD3 (1.60 m) was 25% greater than at SD2 (1.18 m), yet the wells are only 45 m apart and are screened in the same lithology. At SD4, annual recharge increased by 221% between 2006 and 2007, decreased by 17% in 2008, increased by 0.7% in 2009, and increased again by 130% in 2010.

Variations in recharge rates across the study site suggest that recharge was largely dependent on precipitation. The high spatial variation in the distribution of precipitation, particularly of snow, which results from strong winds interacting with complex topography at the Saddle site, contributed to variations in recharge rates. Compared with the other well sites, the ground at SD1 remained relatively snow-free. As a result, SD1 often received less recharge than the other three wells.

The results from this study generally agree with recharge estimates made in similar field settings. Mean annual recharge at the Saddle site was estimated to be 1.25 m or 52.5% of mean annual precipitation. Recharge was 22% of precipitation in the Wasatch Range in Utah (Feth et al., 1966) and 14% in the Sangre de Cristo Mountains in San Luis Valley, Colorado (Huntley, 1979). Earman et al. (2004) found that 40−70% of groundwater recharge was derived from snow in the mountains of Arizona and New Mexico, where snow makes up 25−49% of annual precipitation.

The uncertainty in recharge estimates obtained in this study reflects in part the limitations of the WTF method due to underlying assumptions. Future work should aim to refine estimates of S_y thorough field and laboratory measurements. The observed water table fluctuations and recharge rates were representative of only the area near the Saddle wells. The results present a reasonable first approximation of recharge at the Niwot Ridge study area. In addition, the results provide estimates of S_y and R, which can be used as input parameters to groundwater flow models.

Chapter 5
Estimation of groundwater recharge using numerical model SUTRA

5.1 Background on groundwater modeling of mountain regions

Groundwater flow modeling is a useful tool for studying groundwater systems and developing a conceptual understanding of the flow system. Through model calibration, a groundwater flow model can be used to estimate groundwater recharge rates and distribution (Sanford, 2002). One method to constrain the rate of recharge is to obtain stream baseflow (the groundwater component of streamflow) measurements, which are often considered a proxy for recharge. The success of estimating recharge via modeling depends on the quality of estimates of model input parameters and the degree to which the conceptual model represents the actual groundwater system.

There are many challenges in modeling groundwater in mountainous terrain. Steep topographic and hydraulic gradients are difficult to represent in models. Field data for model input are hard to obtain due to access difficulties and harsh conditions. Even when data are available, they are rarely collected on a fine enough spatial scale to represent the heterogeneities in ground cover, geology, hydrology, and meteorology that are ubiquitous in mountain regions.

Several studies have modeled groundwater flow in mountainous areas. Forster and Smith (1988a and 1988b) used a coupled fluid flow and heat transfer model to study the sensitivity of water table elevation to surface topography, geology, and climate. They found that rock permeability had the greatest impact on mountain water table elevation. Flerchinger et al. (1993) modeled groundwater response to snowmelt in a mountainous watershed in southwestern Idaho to improve their understanding of the relation between groundwater levels and shallow confining layers. Johnson (2007) used groundwater modeling and sensitivity analyses to guide field data

collection in a mountain watershed. He found that hydraulic heads at high elevations were the most important observation data for determining recharge and hydraulic conductivity input values. Gleeson and Manning (2008) extended the two-dimensional Tóthian model of interbasinal groundwater flow systems (Tóth, 1963) to three dimensions. Results of their study indicated that regional groundwater flow is limited in mountain areas with topography-controlled water tables and is significant in mountain areas with recharge-controlled water tables. Wolf et al. (2008) developed a new modeling approach to better simulate the steep hydraulic gradients characteristic of mountain watersheds.

5.2 Modeling groundwater flow at Niwot Ridge

The purpose of modeling was to gain a better understanding of the Niwot Ridge hydrogeologic system and use the results to refine the conceptual model (Chapter 2). The specific goals of modeling the Martinelli catchment were to (1) estimate the rate of groundwater recharge, (2) determine the distribution of recharge, and (3) examine the sensitivity of recharge to hydrogeologic parameters. To achieve the first goal, the model was calibrated by adjusting hydraulic conductivity until modeled groundwater discharge matched measured baseflow in the Martinelli stream. The second goal was accomplished though graphical visualization of model results. Goal (3) was achieved by varying model input parameters and then examining the effect on the rate and distribution of recharge.

The Martinelli catchment was modeled as a two-dimensional cross section. The model was run under transient and saturated conditions. The numerical code, SUTRA (Saturated-Unsaturated TRAnsport) (Voss and Provost, 2009), was used to simulate groundwater flow. The graphical user interface (GUI), SUTRA GUI (Winston and Voss, 2004), was used to visualize the groundwater flow regime and was implemented in Argus ONE software. Model Viewer

software was also used to aid in visualization of model results (Hsieh and Winston, 2002).

5.2.1 Numerical model SUTRA

The SUTRA numerical code (Voss and Provost, 2009) was developed to simulate variable-density, saturated and unsaturated groundwater flow with solute or energy transport. It can be applied to steady state or transient conditions in two or three dimensions. Fluid may flow through the medium and across permeable boundaries. Flow is driven by differences in fluid pressure.

Discretizing the model is the first step in model setup. Spatial discretization in SUTRA is achieved with a finite element mesh consisting of quadrilateral elements. Each element is defined by a node at each of its four corners. Pressure (or hydraulic head) is simulated at each node inside the model domain. Permeability (or hydraulic conductivity) and anisotropy are specified in each element. The advantage of a finite element model, as opposed to a finite difference model like MODFLOW (Harbaugh et al., 2000), is that pressure values are spread out smoothly between nodes. The finite element mesh should be fine enough to best represent spatial variation in physical parameters. For a transient model, time should be discretized on a scale that reasonably approximates the temporal variation of the physical system.

Input to SUTRA includes a description of the physical system. Describing the physical system involves defining the geometry of the model domain, initial conditions, boundary conditions, physical parameters, and fluid sources and sinks. Initial conditions refer to initial values of fluid pressure (or hydraulic head). They are necessary for a transient model. Boundary conditions (e.g. specified pressures or specified fluxes) describe hydrologic conditions along the boundaries of the domain. Boundary conditions can be kept constant or vary with time. Physical parameters include thicknesses of lithologic layers, permeability (or hydraulic conductivity),

porosity, and specific storage. SUTRA can incorporate heterogeneity and anisotropy of the porous medium. Fluid sources are any external addition (e.g. precipitation). Fluid sinks are any external withdrawal (e.g. pumping) of water.

Output from SUTRA includes pressure (or hydraulic head), fluid velocities, and a fluid budget. Pressure is calculated at every node in the domain. Velocity is calculated in every element in the domain. The fluid budget consists of the inflows entering (e.g. recharge) and outflows exiting (e.g. stream baseflow) the model. For a steady state system, net inflows and net outflows are equal. In a transient system, there may be a change in storage due to differences in net inflows and net outflows.

5.2.2 Governing equations

Groundwater flow is governed by a partial differential equation that combines Darcy's law with a fluid mass-balance equation. Direct solution of the governing flow equation is generally impossible, but an approximate solution can be obtained by numerical methods and implemented by a computer model (e.g. SUTRA).

Darcy's law states that the average linear velocity of fluid flow through a porous medium is proportional to hydraulic conductivity and inversely proportional to porosity. Darcy's law also specifies that groundwater moves from regions of higher hydraulic head to regions of lower hydraulic head. In Chapter 3, Darcy's law was written in terms of hydraulic conductivity and hydraulic head gradient (Equation 3.3). The governing equations in SUTRA define Darcy's law in terms of permeability and fluid pressure. When permeability values differ in different directions, the permeability is said to be anisotropic. Hydraulic conductivity is related to permeability by:

$$K = \frac{k\rho g}{\mu} \qquad [5.1]$$

where K is hydraulic conductivity [L/T], k is permeability [L^2], ρ is fluid density [M/L^3], g is acceleration due to gravity [L^2/T], and μ is fluid viscosity [M/LT]. Hydraulic head is defined as:

$$h = z + h_p = z + \frac{p}{\rho g} \quad [5.2]$$

where h is hydraulic head [L], z is elevation head [L], h_p is pressure head [L], and p is fluid pressure [M/LT^2]. Darcy's law written in terms of permeability, k, and fluid pressure, p, is:

$$v = -\frac{K}{n} \cdot \nabla h = -\left(\frac{k\rho g}{\mu n}\right) \cdot \nabla \left(z + \frac{p}{\rho g}\right) \quad [5.3]$$

where v is average linear velocity of fluid [L/T], n is porosity [1], and ∇ is the gradient operator. For this study, ρ, g, and μ were assumed constant and uniform.

The fluid mass balance states that differences in fluid mass flowing into and out of a given system must equal the change in mass of fluid within the system. Assuming the solid matrix is incompressible, for saturated groundwater flow the fluid mass balance written in terms of fluid pressure is (Voss and Provost, 2009):

$$\left(\rho \frac{S_s}{\rho g} + n\rho \frac{\partial}{\partial p}\right) \frac{\partial p}{\partial t} = -\nabla \cdot (n\rho v) + W \quad [5.4]$$

where S_s is specific storage [L^{-1}], t is time [T], and W is a fluid mass source or sink [M/L^3T]. S_s is the volume of fluid released from a unit volume of aquifer due to a unit drop in hydraulic head. The left-hand side of Equation 5.4 describes the total change in fluid mass in the aquifer over time. The first term of the right-hand side represents changes to fluid mass due to fluid inflows or outflows. W accounts for external additions or withdrawals of fluid from the system under study. Substituting Darcy's law (Equation 5.3) into the fluid mass balance (Equation 5.4) gives the equation governing transient saturated groundwater flow in terms of pressure (Voss and Provost, 2009):

$$\left(\rho\frac{S_s}{\rho g}+n\rho\frac{\partial}{\partial p}\right)\frac{\partial p}{\partial t}=-\nabla\left[n\rho\left(\frac{k\rho g}{n\mu}\cdot\nabla\left(z+\frac{p}{\rho g}\right)\right)\right]+W \qquad [5.5].$$

With specified boundary and initial conditions, SUTRA solves the governing flow equation for the distribution of fluid pressure across the model domain.

The model developed in this study was run using the governing equation in terms of hydraulic head. Using Equations 5.1 and 5.2, Equation 5.5 becomes (Voss and Provost, 2009):

$$S_s\frac{\partial h}{\partial t}=\nabla\cdot(K\nabla h)+\frac{W}{\rho} \qquad [5.6].$$

The governing flow equation assumes flow occurs in a porous media having continuous interconnected pores. Fractured material consists of solid rock with a primary porosity broken by joints and fractures that have a secondary porosity. Groundwater flow in fractured media is assumed to occur primarily within the joint and fracture network. To simulate flow in a fractured medium in which fractures are randomly distributed throughout, it is common to designate the physical system as an equivalent porous medium (EPM). The primary assumption of an EPM is that the structure of the fractured material is hydraulically analogous to a medium having continuous interconnected pores. At a site 60 km southeast of Niwot Ridge, Caine and Tomusiak (2003) determined that the upper portion of an aquifer (< 100 m) composed of fractured Silver Plume quartz monzonite could be modeled as an EPM. In the present study, fracture apertures and flow velocities were assumed small for the fractured igneous bedrock underlying Niwot Ridge so that Darcy's law and Equation 5.6 applied (Anderson and Woessner, 2002). The fractured bedrock underlying the surficial sediments at the Martinelli catchment was represented in the model as an EPM and an effective value of hydraulic conductivity was defined for the entire fractured bedrock unit in the model (Table 5.1).

Unit	Observed geology	Calibrated K (m/s)	Measured K (m/s)	Source of measured K
1	Quaternary/Tertiary diamicton	2.5×10^{-6}	3.5×10^{-5}–3.4×10^{-4}	Infiltration tests
			9.8×10^{-5}–2.9×10^{-4}	Slug tests
			2.0×10^{-7}–3.0×10^{-2}	Sand/Gravel*
			1.0×10^{-12}–2.0×10^{-6}	Till*
2	Fractured Tertiary quartz monzonite/syenite	1.0×10^{-7}	8.0×10^{-9}–3.0×10^{-4}	Fractured plutonic bedrock*

K = hydraulic conductivity
*Domenico and Schwartz (1990)

Table 5.1. Observed geology based on Gable and Madole (1976) and drillers' logs, calibrated values of hydraulic conductivity (K), and measured K for each unit in the Martinelli model.

5.2.3 Domain, boundary conditions, and temporal discretization

The domain of the model represented a vertical cross section through the Martinelli catchment. The model was simulated in two dimensions because hydrogeologic data were not available to reasonably approximate the physical system in three dimensions. Figure 5.1 shows the location of the model cross section within the catchment. The cross section was oriented approximately northwest to southeast, which was assumed parallel to the dominant direction of groundwater flow (i.e. toward the Martinelli stream). Groundwater flow in the third direction was assumed zero. However, the dominant topographic gradient of the Martinelli catchment is toward the southeast, which suggests that there is groundwater flow in the third direction. Therefore, the two-dimensional model probably underestimates groundwater flow.

The source of groundwater to the Martinelli model was water table recharge from snowmelt and precipitation. Groundwater exited the modeled domain as baseflow to the Martinelli stream. Evapotranspiration was assumed negligible because there is little vegetation in the Martinelli catchment.

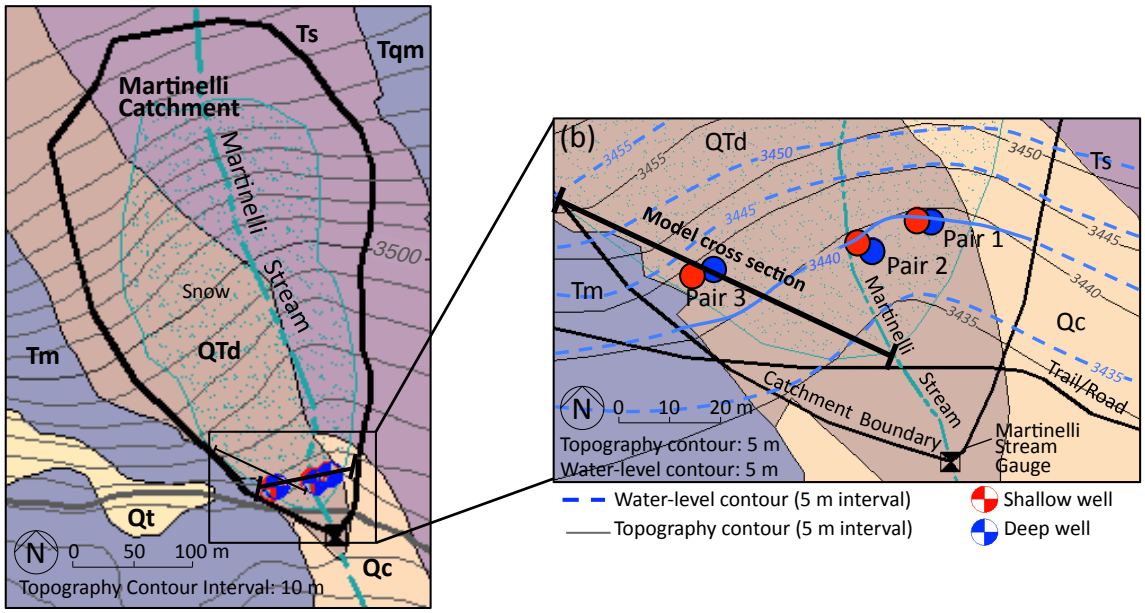

Figure 5.1. Location of model cross section. Cross section was oriented parallel to the dominant direction of groundwater flow with the southeast edge at the Martinelli stream.

Figure 5.2 shows the domain and boundary conditions for the Martinelli model. The two-dimensional finite-element mesh consisted of 2171 nodes and 2046 elements. Because groundwater flow is assumed to display more variation near the ground surface than at depth, the mesh near the top of the model was discretized at a finer scale than the mesh in the rest of the model. Elements in the top 1 m depth were approximately 0.5 m wide. Elements between 2 and 11 m depth were approximately 1.0 m wide. Elements in the lower portion of the model were approximately 5.0 m wide.

The distribution of hydraulic conductivity in the model is largely dependent on lithology. Seismic testing by Leopold et al. (2008) showed that the subsurface of Niwot Ridge is complex with heterogeneities within the surficial layer, an undulating bedrock surface, and an unknown distribution of fractures within the bedrock. The complicated subsurface geometry (Figure 2.4b) was simplified in the model to include two hydrogeologic units corresponding to unconsolidated surficial sediments (Quaternary-Tertiary diamicton composed of sand and gravel) and fractured

granitic bedrock (Tertiary quartz monzonite and/or syenite) (Figure 5.2). The thickness of the surficial unit, based on the results of Leopold et al. (2008) and driller's logs, ranged from 2.5 to 10.3 m. The thickness of the bedrock ranged from 49.7 to 75.7 m.

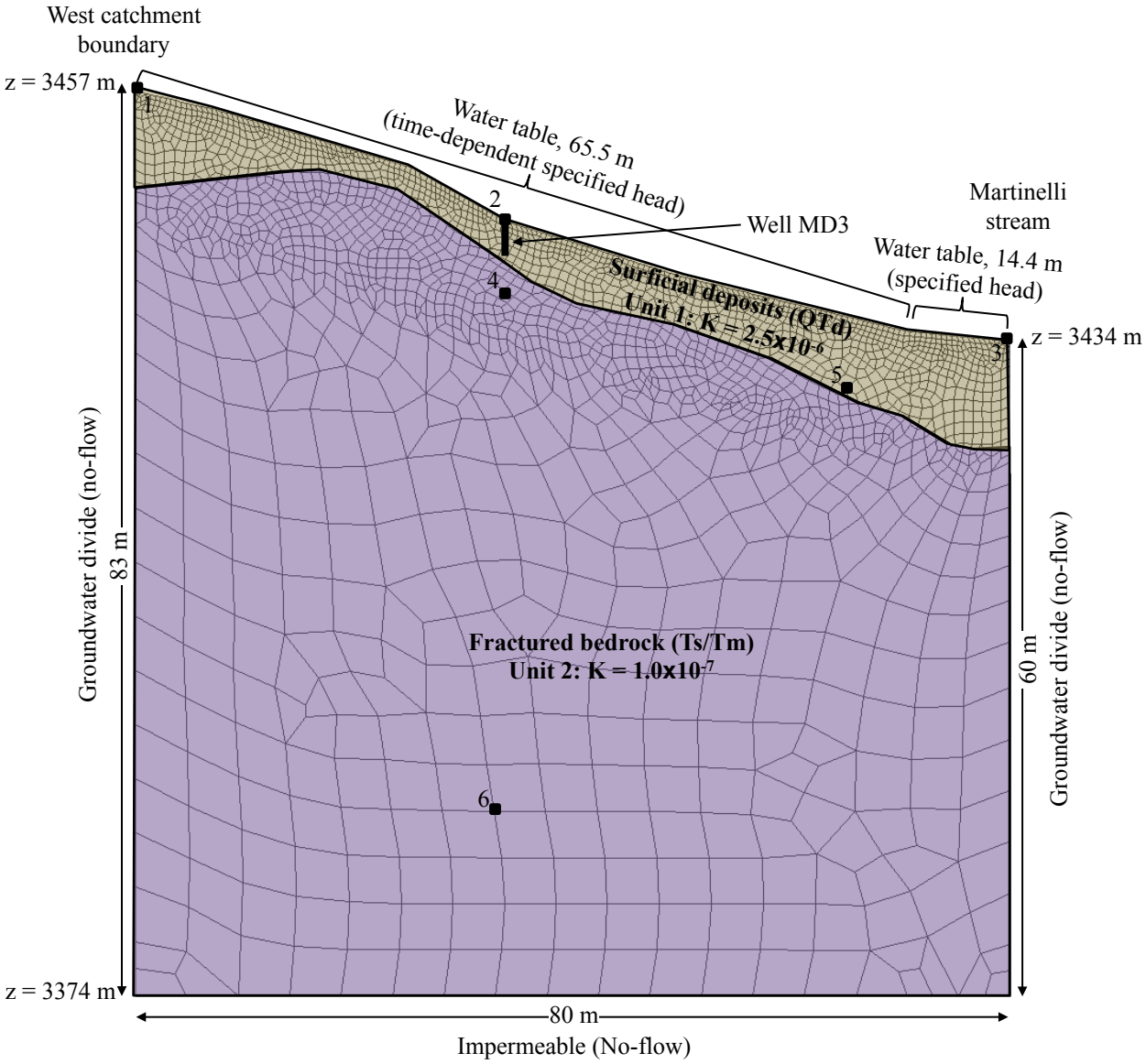

Figure 5.2. Domain and boundary conditions for the model. The domain is 80 m wide and is composed to two hydrogeologic units: (1) Quaternary-Tertiary diamicton (QTd) and (2) fractured Tertiary syenite (Ts) and monzonite (Tm). Elevations range from 3457 at the west catchment boundary on the left side of the model to 3434 m at the stream on the right side of the model. The sides and base are no-flow boundaries. The top is a specified head water table boundary. Locations of 10 observation points are also shown.

The horizontal domain extended from the west catchment boundary to the Martinelli stream at a location roughly 30 m upstream from the stream gauge and 400 m downstream of the stream headwaters. The width of the model was 80 m. The left side of the model was defined as a no-flow boundary representative of the groundwater divide at the west catchment boundary. The right side of the model was defined as a no-flow boundary representative of the groundwater divide at the catchment stream.

The vertical domain was bounded on the bottom by relatively impermeable bedrock and on the top by the water table. Snow (1968) noted that fractured bedrock permeability in the Front Range "vanishes" at 200 ft (~60 m). Therefore, the bottom of the model represented an impermeable base, which was defined as a no-flow boundary 60 m below the elevation of the catchment stream. The top of the model was defined as a time-dependent specified head boundary representing the water table.

A solution was estimated on a 6-hour timestep and model output was printed every 28 timesteps (every week). Water level data from the Saddle and Martinelli study sites indicated that the water table was shallow and was a subdued replica of the topography (Chapter 3). Therefore, for the first week, hydraulic head along this boundary was set equal to the elevation of the top row of nodes, which ranged from 3457 m at the west catchment boundary to 3434 m at the Martinelli stream. Subsequently, hydraulic head was specified every 28 timesteps (once per week) along 65.5 m of the water table (Figure 5.2) according to field measurements of hydraulic head at the Saddle site, specifically weekly measurements from well SD4 in 2010 (Figure 5.3). Hydraulic head values from the Martinelli site were not used because measurements were made only during the summer. It was assumed that the water table at the Martinelli site fluctuated the same as the water table at the Saddle site. Head values along the remaining 14.4 m of the water

table (Figure 5.2), which represented the stream discharge region, equaled land surface elevation and were held constant throughout the simulation.

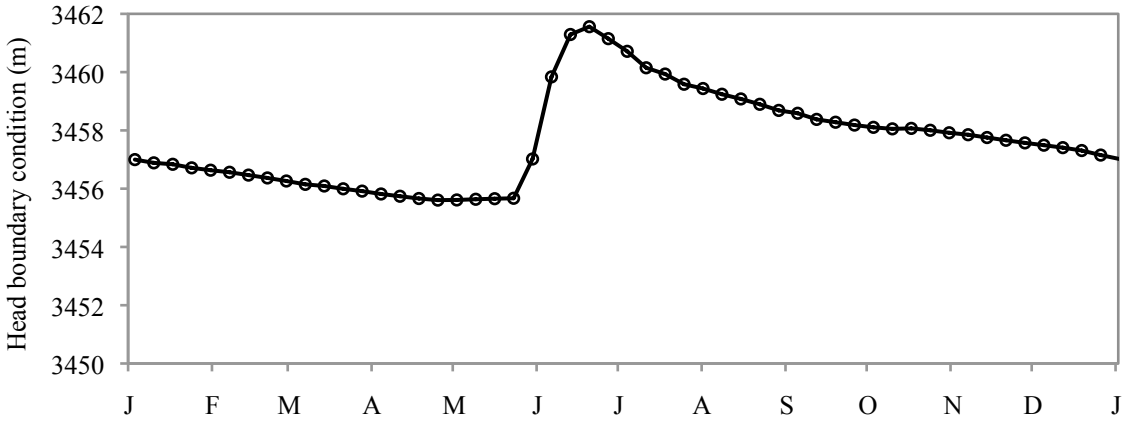

Figure 5.3. Time series of weekly hydraulic head data from well SD4 in 2010 that were used to define the time-dependent water table boundary condition along 65.5 m of the top of the model.

Field measurements indicated that the water table at Niwot Ridge fluctuates similarly each year (Chapter 3). Therefore, the weekly specified head boundary condition was repeated each year using 2010 data. The model was run until quasi-steady state conditions were reached (i.e. until peak model outflow repeated each year), which took about 18 years (26,264 timesteps).

5.2.4 Input parameters

Physical parameters input to the Martinelli model included values of hydraulic conductivity. Hydraulic conductivity was specified for both model units. The model was developed under heterogeneous conditions because the subsurface geology varies spatially. The surficial unit (Unit 1) was assumed isotropic because it is composed of poorly sorted sediments. The fractured bedrock unit (Unit 2) was assumed isotropic because at this relatively shallow depth fractures were assumed not to exhibit significant preferential orientation.

Hydraulic conductivity values for each model unit were initially set at a mid-range value based on the range of values determined from field-testing (Chapter 3) or the range of values for similar lithologies reported by Domenico and Schwartz (1990) (Table 5.1). Infiltration tests at

the Martinelli catchment indicated that hydraulic conductivity of near-surface deposits composed of poorly sorted sand and gravel ranged from 3.46×10^{-5} to 3.41×10^{-4} m/s (Unit 1). Slug tests conducted at the Martinelli site indicated that hydraulic conductivity of subsurface diamicton ranged from 9.82×10^{-5} to 2.85×10^{-4} m/s (Unit 1). Values of hydraulic conductivity for sand and gravel typically range from 2.0×10^{-7} to 3.0×10^{-2} m/s and for till typically range from 1.0×10^{-12} to 2.0×10^{-6} m/s (Domenico and Schwartz, 2004) (Unit 1). Values of hydraulic conductivity for fractured igneous and metamorphic rocks typically range from 8.0×10^{-9} to 3.0×10^{-4} m/s (Domenico and Schwartz, 2004) (Unit 2). Final values of hydraulic conductivity were determined during model calibration and are listed in Table 5.1.

5.2.5 Model calibration

The purpose of simulating groundwater flow at the Martinelli catchment was to estimate groundwater recharge during spring when groundwater levels were at their annual peak. The modeling approach required calibrating hydraulic conductivity until modeled peak groundwater outflow equaled measured peak groundwater outflow. Net model outflow is equal to the volume flux of fluid out of specified head nodes along the water table. It was assumed that all groundwater outflow discharged to the Martinelli stream as baseflow. In a system where recharge and baseflow are the only input and output of water, baseflow may be used as a proxy for recharge. Because hydraulic head observations were limited in the Martinelli catchment, the model was not calibrated with hydraulic head observations.

Liu et al. (2004) used geochemical and isotopic tracers and determined that baseflow contributed 54% to total flow in the Martinelli stream. In 2010, streamflow measured at the Martinelli stream gauge peaked during week 23 (June 6−12) and was on average 3.18×10^{-2} m^3/s. Therefore, the flux of baseflow was 1.72×10^{-2} m^3/s. This value was the targeted value during

model calibration. Measured peak baseflow was examined over a weeklong period because hydraulic head was specified at the water table on a weekly timescale.

Modeled outflow from the two-dimensional cross section represented baseflow to a unit length of stream in the three-dimensional Martinelli catchment. To scale the value of modeled outflow up to a value equivalent to measured baseflow, modeled outflow was multiplied by the length of the Martinelli stream above the cross section location (400 m) and multiplied by 2 because the model cross section is half of the catchment.

During calibration, hydraulic conductivity values were systematically adjusted until an acceptable match between simulated peak baseflow and measured peak baseflow was produced. After calibration, the value of modeled peak baseflow was assumed to equal peak groundwater recharge. Table 5.1 lists values of hydraulic conductivity that produced the best model fit. Calibrated hydraulic conductivity of the surficial deposit (Unit 1) was within approximately one order of magnitude of the results of field-testing and equaled 2.50×10^{-6} m/s. Deviation of modeled hydraulic conductivity from the results of infiltration and slug tests was expected. As both types of tests only test a small volume of aquifer material, results may not represent aquifer heterogeneity beyond the tested volume. In addition, the movement of water in the filter pack during slug testing may have lead to overestimates of hydraulic conductivity.

There were no available data for hydraulic conductivity of the fractured bedrock at the Martinelli catchment. Therefore, hydraulic conductivity of Unit 2 was calibrated to within the range of values reported by Domenico and Schwartz (1990) for fractured plutonic bedrock. Calibrated hydraulic conductivity of Unit 2 was 1.00×10^{-7} m/s.

5.3 Modeling results

Peak groundwater outflow was 2.16×10^{-5} m/s from the calibrated model. Scaled up to

represent the three-dimensional Martinelli catchment, modeled peak baseflow was 1.73×10^{-2} m^3/s, which was 0.6% greater than measured peak baseflow. Because the inflow of groundwater (recharge) equaled the outflow of groundwater (baseflow) for each timestep, peak recharge was assumed to equal peak modeled baseflow or 1.73×10^{-2} m^3/s. Spread over the area of the catchment (142,000 m^2), annual recharge peaked at the end of June at a rate of 1.22×10^{-7} m/s.

Figure 5.4 illustrates the results of the transient simulation once quasi-steady state conditions were reached. The time series shows measured weekly baseflow, modeled weekly baseflow, and measured hydraulic head specified weekly at the water table boundary over the course of a year. The timing of peak measured and peak modeled baseflow do not correspond because measured baseflow was calculated as a percentage of total streamflow (NWT Hydrology, 2011), modeled baseflow was affected by changes in head specified at the water table, and total streamflow peaks prior to peak water levels. The shape of the three curves was similar, suggesting that the model reasonably simulated baseflow to the Martinelli stream and that baseflow is strongly affected by changes in the position of the water table.

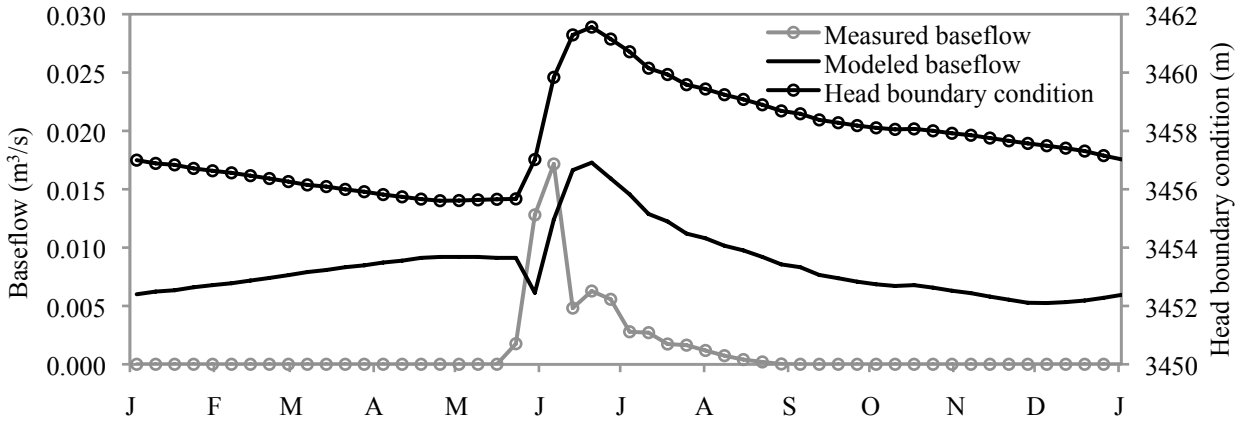

Figure 5.4. Annual time series of measured weekly baseflow, modeled weekly baseflow, and measured hydraulic head specified weekly at the water table boundary.

Figure 5.5 shows the distribution of modeled hydraulic head in the Martinelli catchment on April 25 when modeled baseflow was at its annual minimum, while Figure 5.6 shows the

distribution of head on June 20 when modeled baseflow was at its annual peak. At both times, hydraulic head decreased from the catchment boundary to the stream. Below the catchment boundary, hydraulic head decreased with depth indicating a recharge zone. Below the stream, hydraulic head increased with depth indicating a groundwater discharge zone. Groundwater flowed downward from the recharge zone, then from left to right following the decrease in elevation, and finally upward toward the discharge zone. The width of the recharge zone near the catchment boundary did not change significantly between minimum and peak modeled baseflow.

Hydraulic head at the stream did not vary between April 25 (Figure 5.5) and June 20 (Figure 5.6) because of the constant head boundary at the stream. Hydraulic head west of the stream discharge zone increased over 5 m between April 25 and June 20 reflecting the nearly 6 m rise in the water table the occurred in May and June.

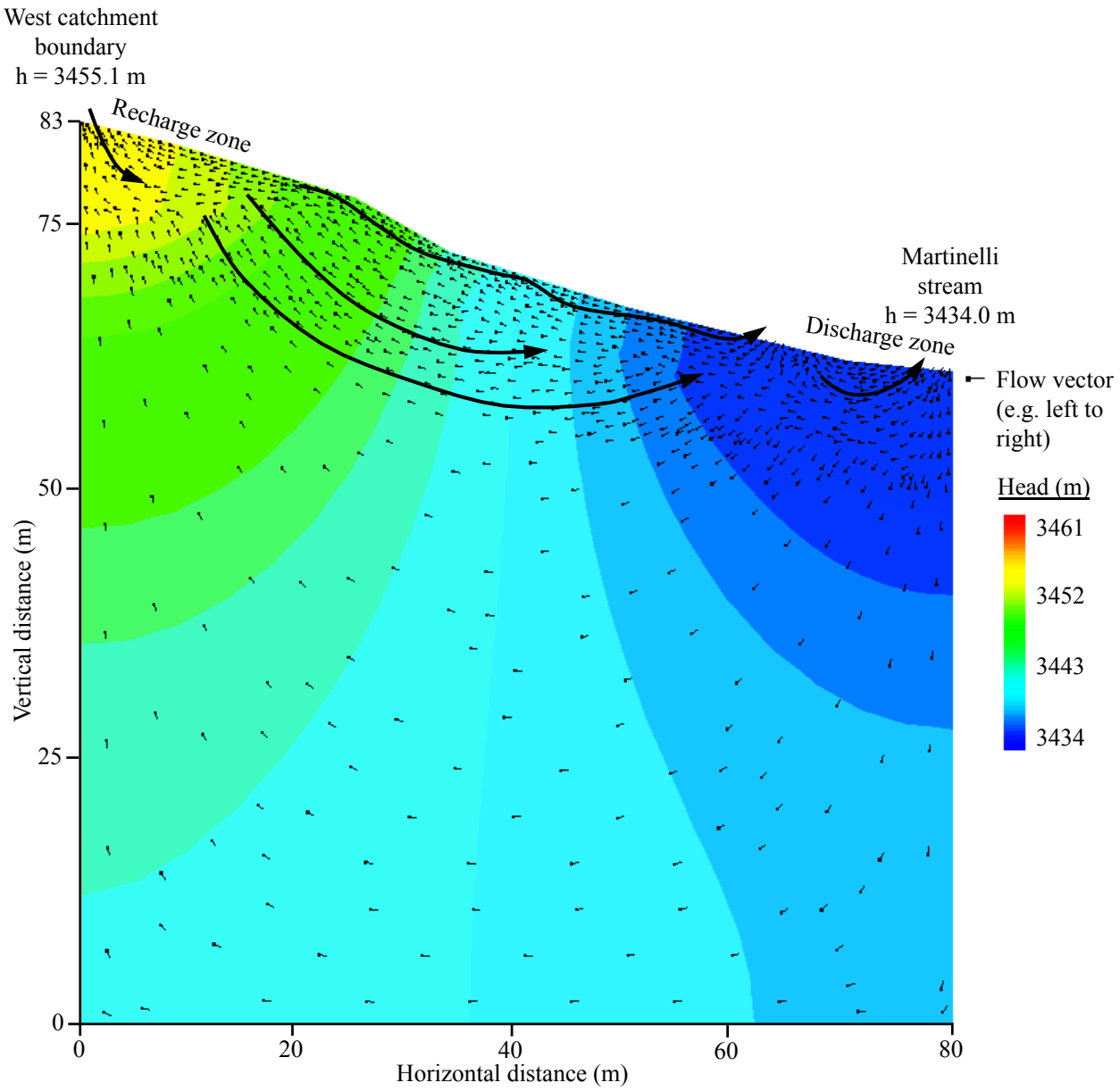

Figure 5.5. Distribution of modeled hydraulic head and groundwater flow in the Martinelli catchment on April 25 when modeled baseflow was at its annual minimum. Groundwater flowpaths are shown with long black arrows.

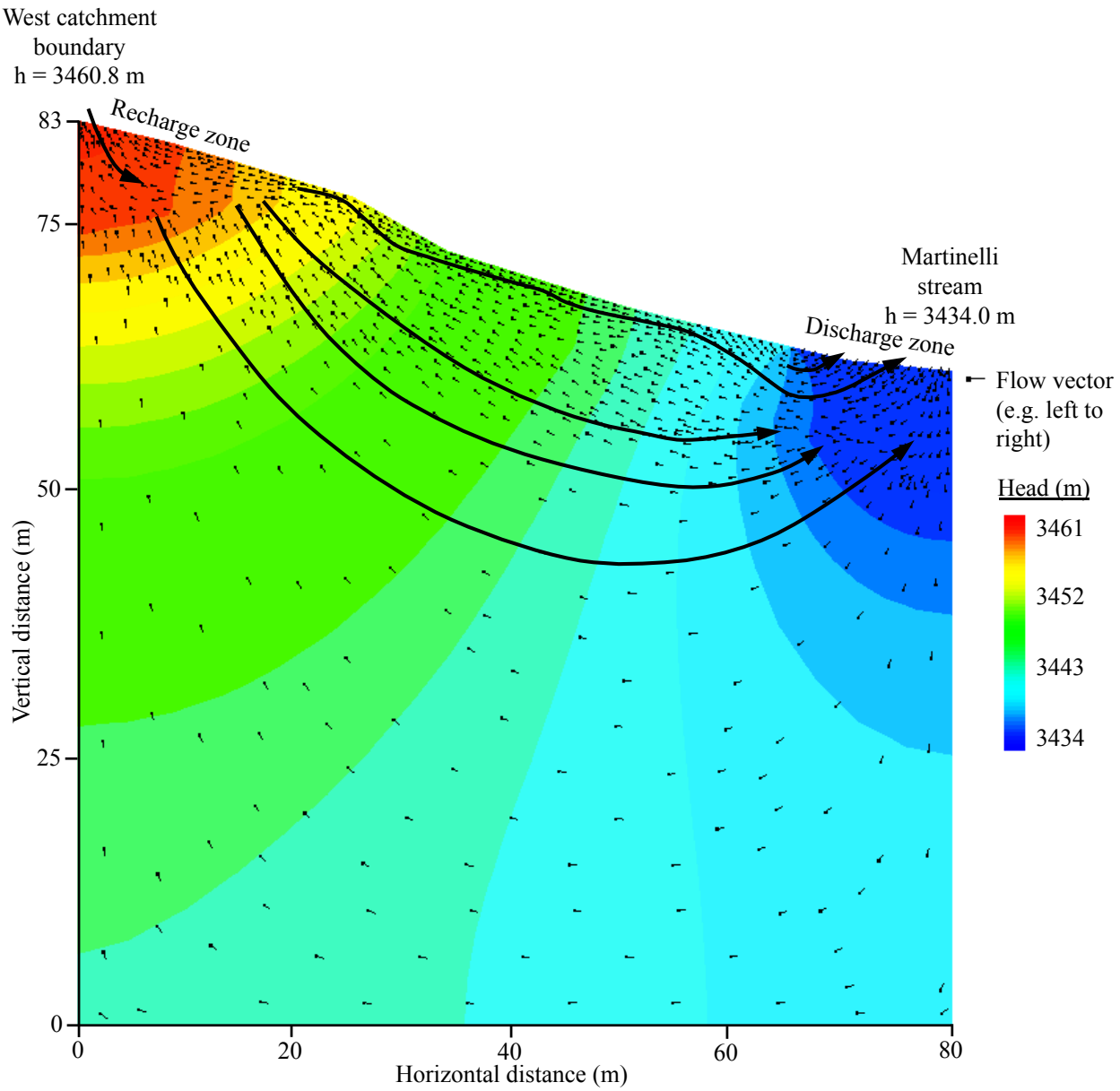

Figure 5.6. Distribution of modeled hydraulic head and groundwater flow in the Martinelli catchment on June 20 when modeled baseflow was at its annual peak. Groundwater flowpaths are shown with long black arrows.

Observation points were established at six nodes in the model (Figure 5.2) to examine changes in hydraulic head throughout the domain over the course of a year. Time series of head from the six points showed that head decreased with depth near the recharge zone (Figure 5.7). For example, time series from observation points 2 and 4, which are located 34 m from the catchment boundary with point 2 positioned 6 m above point 4, showed that head decreased from

point 2 to point 4 throughout the year. The results from the observation points also showed that the magnitude of the annual hydraulic head fluctuation decreased with depth. For example, the annual fluctuation at point 2 was about 6 m while the annual fluctuation at point 6, which is 54 m below point 2, was about 3 m. The time series from point 3 in the Martinelli stream showed that head did not change over time because head was held constant in the stream discharge region.

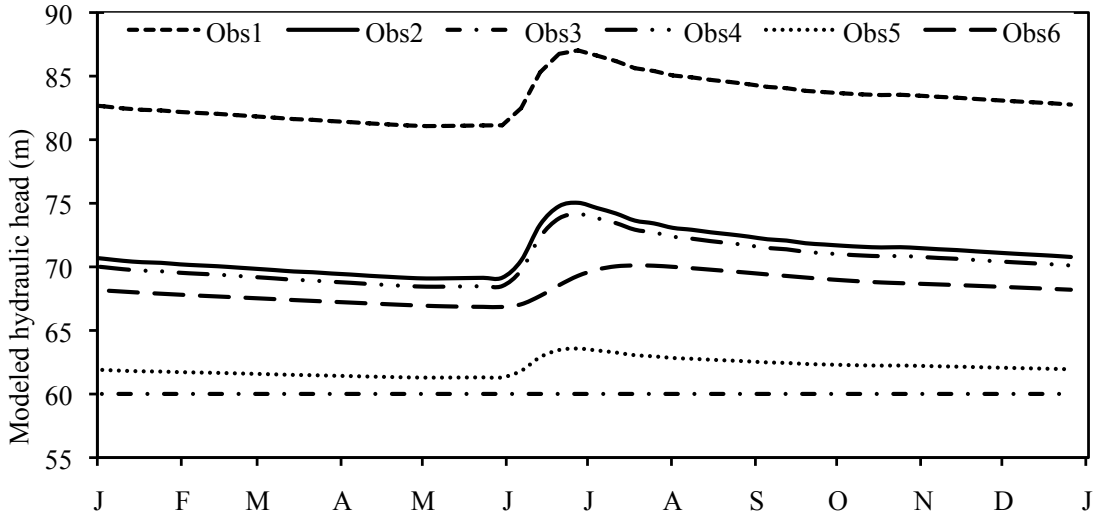

Figure 5.7. Annual time series of hydraulic head at six observation points in the Martinelli model. Locations of observation points are shown in Figure 5.2.

Figures 5.8 and 5.9 show distribution of modeled groundwater velocity in the Martinelli catchment on April 25 (minimum baseflow conditions) and June 20 (peak baseflow conditions). At both times, velocity decreased with depth and increased with topographic gradient. Velocity was highest in surficial deposit (~10^{-5} m/s or 1 m/d) and slowest in fractured bedrock (~10^{-9} m/s or ~10^{-4} m/d) due to the lower permeability of bedrock. Velocity was faster in surficial deposit in June than in April due to the higher hydraulic gradient resulting from the higher water table west of the stream during May and June. Groundwater velocity in bedrock did not change significantly between minimum and peak baseflow conditions. Modeled groundwater velocity of surficial deposit (~10^{-5} m/s or 1 m/d) agreed with estimates of velocity (i.e. specific discharge) using field data from the Martinelli site (1.1×10^{-5} m/s or 1.0 m/d) (Chapter 3).

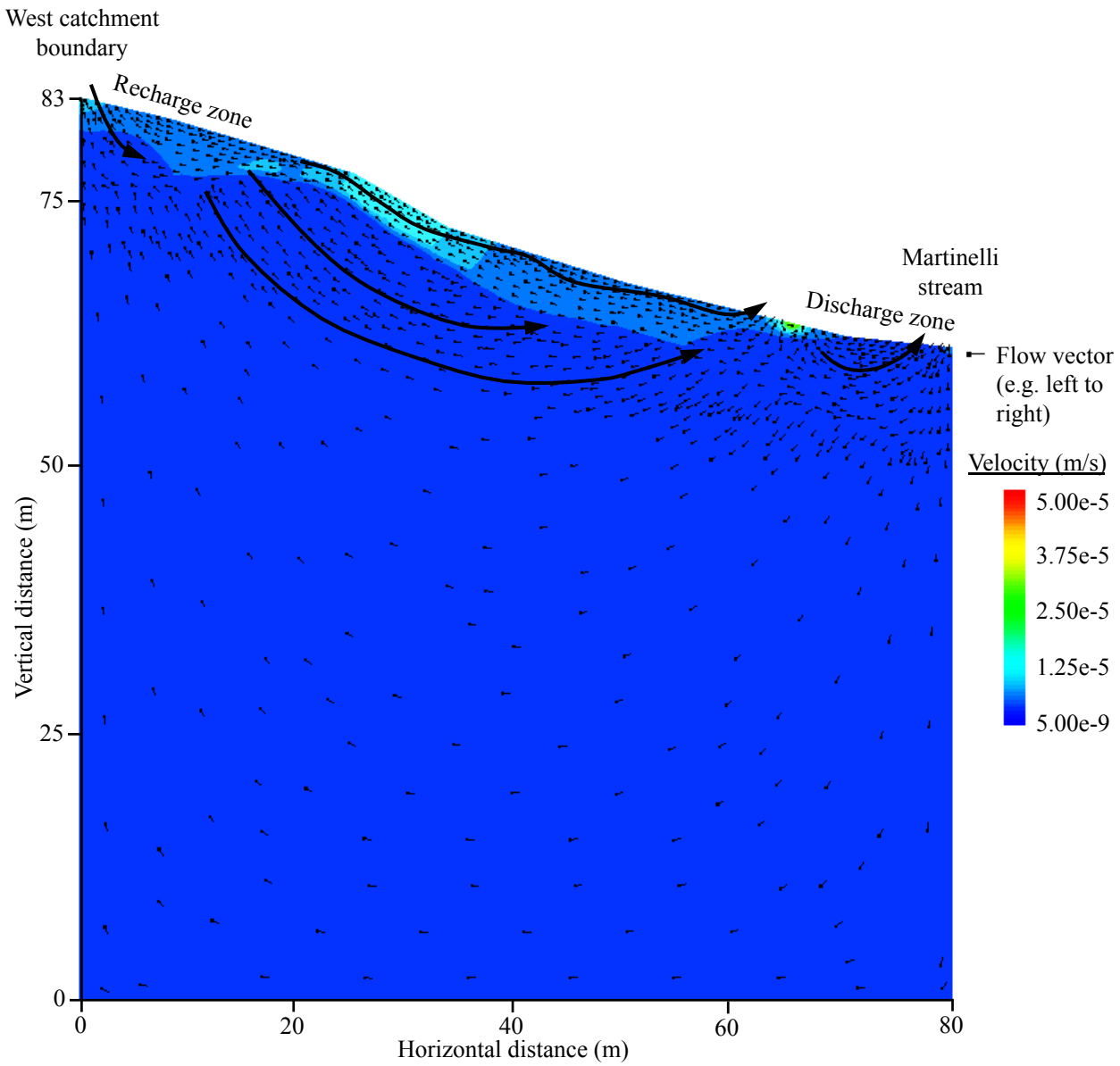

Figure 5.8. Distribution of modeled groundwater velocity and flow in the Martinelli catchment on June 20 when modeled baseflow was at its annual peak. Groundwater flowpaths are shown with long black arrows.

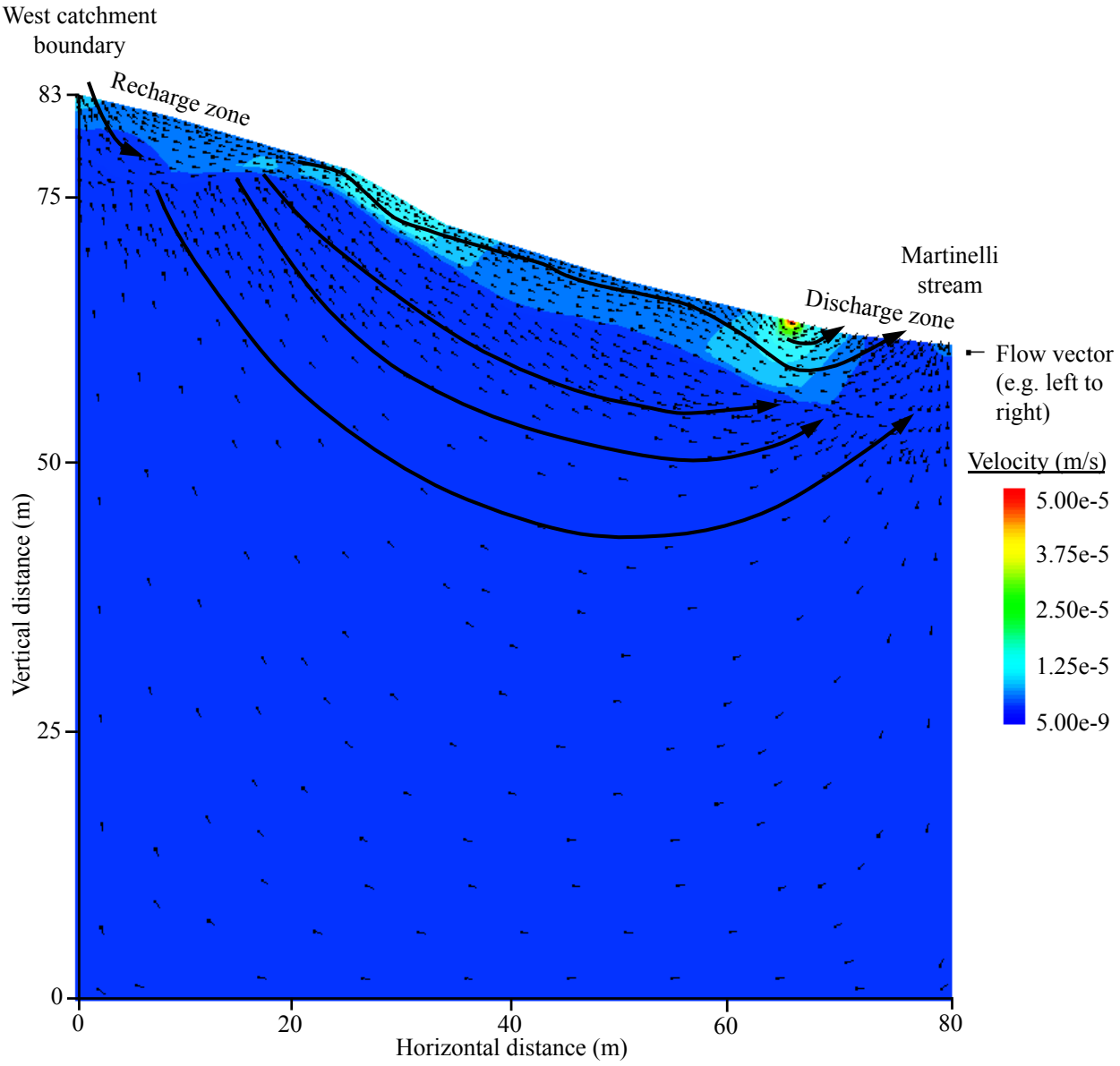

Figure 5.9. Distribution of modeled groundwater velocity and flow in the Martinelli catchment on June 20 when modeled baseflow was at its annual peak. Groundwater flowpaths are shown with long black arrows.

During minimum baseflow conditions, groundwater flowpaths showed that flow was concentrated in the upper 10 m of the shallow surficial deposit (Figure 5.8). During peak baseflow conditions, groundwater flowpaths showed that flow moved slightly deeper into the fractured bedrock (~20 m depth) due to the greater head specified at the water table (Figure 5.9); although, flow was still focused in the surficial layer. Flow occurred in the bedrock, suggesting

that the bedrock on Niwot Ridge is not a no-flow boundary. However, flow rates were significantly less in the bedrock (~10^{-9} m/s) than in the surficial deposits (~10^{-5} m/s).

5.4 Sensitivity analysis

Sensitivity analysis was conducted to identify which model parameters were the dominant controls on groundwater flow and recharge. Model sensitivity was studied by varying hydraulic conductivity and the water table boundary condition and noting the effect on peak model outflow, which is a proxy for recharge. Hydraulic conductivity of one unit was doubled while holding hydraulic conductivity of the other unit constant. The effect on peak model outflow was noted. Hydraulic conductivity of that unit was then halved and the effect on model outflow was noted. The same steps were performed on the other model unit. The width of the time-dependent water table boundary condition was increased by 5 m, which decreased the width of the constant head portion of the water table boundary, and the effect on peak model outflow was noted. The width of the time-dependent water table boundary was then decreased by 5 m and the effect on outflow was noted.

Figure 5.10 shows the results of sensitivity analysis. In the surficial deposit (Unit 1), increasing hydraulic conductivity had a greater effect on peak model outflow, or recharge, than decreasing hydraulic conductivity. Doubling hydraulic conductivity of the surficial deposit from the calibrated value of 2.50×10^{-6} m/s to 5.00×10^{-6} m/s resulted in a 97% increase in peak model outflow, from 1.73×10^{-2} m^3/s to 3.41×10^{-2} m^3/s. Halving hydraulic conductivity of the surficial deposit from 2.50×10^{-6} m/s to 1.25×10^{-6} m/s resulted in only a 49% decrease in peak model outflow, from 1.73×10^{-2} m^3/s to 8.86×10^{-3} m^3/s. Neither changing hydraulic conductivity of the fractured bedrock unit (Unit 2) nor changing the width of the time-dependent specified head water table boundary had much effect of peak model outflow. In the fractured bedrock (Unit 2),

doubling or halving hydraulic conductivity resulted in only a 1% increase or 1% decrease in peak model outflow, respectively. Increasing or decreasing the width by 5 m resulted in a 3% increase or 3% decrease in peak outflow, respectively. Peak outflow from the model was most sensitive to an increase in hydraulic conductivity the surficial deposit. Outflow was least sensitive to an increase or decrease in hydraulic conductivity of the fractured bedrock.

The results of sensitivity analysis indicated that peak modeled outflow, or recharge, was sensitive to changes in hydraulic conductivity, particularly an increase in hydraulic conductivity of the surficial deposit. It is therefore important to properly characterize the permeability of the shallow subsurface. Future investigation should focus on the surficial deposit because variation in hydraulic conductivity of this unit had the greatest effect on modeled recharge.

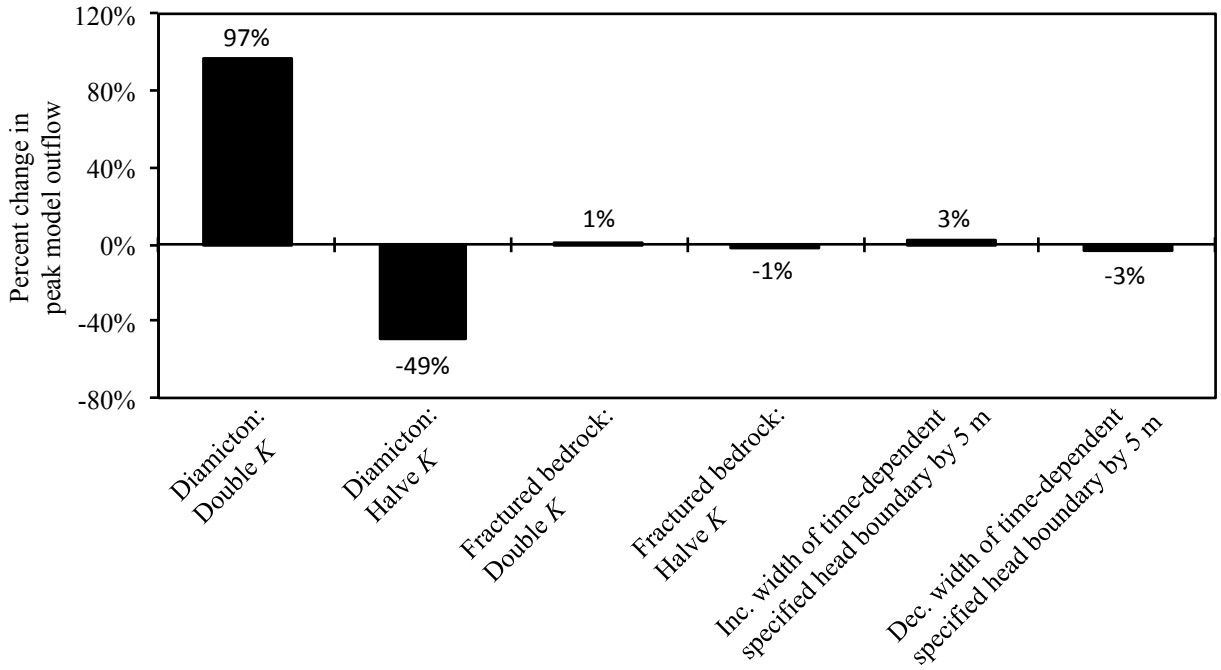

Figure 5.10. The results of sensitivity analysis performed on the Martinelli model. Results are indicated as a percent increase or decrease in modeled outflow, which is a proxy for recharge, in response to doubling or halving hydraulic conductivity (*K*) of a model unit or to increasing or decreasing the width of the time-dependent specified head boundary condition by 5 m.

5.5 Limitations

There were several limitations of the model examined in this study. The lack of adequate field data for the Martinelli catchment meant that model simulations were somewhat ambiguous. The model did not take into account the presence of local heterogeneities (e.g. lithology, fracture networks, ice lenses) or time-dependent variables other than the elevation of the water table (e.g. water input from snowmelt, temperature, variation in the proportion of streamflow that is baseflow). These factors may have significant effects on recharge and should be explored in future work. Still, the results of this study are useful for determining the particular types of data and research that are needed to better understand the hydrogeology of Niwot Ridge.

The model was run under two-dimensional, fully saturated, quasi-steady state conditions. Modeling in 2-D restricts flow patterns to two dimensions when in reality flow occurs in three dimensions. Therefore, the estimate of peak recharge (1.22×10^{-7} m/s) is likely a lower bound on peak recharge to the Martinelli catchment because the two-dimensional model probably underestimated groundwater flow. Incorporation of the unsaturated zone would improve understanding of how groundwater recharges the aquifer and at what depth below ground surface. Modeling at quasi-steady state did not permit study of recharge variability over timescales greater than 1 year, which has important implications for flowpath calculation, nutrient cycling, and groundwater budget calculations (Dripps et al., 2006).

Perhaps the biggest limitation is that the model solutions are nonunique. Multiple calibrations of the model were possible by varying boundary conditions and aquifer parameters. The model presented represents the best estimate of aquifer conditions. Other recharge estimation methods should be employed to provide insight on nonuniqueness, measurement error, and invalid assumptions (Healy, 2010). Furthermore, the use of additional methods would

help refine the conceptual model of groundwater flow and recharge.

5.6 Summary and discussion

This chapter presented a model of groundwater flow in the Martinelli catchment. The model was developed and run using the SUTRA numerical code. Model results indicated that peak annual baseflow to the Martinelli stream occurs at a rate of 1.73×10^{-2} m^3/s and recharge to the Martinelli catchment occurs at a rate of 1.22×10^{-7} m/s. Peak baseflow and peak recharge occurred at the end of June. These rates were calibrated using estimates of hydraulic conductivity. Clow et al. (2003) showed that a high-conductivity surficial unit, such as the diamicton, could account for high rates of groundwater discharge to streams following major events such as snowmelt. The results of this study showed a similar trend. Modeled peak baseflow occurred at the end of June, which was roughly two weeks after snowmelt peaked on June 6 (Rory Cowie, personal communication, 25 April 2011). Furthermore, results of sensitivity analysis indicated that the primary control on recharge to the Martinelli catchment is the hydraulic conductivity of the surficial deposit.

Model results showed that groundwater flowed primarily in the upper 10 m of the surficial unit, suggesting that the surficial deposits are most important for recharge. Groundwater velocity was fast within the surficial deposit, due to higher hydraulic conductivity, and slow through the deeper fractured bedrock, due to lower hydraulic conductivity. Groundwater recharged at the catchment boundary and discharged to the stream. In addition, changes in baseflow throughout the year were strongly affected by the position of the water table. Results of this study agree with prior work that alpine streams generally gain groundwater (Clow et al., 2003; Liu et al., 2004), that groundwater flowpaths on Niwot Ridge are shallow, and that groundwater plays an important role in streamflow generation (Cowie, 2010).

Modeled recharge at the Martinelli catchment (1.22×10^{-7} m/s) was significantly higher than recharge determined by the water table fluctuation (WTF) method at the Saddle site (1.25 m/y or 3.96×10^{-8} m/s) (Chapter 4). The difference in recharge rates does not likely reflect differences between the Martinelli and Saddle catchments, because the catchments are adjacent to each other. Instead, the difference resulted because the value from the Martinelli catchment was the annual maximum rate and the value from the Saddle catchment was the annual mean rate. Assuming annual mean and annual maximum recharge rates are similar for both catchments, peak recharge to the Niwot Ridge groundwater system occurs roughly 3.1 times faster than recharge averaged over the course of a year.

Chapter 6
Conclusions

6.1 Summary

The goal of this study was to improve understanding of the spatial and temporal variability of groundwater flow and recharge in a high-altitude mountainous watershed. It is the first attempt to characterize the shallow subsurface hydrogeology of the snowmelt-dominated aquifer on Niwot Ridge, Front Range, Colorado. In particular, two small alpine catchments were examined, the Saddle catchment and Martinelli catchment. The study site was characterized using results of groundwater level monitoring, infiltration tests, and slug tests. Recharge was estimated using the water table fluctuation (WTF) method and groundwater modeling. The water budget for Niwot Ridge was determined using the results of field characterization.

The results of this thesis contribute to the scientific knowledge about the Niwot Ridge hydrologic system as well as to the broader understanding of how groundwater is replenished at its source by mountain recharge. The primary conclusion is that recharge to groundwater on Niwot Ridge is significant (mean rate = 1.25 m/y or 3.96×10^{-8} m/s, peak rate = 1.22×10^{-7} m/s) and that the subject of mountain hydrogeology should be further studied.

6.2 Conclusions

Major results from this study are summarized in Table 6.1 and are described below.

Hydrogeologic variable		Range of values or mean value	Method used
Depth to water table from ground surface		-0.4−8.5 m	Groundwater level monitoring
Infiltration capacity		2.87×10^{-5}−6.71×10^{-4} m/s	Infiltration tests
Hydraulic conductivity:	Quaternary-Tertiary diamicton	1.92×10^{-4} m/s, 2.50×10^{-6} m/s	Slug tests, Model calibration
	fractured Tertiary bedrock	8.74×10^{-4} m/s, 1.00×10^{-7} m/s	Slug tests, Model calibration
	fractured Precambrian bedrock	8.42×10^{-6} m/s	Slug tests
Groundwater flow rate		1.1×10^{-5}− 8.9×10^{-5} m/s	Darcy's law
Specific yield at the Saddle site		0.033	Water budget
Recharge rate at Saddle site		0.57−1.64 m/y (mean 1.25 m/y)	Water table fluctuation
Peak recharge rate at Martinelli site		1.22×10^{-7} m/s (in June)	Groundwater modeling

Table 6.1. Major results from this study.

1. Depth of the water table at Niwot Ridge is shallow, at most 8.5 m below ground surface, and is a subdued replica of topography. Because of its ridge-top location, depth to water at the Saddle site was slightly greater than at the Martinelli site, which is located mid-slope. Water levels at both sites fluctuated seasonally, rising steeping in late spring following snowmelt and gradually declining through the rest of the year when water inputs were minimal. The single rise and fall of water levels implied that one significant recharge period occurred per year. The near-surface aquifers at both sites are unconfined.

2. Infiltration capacity was similar for the two catchments and ranged 2.87×10^{-5} to 6.71×10^{-4} m/s. Infiltration capacity was greatest in material with a large proportion of gravel and material that was either dry or slightly wet suggesting that recharge rates in these materials is also high.

3. Slug test results showed that hydraulic conductivity of the Quaternary-Tertiary diamicton at the Martinelli site was 1.92×10^{-4} m/s. Hydraulic conductivity of fractured Tertiary bedrock and fractured Precambrian at the Saddle site were 8.74×10^{-4} m/s and 8.42×10^{-6} m/s, respectively. Calibration of the groundwater flow model of the Martinelli catchment indicated that hydraulic conductivity was 2.50×10^{-6} m/s for the diamicton and 1.00×10^{-7} m/s for the Tertiary bedrock.

4. Groundwater flow rate ranged 1.1×10^{-5} to 8.9×10^{-5} m/s (1.0−7.7 m/d). In the model of the Martinelli catchment, high contrast in hydraulic conductivity between surficial deposit and bedrock resulted in quick and shallow groundwater flow in surficial deposit. Flow in bedrock was significantly slower. Hydraulic gradients indicated that groundwater flows from high to low topography and toward streams. Groundwater recharged at ridgetops and discharged to streams.

5. At the Saddle site, results from WTF method indicated that recharge averaged 1.25 m/y, or 52.5% of mean annual precipitation, and ranged from 0.57 m/y in areas where little snow accumulates to 1.64 m/y in areas where snow depths reach several meters. Variation in recharge

over short horizontal distances most likely reflects high spatial variability of snow and snowmelt.

6. At the Martinelli site, results from groundwater flow modeling indicated peak recharge occurred in June at a rate of 1.22×10^{-7} m/s. Peak recharge was most sensitive to increases in hydraulic conductivity of surficial deposit. Modeled recharge was at a minimum through winter months, rose quickly to a maximum in June when the water table was highest, and gradually declined through the remainder of the year. Assuming annual mean and annual maximum recharge rates are similar for the Saddle and Martinelli catchments, peak recharge to the Niwot Ridge groundwater system occurs roughly 3.1 times faster than recharge averaged over a year.

7. Assuming 100% water input from precipitation, the annual water budget at Niwot Ridge, specifically the Saddle site, included 33% evapotranspiration, 15% sublimation, 13% runoff, and 52% recharge (with 13% total error).

6.3 Future work

Based on the results of this study, recommendations are made for extending this work in the future to improve understanding of the complex hydrogeology of the study site. Continued monitoring of groundwater levels is recommended. Because the water table is shallow and water level response to recharge is rapid, improvement would be made by measuring water levels more frequently. Finer resolution of water level data would permit study of short-term trends (e.g. diurnal) and improve use of the WTF method for estimating recharge. A more spatially dense monitoring well network could be used to better delineate recharge and discharge zones and groundwater flow patterns. The installation of deeper monitoring wells would allow for improved understanding of the geology at depth.

Any uncertainty in estimation of hydraulic conductivity and measured baseflow is carried through to the uncertainty in the recharge estimate by groundwater modeling methods. To

reduce the uncertainty in hydraulic conductivity, future work should include pumping tests to determine hydraulic conductivity of a larger volume of aquifer. Delineation of fracture networks would also refine estimates of hydraulic conductivity. To reduce the uncertainty in measured baseflow, future work should incorporate groundwater travel times estimated using groundwater ages obtained from environmental tracer concentrations (Sandford, 2002). Future modeling efforts would be greatly improved by reducing uncertainty in input and calibration parameters as well as incorporating three dimensions and the unsaturated zone.

Better climate data would improve estimates of water available for recharge. Increasing the spatial density of precipitation and snow depth measurements at both the Saddle and Martinelli catchments is recommended. In addition, measurements of ground temperature over several depths at multiple locations across the study site would improve understanding of how freezing conditions affect infiltration and groundwater flow.

The use of global information systems (GIS) in groundwater hydrology has not been explored at Niwot Ridge. GIS and a digital elevation model (DEM) could be used to delineate hydrogeomorphic settings (landforms caused by action of water (Scheidegger, 1973)) based on topography and vegetation, which could then be used to locate recharge and discharge zones on a fine spatial scale. Information gained from use of GIS would also improve three-dimensional groundwater modeling efforts.

Additional recharge estimation methods should be used as more data become available. For example, Darcy's law could be used to calculate recharge using available soil moisture data from Niwot Ridge. Recharge estimation is an iterative process (Healy, 2010) and requires continued field data collection, data analysis, and revision of the conceptual model of recharge.

References

Abbott, M. D., Lini, A., and Bierman, P. R. (2000). $\delta^{18}O$, δD, and ^{3}H measurements constrain groundwater recharge patterns in an upland fractured bedrock aquifer, Vermont, USA. *Journal of Hydrology*, *228*(1−2), 101−112.

Aleinikoff, J. N., Reed, J.C., and de Witt, E. (1993). The Mount Evans batholith in the Colorado Front Range: revision of its age and reinterpretation of its structure. *Geological Society of America Bulletin*, *105*, 791–806.

Allen, D. M., Whitfield, P. H., and Werner, A. (2010). Groundwater level responses in temperate mountainous terrain; regime classification, and linkages to climate and streamflow. *Hydrological Processes*, *24*(23), 3392−3412. doi:10.1002/hyp.7757.

Anderson, M. P. (2005). Review paper: Heat as a ground water tracer. *Ground Water*, *43*(6), 951−968. doi:10.1111/j.1745-6584.2005.00052.x.

Anderson, M. P., and Woessner, W. W. (2002). *Applied Groundwater Modeling*. San Diego, CA: Academic Press.

Anderson, R. S., Riihimaki, C. A., Safran, E. B., and MacGregor, K. R. (2006). Facing reality: Late Cenozoic evolution of smooth peaks, glacially ornamented valleys, and deep river gorges of Colorado's Front Range, in: Willett, S.D., Hovius, N., Brandon, M.T., and Fisher, D.M., (eds.), *Tectonics, Climate, and Landscape Evolution*: Geological Society of America Special Paper 398. Boulder, CO: Geological Survey Society of America, p. 397–418. doi: 10.1130/2006.2398(25).

Bales, R. C., Molotch, N. P., Painter, T. H., Dettinger, M. D., Rice, R., and Dozier, J. (2006). Mountain hydrology of the western United States. *Water Resour. Res.*, *42*(8). doi:10.1029/2005WR004387.

Belan, R. A., and Matlock, W. G. (1973). Groundwater recharge from a portion of the Santa Catalina Mountains. *Hydrology and Water Resources in Arizona and the Southwest*, *3*, 33−40.

Benedict, J. B., (1970). Downslope soil movement in a Colorado alpine region: rates, processes, and climatic significance. *Arctic and Alpine Research*, *2*, 165–226.

Berg, N.H. (1986). Blowing snow at a Colorado alpine site: measurements and implications. *Arctic and Alpine Research*, *18*, 147−161.

Bossong, C. R., Caine, J. S, Stannard, D. I., Flynn, J. L., Stevens, M. R., and Heiny-Dash, J. S. (2003). *Hydrologic Conditions and Assessment of Water Resources in the Turkey Creek Watershed, Jefferson County, Colorado,1998−2001*. (U.S. Geological Survey Water-Resources Investigation Report 03-4034). Reston, VA: U.S. Geological Survey.

Bouwer, H., and Rice, R. C. (1976). A slug test for determining hydraulic conductivity of unconfined aquifers with completely or partially penetrating wells. *Water Resources Research*, *12*(3), 423−428. doi:10.1029/WR012i003p00423

Bowman, W. D. (2001). Introduction: Historical Perspective and Significance of Alpine Ecosystem Studies. In Bowman, W. and Seastedt, T.R., (eds.), *Alpine Dynamics: The Structure and Function of an Alpine Ecosystem: Niwot Ridge, Colorado* (pp. 3−12). New York, NY: Oxford University Press.

Burgy, R. H., and J. N. Luthin (1956). A test of the single- and double-ring infiltrometers. *American Geophysical Union Transactions*, *37*, 189−191.

Burns, S. F. (1980). *Alpine soil distribution and development, Indian Peaks, Colorado Front Range*. (Doctoral dissertation). University of Colorado at Boulder, Boulder, CO.

Butler, J. J., Jr. (1998). *The Design, Performance, and Analysis of Slug Tests*. Boca Raton, FL: Lewis Publishers.

Butler, J.J., Jr., Garnett, E.J., and Healey, J.M., (2003). Analysis of slug tests in formations of high hydraulic conductivity. *Ground Water*, *41*(5), 620−630.

Caine, J. S., A. H. Manning, P. L. Verplanck, D. J. Bove, K. G. Kahn, and S. Ge, (2006). *Well Construction Information, Lithologic Logs, Water Level Data, and Overview of Research in Handcart Gulch, Colorado: An Alpine Watershed Affected by Metalliferous Hydrothermal Alteration*. (U.S. Geological Survey Open-File Report 2006-1189). Reston, VA: U.S. Geological Survey.

Caine, J. S., and Tomusiak, S. R. A. (2003). Brittle structures and their role in controlling porosity and permeability in a complex Precambrian crystalline-rock aquifer system in the Colorado Rocky Mountain Front Range. *Geological Society of America Bulletin*, *115*(11), 1410−1424. doi:10.1130/B25088.1

Caine, N. (1989a). Diurnal variations in the quality of water draining from an alpine snowpack. *Catena*, *16*,153−162.

Caine, N. (1989b). Hydrograph separation in a small alpine basin based on inorganic solute concentrations. *J. Hydrol.*, *112*, 89−101.

Caine, N. (1992). Sediment transfer on the floor of the Martinelli snowpatch, Colorado Front Range, USA. *Geografiska Annaler. Series A: Physical Geography*, *74*(2−3), 133−144.

Caine, N. (1995). Snowpack Influences on Geomorphic Processes in Green Lakes Valley, Colorado Front Range. *The Geographic Journal*, *161*(1), 55−68.

Caine, N. (2001). Geomorphic systems of Green Lakes Valley. In Bowman, W. and Seastedt, T.R., (eds.), *Alpine Dynamics: The Structure and Function of an Alpine Ecosystem: Niwot Ridge, Colorado* (pp. 45−74). New York, NY: Oxford University Press.

Caine, N., and Thurman, E. M. (1990). Temporal and spatial variations in the solute content of an alpine stream, Colorado Front Range. *Geomorphology*, *4*(1), 55−72.

Chen, W., and Lee, C. (2003). Estimating ground-water recharge from streamflow records. *Environmental Geology (Berlin)*, *44*(3), 257−265.

Cherkauer, D. S. (2004). Quantifying ground water recharge at multiple scales using PRMS and GIS. *Ground Water*, *42*(1), 97-110.

Cherkauer, D. S., and Ansari, S. A. (2005). Estimating ground water recharge from topography, hydrogeology, and land cover. *Ground Water*, *43*(1), 102−112.

Cline, D. W., (1997). Effect of seasonality of snow accumulation and melt on snow surface energy exchanges at a continental alpine site, *Journal of Applied Meteorology*, *36*, 32−51. doi: 10.1175/1520-0450(1997)036<0032:EOSOSA>2.0.CO;2.

Clow, D. W., Schrott, L., Webb, R., Campbell, D. H., Torizzo, A., and Dornblaser, M. M. (2003). Ground water occurrence and contributions to streamflow in an alpine catchment, Colorado Front Range. *Ground Water*, *41*(7), 937−950.

Coes, A. L., T. B. Spruill, and M. J. Thomasson (2007). Multiple-method estimation of recharge rates at diverse locations in the North Carolina Coastal Plain, USA. *Hydrogeology Journal*, *15*, 773−788.

Cowie, R. (2010). *The hydrology of headwater catchments from the plains to the Continental Divide, Boulder Creek Watershed, Colorado*. (Master's thesis). University of Colorado at Boulder, Boulder, CO.

Cutillo, P. A., and Bredehoeft, J. D. (2010). Estimating aquifer properties from the water level response to earth tides. *Ground Water*. doi:10.1111/j.1745-6584.2010.00778.x

Dagan, G., (1978). A note on packer, slug, and recovery tests in unconfined aquifers. *Water Resources Research*, *14*(5), 929−934.

Davinroy, T. C. (2000). *Hydrological and biogeochemical characteristics of alpine talus, Colorado Front Range*. (Doctoral dissertation). University of Colorado at Boulder, Boulder, CO.

Delin, G., Healy, R., Lorenz, D., and Nimmo, J. (2007). Comparison of local- to regional-scale estimates of ground-water recharge in Minnesota, USA. *Journal of Hydrology*, *334*(1−2), 231−249.

Delin, G. N., and Risser, D. W. (2007). *Ground-Water Recharge in Humid Areas of the United States−A Summary of Ground-Water Resources Program Studies, 2003-06*. (U.S. Geological Survey Fact Sheet FS-2007-3007). Reston, VA: U.S. Geological Survey.

Dethier, D. P., Benedict, J. B., Birkeland, P. W., Caine, N., Davis, P. T., Madole, R. F., … Shroba, R. R. (2003). Quaternary stratigraphy, geomorphology, soils, and alpine archaeology in an alpine-to-plains transect, Colorado Front Range. In D. J. Easterbrook (Ed.), *Quaternary geology of the United States; INQUA 2003 field guide*. Reno, NV: Desert Research Institute.

de Vries, J. J., and Simmers, I. (2002). Groundwater recharge: An overview of processes and challenges. *Hydrogeology Journal*, *10*(1), 5−17. doi:10.1007/s10040-001-0171-7

Dingman, S. L. (2002). *Physical Hydrology* (2nd ed.). Long Grove, IL: Waveland Press, Inc.

Domenico, P. A., and Schwartz, F. W., (1990). *Physical and Chemical Hydrogeology*. New York, NY: John Wiley and Sons.

Dripps, W. R., Hunt, R. J., and Anderson, M. P. (2006). Estimating recharge rates with analytic element models and parameter estimation. *Ground Water*, *44*(1), 47−55. doi:10.1111/j.1745-6584.2005.00115.x

Duffield, G. M. (2007). *AQTESOLV for Windows Version 4.5 User's Guide*. Reston, VA: HydroSOLVE, Inc.

Earman, S., Campbell, A. R., and Phillips, F. M. (2004). Where does groundwater in mountainous terrain come from? The importance of high-elevation precipitation and snow as contributors to mountain groundwater. *Geological Society of America, 2004 Annual Meeting, Abstracts with Programs*, *36*(5), 538.

Erickson, T. A., Williams, M. W., and Winstral, A. (2005). Persistence of topographic controls on the spatial distribution of snow in rugged mountain terrain, Colorado, United States. *Water Resources Research*, *41*(4), W04014. doi:10.1029/2003WR002973

Feth, J. H., D. A. Barker, L. G. Moore, R. J. Brown, and C. E. Veirs (1966). *Lake Bonneville: geology and hydrology of the Weber Delta District, including Ogden, Utah*. (U.S. Geological Survey Professional Paper 518). Reston, VA: U.S. Geological Survey.

Fetter, C. W., (2001). *Applied Hydrogeology* (4th ed.). New York, NY: Macmillan.

Flerchinger, G. N., Deng, Y., and Cooley, K. R. (1993). Groundwater response to snowmelt in a mountainous watershed; testing of a conceptual model. *Journal of Hydrology*, *152*(1−4), 201−214.

Flint, A. L., Flint, L. E., Kwicklis, E. M., Fabryka-Martin, J. T., and Bodvarsson, G. S. (2002). Estimating recharge at Yucca Mountain, Nevada, USA; comparison of methods. *Hydrogeology Journal*, *10*(1), 180−204.

Flynn, R. H., and Tasker, G. D. (2004). *Generalized estimates from streamflow data of annual and seasonal ground-water-recharge rates for drainage basins in New Hampshire*. (21, Hydrogeology No. SIR 2004-5019). Reston, VA: U.S. Geological Survey.

Forster, C., and Smith, L. (1988a). Groundwater flow systems in mountainous terrain; 1, numerical modeling technique. *Water Resources Research*, *24*(7), 999−1010. doi:10.1029/WR024i007p00999

Forster, C., and Smith, L. (1988b). Groundwater flow systems in mountainous terrain; 2, controlling factors. *Water Resources Research*, *24*(7), 1011−1023. doi:10.1029/WR024i007p01011

Freeze, R.A. and Cherry, J.A., (1979). *Groundwater*. Englewood Cliffs, NJ: Prentice Hall.

Freeze, R. A., and Witherspoon, P. A. (1967). Theoretical analysis of regional groundwater flow; part 2, effect of water-table configuration and subsurface permeability variation. *Water Resources Research*, 3(2), 623−634. doi:10.1029/WR003i002p00623

Gable, D. J. (2000). *Geologic map of the Proterozoic rocks of the central Front Range, Colorado*. (14, Geologic maps No. I-2605). Reston, VA: U.S. Geological Survey.

Gable, D. J., and Madole, R. F. (1976). *Geologic map of the Ward quadrangle, Boulder County, Colorado* [map]. 1:24,000. (Geologic Quadrangle Map Series, map GQ-1277). Reston, VA: U.S. Geological Survey.

Gburek, W. J., Folmar, G. J., and Urban, J. B. (1999). Field data and ground water modeling in a layered fractured aquifer. *Ground Water*, *37*(2), 175−184.

Gleeson, T., and Manning, A. H. (2008). Regional groundwater flow in mountainous terrain: Three-dimensional simulations of topographic and hydrogeologic controls. *Water Resour. Res.*, *44*, W10403. doi:10.1029/2008WR006848.

Gleeson, T., Marklund, L., Smith, L., and Manning, A. H. (2011). Classifying the water table at regional to continental scales. *Geophys. Res. Lett.*, *38*, L05401. doi:10.1029/2010GL046427.

Gleeson, T., Novakowski, K., and Kurt Kyser, T. (2009). Extremely rapid and localized recharge to a fractured rock aquifer. *Journal of Hydrology (Amsterdam)*, *376*(3−4), 496−509. doi:10.1016/j.jhydrol.2009.07.056

Greenland, D. (1989). The climate of Niwot Ridge, Front Range, Colorado, U.S.A. *Arctic and Alpine Research*, *21*(4), 380−391.

Greenland, D., and M. Losleben (2001). Climate. In Bowman, W. and Seastedt, T.R., (eds.), *Alpine Dynamics: The Structure and Function of an Alpine Ecosystem: Niwot Ridge, Colorado* (pp. 15−31). New York, NY: Oxford University Press.

Greenstein, L. A., Pewe, T. L., and Brown, J. (1983). An investigation of midlatitude alpine permafrost on Niwot Ridge, Colorado Rocky Mountains, USA; permafrost; fourth international conference, proceedings. *International Conference on Permafrost, Proceedings*, *4*, 380−383.

Halford, K. J., and Mayer, G. C. (2000). Problems associated with estimating ground water discharge and recharge from stream-discharge records. *Ground Water*, *38*(3), 331−342.

Hall, D. W., and Risser, D. W. (1993). Effects of agricultural nutrient management on nitrogen fate and transport in Lancaster County, Pennsylvania. *Water Resources Bulletin*, *29*(1), 55−76.

Hamann, H. B. (2002). *The ionic pulse, snowmelt flowpaths, and surface water chemistry in two alpine basins, Colorado Rocky Mountains, United States*. (Doctoral dissertation). University of Colorado at Boulder, Boulder, CO.

Hamlet, A. F., Mote, P. W., Clark, M. P., and Lettenmaier, D. P. (2005). Effects of temperature and precipitation variability on snowpack trends in the western United States. *Journal of Climate*, *18*, 4545−4561.

Harbaugh, A. W., Banta, E. R., Hill, M. C., and McDonald, M. G. (2000). *MODFLOW-2000, the U.S. geological survey modular ground-water models; user guide to modularization concepts and the ground-water flow process*. (21, Hydrogeology No. OF 00-0092). Reston, VA: U.S. Geological Survey.

Healy, R. (2010). *Estimating Groundwater Recharge*. Cambridge University Press Textbooks. Retrieved 5 July 2011, from <http://lib.myilibrary.com?ID=277150>

Healy, R. W., and P. G. Cook (2002). Using groundwater levels to estimate recharge. *Hydrogeology Journal*, *10*, 91−109. doi 10.1007/s10040-001-0178-0.

Hely, A. G., Mower, R. W., and Harr, C. A. (1971). *Water resources of Salt Lake County, Utah*. Salt Lake City, UT: Utah Department of Natural Resources.

Heppner, C. S., Nimmo, J. R., Folmar, G. J., Gbruek, W. J., and Risser, D. W. (2007). Multiple-methods investigation of recharge at a humid-region fractured rock site, Pennsylvania, USA. *Hydrogeology Journal*, *15*, 915–927.

Hill, K. (2005). *Potential climate impacts on hydrochemistry, source waters, and flowpaths in two alpine catchments, Green Lakes Valley, Colorado*. (Master's thesis). University of Colorado at Boulder, Boulder, CO.

Hood, E., M. Williams, and D. Cline (1999). Sublimation from a seasonal snowpack at a continental, mid-latitude alpine site. *Hydrological Processes*, *13*, 1781–1797. doi: 10.1002/(SICI)1099-1085(199909)13:12/13<1781::AID-HYP860>3.0.CO;2-C

Hsieh, P.A., and Winston, R.B. (2002). *User's Guide to Model Viewer, a Program for Three-Dimensional Visualization of Ground-water Model Results*. (U.S. Geological Survey Open-File Report 02-106). Reston, VA: U.S. Geological Survey.

Huntley, D. (1979). Ground-water recharge to the aquifers of northern San Luis Valley, Colorado. *Geological Society of America Bulletin*, *90*(8), 707−709, 1196−1281.

Hvorslev, M. J. (1951). Time lag and soil permeability in ground water observations. *U.S. Army Corps of Engineers Waterway Experimentation Station, Bulletin*, *36*.

Ives, J.D., (1973). Permafrost and its relationship to other environmental parameters in a mid-latitude, high-altitude setting, Front Range, Colorado Rocky Mountains. In *Permafrost - the North American Contributions to the 2nd Int. Permafrost Conf*. (pp. 13–28). Washington, D.C.: National Academy of Sciences.

Ives, J. D. (1974). Permafrost. In Ives, J. D., and Barry, R. G., (Eds.), *Arctic and alpine environments*. London, United Kingdom (GBR): Methuen.

Ives, J. D., and Fahey, B. D. (1971). Permafrost occurrence in the Front Range, Colorado Rocky Mountains, U.S.A. *Journal of Glaciology*, *10*(58), 105−111.

Janke, J. R. (2005). The occurrence of alpine permafrost in the Front Range of Colorado. *Geomorphology*, *67*(3−4), 375−389. doi:10.1016/j.geomorph.2004.11.005

Johnson, R. H. (2007). Ground Water Flow Modeling with Sensitivity Analyses to Guide Field Data Collection in a Mountain Watershed. *Ground Water Monitoring Review*, *27*(1), 75. doi:10.1111/j.1745-6592.2006.00125.x.

Kahn, K. G. (2005). *Analysis of the shallow groundwater system in an alpine basin; Handcart Gulch, Colorado*. (Master's thesis). University of Colorado at Boulder, Boulder, CO.

Karl, T. R., Groisman, P. Y., Knight, R. W., and Heim, R. R. (1993). Recent variations of snow cover and snowfall in North America and their relation to precipitation and temperature variations. *Journal of Climate*, *6*, 1327−1344.

Knowles, N., Dettinger, M. D., and Cayan, D. R. (2006). Trends in snowfall versus rainfall in the Western United States. *Journal of Climate*, *19*(18), 4545−4559.

Lee, C., Chen, W., and Lee, R. (2006). Estimation of groundwater recharge using water balance coupled with base-flow-record estimation and stable-base-flow analysis. *Environ. Geol.*, *51*, 73−82. doi: 10.1007/s00254-006-0305-2

Leopold, M., Dethier, D., Voelkel, J., Raab, T., Rikert, T. C., and Caine, N. (2008). Using geophysical methods to study the shallow subsurface of a sensitive alpine environment, Niwot Ridge, Colorado Front Range, U.S.A. *Arctic, Antarctic, and Alpine Research*, *40*(3), 519−530. doi:10.1657/1523-0430(06−124)[LEOPOLD]2.0.CO;2

Leopold, M., Voelkel, J., Dethier, D., Williams, M., and Caine, N. (2010). Mountain Permafrost – A Valid Archive to Study Climate Change? Examples from the Rocky Mountains Front Range of Colorado, USA. *Nova Acta Leopoldina NF*, *112*(384), 281−289.

Lester, A. P. (1992). *Mineralogic, isotopic, and paleomagnetic variations in the contact aureole of the Audubon-Albion stock, Front Range, Colorado*. (Doctoral dissertation). University of Colorado at Boulder, Boulder, CO.

Linsley, R.K., Kohler, M.A., and Paulhus, J.L.H. (1982). *Hydrology for engineers* (3rd ed.). New York, NY: McGraw-Hill.

Liu, F., Williams, M. W., and Caine, N. (2004). Source waters and flow paths in an alpine catchment, Colorado Front Range, United States. *Water Resources Research*, *40*(9) doi:10.1029/2004WR003076

Loague, K. (1990). Simple design for simultaneous steady-state infiltration experiments with ring infiltrometers. *Water Resources Bulletin*, *26*:935−938.

Lovering, T. S., and Goddard, E. N. (1950). *Geology and ore deposits of the Front Range, Colorado*. (27A Economic geology, geology of ore deposits; 13 Areal geology No. P 0223). Reston, VA: U.S. Geological Survey.

Lu, G., Liu, H., and Salve, R. (2011). Long term infiltration and tracer transport in fractured rocks: Field observations and model analyses. *Journal of Hydrology (Amsterdam)*, *396*(1−2), 33−48. doi:10.1016/j.jhydrol.2010.10.030

Madole, R. F. (1982). *Possible origins of till-like deposits near the summits of the Front Range in north-central Colorado*. (U.S. Geological Survey Professional Paper 1243). Reston, VA: U.S. Geological Survey.

Maréchal, J. C., Dewandel, B., Ahmed, S., Galeazzi, L., and Zaidi, F. K. (2006). Combined estimation of specific yield and natural recharge in a semi-arid groundwater basin with irrigated agriculture. *Journal of Hydrology*, *329*(1−2), 281−293. doi:10.1016/j.jhydrol.2006.02.022

Marler, J., and Ge, S. (2003). The permeability of the Elkhorn fault zone, South Park, Colorado. *Ground Water*, *41*(3), 321−332.

Mau, D. P., and Winter, T. C. (1997). Estimating ground-water recharge from streamflow hydrographs for a small mountain watershed in a temperate humid climate, New Hampshire, USA. *Ground Water*, *35*(2), 291−304.

Maurer, D. K. and Berger, D. L. (1997). *Subsurface flow and water yield from watersheds tributary to eagle valley hydrographic area, west-central Nevada*. (21, Hydrogeology No. WRI 97-4191). Reston, VA: U.S. Geological Survey.

McIntosh, J., McDonnell, J. J., and Peters, N. E. (1999). Tracer and hydrometric study of preferential flow in large undisturbed soil cores from the Georgia Piedmont, USA. *Hydrological Processes*, *13*(2), 139−155.

Memon, B. A. (1995). Quantitative analysis of springs. *Environmental Geology*, *26*, 111–120.

Moon, S., Woo, N. C., and Lee, K. S. (2004). Statistical analysis of hydrographs and water-table fluctuation to estimate groundwater recharge. *Journal of Hydrology*, *292*(1-4), 198-209. doi:10.1016/j.jhydrol.2003.12.030

Mote, P. W. (2003). Trends in snow water equivalent in the Pacific Northwest and their climatic causes. *Geophysical Research Letters*, *30*, 1601−1604.

Mote, P. W. (2006). Climate-driven variability and trends in mountain snowpack in western North America. *Journal of Climate*, *19*, 6209−6220.

Nathan, R. J., and McMahon, T. A. (1990). Evaluation of automated techniques for base flow and recession analyses. *Water Resources Research*, *26*(7), 1465−1473. doi:10.1029/WR026i007p01465

Niswonger, R. G., and Constantz, J. (1999). *Using heat as a tracer to estimate mountain-front recharge at Bear Canyon, Sandia Mountains, New Mexico; U.S. Geological Survey Middle Rio Grande Basin Study; Proceedings*. (21, Hydrogeology No. OF 99-0203). Reston, VA: U.S. Geological Survey.

NWT Hydrology (2011). *Niwot Ridge Long-Term Ecological Research program*. http://culter.colorado.edu/NWT/, downloaded 31 August 2011.

NWT Meteorology/Climatology (2011). *Niwot Ridge Long-Term Ecological Research program*. http://culter.colorado.edu/NWT/, downloaded 31 August 2011.

Pearson, R. C. and U.S. Bureau of Mines (1980). *Mineral resources of the Indian Peaks study area, Boulder and Grand Counties, Colorado*. (27, Economic geology of ore deposits No. B 1463). Reston, VA: U.S. Geological Survey.

Regonda, S. K., Rajogopalan, B., Clark, M., and Pitlick, J. (2005). Seasonal cycle shifts in hydroclimatology over the western United States. *Journal of Climate*, *18*, 372−384.

Risser, D., Gburek, W., and Folmar, G. (2005). *Comparison of methods for estimating ground-water recharge and base flow at a small watershed underlain by fractured bedrock in the eastern United States*. (U.S. Geological Survey Scientific Investigations Report 2005-5038). Reston, VA: U.S. Geological Survey.

Risser, D. W., Gburek, W. J., and Folmar, G. J. (2009). Comparison of recharge estimates at a small watershed in east-central Pennsylvania, USA. *Hydrogeology Journal*, *17*(2), 287−298. doi:10.1007/s10040-008-0406-y

Rutledge, A. T. (1998). *Computer programs for describing the recession of ground-water discharge for estimating mean ground-water recharge and discharge from streamflow records; update*. (21, Hydrogeology No. WRI 98-4148). Reston, VA: U.S. Geological Survey.

Saines, M. (1981). Errors in interpretation of ground-water level data. *Ground Water Monitoring Review*, *1*(1), 56−61.

Sanford, W. (2002). Recharge and groundwater models: an overview. *Hydrogeology Journal*, *10*:110–120.

Scanlon, B. R., Healy, R. W., Cook, P. G. (2002). Choosing appropriate techniques for quantifying groundwater recharge. *Hydrogeology Journal*, *10*:18–39.

Scanlon, B. R., Keese, K. E., Flint, A. L., Flint, L. E., Gaye, C. B., Edmunds, W. M., and Simmers, I. (2006). Global synthesis of groundwater recharge in semiarid and arid regions. *Hydrological Processes*, *20*(15), 3335−3370. doi:10.1002/hyp.6335

Scheidegger, A. E. (1973). Hydrogeomorphology review. *Journal of Hydrology*, *20*(3), 193−215.

Schilling, K. E. (2009). Investigating local variation in groundwater recharge along a topographic gradient, Walnut Creek, Iowa, USA. [Etude des variations locales de recharge d'un aquifere le long du gradient topographique: Walnut Creek, Iowa, USA] *Hydrogeology Journal*, *17*(2), 397−407. doi:10.1007/s10040-008-0347-5

Smerdon, B. D., Allen, D. M., Grasby, S. E., and Berg, M. A. (2009). An approach for predicting groundwater recharge in mountainous watersheds. *Journal of Hydrology*, *365*(3−4), 156−172. doi:10.1016/j.jhydrol.2008.11.023

Snow, D. T. (1968). Hydraulic character of fractured metamorphic rocks of the Front Range and implications of the Rocky Mountain arsenal well; geophysical and geological studies of the relationships between the Denver earthquake and the Rocky Mountain arsenal well, part A. *Colorado School of Mines Quarterly*, *63*(1), 167−199.

Snow, D. T. (1973). Mountain groundwater supplies. *The Mountain Geologist*, *10*(1), 19−24.

Sophocleous, M. A. (1991). Stream-floodwave propagation through the great bend alluvial aquifer, Kansas; field measurements and numerical simulations. *Journal of Hydrology*, *124*(3−4), 207−228.

Springer, R.K. and Gelhar, L.W., (1991). *Characterization of large-scale aquifer heterogeneity in glacial outwash by analysis of slug tests with oscillatory response, Cape Cod, Massachusetts*. (U.S. Geol. Surv. Water Res. Invest. Rep. 91-4034). Reston, VA: U.S. Geological Survey.

Stonestrom, D. A. and Harrill, J. R. (2007). Ground-water recharge in the arid and semiarid southwestern United States: climatic and geologic framework. In Stonestrom, D. A., Constantz, J., Ferre, T. P. A., and Leake, S. A., (eds.), *Ground-water Recharge in the Arid and Semiarid Southwestern United States*. (U.S. Geological Survey Professional Paper 1703, Chapter A, 1−28). Reston, VA: U.S. Geological Survey.

Susong, D. D., Spangler, L. E., and Heasler, H. P. (2005). Use of fluorescein dye tracing to determine ground-water flow in a glaciated, alpine valley, Sylvan Pass, Yellowstone National Park, Wyoming. *Geological Society of America, 2005 Annual Meeting. Abstracts with Programs*, *37*(7), 455.

Theis, C. V. (1935). The lowering of the piezometer surface and the rate and discharge of a well using ground-water storage. *Transactions, American Geophysical Union*, *16*, 519−24.

Thiem, D. (1906). Hydrologische methoden. Leipzig: Gebhardt, 56 pgs.

Tóth, J. (1963). A theoretical analysis of groundwater flow in small drainage basins. *Journal of Geophysical Research*, *68*(16), 4795−4812.

Tweto, O. (1968). Geologic setting and interrelationships of mineral deposits in the Mountain Province of Colorado and south-central Wyoming. In Ridge, J. D., (ed.), *Ore deposits of the United States 1933/1967* (pp. 551–588). New York, NY: The American Institute of Mining, Metallurgical, and Petroleum Engineers.

Tweto, O. (1987). *Rock units of the Precambrian basement in Colorado*. (12, Stratigraphy No. P 1321-A). Reston, VA: U.S. Geological Survey.

U.S. Geological Survey (1957). *Ward quadrangle, Colorado* [map]. 1:24,000. (7.5 Minute Series, map N4000-W10530). Reston, VA: U.S. Geological Survey.

Viviroli, D., H. H. Du¨rr, B. Messerli, M. Meybeck, and R. Weingartner (2007). Mountains of the world, water towers for humanity: Typology, mapping, and global significance, *Water Resour. Res.*, *43*, W07447. doi:10.1029/2006WR005653.

Voss, C. I. and Provost, A. M. (2009). *SUTRA, A model for saturated-unsaturated, variable-density ground-water flow with solute or energy transport*. (U.S. Geological Survey Water-Resources Investigations Report 02-4231). Reston, VA: U.S. Geological Survey.

Wahlstrom, E. E. (1933). *Geology of the Lake Albion region, Boulder County, CO*. (Master's thesis). University of Colorado at Boulder, Boulder, CO.

Wahlstrom, E. E. (1940). Audubon-Albion stock, Boulder County, Colorado. *Geological Society of America Bulletin*, *51*(12), 1789−1820.

Weider, K., and D. F. Boutt (2010). Heterogeneous water table response to climate revealed by 60 years of ground water data. *Geophys. Res. Lett.*, *37*, L24405. doi:10.1029/2010GL045561.

Weight, W. D. (2008). *Hydrogeology Field Manual* (2nd ed.). New York, NY: McGraw-Hill.

White, S. E. (1982). Physical and Geological Nature of the Indian Peaks, Colorado Front Range. *Institute of Arctic and Alpine Research Occasional Paper 37*, *37*, 1−12.

Williams, M. W., Bardsley, T., and Rikkers, M. (1998). Overestimation of snow depth and inorganic nitrogen wetfall using NADP data, Niwot Ridge, Colorado. *Atmospheric Environment*, *32*(22), 3827−3833.

Wilson, J. L., and H. Guan (2004). Mountain-block hydrology and mountain-front recharge. In Hogan, J. F., Phillips, F. M., and Scanlon, B. R., (eds.), *Groundwater Recharge in a Desert Environment: The Southwestern United States Volume 9* (pp. 113−137). Washington, D.C.: American Geophysical Union.

Winston, R. B., and Voss, C.I., (2004). *SutraGUI: A Graphical User Interface for SUTRA, A Model for Ground-Water Flow with Solute or Energy Transport*. (U.S. Geological Survey Open-File Report 03-285). Reston, VA: U.S. Geological Survey.

Winter, T. C. (1984). *Geohydrologic setting of Mirror Lake, West Thornton, New Hampshire*. (21, Hydrogeology No. WRI 84-4266). Reston, VA: U.S. Geological Survey.

Winter, T. C., Buso, D. C., Parkhurst, R. S., Rosenberry, D. O., and Martinez, M. L. (1999). *Hydrographs of lake stage, stream discharge, and hydraulic head in ground water for the Mirror Lake area, New Hampshire, 1979−1995*. (21, Hydrogeology No. OF 99-0239). Reston, VA: U.S. Geological Survey.

Wolf, J., Barthel, R., and Braun, J. (2008). Modeling ground water flow in alluvial mountainous catchments on a watershed scale. *Ground Water*, *46*(5), 695−705. doi:10.1111/j.1745-6584.2008.00456.x

Zhang, H., Schwartz, F. W., Wood, W. W., Garabedian, S. P., and LeBlanc, D. R. (1998). Simulation of variable-density flow and transport of reactive and nonreactive solutes during a tracer test at Cape Cod, Massachusetts. *Water Resources Research*, *34*(1), 67−82. doi:10.1029/97WR02918

Appendix I
List of notation

A cross-sectional area of the aquifer through which water flows [L^2]
A_s surface area that contributes to flow [L^2]
A_{Saddle} are of the Saddle catchment [L^2]
B formation thickness [L]
C_d damping parameter for slug tests in high-conductivity formations [1]
E evaporation [L/T], [L^2/T], [L^3/T], or [M/T]
E^{gw} evaporation from groundwater [L/T], [L^2/T], [L^3/T], or [M/T]
E^{sw} evaporation from surface water [L/T], [L^2/T], [L^3/T], or [M/T]
ET evapotranspiration [L/T], [L^2/T], [L^3/T], or [M/T]
ET^{uz} evapotranspiration from unsaturated zone [L/T], [L^2/T], [L^3/T], or [M/T]
g gravitational acceleration [L/T^2]
H measured displacement from static conditions [L]
H_0 measured initial displacement [L]
H_0^* expected initial displacement [L]
H_0^+ apparent magnitude of the initial displacement [L]
h total hydraulic head or water table elevation in an unconfined aquifer [L]
h_{mp} matric pressure head [L]
h_p pressure head [L]
K saturated hydraulic conductivity [L/T]
$K(\theta)$ hydraulic conductivity at the ambient water content [L/T]
K_r radial component of saturated hydraulic conductivity [L/T]
K_z vertical component of saturated hydraulic conductivity [L/T]
k permeability [L^2]
L screen length [L]
L_e effective length of water column in well [L]
l length of flow [L]
n effective or drainable porosity [1]
P precipitation that reaches the ground surface [L/T], [L^2/T], [L^3/T], or [M/T]
P_D flow parameter used in Dagan method [1]
p fluid pressure [M/LT^2]
Q discharge or volume flow rate [L^3/T]
Q_{in} water flow into a basin [L/T], [L^2/T], [L^3/T], or [M/T]
Q_{in}^{gw} groundwater flow into a basin [L/T], [L^2/T], [L^3/T], or [M/T]
Q_{in}^{sw} surface water flow into a basin [L/T], [L^2/T], [L^3/T], or [M/T]
Q_{out} water flow out of a basin [L/T], [L^2/T], [L^3/T], or [M/T]
Q_{out}^{gw} groundwater flow out of a basin [L/T], [L^2/T], [L^3/T], or [M/T]
Q_{out}^{sw} surface water flow out of a basin [L/T], [L^2/T], [L^3/T], or [M/T]
q specific discharge or Darcy velocity [L/T]
R recharge [L/T], [L^2/T], [L^3/T], or [M/T]
R_e effective radius over which head is dissipated during a slug test [L]
r_c effective well casing radius [L]
r_{nc} nominal well casing radius [L]
r_w effective well screen radius [L]

r_w^* equivalent well radius or radius of filter pack [L]
S water stored in a basin [L/T], [L^2/T], [L^3/T], or [M/T]
S^{gw} groundwater stored in a basin [L/T], [L^2/T], [L^3/T], or [M/T]
S^{sw} surface water stored in a basin [L/T], [L^2/T], [L^3/T], or [M/T]
S^{uz} water stored in the unsaturated zone in a basin [L/T], [L^2/T], [L^3/T], or [M/T]
S_s specific storage [L^{-1}]
S_y specific yield [1]
T_0 time at which normalized head of 0.37 is obtained [T]
t time; for slug tests, total time since test initiation [T]
t_0 time of test initiation [T]
t_d $(g/L_e)^{0.5}t$ [1]
v average linear velocity [L/T]
W source or sink of groundwater [M/L^3T]
w deviation of static water level from static [L]
w_d w/H_0 [1]
x horizontal distance [L]
z elevation head [L]
ρ density [M/L^3]
μ fluid viscosity [M/LT]

Appendix II
Methods for estimating groundwater recharge in mountain settings

Hydrogeologists have employed many different methods to estimate groundwater recharge, however few methods have been applied to mountain settings. Deciding what methods to use depends on the resources and data available and on the applicability and limitations of each method. Many studies recommend using multiple methods and comparing the results since much of the error associated with a recharge estimate is not quantifiable (Sophocleous, 1991; Halford and Mayer, 2000; de Vries and Simmers, 2000; Healy and Cook, 2002; Scanlon et al., 2002; Healy, 2010). Because of the complex interaction of climate, topography, geology, and other factors, recharge to mountain watersheds is difficult to quantify (Winter et al., 1999). The selected estimation technique must take into account the mechanisms influencing recharge to the aquifer under study (de Vries and Simmers, 2000). It is therefore important to have high-quality, long-term, continuous hydrologic and climatic data. In mountain settings, groundwater data are rarely available for mountain regions because of the practical challenges of installing wells and collecting groundwater data in remote settings with rugged terrain and harsh weather. These factors often limit the type and number of methods that may be utilized.

It is important to consider spatial and temporal scales of recharge (Delin and Risser, 2007). Local-scale estimates of recharge are highly variable and may not be accurately extended to larger scales. Regional-scale estimates do not account for high spatial variability of recharge, particularly in the mountains, and should be used with caution. Because the source of recharge, precipitation and snowmelt, varies in time, temporal variability of recharge should be considered.

Darcy's law

Using Darcy's law, recharge in the unsaturated zone is calculated as (Scanlon et al., 2002):

$$R = -K(\theta)\frac{dh}{dz} = -K(\theta)\frac{d}{dz}(h_{mp} + z) = -K(\theta)\left(\frac{\partial h_{mp}}{\partial z} + 1\right) \quad [II.1]$$

where $K(\theta)$ is the hydraulic conductivity at the ambient water content [L/T], h total hydraulic head [L], h_{mp} is the matric pressure head [L], and z is elevation head [L]. This method assumes that the hydraulic gradient is uniform with depth, all water that infiltrates becomes recharge, and most of the flow is through the rock matrix rather than through fractures.

In the saturated zone, the equation for recharge using Darcy's law is simplified to (Scanlon et al., 2002):

$$R = \left(-K\frac{\partial h}{\partial l}\right)\frac{A}{A_s} \quad [II.2]$$

where K is the saturated hydraulic conductivity [L/T], $\delta h/\delta l$ is the hydraulic gradient [L/L], A is the vertical cross-section of the aquifer through which water flows [L^2], and A_s is the surface area that contributes to flow [L^2]. This method assumes steady flow, no pumping, and that A is aligned with an equipotential line.

A recharge estimation using Darcy's law depends on estimates of hydraulic conductivity and hydraulic gradient. Estimating hydraulic conductivity can be difficult since it varied by several orders of magnitude and because of the complex relation between unsaturated hydraulic conductivity and saturation (de Vries and Simmers, 2002; Scanlon et al., 2002). Hely et al. (1971) used the Darcy method and found that 19% of precipitation recharged groundwater in the Wasatch Range, Utah. Belan and Matlock (1973) used the Darcy method to estimate mountain recharge (4.14×10^5 m^3/y) to the Tucson Basin, Arizona.

Lysimeters

A lysimeter is soil-filled container placed in the unsaturated zone at a depth such that the base of the lysimeter is below the root zone (Scanlon et al., 2002). Water percolating downward

through the unsaturated zone enters the lysimeter. Recharge is estimated either as the change in weight of the lysimeter (e.g. weighing lysimeter) or as the volume of water which drains from the lysimeter into a collection device (e.g. drainage lysimeter). Care must be taken so that the soil inside the lysimeter represents the surrounding environment (i.e. soil and vegetation).

The primary assumption of recharge estimates made with lysimeters is that water collected by a lysimeter would proceed to recharge the water table under natural conditions in the absence of the lysimeter (Heppner et al., 2007). Lysimeters provide the rate of potential recharge, but not necessarily the timing (Risser et al., 2009).

The advantage of lysimeters is they can be very accurate and measurements incorporate the various components of the water budget. The disadvantage of lysimeters is they are expensive, difficult to install without disturbing native soil conditions, and only represent a small area. Lysimeters were used to estimate recharge (0.31 m/y) in a fractured-rock aquifer in Pennsylvania (Risser et al., 2009), which suggests they may be used in mountain settings.

Water table fluctuations in wells

Water table fluctuations occur in unconfined aquifers in response to groundwater recharge and discharge. The water table fluctuation (WTF) method uses water table fluctuations measured in observation wells, to provide an estimate of recharge that reaches the water table. Additional details on the WTF method are found in Chapter 4. This method is based on the relation between changes in measured water level and changes in the amount of water stored in the aquifer. Recharge is calculated as (Healy, 2010):

$$R = S_y \frac{dh}{dt} = S_y \frac{\Delta h}{\Delta t} \qquad \text{[II.3]}$$

where S_y is specific yield [1], h is water table elevation [L], and t is time [T]. The change in water table elevation due to recharge, Δh, is equal to the difference in the peak of the rise at time

t and the low point on the extrapolated antecedent recession curve at the time of the peak (Figure 4.1).

Stream discharge records

Estimating recharge from stream discharge records (i.e. stream hydrograph separation) is a commonly used method because the only measurements needed are streamflow rates over time from gaining streams. The method is based on a simplified water budget approach where the residual, recharge, is equated to discharge of groundwater to the stream (i.e. baseflow). Various techniques are available to determine baseflow from streamflow records (Rutledge, 1998; Nathan and McMahon, 1990). Several studies have compared recharge amounts using multiple approaches to stream hydrograph separation for mountain watersheds and determined that multiple methods should be employed (Mau and Winter, 1997; Chen and Lee, 2003). Chemical and isotopic hydrograph separation techniques have been used to infer the sources of streamflow from end members such as rain, snowmelt, and groundwater (Liu et al., 2004).

The accuracy of recharge estimates obtained by hydrograph separation depends on the validity of and adherence to the various assumptions of the particular estimation technique (Halford and Mayer, 2000). Techniques that depend on empirical relations to estimate baseflow may result in error if extended beyond the study area that was used to develop the empirical relations. Halford and Mayer (2000) describe in detail the limitations and requirements of the hydrograph separation method.

Tracers

Tracers are commonly used to quantify recharge, determine groundwater sources and flowpaths, and estimate groundwater velocities and travel times (Healy, 2010). A tracer is a substance (chemical, isotopic, or heat) that moves with water and can be measured in the

atmosphere, surface of the Earth, and/or subsurface. When tracers are used in the unsaturated zone, only estimates of potential recharge are provided. In the saturated zone, actual recharge can be quantified. In systems where preferential flow dominates, such as fractured rock aquifers, recharge estimated using tracer techniques might be erroneous (Healy, 2010). The accuracy of the recharge estimate depends on the extent to which the assumptions of the particular tracer method are met for the system under study. The main categories of tracers include natural environmental tracers, historical tracers, applied tracers, and heat tracer (Scanlon et al., 2002).

Natural environmental tracers are transported to the ground as wet or dry atmospheric deposition. Most of these tracers come from evaporated ocean water or are formed in the atmosphere. Natural environmental tracers are useful in determining recharge over long time scales. The staple isotopes of water (δ^2H and $\delta^{18}O$) are the most frequently used natural environmental tracer because they are abundant throughout the hydrologic cycle and can be detected with great precision. Abbott et al. (2000) compared δ^2H and $\delta^{18}O$ in precipitation and groundwater to trace the source of groundwater recharge to a mountain in Vermont. They found that snowmelt contributed most of the recharge and that recharge at higher elevations (800−1330 m) may occur year round while recharge at lower elevations (250−800 m) may only occur during the winter when evapotranspiration rates are lower. Liu et al. (2004) used water isotopes to show that subsurface flow, even during peak spring streamflow, contributed significantly to alpine streamflow in Green Lakes Valley, Colorado.

Historical tracers are chemicals or isotopes that have been added to the atmosphere by human activity. They are transported to the ground by either wet or dry atmospheric deposition or diffusion of gasses from the atmosphere into the subsurface. Historical tracers are most useful when they mark an event in time, such as the use of tritium (^3H) and chlorine-36 (^{36}Cl), which

were added to the atmosphere during the 1950s and early 1960s as the result of nuclear weapons testing. The presence of an historical event tracer in groundwater suggests that at least part of that groundwater recharge at the time of the event. Abbott et al. (2000) used ^{3}H measurements and determined the age of groundwater recharge was 40−50 years in a mountain aquifer in Vermont.

Applied tracers are applied directly to the land surface or subsurface by human application and transported to the subsurface by infiltrating water. Commonly used applied tracers include bromide (Br^-), chloride (Cl^-), tritium (^{3}H), and visible dyes (Scanlon et al., 2002). Applied tracer techniques can be difficult in mountain regions, which are often protected from the application of artificial chemicals. Nevertheless, several studies have used bromide and dyes to determine the source and flowpaths of groundwater recharge to mountain regions (Susong et al., 2005; Lu et al., 2011).

Heat moves with the flow of water and can therefore be used as a tracer to detect groundwater recharge. Borehole temperature profiles can be used to trace the downward movement of water and were used to determine that recharge occurred at a rate of 0.5−20 mm/y at Yucca Mountain, Nevada (Flint et al., 2002) and 1.4−6.6 m/d in the Sandia Mountains, New Mexico, depending on the time of year (Niswonger and Constantz, 1999). Temperature measurements in streams and lakes can be used to estimate infiltration from the surface water (Scanlon et al., 2002). The advantage of the heat tracer method is that temperature measurements can be made with great accuracy, at low cost, at high frequency, and without the need to obtain water samples (Healy, 2010). A review of heat as a groundwater tracer is provided in Anderson (2005).

Numerical models

Water budget equations and Darcy's law form the basis of many numerical groundwater models (e.g. Harbaugh et al., 2000; Voss and Provost, 2009). Recharge rates, distribution, and the fate of recharge can be estimated using modeling techniques (Sanford, 2002). The recharge estimate depends on the conceptual model on which the numerical model is based and on the quality of hydrogeologic data input to the model. Groundwater recharge is typically estimated in numerical models by calibration to hydrogeologic observations. If hydraulic conductivity is used as the only observation data, only the ratio of recharge to hydraulic conductivity can be estimated. In order to quantify recharge by calibration, observations of groundwater flux (e.g. baseflow), groundwater ages, or groundwater temperatures are needed. The advantage of numerical modeling to estimate recharge is that recharge can be estimated across space and time scales that would otherwise be impossible to study. The disadvantages are that modeling requires specialized software and expertise, costs can be high, and data inputs are extensive. Groundwater modeling was used to estimate recharge in Chapter 5. Sandford (2002) reviews the use of groundwater models to estimate recharge.

Other methods

Other methods are available to estimate groundwater recharge in mountain regions, however their use is less widespread than the methods discussed above. Methods that rely on spatial data and a global information system (GIS) are available to examine recharge (Cherkauer, 2004; Cherkauer and Ansari, 2005). Regression models, which relate recharge to precipitation, elevation, or other parameters, are available and can be used for mountain regions (Flint et al., 2002; Flynn and Tasker, 2004). However, the empirical nature of a regression model limits its use beyond the region and timescale for which it was developed (Wilson and Guan, 2004).

Appendix III
Theoretical models for analysis of slug test data

This Appendix describes the theoretical models used to analyze the results of slug tests presented in Chapter 3.

Hvorslev method

For normalized slug test response data that coincided when plotted together, were not dependent on H_0, and did not display evidence of filter pack drainage, the Hvorslev solution was matched to the response data. Hvorslev (1951) originally created this method for confined aquifers, however if the well screen is far from the water table in an unconfined aquifer, the water table can be assumed to have little effect on slug test response and the Hvorslev method for confined aquifers may be used (Fetter, 2001). Assumptions of the Hvorslev method include (1) effects of elastic storage are negligible, (2) the position of the water table and the saturated thickness do not change during testing, and (3) the aquifer is homogeneous, isotropic, of uniform thickness, and has infinite areal extent.

The empirical relationship for the water-level response due to the displacement of a known volume of water in a fully or partially penetrating well is written as:

$$\ln\left(\frac{H_0}{H}\right) = -\frac{2K_r L t}{r_c^2 \ln\left(L/2r_w^* + \sqrt{1+(L/2r_w^*)^2}\right)} \qquad \text{[III.1a]}$$

where H_0 is measured initial displacement [L], H is displacement [L] at time t [T], K_r is radial hydraulic conductivity [L/T], L is screen length [L], and r_c is effective casing radius [L]. r_w^* is equivalent well radius [L] and is defined as $r_w^* = r_w(K_z/K_r)^{1/2}$ where r_w is the effective radius of the well screen [L] and K_z is vertical hydraulic conductivity [L/T]. Alternatively, the radius of the filter pack may be used for r_w^* (Fetter, 2001). Equation III.1a solved for K_r is:

$$K_r = \frac{r_c^2 \ln(R_e / r_w)}{2LT_0} \qquad \text{[III.1b]}$$

where R_e is an empirical parameter designated as the effective radius over which head is dissipated [L] and T_0 is the time at which normalized head equals 0.37 [T]. R_e is defined as 200 times the effective radius of the well screen (Butler, 1998). T_0 was obtained by fitting a straight line to the normalized response data plotted on semilog axes and locating the point on the line where normalized head equals 0.37. The corresponding value of t was used for T_0. If a concave-up curve formed, the straight line was fit to normalized heads in the range of 0.15−0.25 (Butler, 1998).

Bouwer and Rice method

For normalized response data that coincided when plotted together, were not dependent on H_0, and displayed evidence of filter pack drainage (e.g. double straight-line effect), the Bouwer and Rice solution was matched to the data. Bouwer and Rice (1976) developed a conventional theoretical method for the analysis of a slug test performed in a fully or partially penetrating well in an unconfined aquifer. Assumptions of the Bouwer and Rice method include (1) effects of elastic storage are negligible, (2) the position of the water table and the effective screen length do not change during testing, and (3) the aquifer is homogeneous, isotropic, of uniform thickness, and has infinite areal extent. A disadvantage of the Bouwer and Rice method is that it is difficult to recognize the presence of a low-permeability well skin, so hydraulic conductivity estimated with the Bouwer and Rice method must be considered a lower bound on the hydraulic conductivity of the aquifer.

The empirical relationship describing the response of water level in a well due to the displacement of a known volume of water in a well is written as:

$$\ln\left(\frac{H}{H_0}\right) = -\frac{2K_r Lt}{r_c^2 \ln\left(R_e / r_w^*\right)} \qquad \text{[III.2a].}$$

The terms in Equation III.2a were previously defined. Equation III.2a solved for K_r is:

$$K_r = \frac{r_c^2 \ln(R_e / r_w^*)}{2L} \frac{1}{t} \ln \frac{H_0}{H} \qquad \text{[III.2b]}$$

where $\frac{1}{t} \ln \frac{H_0}{H}$ is the slope of a straight line fit to the normalized response data plotted on log-linear axes. If a concave-up curve formed, the straight line was fit to normalized heads in the range of 0.20−0.30 (Butler, 1998).

Dagan method

For normalized response data that coincided when plotted together and displayed a reproducible dependence on H_0, the Dagan solution was matched to the data. Dagan (1978) developed a method for the analysis of a slug test performed in a partially penetrating well in an unconfined aquifer in which the water table intersects the screened interval. Assumptions of the Dagan method include (1) effects of elastic storage are negligible, (2) unlike the Bouwer and Rice method, the Dagan method assumes that the water table may change position during a slug test, and (3) the aquifer is homogeneous, of uniform thickness, and has infinite areal extent. Similar to the Bouwer and Rice method, it is difficult to recognize the presence of a low-permeability well skin with the Dagan method and estimates of hydraulic conductivity much be considered a lower bound on the hydraulic conductivity of the aquifer.

The empirical relationship that is the Dagan solution is written as:

$$\ln\left(\frac{H}{H_0(2L-H)/2L-H_0}\right) = -\frac{2K_r Lt}{r_c^2 / P_D} \qquad \text{[III.3]}$$

where P_D is the Dagan method flow parameter [1]. The other terms in Equation III.3 have been previously defined. The Dagan solution takes into account changes in the position of the water table through the term P_D, which depends on well geometry and hydraulic conductivity anisotropy. To determine P_D, the normalized length of the well screen was calculated as L/B, where L is screen length [L] and B is formation thickness [L]. Anisotropy was related to well geometry by $(K_z/K_r)^{1/2}/(L/r_w)$, for which the terms have been previously defined. K_z/K_r was assumed to equal one. P_D was then determined from Table 6.7 in Butler (1998).

To estimate K_r, the response data were plotted on semilog axes and a straight line was fit to the data. If a concave-up curve formed, the straight line was fit to normalized heads in the range of 0.20−0.30 (Butler, 1998). Then, similar to the Hvorslev method, the time at which normalized head equaled 0.37, T_0, was determined from the best-fit straight line. Hydraulic conductivity was estimated using the equation:

$$K_r = \frac{r_c^2 (1/P_D)}{2LT_0} \quad . \qquad \text{[III.4]}$$

Springer and Gelhar method

In highly conductive aquifers, the displaced column of water may recover quickly enough such that the momentum of the water column overcomes the viscous forces of the water. As a result, the water level in the well oscillates from above to below static water level. This response is termed underdamped. Normalized response data that displayed an oscillatory response were analyzed using the method of Springer and Gelhar (1991). The Springer and Gelhar solution extends the Bouwer and Rice (1976) solution for a slug test in an unconfined aquifer and approximates the oscillations as an exponentially decaying sinusoidal function. Assumptions of the Springer and Gelhar solution are the same as for the Bouwer and Rice solution and include (1) effects of elastic storage are negligible, (2) the position of the water table and the saturated

thickness do not change during testing, and (3) the aquifer is homogeneous, isotropic, of uniform thickness, and has infinite areal extent.

The Springer and Gelhar method stems from the solution for a damped spring:

$$\frac{d^2 w_d}{dt_d^2} + C_d \frac{dw_d}{dt_d} + w_d = 0 \qquad \text{[III.5]}$$

where $w_d = w/H_0$ [1] and $t_d = (g/L_e)^{0.5} t$ [1]. w is deviation of static water level from static [L], H_0 is measured initial displacement [L], g is gravitational acceleration [L/T^2], and L_e is the effective length of the water column in the well [L]. C_d is the damping parameter for slug tests in high-conductivity formations [1] and is defined as:

$$C_d = \sqrt{\frac{g}{L_e}} \frac{r_c^2 \ln(R_e / r_w)}{2 K_r L} \qquad \text{[III.6a]}$$

for which the terms on the right-hand side have been previously defined.

To apply the Springer and Gelhar method, normalized response data were plotted against time on linear axes. The translation method was used to eliminate early noise in the data record. Type curves, determined from Equation III.6a and well geometry, were plotted as w_d versus t_d on linear axes. The plot of normalized response data was matched to the best-fit C_d type curve. Values of t_d and C_d were determined from the best-fit match between type curve and response data. L_e was determined from the definition of t_d (given above). Hydraulic conductivity of the aquifer was estimated from Equation III.6a, which solved for Kr is rewritten as:

$$K_r = \sqrt{\frac{g}{L_e}} \frac{r_c^2 \ln(R_e / r_w)}{2 L C_d} \qquad \text{[III.6b]}$$

.

Appendix IV
Groundwater temperature data

Groundwater temperature was measured using the In-Situ Inc. Level Troll® 100 non-vented pressure transducers installed in Saddle wells SD3 and SD4. The bottom of the pressure transducer was set 8.57 m below ground surface (elevation 3515.21 m) in SD3 and 6.12 m below ground surface in SD4 (elevation 3525.73 m). Groundwater temperature data were collected twice daily, measured at noon and midnight, between January 2010 and September 2011. Measurements of temperature were made in conjunction with measurements of groundwater level. The accuracy of the In-Situ Inc. Level Troll® 100 temperature sensor is ± 0.3°C. The operational temperature range is -20 °C to 50 °C. There temperature data were downloaded 1 to 2 times per year using Win-Situ® v5.6.4.6 software.

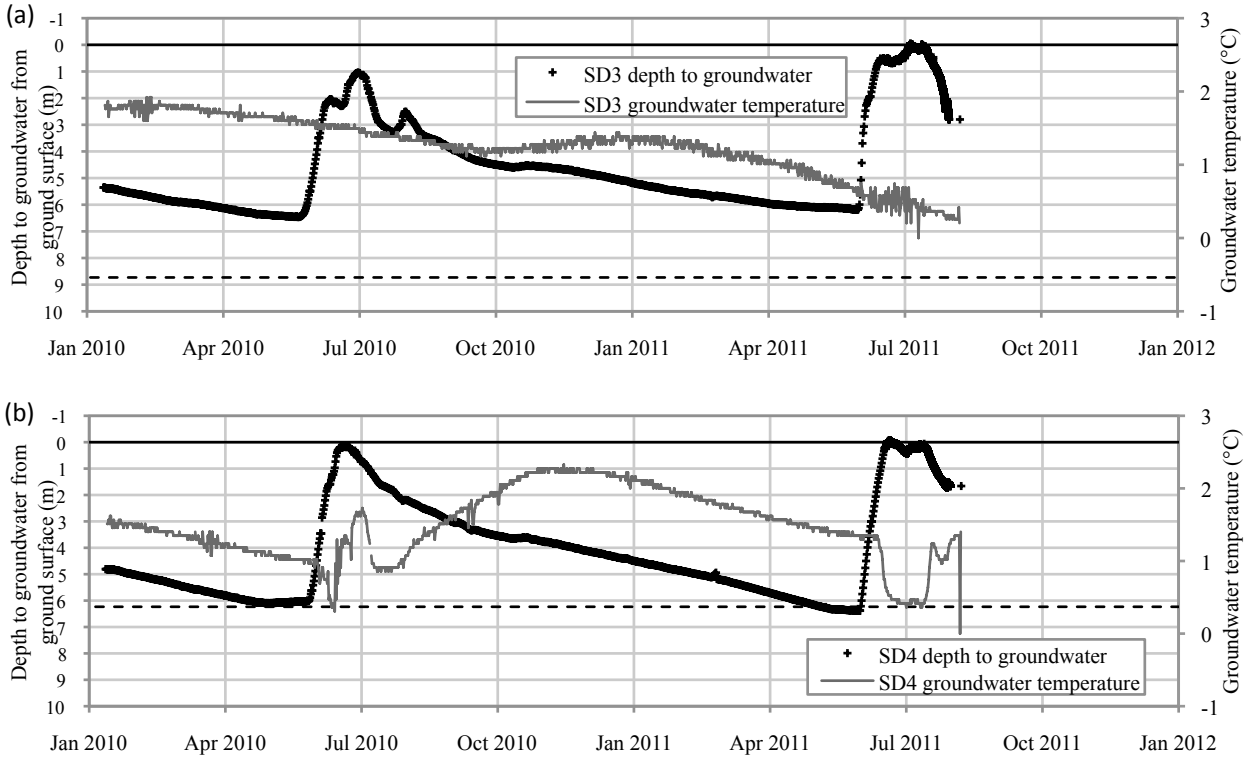

Figure IV.1. Graph of depth to groundwater and groundwater temperature measured in Saddle wells (a) SD3 and (b) SD4 for the period of measurement (Jan. 2009 to Aug. 2011). Dashed line represents bottom of each well.